

Production and Application of Different Waste-derived Sustainable Materials for the Removal of  
Naphthenic Acids Related to Oil Sands Process Water

by

Zhexuan An

A thesis submitted in partial fulfillment of the requirements for the degree of

Doctor of Philosophy

in

Environmental Engineering

Department of Civil and Environmental Engineering  
University of Alberta

© Zhexuan An, 2024

## ABSTRACT

Oil sands process water (OSPW) is generated in a large volume during the bitumen extraction process from the oil sands. Naphthenic acids (NAs) are recalcitrant compounds that contribute to the toxicity of OSPW, which need effective treatment before being released into the environment. In the meantime, various undervalued waste materials and by-products from industry are facing a continuous accumulation problem. This study applied different waste-derived materials and evaluated their potential for OSPW remediation, including petroleum coke to remove the acid extractable fraction (AEF) in real OSPW, and coarse sand tailing, peat mineral mix, and wood waste-based biochar, to remove or degrade model NAs. All the assessed results contribute as an essential insight for the further practical implementation of real OSPW remediation.

Firstly, a large-scale field pilot study was conducted to examine the feasibility and effectiveness of residual waste petroleum coke (PC) as an adsorbent for OSPW treatment. The quality of treated OSPW was evaluated as a function of residence time in the PC deposit under natural climatic conditions. The results indicated the AEF adsorption by PC followed a pseudo-second order (PSO) kinetics with overall removal efficiency of over 80%. The dissolved organic carbon (DOC) decreased by about 50% after 4 weeks of retention in the PC deposit. In addition, treated OSPW exhibited no acute toxic response in the whole effluent toxicity testing. This field pilot study proved that PC adsorption is a potentially commercially viable technology for OSPW treatment.

Secondly, the adsorption behavior of NAs on coarse sand tailings (CST) and peat-mineral mix (PMM) was assessed. Both CST and PMM are leftovers of oil sands industry operations in Alberta and are readily available at the mining site. In this study, mono-compound and mixture solutions of NAs were applied to evaluate the removal efficiency and adsorption performance. The

adsorption of dodecanoic acid (DDA) on CST and PMM followed PSO kinetics and intra-particle diffusion (IPD) model. The isotherm of DDA adsorption was best fitted with the Freundlich model for both materials. At equilibrium, the adsorption capacity of PMM for DDA (2.4 mg/g) was higher than CST (0.05 mg/g). The competing adsorption of different NAs was observed in the mixture solution where NAs with longer chain structures showed more competition capacity. The predominant adsorption mechanism for NAs on CST and PMM was identified as hydrophobic interaction. PMM could be a potential alternative material for NAs removal due to the better performance of removing most of the NAs in 96 h from the mixture solution.

Finally, biochar ZnO (BC/ZnO) composites were synthesized using wood waste with different ZnO content and applied under simulated solar light for the photocatalytic degradation of NAs. The best experimental conditions were determined as 0.5 g/L BC/30%ZnO and 4 h of solar irradiation time, achieving 93.7% degradation of cyclohexanecarboxylic acid (CHA) following a pseudo-first order (PFO) kinetics. BC, with a porous structure and roughened surface, acted as an excellent platform for ZnO particles, as well as an electron reservoir to inhibit the recombination of photogenerated electron-hole pairs. Hydroxyl radicals ( $\cdot\text{OH}$ ) were identified to play the dominant role in CHA degradation, and the enhanced photocatalytic performance of the BC/30%ZnO composite was proved by more  $\cdot\text{OH}$  species detected by EPR measurements compared to synthesized ZnO (Syn-ZnO). The composite showed good reusability and stability after 4 successive cycles of use. Moreover, for the first time, BC/30%ZnO composite was applied for the simultaneous removal of a complex mixture of 8 NAs with significantly different chemical structures. A competition tendency was observed in which NAs with S atom, as well as large, branched, and cyclic NAs showed a better degradation performance, finally reaching a total NAs degradation efficiency of more than 95% after 6 h solar irradiation. The excellent performance of

BC/ZnO composite under solar light, as well as its good reusability and stability, make the composite a sustainable approach for OSPW remediation.

This research provides valuable insight into developing and applying eco-friendly and effective alternatives for OSPW remediation. At the same time, it enhances the understanding of different waste-derived materials and highlights the possible future applications. More importantly, the outcomes are essential contributions that can be meaningful guidance for pursuing sustainable development by promoting economically feasible waste material management and environmental remediation.

## PREFACE

All the research completed in this thesis was performed by myself under the supervision of Dr. Mohamed Gamal El-Din in the Department of Civil and Environmental Engineering at the University of Alberta. I conducted all data analysis as well as the preparation of the manuscripts. Some colleagues and collaborators have contributed to sample analysis or manuscript edits, and some of them were co-authors in the published paper or manuscripts prepared for publication. The contributions to each chapter are described below.

Chapter 2 has been published as “Zubot, W., An, Z., Benally, C., and Gamal El-Din, M. 2021. Treatment of oil sands process water using petroleum coke: Field pilot. *Journal of environmental management*, 289: 112407. DOI: 10.1016/j.jenvman.2021.112407”. I accomplished all the data mining and plotting, as well as the manuscript writing. Dr. Mohamed Gamal El-Din contributed to the supervision, reviewing the paper, and funding acquisition. Dr. Warren Zubot contributed to the design and operation of the field pilot program. Dr. Chelsea Benally and Dr. Pamela Chelme-Ayala contributed to the editing and revision of the manuscript.

Chapter 3 is under review in *Chemosphere* as “An, Z., Muhammad, A., Chelme-Ayala, P., Chen, C., and Gamal El-Din, M. Adsorption Assessment of Naphthenic Acids on Different Types of Reclamation Materials: Coarse Sand Tailings and Peat Mineral Mix”. I prepared the reclamation materials, conducted the experiments, and analyzed the data discussed in Chapter 3. Dr. Mohamed Gamal El-Din contributed to the supervision, planning, final editing, and funding acquisition. Dr. Muhammad Arslan and Dr. Pamela Chelme-Ayala contributed to the manuscript revision and editing. Dr. Zuo Tong How and Dr. Lingling Yang contributed to the analytical measurement of NAs in the samples. The following analyses were performed in multiple laboratories and facilities at the University of Alberta: scanning electron microscopy (SEM) and X-ray diffraction (XRD)

were performed in the EAS SEM and X-ray Diffraction Laboratory, while Fourier transform infrared spectrometry (FTIR) was conducted in the Analytical and Instrumentation Laboratory. Texture composition, elemental analysis, cation exchange capacity (CEC), and total organic carbon (TOC) were analyzed in the Natural Resources Analytical Laboratory.

Chapter 4 is under review in *Chemical Engineering Journal* as “An, Z., Sánchez-Montes, I., Chelme-Ayala, P., Chen, C., and Gamal El-Din, M. Efficient Degradation of Naphthenic Acids in Water Using a Sustainable Engineered Biochar/ZnO Composite Under Solar Light”. I designed and synthesized the wood waste-based biochar and the BC/ZnO composites, conducted the experiments, and analyzed the data discussed in Chapter 4. Dr. Mohamed Gamal El-Din contributed to the supervision, planning, final editing, and funding acquisition. Dr. Isaac Sánchez-Montes and Dr. Pamela Chelme-Ayala contributed to the manuscript revision and editing. Dr. Lingling Yang contributed to the analytical measurement of NAs in the samples. The following analyses were performed in multiple laboratories and facilities at the University of Alberta: SEM and XRD were performed in the EAS SEM and X-ray Diffraction Laboratory, while The X-ray photoelectron spectroscopy (XPS) was conducted at the NanoFab Fabrication and Characterization Centre. The optical properties of materials were conducted in the Analytical and Instrumentation Laboratory. The elemental analysis was analyzed in the Natural Resources Analytical Laboratory.

I performed all the work associated with this thesis except for the contributions from the collaborators and co-authors described above.

## DEDICATION

*To my dearest grandparents who have cheered me up all the time; Zouhui Cao &  
Jichang Yang.*

*To my beloved parents who always support me with no doubt; Ying Yang &  
Xiangguang An.*

*To all my friends who accompany me through this treasured journey.*

*To everyone who seeks the truth.*

## ACKNOWLEDGEMENTS

First and foremost, I would like to express my sincere gratitude to my supervisor, Dr. Mohamed Gamal El-Din, for offering me the precious opportunity to work on wastewater treatment-related projects under his professional tutelage. His invaluable academic guidance, supervision, and generous financial assistance supported me to pursue my research goal. It is my honor to be a member of his research group. And the fantastic experience in his group improved me a lot. I appreciate all the understanding and support from him.

I would like to thank all of those I have had the pleasure to work with. I am especially indebted to Dr. Pamela Chelme-Ayala for her inspiring encouragement at every stage of my research. The dedicated support from her towards all the students and the staff inspires me a lot. My grateful gratitude also goes to Mr. Warren Zubot, Dr. Isaac Sánchez-Montes, Dr. Chelsea Benally, and Dr. Muhammad Arslan, who have provided professional and treasured advice on my work. I would especially like to thank Dr. Lingling Yang and Dr. Zuo Tong How for the numerous analytical measurements of NAs throughout my projects. My appreciation also goes to the postdoctoral fellows and graduate students who helped me gain a better understanding of the water treatment processes, especially Dr. Jia Li and Dr. Lingjun Meng, for their assistance in the training of various instruments.

I sincerely acknowledge the generous financial support from the University of Alberta's Future Energy Systems research initiative, supported by the Canada First Research Excellence Fund, as well as the assistance from the Natural Sciences and Engineering Research Council of Canada (NSERC) Senior Industrial Research Chair (IRC) in Oil Sands Tailings Water Treatment and Canada's Oil Sands Innovation Alliance (COSIA). I am also thankful for the following for their support: Syncrude Canada Ltd., Suncor Energy Inc., Canadian Natural Resources Ltd.,

Imperial Oil Resources, Teck Resources Limited., EPCOR Water Services, Alberta Innovates, and Alberta Environment and Protected Areas. I appreciate the recognition of the following awards: the Alberta Graduate Excellence Scholarship, the Jacob H. Masliyah Graduate Award in Oil Sands Engineering, and the Gordon R. Finch Memorial Graduate Scholarship in Environmental Engineering.

In the end, I would like to express my heartfelt gratitude to my loving family, who had my back and supported me with no doubt all the time. The love and patience given by my family are my source of strength, faith, and motivation. All my accomplishments are dedicated to them.

# TABLE OF CONTENTS

ABSTRACT.....	ii
PREFACE.....	v
DEDICATION.....	vii
ACKNOWLEDGEMENTS .....	viii
TABLE OF CONTENTS.....	x
LIST OF TABLES .....	xv
LIST OF FIGURES.....	xvii
LIST OF ABBREVIATIONS .....	xxi
CHAPTER 1: GENERAL INTRODUCTION AND RESEARCH OBJECTIVES.....	1
1.1 Background.....	1
1.1.1 Oil sands process water.....	1
1.1.2 Naphthenic acids.....	2
1.1.3 Treatment methods for OSPW remediation.....	4
1.1.4 Advanced oxidation processes (AOPs).....	5
1.1.5 Photocatalysis as advanced water treatment.....	7
1.1.6 Biochar-supported photocatalysts .....	9
1.1.7 Waste materials with potential for wastewater remediation .....	12
1.2 Research significance and hypotheses .....	16
1.3 Research objectives.....	19
1.4 Thesis organization.....	21

CHAPTER 2: Treatment of oil sands process water using petroleum coke: Field pilot.....	38
2.1 Introduction .....	38
2.2 Materials and Methods .....	40
2.2.1 Pilot program.....	40
2.2.2 Experimental methods.....	43
2.2.2.1 OSPW sampling.....	43
2.2.2.2 Water analyses .....	43
2.2.2.3 Toxicology.....	44
2.3 Results and discussion .....	44
2.3.1 Cell and tank performance.....	44
2.3.2 Removal of organic compounds.....	45
2.3.2.1 AEF and DOC.....	45
2.3.2.2 TPH and Phenols .....	52
2.3.2.3 Polycyclic aromatic hydrocarbons and volatile organic compounds.....	53
2.3.3 Removal of vanadium and changes in other trace element concentrations.....	54
2.3.4 Change in major ions, conductivity, total suspended solids and pH .....	58
2.3.5 Toxicity.....	60
2.4 Conclusions .....	62
2.5 References .....	64

## CHAPTER 3: Adsorption Assessment of Naphthenic Acids on Different Reclamation Materials:

Coarse Sand Tailings and Peat Mineral Mix. ....	72
3.1 Introduction .....	72
3.2 Materials and methods.....	76
3.2.1 Reagents.....	76
3.2.2 Material preparation.....	76
3.2.3 Characterization of materials .....	77
3.2.4 Adsorption experiments.....	77
3.3 Results and discussions.....	80
3.3.1 Material characterization .....	80
3.3.1.1 Physicochemical properties .....	80
3.3.1.2 SEM and EDX analysis.....	81
3.3.1.3 FTIR and XRD analysis .....	83
3.3.2 Single NA model compound adsorption.....	87
3.3.2.1 Kinetics study .....	87
3.3.2.2 Isotherm study .....	89
3.3.3 Adsorption behavior towards NAs model compound mixture solution .....	91
3.3.4 Mechanism insight.....	94
3.4 Conclusions .....	97
3.5 References .....	98

CHAPTER 4: Efficient Degradation of Naphthenic Acids in Water Using a Sustainable Engineered Biochar/ZnO Composite Under Solar Light.....	111
4.1 Introduction .....	111
4.2 Materials and methods.....	114
4.2.1 Material and reagents.....	114
4.2.2 Experimental methods.....	115
4.2.2.1 Synthesis of BC and BC/ZnO.....	115
4.2.2.2 Characterization of BC/ZnO.....	116
4.2.3 Photocatalytic degradation experiments .....	117
4.2.4 Reactive oxygen species (ROS) and reusability tests .....	118
4.2.5 Performance of the BC/ZnO in the degradation of a mixture of NAs.....	118
4.2.6 Analytical methods .....	120
4.3 Results and discussions.....	120
4.3.1 Characterization of BC/ZnO.....	120
4.3.1.1 SEM and EDX analysis.....	120
4.3.1.2 XRD and XPS analysis.....	121
4.3.1.3 Optical properties.....	124
4.3.2 Effect of ZnO content and catalyst dosage on CHA degradation .....	127
4.3.3 ROS and possible mechanism of BC/ZnO under solar irradiation.....	132
4.3.4 Reusability of BC/ZnO.....	135

4.3.5 Degradation performance of BC/30%ZnO towards NAs mixture .....	137
4.3.6 Leaching test.....	141
4.4 Conclusions and future perspectives.....	142
4.5 References .....	143
CHAPTER 5. GENERAL CONCLUSIONS AND RECOMMENDATIONS.....	151
5.1 Thesis overview .....	151
5.2 Conclusions .....	153
5.3 Recommendations for future studies.....	157
BIBLIOGRAPHY .....	160
APPENDIX A.....	187
APPENDIX B.....	209
APPENDIX C .....	220

## LIST OF TABLES

Table 2.1: PSO kinetics coefficient for AEF.....	50
Table 2.2: Results of toxicity evaluation. ....	61
Table 3.1: The name, formula, molecular weight and structure of selected model compounds...	79
Table 3.2: Physicochemical properties of CST and PMM. ....	81
Table 3.3: Kinetics models and parameters for DDA adsorption by CST and PMM. ....	89
Table 4.1: NAs models investigated in this study.....	119
Table 4.2: PFO kinetics parameters of BC/30%ZnO composite. ....	132
Table S1: Summary of OSPW samples collected and sample locations. ....	195
Table S2: Analytical methods used. ....	196
Tables S3: General water chemistry of OSPW .....	197
Table S3 (a): General water chemistry – OSPW prior to treatment.....	197
Table S3 (b): General water chemistry – OSPW treatment after R1.....	197
Table S3 (c): General water chemistry – Treated OSPW after Reactor 2 (cells). ....	198
Table S3 (d): General water chemistry – Treated OSPW after Reactor 2 (tanks). ....	198
Tables S4: Trace Elements (Dissolved) in OSPW.....	199
Table S4 (a): Trace Elements (Dissolved) – OSPW prior to Treatment.....	199
Table S4 (b): Trace Elements (Dissolved) – OSPW Treatment after Reactor 1.....	199
Table S4 (c): Trace Elements (Dissolved) – OSPW Treatment after Reactor 2 (cells).....	200
Table S4 (d): Trace Elements (Dissolved) – OSPW Treatment after Reactor 2 (tanks). ....	200
Tables S5: PAH concentrations in OSPW .....	201
Table S5 (a): PAH concentrations in OSPW (pre-treatment).....	201
Table S5 (b): PAH concentrations after R1.....	202

Table S5 (c): PAH concentrations in OSPW after R2 (cells). .....	203
Table S5 (d): PAH concentrations in OSPW after R2 (tanks). .....	204
Tables S6: VOC concentration in OSPW .....	205
Table S6 (a): VOC concentrations in OSPW (pre-treatment).....	205
Table S6 (b): VOC concentrations in OSPW after R1.....	206
Table S6 (c): VOC concentrations in OSPW after R2 (cells).....	207
Table S6 (d): VOC concentrations in OSPW after R2 (tanks). .....	208
Table S7: The parameters of UPLC-MS analysis of each NA compound.....	219
Table S8: Comparison of kinetics for different NAs sorption on CST.....	219
Table S9: Compound-dependent parameters in LC-QQQMS analysis.....	221

## LIST OF FIGURES

Figure 2.1: Two earthen containment cells (~600 m <sup>3</sup> each, Cell A, Cell B) and two steel tanks (~60 m <sup>3</sup> each, Tank A and Tank B) that acted as water treatment units. ....	41
Figure 2.2: Acid extractable fraction (AEF) and dissolved organic carbon (DOC) concentrations in OSPW and after R1 and R2 (residence time: 4 weeks). ....	46
Figure 2.3: Comparison of (a) AEF concentration and (b) DOC concentration in OSPW for residence time up to week 17. ....	47
Figure 2.4: Correlation of AEF and DOC by % removal.....	49
Figure 2.5: PSO model for the adsorption of AEF in OSPW treated by PC in Cell A and Tank A. ....	50
Figure 2.6: Vanadium concentrations upon exit from Cell A and Tank A with time. ....	55
Figure 3.1: Scheme for the source of the CST and PMM. ....	76
Figure 3.2: SEM images of CST (a) and (b); PMM (c) and (d).....	82
Figure 3.3: FTIR results of CST (a) and PMM (b).....	84
Figure 3.4: XRD results of CST (a) and PMM (b).....	86
Figure 3.5: Kinetics of DDA adsorption by CST (a) and PMM (b).....	88
Figure 3.6: The linearized Freundlich models for DDA adsorption by CST (a) and PMM (b)....	90
Figure 3.7: NAs mixture adsorption (a) by CST (b) by PMM. ....	93
Figure 3.8: NAs mixture adsorption capacity (a) by CST (b) by PMM.....	94
Figure 3.9: Possible adsorption mechanism.....	97
Figure 4.1: The scheme of the synthesis steps of BC/ZnO composites. ....	115
Figure 4.2: Setup of the photocatalytic experiments using BC/ZnO composites. ....	117
Figure 4.3: SEM images of the BC/30%ZnO composite.....	121

Figure 4.4: XRD results of the BC/30%ZnO composite. ....	122
Figure 4.5: (a) XPS survey scan spectrum of the BC/30%ZnO composite and high-resolution XPS spectra of (b) C 1s (c) O 1s and (d) Zn 2p. ....	124
Figure 4.6 (a) PL spectrum; (b) UV-vis DRA reflectance; (c) Absorbance response plot spectrum of the BC/30%ZnO composite and Syn-ZnO; Tauc plot of (d) BC/30%ZnO and (e) Syn-ZnO were obtained with diffusion reflectance spectroscopy.....	127
Figure 4.7: Dark adsorption control of (a) BC; (b) Syn-ZnO; and (c) BC/ZnO composite; and (d) CHA photolysis control. The dosage of BC, Syn-ZnO, and BC/ZnO is 0.5 g/L. $[CHA]_0 = 25$ mg/L. ....	129
Figure 4.8: CHA degradation using different BC/ZnO composites under solar irradiation: (a) $C/C_0$ vs. Time; (b) Comparison of different content of ZnO.....	130
Figure 4.9: CHA degradation using different dosages of BC/30%ZnO under solar irradiation: (a) $C/C_0$ vs. Time; (b) Comparison on solar irradiation time. ....	131
Figure 4.10: CHA degradation using same ZnO content of the BC/30%ZnO composite and Syn-ZnO. ....	131
Figure 4.11: EPR spectra using (a) DMPO; (b) BMPO, and (c) TEMP as trapping agents.....	134
Figure 4.12: Schematic representation of photocatalytic mechanism for the degradation of NAs using BC/ZnO composite under solar irradiation.....	135
Figure 4.13: Reusability tests for the BC/30%ZnO composite. ....	136
Figure 4.14: SEM images of BC/30%ZnO after 4 cycles of use.....	137
Figure 4.15: Control experiment: photodegradation of the NAs in the mixture in the absence of the composite.....	138

Figure 4.16: Simultaneous degradation of a mixture of NAs using the BC/30%ZnO composite under solar irradiation: (a) $C/C_0$ vs. Time; (b) Degradation efficiency of different NAs after 2, 4, and 6 h solar irradiation; (c) PFO rate constants of different NAs. ....	139
Figure S1: (a) Field pilot study sample locations; (b) Under-drain system prior to PC deposition: Cells and Tanks; (c) Tanks on pad being filled with PC/OSPW slurry; d) Top view Tank B showing Tee-distributor (10”) and under-drain manifold (insets).....	191
Figure S2: PSO model for the adsorption of AEF in OSPW treated by PC in different R2 reactors. ....	192
Figure S3: Change in TPH concentrations for different reactors at different residence times. .	192
Figure S4: Average phenol concentration in source OSPW and in OSPW after treatment by R1, R2 cells, and R2 tanks over the entire sampling period (OSPW-4 weeks, R1-4weeks, R2 cells - 59 weeks, R2 tanks – 55 weeks).....	193
Figure S5: Polycyclic aromatic hydrocarbons concentrations before and after treatment.....	194
Figure S6: Change in TSS concentrations for different reactors at different residence times....	195
Figure S7: The raw materials and well-prepared samples. ....	210
Figure S8: The scheme for the kinetics study. ....	211
Figure S9: EDX results of CST (a) and PMM (b).....	211
Figure S10: $C/C_0$ vs. contact time for DDA adsorption by CST(a), and PMM (b).....	211
Figure S11: Different kinetics models of DDA adsorption by CST: (a) PFO, (b) IPD, and (c) Elovich.....	212
Figure S12: Different kinetics models of DDA adsorption by PMM: (a) PFO, (b) PSO, and (c) Elovich.....	213
Figure S13: The linearized Langmuir models for DDA adsorption by CST (a) and PMM (b)..	214

Figure S14: DDA (a) and DA (b) adsorption PSO kinetics in mixture by CST.....	214
Figure S15: Adsorption kinetics (IPD model) in NAs mixture by PMM for DDA (a) DA (b), CHPA (c), and PVA (d).....	215
Figure S16: FITR spectra for CST (a) and PMM (b) before and after adsorption process.....	216
Figure S17: XRD results for CST (a) and PMM (b) before and after adsorption process.....	217
Figure S18: SEM results for CST (a, b) and PMM (c, d) after adsorption process.....	218
Figure S19: EDX results for CST (a) and PMM (b) after adsorption process.....	219

## LIST OF ABBREVIATIONS

1/n	Freundlich heterogeneity parameter
$^1\text{O}_2$	singlet oxygen
4-MHA	4-methylheptanoic acid
AC	activated carbon
AEF	acid extractable fraction
AOP	advanced oxidation processes
BC	biochar
BC/ZnO	biochar ZnO composite
BMPO	5-tert-butoxycarbonyl 5-methyl-1-pyrroline <i>N</i> -oxide
BSPs	biochar-supported photocatalysts
BTEX	benzene, toluene, ethyl benzene, and xylenes
$C_0$	initial concentration
CB	conduction band
CEC	cation exchange capacity
C-H, C-H <sub>2</sub> , C-H <sub>3</sub>	aliphatic groups
CHA	cyclohexanecarboxylic acid
CHPA	cyclohexanepentanoic acid
CST	coarse sand tailings
$C_t$	the concentration of the target NAs compound at time t
CX	carbon xerogel
DA	decanoic acid
DDA	dodecanoic acid
DMPO	5,5-dimethyl-1-pyrroline <i>N</i> -oxide
dMRM	dynamic multiple reaction monitoring
DOC	dissolved organic carbon
$e^-$	photogenerated electron
EC	electrical conductivity
EC	effective concentrations
EDX	energy-dispersive X-ray spectroscopy
EPR	electron paramagnetic resonance
ESI	electrospray ionization
FT-ICR-MS	Fourier transform ion cyclotron resonance mass spectrometry
FTIR	Fourier transform infrared spectrometry
FV	fragmentor voltage
GAC	granular activated carbon
$h^+$	hole
H <sub>2</sub> O <sub>2</sub>	hydrogen peroxide
HA	hexanoic acid
HDPE	high density polyethylene
IA	isonipecotic acid
IC	inhibitory concentrations
ICP-OES	inductively coupled plasma-optical emission spectroscopy
IMS	ion mobility spectrometry
IPD	intra-particle diffusion

k	rate constant
$K_F$	Freundlich adsorption coefficient
$K_L$	Langmuir rate constant
LC	lethal concentrations
MBR	membrane bioreactor
$Na_2CO_3$	anhydrous sodium carbonate
$NaHCO_3$	sodium bicarbonate
NAs	naphthenic acids
$O_2$	molecular oxygen
$O_2^{\bullet-}$	superoxide radicals
ODT/yr	oven-dry tonnes per year
$\bullet OH$	hydroxyl radical
$O_L$	oxygen lattice
OSPW	oil sands process water
$O_v$	oxygen vacancies
Oxy-NAs	oxidized naphthenic acids
PAHs	polycyclic aromatic hydrocarbons
PC	petroleum coke
PFO	pseudo-first order
PL	photoluminescence spectroscopy
PMM	peat-mineral mix
PSO	pseudo-second order
PVA	5-phenylvaleric acid
PZC	point of zero charge
$q_e$	equilibrium adsorption capacity
QQMS	triple quadrupole mass spectrometer
$q_t$	adsorption capacity at time t
R1, R2, and R3	reactor 1, reactor 2, and reactor 3
$R^2$	correlation coefficient
$ROO\bullet$	organic peroxy radicals
ROS	reactive oxygen species
SEM	scanning electron microscopy
$SO_4^{\bullet-}$	sulfate radicals
SQMS	single quadrupole mass spectrometry
Syn-ZnO	synthesized ZnO
T-2H-T4CA	tetrahydro-2H-thiopyran-4-carboxylic acid
T4CA	tetrahydropyran-4-carboxylic acid
TDS	total dissolved solids
TEMP	2,2,6,6-tetramethylpiperidine
TOC	total organic carbon
TPH	total petroleum hydrocarbons
TSS	total suspended solids
UHPLC	ultra-high performance liquid chromatography
UPLC-TOF-MS	ultra-performance liquid chromatography time-of-flight mass spectrometry
UV-Vis DRS	ultraviolet-visible diffused reflectance spectroscopy

V	volume of the solution
VB	valence band
VOCs	volatile organic compounds
XPS	X-ray photoelectron spectroscopy
XRD	X-ray diffraction
ZnO	zinc oxide
$\alpha$	initial sorption rate
$\beta$	desorption constant

# **CHAPTER 1: GENERAL INTRODUCTION AND RESEARCH OBJECTIVES**

## **1.1 Background**

### **1.1.1 Oil sands process water**

Canada owns the third largest oil reserve in the world, and more than 166 billion barrels of crude oil are contained in the oil sands spread in Northern Alberta, which accounts for more than 95% of the total reserves of the country (NRCAN 2020). Oil sands are composed of approximately 85% mineral solids, 10% bitumen, and 5% water (Allen 2008a; Zubot et al. 2012). Due to the high content of mineral solids, the Clark caustic hot water extraction process has been widely applied by oil sands companies as a bitumen extraction technique. During the extraction process, every barrel of bitumen consumes about 0.2 to 2.6 barrels of fresh water, resulting in a large volume production of oil sands process water (OSPW) (Canada 2020). OSPW is a complex saline mixture solution that may contain at varied concentrations, suspended solids, heavy metals, inorganic compounds, and organic compounds, including some recalcitrant contaminants such as naphthenic acid (NAs), total petroleum hydrocarbons (TPH), polycyclic aromatic hydrocarbons (PAHs), trace elements, BTEX components (benzene, toluene, ethyl benzene, and xylenes), and phenols (Allen 2008a; Gamal El-Din et al. 2011).

Since 1967, when Suncor Energy Ltd. Began operating the first commercial oil sands project, there has been no operational releases of OSPW to the environment. In this case, and in accordance with Alberta's zero discharge approach requirement, OSPW is stored in on-site tailings ponds, which poses significant challenges due to its continuous accumulation (Allen 2008a). For

instance, fluid tailings increased by about 29% in volume in the Athabasca oil sands region since 2015 and reached 1.39 billion m<sup>3</sup> in 2022 (Alberta Energy Regulator 2023). Therefore, it is necessary to develop new approaches for the treatment of OSPW that the industry can adopt to ensure the safe release of treated OSPW and protect the downstream environment.

### 1.1.2 Naphthenic acids

Naphthenic acids (NAs) are broadly recognized as a family of saturated aliphatic and alicyclic carboxylic acids that are naturally present in the oil sands in Northern Alberta and other oil reserves (Quinlan and Tam 2015). During the bitumen extraction process, NAs are concentrated in the OSPW. NAs are generally represented by the formula  $C_nH_{2n+z}O_x$ , in which “n” means the carbon number ( $7 \leq n \leq 26$ ), “z” indicates the hydrogen deficiency due to the formation of ring or double bond structures (even integer,  $0 \leq -Z \leq 18$ ), and “x” means the oxygen number (typically  $2 \leq x \leq 6$ ) (Huang et al. 2018). Classical NAs contain an oxygen number equal to 2 in their chemical structures, and the oxidized NAs (Oxy-NAs) have an oxygen number ranging from 3 to 6. In addition, heteroatomic NAs could be represented by  $C_nH_{2n+z}SO_x$  and  $C_nH_{2n+z}NO_x$  for NAs containing sulfur and nitrogen atoms, respectively (Huang et al. 2018).

The quantification of NAs can be conducted by several analytical techniques, including ultra-performance liquid chromatography time-of-flight mass spectrometry (UPLC-TOF-MS), Fourier transform ion cyclotron resonance mass spectrometry (FT-ICR-MS), and ion mobility spectrometry (IMS) (Sun et al. 2014). Grewer et al. (2010) indicated that classical and Oxy-NAs account for more than 50% of the total organic components in studied OSPW. In addition, Nyakas et al. (2013) characterized a typical OSPW using FT-ICR-MS, revealing a composition of 64% classical and oxy-NAs, 23% sulfur-containing NAs, and 8% nitrogen-containing NAs. Suara et al.

(2022a) reported that classical NAs were up to 55% of the total NAs in the studied OSPW, while Huang et al. (2021) found that classical NAs were 40% of total NAs and the remaining 60% were reported to be oxy-NAs. Over the years, most studies have focused on the classical and oxy-NAs removal, however, studies on the degradation of heteroatomic NAs are also indispensable in OSPW (Meng et al. 2021).

The presence of NAs in OSPW has brought increasing environmental and process-related concerns. For example, NAs were reported as one of the main reasons that could cause the corrosion problems of the plant infrastructure (Fan 1991; Quinlan and Tam 2015). More importantly, several studies have pointed out that NAs have acute and chronic toxicity to aquatic and mammalian species (Clemente and Fedorak 2005; Frank et al. 2009; Hagen et al. 2013; Li et al. 2017; MacKinnon and Boerger 1986). Scarlett et al. (2013) studied the acute toxicity of NAs to zebrafish larvae. Their findings revealed that zebrafish larvae exposed to OSPW fractions containing classical NAs exhibited a 96h-LC<sub>50</sub> of 13.1 mg/L, while those exposed to OSPW fractions containing aromatic NAs had a result of 8.1 mg/L. These results suggested that the toxicity of OSPW is depended on the composition and structure of NAs. Furthermore, some aromatic NAs have a similar structure as estrogens, resulting in endocrine disruptive effects on fish (Rowland et al. 2011; Scarlett et al. 2012; Wang et al. 2015b). Moreover, it was reported that the diverse bone marrow-derived macrophage functions and the expression of many pro-inflammatory cytokine and chemokine genes in the liver of mice could be affected by the dissolved organics in OSPW (Garcia-Garcia et al. 2011). Consequentially, the removal of NAs is a crucial task for the remediation of OSPW.

### 1.1.3 Treatment methods for OSPW remediation

The studies of OSPW initially focused on solid-liquid separation aimed at enhancing tailings settling rates and process water recovery (Allen 2008b). With the increasing concerns about the environmental risks of OSPW, effective treatment methods are needed for the safe release of OSPW. The remediation methods for OSPW are based on physical, chemical, and biological techniques. Adsorption has been recognized as one of the most common physical methods that could effectively remove organic compounds from OSPW, which includes NAs and acid extractable fraction (AEF) (Pourrezaei et al. 2014b; Zubot et al. 2012).

Currently, several bench-scale studies have investigated the effectiveness of the adsorption process towards OSPW and have provided various alternatives as adsorbent materials, such as activated carbon (AC) (Islam et al. 2015; Islam et al. 2018), petroleum coke (PC) (Gamal El-Din et al. 2011; Pourrezaei et al. 2014a; Pourrezaei et al. 2014b; Zubot et al. 2012), carbon xerogel (CX) (Benally et al. 2019; Rashed et al. 2020), and biochar (Bhuiyan et al. 2017; Frankel et al. 2016). For example, Islam et al. (2018) studied the isotherm and kinetics of the adsorption process towards raw OSPW by granular activated carbon (GAC) (0.4 g/L in 24 h of treatment), which resulted in the adsorption capacity of 60 mg/g. Benally et al. (2019) reported that the adsorption by CX of OSPW achieved 88.8% removal of classical NAs but only 6% removal of AEF. Using PC as an adsorbent, Gamal El-Din et al. (2011) found that the AEF concentration in OSPW was reduced from 63 mg/L to 5.7 mg/L.

Natural materials have been studied by many other researchers as potential adsorbents to remove organic contaminants (e.g., NAs, toluene, etc.) and heavy metal ions (e.g., Cd, Zn, Pb, Cu, etc.) (Arthur et al. 2017; Janfada et al. 2006; Li et al. 2020; Lim and Lee 2015; Peng et al. 2002;

Rao et al. 2020; Smaranda et al. 2017). For instance, Janfada et al. (2006) observed a strong and selective adsorption of OSPW-derived NAs on soil. Lim and Lee (2015) also reported that soil can be applied as a feasible, low-cost, and naturally abundant adsorbent to remove Zn (II), Pb (II), and Cu (II) from wastewater. Based on previous studies, adsorption is a promising treatment method for the remediation of OSPW; however, the feasibility and effectiveness of these natural adsorbents need to be investigated in larger-scale applications, such as column tests or pilot scale studies.

Other remediation methods for OSPW have been developed and studied with various techniques, which include advanced oxidation processes (AOPs) (Abdalahman et al. 2019; Abdalahman 2019; Anderson et al. 2012; Fang et al. 2019; Fang et al. 2020; Gamal El-Din et al. 2011; Islam et al. 2014b; Klamerth et al. 2015; Martin et al. 2010; Meng et al. 2021; Meshref et al. 2017; Qin et al. 2019; Shu et al. 2014; Song et al. 2022), coagulation and flocculation (Pourrezaei et al. 2011; Wang et al. 2015a), biofiltration (Zhang et al. 2018a, 2019; Zhang et al. 2020), biofilm reactors (Islam et al. 2015; Islam et al. 2014a; Islam et al. 2014b), and anoxic aerobic membrane bioreactor (MBR) (Huang et al. 2017; Xue et al. 2016; Zhang et al. 2016a, 2018b).

#### 1.1.4 Advanced oxidation processes (AOPs)

In the 1980s, AOPs were initially introduced for drinking water treatment, but their application was expanded to include the treatment of various types of wastewaters (Deng and Zhao 2015). AOPs are characterized by the *in-situ* production of reactive oxygen species (ROS), including hydrogen peroxide ( $H_2O_2$ ), ozone ( $O_3$ ), and hydroxyl ( $\cdot OH$ ), superoxide ( $O_2^{\cdot-}$ ), and sulfate ( $SO_4^{\cdot-}$ ) radicals, resulting in the efficient elimination of recalcitrant organic pollutants (Ong et al. 2018).

Among these radicals,  $\cdot\text{OH}$  is one of the most reactive and powerful oxidizing agent in the water treatment process, with an oxidation potential ( $E^0$ ) between 2.8 V (pH = 0) and 1.95 V (pH = 14) (Deng and Zhao 2015). As a non-selective ROS,  $\cdot\text{OH}$  can rapidly react with numerous species with rate constants of  $10^8$  to  $10^{10} \text{ M}^{-1} \text{ s}^{-1}$  (Deng and Zhao 2015). The four basic pathways for  $\cdot\text{OH}$  oxidizing organic contaminants include radical addition, hydrogen abstraction, electron transfer, and radical combination (Solarchem Environmental 1994). The reaction between  $\cdot\text{OH}$  and the targeted organic compounds can generate carbon-centered radicals in the form of  $\text{R}\cdot$  or  $\text{R}\cdot\text{-OH}$ , and then these radicals may be transformed into organic peroxy radicals ( $\text{ROO}\cdot$ ) in the presence of molecular oxygen ( $\text{O}_2$ ). All the produced radicals undergo further reactions accompanied by the formation of more reactive species such as  $\text{H}_2\text{O}_2$  and  $\text{O}_2^{\cdot-}$ , consequently leading to the degradation and mineralization of the targeted organic contaminants (Deng and Zhao 2015).  $\cdot\text{OH}$  can be only *in-situ* generated from different technologies, including UV radiation or ultrasound, the combination of oxidizing agents such as ozone and  $\text{H}_2\text{O}_2$ , and the use of catalysts such as  $\text{Fe}^{2+}$  (Huang et al. 1993).

So far, the great potential of AOPs for the treatment of OSPW has been proved by various studies, for instance, ozonation (Pérez-Estrada et al. 2011; Qin et al. 2020), sulfate radical-based AOPs (Arslan et al. 2023), Fenton-related process (Zhang et al. 2016b), ferrate (VI) oxidation (Wang et al. 2016), UV-based processes (Fang et al. 2020), among others. Pérez-Estrada et al. (2011) reported that ozonation achieved effective degradation of NAs with multiple rings and alkyl branching, and the degradation rate improved while the pH increased. Wang et al. (2016) performed a study of ferrate oxidation with the dosage of Fe (VI) as 200 and 400 mg/L and achieved 64.0% and 78.4% removal of NAs, respectively, while the preferential removal of NAs

with high carbon number and ring number was observed. Besides, Zhang et al. (2016b) applied the UV-Fenton process at natural pH with the presence of chelating agents (nitrilotriacetic acid), while the removal rates for classical NAs, mono-oxidized and di-oxidized NAs were reported as 98.4%, 86.0%, and 81.0%, respectively. Nevertheless, significant challenges hinder the practical implementation of these AOPs, mainly due to the high operating costs associated with energy consumption and chemical inputs (Miklos et al. 2018).

#### 1.1.5 Photocatalysis as advanced water treatment

Solar energy has attracted increasing noteworthy research interests since it has been regarded as an unlimited, pollution-free, and renewable green energy source (Ahmad et al. 2023). Since photocatalysis can utilize renewable solar energy and eco-friendly materials, it has been regarded as a sustainable route to overcome environmental and energy issues (Ahmad et al. 2023). Particularly, with the increasing research interest in photocatalysis, various semiconductors have been developed as promising materials in several applications, including water treatment (Yang et al. 2019). According to Wang et al. (2014), the fundamental mechanisms of semiconductor-based photocatalysis could be described as follow: the photocatalytic reactions are initiated when photons with energies larger than that of the band gap of the material reach the surface of the photocatalyst, exciting the photogenerated electron ( $e^-$ ) from the valence band (VB) to the conduction band (CB) while producing a positive hole ( $h^+$ ) on the surfaces of the particles, then, with simultaneous dissipation of heat or light energy, the recombination of the  $e^-$  and  $h^+$  could decrease the photocatalysis efficiency. The  $e^-$ - $h^+$  pairs act as oxidant and reductant to react with electron acceptors and donors absorbed on the surface of the semiconductor. Meantime,  $\cdot\text{OH}$  could be formed by the reaction of the  $h^+$  with  $\text{OH}^-$ . The presence of  $\text{O}_2$  could also act as an electron

scavenger to prolong the recombination of the photoinduced  $e^-h^+$  pairs and produce the  $O_2^{\cdot-}$  simultaneously.

The heterogeneous photocatalytic treatment of wastewater employs various semiconductor catalysts, such as titanium dioxide ( $TiO_2$ ), zinc oxide (ZnO), iron (III) oxide ( $Fe_2O_3$ ), etc. (Ibhadon and Fitzpatrick 2013; Wang et al. 2022). Among those semiconductors,  $TiO_2$  has been the most studied photocatalyst in the past decade owing to its relatively low production cost and good chemical stability. Leshuk et al. (2016) reported that the concentration of AEF of target OSPW was significantly decreased by the photocatalysis process using  $TiO_2$ , while also effectively reducing the acute toxicity toward the bacteria *Vibrio fischeri*.  $TiO_2$  has been also reported for the oxidative decomposition of NAs (de Oliveira Livera et al. 2018). However, due to its wide band gap (3.2 eV),  $TiO_2$  usually requires UV excitation, which only covers about 4% of the natural solar spectrum (Wu et al. 2013).

ZnO is considered a prominent photocatalyst candidate for photodegradation due to its non-toxic properties and more light absorption capacity under solar radiation than  $TiO_2$  (Ong et al. 2018). In addition, the production cost of ZnO is up to 75% lower than that of  $TiO_2$  (Liang et al. 2012). Similar to  $TiO_2$ , ZnO has excellent electrical, mechanical, and optical characteristics, and it also possesses antifouling and antibacterial properties (Ong et al. 2018). Herrmann (1999) indicated the main steps of the heterogeneous photocatalytic oxidation process by ZnO particles as follows: 1) organic contaminants diffuse from the liquid phase to the surface of ZnO particles; 2) adsorption of the targeted pollutants on the surface of ZnO particles; 3) oxidation and reduction reactions occur in the adsorbed phase; 4) desorption of the by-products and 5) removal of the by-products from the interface region. Regarding the application of ZnO for the treatment of OSPW,

Suara et al. (2022b) successfully applied 1 g/L commercial ZnO particles under 4 h of simulated solar irradiation, resulting in more than 99% removal of total NAs.

Despite this, ZnO has some specified drawbacks as photocatalyst. For instance, due to the broad band gap (3.37 eV) and high exciton binding energy (60 meV), it is also difficult to be excited by visible light (Cai et al. 2022). Additionally, the photocorrosion effect and the high rate of photogenerated  $e^-h^+$  pairs recombination constrained the commercialization of ZnO as a suitable photocatalyst for solar-driven water treatment (Mohamed et al. 2023; Yang et al. 2019). Furthermore, there are concerns about the leaching potential of zinc to the environment and the difficulties in collecting and recycling the catalysts from the reaction mixture. In this sense, new strategies have recently been investigated to overcome these problems.

#### 1.1.6 Biochar-supported photocatalysts

Despite the advantages of semiconductor photocatalysts, the quick recombination rate of the photogenerated  $e^-h^+$  pairs and poor visible-light response are still their main limitations (Cui et al. 2020). During the past decade, a variety of strategies have been developed to boost the photocatalytic efficiencies of photocatalysts from several aspects, including enhancing the utilization of solar energy, improving the separation and transportation rate of photoinduced  $e^-h^+$  pairs, or creating sufficient built-in potential for redox reactions. (Wang et al. 2014). For example, the coupling of semiconductors with other semiconductors, the deposition of metal to form semiconductor-metal heterojunctions, the forming of multicomponent heterojunctions, and the combination of semiconductors with carbon-based materials are some of the most promising alternatives (Ahmad et al. 2023; Wang et al. 2014).

Biochar (BC) is recognized as a sustainable carbon-rich material generated by biomass

pyrolysis in an environment with limited oxygen (Zhao et al. 2021). Biochar has numerous advantages, including its eco-friendly nature, high adsorption capacities, tunable structure, low cost for production, and availability in the natural environment, which make it a suitable option for various applications (Kahkeci and Gamal El-Din 2023). Generally, the ease of production and the wide range of feedstock sources for BC contributed to the establishment of local circular economy. Moreover, the physical and chemical properties of BC can be effectively tuned or modified through combinations with other materials, such as semiconductor photocatalysts. Embedding semiconductor particles on the surface of BC materials can produce hybrid heterogeneous photocatalysts, leveraging the combined advantages of BC and nano-metal oxides. These resulted composites exhibit enhanced dispersibility, higher stability, smaller crystallite size, and improved efficiency in the separation and transportation of  $e^-h^+$  pairs. This modification also contributes to lower energy requirements than unmodified materials (Kahkeci and Gamal El-Din 2023; Wang et al. 2019). All these enhanced properties of the biochar-supported photocatalysts (BSPs) result in the boosted photocatalytic degradation performance of target organic contaminants (Bhavani et al. 2022).

The common synthesis methods of BSPs generally include calcination, impregnation, ultra-sonication, hydrothermal, sol-gel, etc. The general synthesis steps are discussed in detail in several review studies in the literature (Bhavani et al. 2022; Cui et al. 2020; Kahkeci and Gamal El-Din 2023). Briefly, calcination is the simplest synthesis method for BSPs, and the general steps include: 1) preparation of photocatalyst nanoparticles; 2) mixing them with the biomass in solution and drying the mixture; 3) pyrolyzing the dried mixture to obtain the final BSPs. The impregnation method usually provides a high product yield and is also easy to handle, during which the biomass

feedstocks are impregnated with metal precursors to achieve the *in-situ* introduction of single metal atoms, precious elements, or metal oxides into BC structures after pyrolysis. In addition, the ultrasonication method is recognized as a cost-effective green pretreatment process that can reduce the loading of chemicals and reaction time. After sonication pretreatment, the solid precursors are collected, dried, and pyrolyzed for final composite products. The hydrothermal synthesis method is performed in autoclaves with high pressure. The mixture solution of BC and the catalyst precursors are placed inside the autoclave, followed by a thermal treatment process (up to 200 °C) for a certain time. The sol-gel method first needs to prepare a uniform mixture of the sol and the BC, followed by ageing to form a gel, and calcination with higher temperature is required as the final step to obtain BSPs. The specific synthesis procedures and corresponding parameters could be adjusted flexibly according to experimental requirements based on the abovementioned basic steps. For example, the thermal treatment process of the hydrothermal synthesis method could be applied to the mixture of biomass and photocatalyst precursors, and then a pyrolysis step would be added to gain the final BSPs.

BC plays a beneficial role in the final prepared composite. First of all, the BC with porous structure and heterogeneous surface can act as a good supporting material for the deposition and dispersion of nanoparticles, meanwhile, the subsequent functionalization strategies can help tune the surface structures of BC and introduce various surface functional groups, such as –OH, –COOH, or –NH<sub>2</sub>, to generate more dispositional sites (Bhavani et al. 2022). Mian and Liu (2018) and Shan et al. (2020) reported that the presence of BC can enhance the surface area and increase the number of active sites of the composite, as well as act as an electron reservoir to improve the transportation and separation efficiency of photoinduced  $e^-h^+$  pairs and reduce the band gap

energy. Besides, Kahkeci and Gamal El-Din (2023) indicated that loaded photocatalysts on BC surfaces can produce composites with greater adsorption capacities, higher chemical stability, and enhanced photocatalytic degradation compared to bare semiconductor photocatalysts. Cai et al. (2022) prepared a novel ZnO/Pic photocatalyst using pine as the biomass and achieved effective degradation of metronidazole under visible light irradiation. Gonçalves et al. (2022) synthesized ZnO/BC composites using biowaste from brewed coffee and chitosan as the feedstock, resulting in an enhanced photocatalytic performance for degrading phenol compared to the pristine ZnO. Although recent studies have proved the great potential of BC/ZnO composite as a photocatalyst, there still needs to be a research gap in assessing the effectiveness and feasibility of using the BC/ZnO composite for solar photocatalytic degradation of OSPW-related NAs.

#### 1.1.7 Waste materials with potential for wastewater remediation

The increasing amount of waste produced by increasing population and human activities leads to growing pressure on waste management worldwide. Waste prevention, recycling, reuse, and recovery are important steps for waste material management, which are also key strategies to help achieve sustainable development goals (Wan et al. 2019). Applying these strategies can help ease the burden on landfills, save energy and costs, and utilize resources effectively and sustainably (Wan et al. 2019). Moreover, according to the current situation of large waste production and the necessity for cost-effective wastewater treatment methods, a pragmatic shift is ongoing for waste material management and wastewater treatment technologies (Hossain et al. 2020). In recent years, the development of novel waste-derived materials for wastewater remediation has become an important research topic and gained increasing attention due to its great potential and eco-friendly nature, which can finally result in improvements in the circular economy (Hossain et al. 2020;

Rodríguez-Padrón et al. 2020). Therefore, various undervalued waste materials have joined the vision of researchers, and different waste-derived adsorbents or catalysts have been studied as eco-friendly alternatives for wastewater treatment.

Petroleum industries face the continuous accumulation problem of industrial waste materials and by-products (Pourrezaei et al. 2014b). For example, petroleum coke (PC) is a common residual of the oil refining process. Approximately 20 kg of PC are generated as by-product during the production of one barrel of synthetic crude oil (Zubot et al. 2012). Typically, the carbon content of the material exceeds 80 wt.% (Hyndman 1981). Rather than undervalued industrial by-products, PC can be considered as a potential adsorbent for OSPW treatment (Zubot et al. 2012). A previous bench-scale study had already shown that when a 19.9 wt% concentration of PC was used in short-term adsorption experiments, it achieved an 82% removal efficiency of NAs, as confirmed by UPLC/MS analysis. Additionally, the treated OSPW did not exhibit acute toxicity towards rainbow trout and *Vibrio fischeri* (Zubot et al. 2012). Another bench-scale study reported that a PC dose of approximately 22 wt% resulted in a 91% decrease of AEF (Gamal El-Din et al. 2011). Applying PC as an *in-situ* adsorbent for treating OSPW offers cost-saving benefits and the potential to repurpose PC from a residual material into a valuable resource. This approach can simultaneously address PC accumulation issues and toxicity concerns in OSPW (Pourrezaei et al. 2014b). Therefore, PC adsorption has great potential to be developed as a cost-effective and efficient treatment method for OSPW.

Coarse sand tailings (CST) are waste tailings materials from the oil sands industry. In the bitumen production process, large volumes of process water are required to produce a slurry that can be gravity-separated, during which the bitumen is recovered, and the coarse sand, fines, and

process water are left behind. The tailings streams are poured into the tailings ponds, where the coarse sands deposit to the bottom, and the water level rises, leading to higher tailings dams (Oil Sands Magazine 2021). The general use for CST materials in-field is to build up the dyke to support the tailings ponds (COSIA 2012). Tailings accumulation and land use have become two of the raising concerns of the oil sands industry. The potential contamination risk of the surrounding environment also increased the concern about whether the reclamation of the tailings waste can be achieved (Cossey et al. 2021; Jones and Forrest 2010). Therefore, the properties and adsorption behavior of OSPW-related contaminants by CST materials are essential information needed by the oil sands industries; however, related studies still need to be completed.

The surface mining process of oil sands is required to excavate the layer above the oil sand ores, which are the muskeg and overburden layers. During this process, the salvaged peat-mineral mixture (PMM) is generated by the removed layers and stored as a reclamation material (Speight 2013). Over the past research, different peat materials have been studied as possible effective adsorbents. Qin et al. (2006) found that the adsorption capacity on the same peat followed the order  $Pb > Cu > Cd$  in a single-solute system, correspondingly, the competitive adsorption phenomenon at low-energy adsorption sites was observed. However, the adsorption performance of PMM obtained from oil sands mining fields toward OSPW-related contaminants has been less reported. The characteristics and adsorption-related results for these reclamation materials are critical for helping the oil sands industry estimate the NAs transport in the environment. Moreover, developing other possible applications for CST and PMM is also essential for the industry.

On the other hand, large amounts of wood waste materials are widely generated by forestry industries, agricultural activities, and energy/food industries every year (Shaheen et al. 2019). It

has been reported by Barrette et al. (2018) that the average biomass of forest residues available after harvest is approximately  $26 \pm 16$  oven-dry tonnes per year (ODT/yr), meantime, for all forests managed in Canada, the total annual availability was 21 million (ODT/yr). Despite being reused as valuable biomass, most wood wastes are disposed directly at landfills, wasting precious land resources and leading to a large amount of greenhouse gas emissions (He et al. 2021). Wood waste-based biochar production could become a prospective way for processing large amounts of residual biomass from forestry (Boguta et al. 2019). In recent studies, researchers have shown great interest in the possibility of biochar applications due to its valuable structure and properties, such as the high porosity, large specific surface area, and high organic matter content (He et al. 2021; S and P 2019). Among various feedstock sources for biochar generation, wood-based biochar typically showed greater specific surface, larger pore volume, and more carbon content (Ippolito et al. 2020). Wood-based biochar has been developed as an effective adsorbent and activator, meanwhile, various modifications were applied to wood-based biochar for enhanced adsorption or catalytic capacity. Shaheen et al. (2019) summarized and concluded that wood-based biochar has great potential for removing potentially toxic elements from water and wastewater due to its high surface area, cation exchange capacity, aromatic character, and carbon content, among other properties. Zhu et al. (2019) prepared wood-based biochar by polar sawdust to active peroxydisulfate and achieved over 99.3% removal of Acid Orange after 14 min of reaction. Therefore, wood-based biochar and relative composite materials can be considered sustainable alternatives for OSPW remediation. Moreover, biochar produced from locally available wood waste could help pursue a “win-win” sustainable development by further promoting economically feasible waste management and environmental remediation at the same time.

## 1.2 Research significance and hypotheses

Adsorption and photodegradation are both considered effective treatments for OSPW remediation. However, developing feasible and cost-effective materials for OSPW remediation is still a crucial research topic. At the same time, large amounts of undervalued waste materials from industry, agriculture, or forestry raise serious environmental problems. Thus, this study focuses on developing and applying waste-derived materials, including petroleum coke, coarse sand tailings, peat-mineral mix, and wood waste-based biochar/ZnO composites, to remove or degrade OSPW-related contaminants and provides essential insights for future implementations in real OSPW treatment.

PC is an undervalued by-product of the fluid coking process, and it was proved to be an effective adsorbent for real OSPW reclamation under bench-scale in previous studies. However, a larger-scale study using PC as an adsorbent to treat real OSPW still needs to be explored. Moreover, the need for the water quality data of treated OSPW as a function of residence time in the PC deposit under natural climatic conditions is also challenging. As such, the treated OSPW quality needs to be assessed in detail. In this research, the first large-scale field pilot study that examined the feasibility and effectiveness of PC as an adsorbent for OSPW treatment was conducted. The adsorption performance by PC towards real OSPW was investigated accordingly.

Many studies indicate that different types of soils showed good adsorption performance for organic pollutants and heavy metals. However, reclamation materials like CST and PMM have yet to be investigated. To understand the transport of NAs in the natural environment, it is necessary to evaluate the adsorption behavior of NA from the aqueous phase on these two materials. The outcomes of this research should offer a better understanding of CST and PMM as reclamation

materials and provide insights into the possible application of these materials.

Biochar has been reported as a good supporting material for photocatalysts. Simultaneously, hardwood wastes are considered promising feedstocks for biochar production as waste materials from forestry residues. This study will use hardwood wastes from forest residue as low-cost biomass for biochar production. By using a simple pyrolysis method, hardwood waste-based biochar could be generated. In addition, biochar-based composite photocatalysts (BC/ZnO) could be applied to degrade NAs under solar light. Currently, the use of BC/ZnO composites towards the photocatalytic degradation of OSPW-related NAs remains a research gap. This study should combine the use of wood wastes as low-cost materials and solar light as a green energy source to develop an eco-friendly and highly efficient approach for the degradation of synthetic NAs. More importantly, the first study using BC/ZnO composite with solar light for the degradation of a complex mixture of NAs should be included as an important research section in this study, providing a proof of concept for further application into OSPW remediation.

The following hypotheses were tested in the corresponding studies.

### **Hypothesis 1 – Treatment of oil sands process water using petroleum coke: Field pilot**

- (1) Previous bench-scale results using PC as an adsorbent should be a reasonable basis to expect similar adsorption performance in pilot-scale experiments.
- (2) A substantial improvement in the quality of OSPW when mixed with a PC slurry at concentrations ranging from 10 to 25 wt% is expected. Specifically, the concentration of AEF and DOC should decrease after treatment.
- (3) The adsorption of AEF from OSPW onto PC is expected to follow a PSO kinetics model.

- (4) Following contact and drainage from PC deposits, changes in OSPW properties should reduce acute toxicity.
- (5) The cost-effectiveness and efficiency of PC adsorption as a treatment method for OSPW should be proved.

### **Hypothesis 2 – Adsorption Assessment of Naphthenic Acids on Different Types of Reclamation Materials: Coarse Sand Tailings and Peat Mineral Mix**

- (1) The removal of the target pollutant should be the result of the adsorption process onto different materials rather than microbial degradation.
- (2) The adsorption mechanism of the NA model compounds on CST and PMM should include both the hydrogen bonding and hydrophobic interaction.
- (3) The target NA model compound adsorption may follow a PSO.
- (4) The equilibrium adsorption data of the target NA model compound may be fitted to the Freundlich isotherm.
- (5) PMM material should be more effective for NAs removal due to its surface properties, including the functional groups, relatively larger specific surface area, and total pore volume compared to CST material.

### **Hypothesis 3 – Efficient Degradation of Naphthenic Acids in Water Using a Sustainable Engineered Biochar/ZnO Composite Under Solar Light**

- (1) Harwood waste-derived biochar should serve as an effective platform for the deposition and dispersion of ZnO particles.
- (2) The composite catalyst is expected to exhibit a cooperative catalytic mechanism during the degradation process, which will result in enhanced degradation performance of NAs.

- (3) The main ROS produced by the composite under solar light should be the  $\cdot\text{OH}$ .
- (4) The photocatalytic degradation of targeted NAs model compounds should follow a PFO kinetics.

### 1.3 Research objectives

In this study, different waste-derived materials, including PC, CST, PMM, and hardwood waste-based BC/ZnO composite, were developed and applied to assess their potential for the removal or degradation of the OSPW-related contaminants, aiming to provide efficient and cost-effective alternatives for OSPW remediation, as well as provide essential insights for further practical implementations. To achieve the goal of the study, the specific sub-objectives were developed and listed below:

#### **Specific objectives 1 – Treatment of oil sands process water using petroleum coke: Field pilot**

- (1) To investigate the reduction of total suspended solids (TSS) that result from filtering OSPW through the PC deposit.
- (2) To evaluate the water chemistry of the under-drained OSPW as a function of residence time within the PC deposit to quantify changes in constituent concentration of AEF, trace elements, parent and alkylated PAHs, volatile organic compounds (VOCs), major cations and anions, pH, total dissolved solids, phenols, TPH, and DOC.
- (3) To assess vanadium concentration in OSPW in contact with freshly produced PC and during storage within the coke deposit to quantify the removal efficiencies as a function of residence time.
- (4) To examine the acute toxicity of treated OSPW using standard commercial bioassays,

including Microtox™, Rainbow trout, *Daphnia magna*, and *Ceriodaphnia dubia*.

**Specific objectives 2 – Adsorption Assessment of Naphthenic Acids on Different Types of Reclamation Materials: Coarse Sand Tailings and Peat Mineral Mix**

- (1) To investigate the characteristics of CST and PMM to help understand the adsorption behaviour.
- (2) To study the adsorption kinetics and isotherm for the targeted NA model in the adsorption process.
- (3) To assess the adsorption performance towards different structured NAs in a mixture of CST and PMM.
- (4) To study the mechanisms for the adsorption process of NAs.

**Specific objectives 3 – Efficient Degradation of Naphthenic Acids in Water Using a Sustainable Engineered Biochar/ZnO Composite Under Solar Light**

- (1) To synthesize the BC/ZnO composites and characterize the composite with the best ZnO content.
- (2) To investigate the degradation kinetics of the NA model compound by BC/ZnO under solar radiation.
- (3) To identify the main reactive oxygen species involved in the photocatalytic degradation mechanism of the NA model compound.
- (4) To investigate the reusability of the BC/ZnO composite photocatalyst.

- (5) To evaluate the photocatalytic performance of the BC/ZnO composite to remove a mixture of different NAs.

## 1.4 Thesis organization

The thesis contains five logically organized chapters based on the above research objectives.

Chapter 1 provides a general introduction and background information on the research and the significance, hypotheses, objectives, and thesis organization. The background information contains a brief review of the OSPW, target contaminant (NAs), OSPW treatment methods, biochar-supported photocatalyst, and the waste materials related to this research.

Chapter 2 showcases the first large-scale field pilot study that examined the feasibility and effectiveness of PC, produced by a Fluid Coking Process, as an adsorbent for oil OSPW treatment. The pilot program consisted of an inline series of two reactors (pipeline reactor 1 and batch reactor 2) and lasted approximately 4 months. The quality of treated OSPW as a function of residence time in the PC deposit under natural climatic conditions was assessed by looking at changes in organic compounds (mainly focus on AEF and DOC), vanadium, and other trace element concentrations, major ions, conductivity, TSS, pH, and toxicity.

Chapter 3 presents the results of the study that investigated the adsorption behavior of NAs related to OSPW onto different reclamation materials from the oil sands industry. CST are waste tailings materials, and PMM is the general leftover material of the mining process, which are both readily available at the mining site. A single NA and a mixture solution containing several NAs were used as a working matrix in this study to evaluate the removal efficiency and adsorption performance. The mechanism of the adsorption process of NAs onto two different industrial

materials was conducted by kinetics and isotherm analysis and the properties investigation for materials before and after adsorption.

Chapter 4 shows the results of developing hardwood wastes-based biochar/ZnO composite for the degradation of NAs under solar irradiation. The BC/ZnO composites were synthesized using impregnant and pyrolysis methods and characterized to study morphology, chemical states, surface composition, and optical properties. A single model NA compound was used to study the best experimental conditions for the bench-scale study, meanwhile, the reusability and the degradation mechanism were also conducted. Additionally, the chapter contains the degradation performance of the selected composite towards a NAs mixture under solar irradiation and the Zn leaching potential of the composite.

Finally, Chapter 5 summarizes the general overview of the thesis and provides the major conclusions and key findings from the above studies. In addition, the future recommendations for further research were presented in the last section of the chapter.

## 1.5 References

- Abdalrhman, A.S., Zhang, Y., and Gamal El-Din, M. 2019. Electro-oxidation by graphite anode for naphthenic acids degradation, biodegradability enhancement and toxicity reduction. *Science of the Total Environment*, 671: 270-279.
- Abdalrhman, A.S.A. 2019. Application of Electro-oxidation for the Degradation of Organics in Oil Sands Process Water (OSPW). Thesis, University of Alberta.
- Ahmad, I., Zou, Y., Yan, J., Liu, Y., Shukrullah, S., Naz, M.Y., Hussain, H., Khan, W.Q., and Khalid, N.R. 2023. Semiconductor photocatalysts: A critical review highlighting the various

- strategies to boost the photocatalytic performances for diverse applications. *Advances in Colloid and Interface Science*, 311: 102830.
- Alberta Energy Regulator. 2023. State of Fluid Tailings Management for Mineable Oil Sands, 2022. Alberta Energy Regulator: Calgary, AB, Canada.
- Allen, E.W. 2008a. Process water treatment in Canada's oil sands industry: I. Target pollutants and treatment objectives. *Journal of Environmental Engineering and Science*, 7(2): 123-138.
- Allen, E.W. 2008b. Process water treatment in Canada's oil sands industry: II. A review of emerging technologies. *Journal of Environmental Engineering and Science*, 7(5): 499-524.
- Anderson, J., Wiseman, S., Wang, N., Moustafa, A., Perez-Estrada, L., Gamal El-Din, M., Martin, J., Liber, K., and Giesy, J.P. 2012. Effectiveness of ozonation treatment in eliminating toxicity of oil sands process-affected water to *Chironomus dilutus*. *Environmental science & technology*, 46(1): 486-493.
- Arslan, M., Ganiyu, S.O., Lillico, D.M.E., Stafford, J.L., and Gamal El-Din, M. 2023. Fate of dissolved organics and generated sulfate ions during biofiltration of oil sands process water pretreated with sulfate radical advanced oxidation process. *Chemical Engineering Journal*, 458: 141390.
- Barrette, J., Paré, D., Manka, F., Guindon, L., Bernier, P., and Titus, B. 2018. Forecasting the spatial distribution of logging residues across the Canadian managed forest. *Canadian Journal of Forest Research*, 48(12): 1470-1481.
- Benally, C., Messele, S.A., and Gamal El-Din, M. 2019. Adsorption of organic matter in oil sands process water (OSPW) by carbon xerogel. *Water research*, 154: 402-411.

- Bhavani, P., Hussain, M., and Park, Y.-K. 2022. Recent advancements on the sustainable biochar based semiconducting materials for photocatalytic applications: A state of the art review. *Journal of cleaner production*, 330: 129899.
- Bhuiyan, T.I., Tak, J.K., Sessarego, S., Harfield, D., and Hill, J.M. 2017. Adsorption of acid-extractable organics from oil sands process-affected water onto biomass-based biochar: Metal content matters. *Chemosphere*, 168: 1337-1344.
- Boguta, P., Sokołowska, Z., Skic, K., and Tomczyk, A. 2019. Chemically engineered biochar – Effect of concentration and type of modifier on sorption and structural properties of biochar from wood waste. *Fuel*, 256: 115893.
- Cai, H., Zhang, D., Ma, X., and Ma, Z. 2022. A novel ZnO/biochar composite catalysts for visible light degradation of metronidazole. *Separation and Purification Technology*, 288: 120633.
- Canada, N.R. 2020. Crude oil facts.
- Clemente, J.S., and Fedorak, P.M. 2005. A review of the occurrence, analyses, toxicity, and biodegradation of naphthenic acids. *Chemosphere*, 60(5): 585-600.
- COSIA. 2012. Guide for Fluid Fine Tailings Management. Online (Available from <https://cosia.ca/node/57>, accessed 23 May 2023).
- Cossey, H.L., Batycky, A.E., Kaminsky, H., and Ulrich, A.C. 2021. Geochemical stability of oil sands tailings in mine closure landforms. *Minerals*, 11(8): 830.
- Cui, J., Zhang, F., Li, H., Cui, J., Ren, Y., and Yu, X. 2020. Recent Progress in Biochar-Based Photocatalysts for Wastewater Treatment: Synthesis, Mechanisms, and Applications. *Applied Sciences* 10(3) [cited].

- de Oliveira Livera, D., Leshuk, T., Peru, K.M., Headley, J.V., and Gu, F. 2018. Structure-reactivity relationship of naphthenic acids in the photocatalytic degradation process. *Chemosphere*, 200: 180-190.
- Deng, Y., and Zhao, R. 2015. Advanced Oxidation Processes (AOPs) in Wastewater Treatment. *Current Pollution Reports*, 1(3): 167-176.
- Fan, T.P. 1991. Characterization of naphthenic acids in petroleum by fast atom bombardment mass spectrometry. *Energy & Fuels*, 5(3): 371-375.
- Fang, Z., Huang, R., Chelme-Ayala, P., Shi, Q., Xu, C., and Gamal El-Din, M. 2019. Comparison of UV/Persulfate and UV/H<sub>2</sub>O<sub>2</sub> for the removal of naphthenic acids and acute toxicity towards *Vibrio fischeri* from petroleum production process water. *Science of the Total Environment*, 694: 133686.
- Fang, Z., Huang, R., How, Z.T., Jiang, B., Chelme-Ayala, P., Shi, Q., Xu, C., and El-Din, M.G. 2020. Molecular transformation of dissolved organic matter in process water from oil and gas operation during UV/H<sub>2</sub>O<sub>2</sub>, UV/chlorine, and UV/persulfate processes. *Science of the Total Environment*, 730: 139072.
- Frank, R.A., Fischer, K., Kavanagh, R., Burnison, B.K., Arsenault, G., Headley, J.V., Peru, K.M., Kraak, G.V.D., and Solomon, K.R. 2009. Effect of Carboxylic Acid Content on the Acute Toxicity of Oil Sands Naphthenic Acids. *Environmental science & technology*, 43(2): 266-271.
- Frankel, M.L., Bhuiyan, T.I., Veksha, A., Demeter, M.A., Layzell, D.B., Helleur, R.J., Hill, J.M., and Turner, R.J. 2016. Removal and biodegradation of naphthenic acids by biochar and attached environmental biofilms in the presence of co-contaminating metals. *Bioresource technology*, 216: 352-361.

- Gamal El-Din, M., Fu, H., Wang, N., Chelme-Ayala, P., Pérez-Estrada, L., Drzewicz, P., Martin, J.W., Zubot, W., and Smith, D.W. 2011. Naphthenic acids speciation and removal during petroleum-coke adsorption and ozonation of oil sands process-affected water. *Science of the Total Environment*, 409(23): 5119-5125.
- Garcia-Garcia, E., Ge, J.Q., Oladiran, A., Montgomery, B., El-Din, M.G., Perez-Estrada, L.C., Stafford, J.L., Martin, J.W., and Belosevic, M. 2011. Ozone treatment ameliorates oil sands process water toxicity to the mammalian immune system. *Water research*, 45(18): 5849-5857.
- Gonçalves, N.P.F., Lourenço, M.A.O., Baleuri, S.R., Bianco, S., Jagdale, P., and Calza, P. 2022. Biochar waste-based ZnO materials as highly efficient photocatalysts for water treatment. *Journal of Environmental Chemical Engineering*, 10(2): 107256.
- Grewer, D.M., Young, R.F., Whittal, R.M., and Fedorak, P.M. 2010. Naphthenic acids and other acid-extractables in water samples from Alberta: what is being measured? *Science of the Total Environment*, 408(23): 5997-6010.
- Hagen, M.O., Katzenback, B.A., Islam, M.D.S., Gamal El-Din, M., and Belosevic, M. 2013. The Analysis of Goldfish (*Carassius auratus* L.) Innate Immune Responses After Acute and Subchronic Exposures to Oil Sands Process-Affected Water. *Toxicological Sciences*, 138(1): 59-68.
- He, M., Xu, Z., Sun, Y., Chan, P.S., Lui, I., and Tsang, D.C.W. 2021. Critical impacts of pyrolysis conditions and activation methods on application-oriented production of wood waste-derived biochar. *Bioresource technology*, 341: 125811.
- Herrmann, J.-M. 1999. Heterogeneous photocatalysis: fundamentals and applications to the removal of various types of aqueous pollutants. *Catalysis Today*, 53(1): 115-129.

- Hossain, N., Bhuiyan, M.A., Pramanik, B.K., Nizamuddin, S., and Griffin, G. 2020. Waste materials for wastewater treatment and waste adsorbents for biofuel and cement supplement applications: A critical review. *Journal of cleaner production*, 255: 120261.
- Huang, C., Shi, Y., Xue, J., Zhang, Y., Gamal El-Din, M., and Liu, Y. 2017. Comparison of biomass from integrated fixed-film activated sludge (IFAS), moving bed biofilm reactor (MBBR) and membrane bioreactor (MBR) treating recalcitrant organics: Importance of attached biomass. *Journal of hazardous materials*, 326: 120-129.
- Huang, C.P., Dong, C., and Tang, Z. 1993. Advanced chemical oxidation: Its present role and potential future in hazardous waste treatment. *Waste Management*, 13(5): 361-377.
- Huang, R., Yang, L., How, Z.T., Fang, Z., Bekele, A., Letinski, D.J., Redman, A.D., and Gamal El-Din, M. 2021. Characterization of raw and ozonated oil sands process water utilizing atmospheric pressure gas chromatography time-of-flight mass spectrometry combined with solid phase microextraction. *Chemosphere*, 266: 129017.
- Huang, R., Chen, Y., Meshref, M.N.A., Chelme-Ayala, P., Dong, S., Ibrahim, M.D., Wang, C., Klammerth, N., Hughes, S.A., Headley, J.V., Peru, K.M., Brown, C., Mahaffey, A., and Gamal El-Din, M. 2018. Characterization and determination of naphthenic acids species in oil sands process-affected water and groundwater from oil sands development area of Alberta, Canada. *Water research*, 128: 129-137.
- Hyndman, A.W. APPLICATION OF FLUID COKING TO UPGRADING OF ATHABASCA BITUMEN. *In* 1981. McGraw Hill., New York. pp. 645-647.
- Ibhadon, A.O., and Fitzpatrick, P. 2013. Heterogeneous Photocatalysis: Recent Advances and Applications. *Catalysts*, 3(1): 189-218.

- Ippolito, J.A., Cui, L., Kammann, C., Wrage-Mönnig, N., Estavillo, J.M., Fuertes-Mendizabal, T., Cayuela, M.L., Sigua, G., Novak, J., Spokas, K., and Borchard, N. 2020. Feedstock choice, pyrolysis temperature and type influence biochar characteristics: a comprehensive meta-data analysis review. *Biochar*, 2(4): 421-438.
- Islam, M.S., Zhang, Y., McPhedran, K.N., Liu, Y., and Gamal El-Din, M. 2015. Granular activated carbon for simultaneous adsorption and biodegradation of toxic oil sands process-affected water organic compounds. *Journal of environmental management*, 152: 49-57.
- Islam, M.S., McPhedran, K.N., Messele, S.A., Liu, Y., and Gamal El-Din, M. 2018. Isotherm and kinetic studies on adsorption of oil sands process-affected water organic compounds using granular activated carbon. *Chemosphere*, 202: 716-725.
- Islam, M.S., Dong, T., Sheng, Z., Zhang, Y., Liu, Y., and Gamal El-Din, M. 2014a. Microbial community structure and operational performance of a fluidized bed biofilm reactor treating oil sands process-affected water. *International biodeterioration & biodegradation*, 91: 111-118.
- Islam, M.S., Dong, T., McPhedran, K.N., Sheng, Z., Zhang, Y., Liu, Y., and Gamal El-Din, M. 2014b. Impact of ozonation pre-treatment of oil sands process-affected water on the operational performance of a GAC-fluidized bed biofilm reactor. *Biodegradation*, 25(6): 811-823.
- Janfada, A., Headley, J.V., Peru, K.M., and Barbour, S. 2006. A laboratory evaluation of the sorption of oil sands naphthenic acids on organic rich soils. *Journal of Environmental Science and Health, Part A*, 41(6): 985-997.
- Jones, R., and Forrest, D. 2010. *Oil Sands Mining Reclamation Challenge Dialogue—Report and Appendices*.

- Kahkeci, J., and Gamal El-Din, M. 2023. Biochar-supported photocatalysts: Performance optimization and applications in emerging contaminant removal from wastewater. *Chemical Engineering Journal*, 476: 146530.
- Klamerth, N., Moreira, J., Li, C., Singh, A., McPhedran, K.N., Chelme-Ayala, P., Belosevic, M., and Gamal El-Din, M. 2015. Effect of ozonation on the naphthenic acids' speciation and toxicity of pH-dependent organic extracts of oil sands process-affected water. *Science of the Total Environment*, 506: 66-75.
- Leshuk, T., Wong, T., Linley, S., Peru, K.M., Headley, J.V., and Gu, F. 2016. Solar photocatalytic degradation of naphthenic acids in oil sands process-affected water. *Chemosphere*, 144: 1854-1861.
- Li, C., Fu, L., Stafford, J., Belosevic, M., and Gamal El-Din, M. 2017. The toxicity of oil sands process-affected water (OSPW): a critical review. *Science of the Total Environment*, 601: 1785-1802.
- Liang, S., Xiao, K., Mo, Y., and Huang, X. 2012. A novel ZnO nanoparticle blended polyvinylidene fluoride membrane for anti-irreversible fouling. *Journal of Membrane Science*, 394-395: 184-192.
- Lim, S.-F., and Lee, A.Y.W. 2015. Kinetic study on removal of heavy metal ions from aqueous solution by using soil. *Environmental Science and Pollution Research*, 22(13): 10144-10158.
- MacKinnon, M.D., and Boerger, H. 1986. Description of two treatment methods for detoxifying oil sands tailings pond water. *Water Quality Research Journal*, 21(4): 496-512.

- Martin, J.W., Barri, T., Han, X., Fedorak, P.M., Gamal El-Din, M., Perez, L., Scott, A.C., and Jiang, J.T. 2010. Ozonation of oil sands process-affected water accelerates microbial bioremediation. *Environmental science & technology*, 44(21): 8350-8356.
- Meng, L., How, Z.T., Ganiyu, S.O., and Gamal El-Din, M. 2021. Solar photocatalytic treatment of model and real oil sands process water naphthenic acids by bismuth tungstate: Effect of catalyst morphology and cations on the degradation kinetics and pathways. *Journal of hazardous materials*, 413: 125396.
- Meshref, M.N., Chelme-Ayala, P., and Gamal El-Din, M. 2017. Fate and abundance of classical and heteroatomic naphthenic acid species after advanced oxidation processes: Insights and indicators of transformation and degradation. *Water research*, 125: 62-71.
- Mian, M.M., and Liu, G. 2018. Recent progress in biochar-supported photocatalysts: synthesis, role of biochar, and applications. *RSC advances*, 8(26): 14237-14248.
- Miklos, D.B., Remy, C., Jekel, M., Linden, K.G., Drewes, J.E., and Hübner, U. 2018. Evaluation of advanced oxidation processes for water and wastewater treatment—A critical review. *Water research*, 139: 118-131.
- Mohamed, K.M., Benitto, J.J., Vijaya, J.J., and Bououdina, M. 2023. Recent Advances in ZnO-Based Nanostructures for the Photocatalytic Degradation of Hazardous, Non-Biodegradable Medicines. *Crystals*, 13(2): 329.
- NRCAN. 2020. Natural Resources Canada Water Management in oil sands. Available from <https://natural-resources.canada.ca/our-natural-resources/energy-sources-distribution/fossil-fuels/crude-oil/what-are-oil-sands/18089>.
- Nyakas, A., Han, J., Peru, K.M., Headley, J.V., and Borchers, C.H. 2013. Comprehensive analysis of oil sands processed water by direct-infusion Fourier-transform ion cyclotron resonance

- mass spectrometry with and without offline UHPLC sample prefractionation. *Environmental science & technology*, 47(9): 4471-4479.
- Oil Sands Magazine. 2021. Tailing Ponds 101. *In* Online (<https://www.oilsandsmagazine.com/technical/mining/tailings-ponds>, Updated on March 3, 2021), Oil Sands Magazine.
- Ong, C.B., Ng, L.Y., and Mohammad, A.W. 2018. A review of ZnO nanoparticles as solar photocatalysts: Synthesis, mechanisms and applications. *Renewable and Sustainable Energy Reviews*, 81: 536-551.
- Pérez-Estrada, L.A., Han, X., Drzewicz, P., Gamal El-Din, M., Fedorak, P.M., and Martin, J.W. 2011. Structure–reactivity of naphthenic acids in the ozonation process. *Environmental science & technology*, 45(17): 7431-7437.
- Pourrezaei, P., Alpatova, A., Khosravi, K., Drzewicz, P., Chen, Y., Chelme-Ayala, P., and Gamal El-Din, M. 2014a. Removal of organic compounds and trace metals from oil sands process-affected water using zero valent iron enhanced by petroleum coke. *Journal of environmental management*, 139: 50-58.
- Pourrezaei, P., Alpatova, A., Chelme-Ayala, P., Perez-Estrada, L., Jensen-Fontaine, M., Le, X., and Gamal El-Din, M. 2014b. Impact of petroleum coke characteristics on the adsorption of the organic fractions from oil sands process-affected water. *International Journal of Environmental Science and Technology*, 11(7): 2037-2050.
- Pourrezaei, P., Drzewicz, P., Wang, Y., Gamal El-Din, M., Perez-Estrada, L.A., Martin, J.W., Anderson, J., Wiseman, S., Liber, K., and Giesy, J.P. 2011. The impact of metallic coagulants on the removal of organic compounds from oil sands process-affected water. *Environmental science & technology*, 45(19): 8452-8459.

- Qin, F., Wen, B., Shan, X.-Q., Xie, Y.-N., Liu, T., Zhang, S.-Z., and Khan, S.U. 2006. Mechanisms of competitive adsorption of Pb, Cu, and Cd on peat. *Environmental Pollution*, 144(2): 669-680.
- Qin, R., How, Z.T., and Gamal El-Din, M. 2019. Photodegradation of naphthenic acids induced by natural photosensitizer in oil sands process water. *Water research*, 164: 114913.
- Qin, R., Chelme-Ayala, P., and Gamal El-Din, M. 2020. The impact of oil sands process water matrix on the ozonation of naphthenic acids: from a model compound to a natural mixture. *Canadian Journal of Civil Engineering*, 47(10): 1166-1174.
- Quinlan, P.J., and Tam, K.C. 2015. Water treatment technologies for the remediation of naphthenic acids in oil sands process-affected water. *Chemical Engineering Journal*, 279: 696-714.
- Rashed, Y., Messele, S.A., Zeng, H., and Gamal El-Din, M. 2020. Mesoporous carbon xerogel material for the adsorption of model naphthenic acids: structure effect and kinetics modelling. *Environmental technology*, 41(27): 3534-3543.
- Rodríguez-Padrón, D., Luque, R., and Muñoz-Batista, M.J. 2020. Waste-derived materials: opportunities in photocatalysis. *Heterogeneous Photocatalysis: Recent Advances*: 1-28.
- Rowland, S.J., West, C.E., Jones, D., Scarlett, A.G., Frank, R.A., and Hewitt, L.M. 2011. Steroidal Aromatic ‘Naphthenic Acids’ in Oil Sands Process-Affected Water: Structural Comparisons with Environmental Estrogens. *Environmental science & technology*, 45(22): 9806-9815.
- S, R., and P, B. 2019. The potential of lignocellulosic biomass precursors for biochar production: Performance, mechanism and wastewater application—A review. *Industrial Crops and Products*, 128: 405-423.

- Scarlett, A.G., West, C.E., Jones, D., Galloway, T.S., and Rowland, S.J. 2012. Predicted toxicity of naphthenic acids present in oil sands process-affected waters to a range of environmental and human endpoints. *Science of the Total Environment*, 425: 119-127.
- Scarlett, A.G., Reinardy, H.C., Henry, T., West, C.E., Frank, R.A., Hewitt, L.M., and Rowland, S.J. 2013. Acute toxicity of aromatic and non-aromatic fractions of naphthenic acids extracted from oil sands process-affected water to larval zebrafish. *Chemosphere*, 93(2): 415-420.
- Shaheen, S.M., Niazi, N.K., Hassan, N.E.E., Bibi, I., Wang, H., Tsang, Daniel C.W., Ok, Y.S., Bolan, N., and Rinklebe, J. 2019. Wood-based biochar for the removal of potentially toxic elements in water and wastewater: a critical review. *International Materials Reviews*, 64(4): 216-247.
- Shan, R., Han, J., Gu, J., Yuan, H., Luo, B., and Chen, Y. 2020. A review of recent developments in catalytic applications of biochar-based materials. *Resources, Conservation and Recycling*, 162: 105036.
- Shu, Z., Li, C., Belosevic, M., Bolton, J.R., and Gamal El-Din, M. 2014. Application of a solar UV/chlorine advanced oxidation process to oil sands process-affected water remediation. *Environmental science & technology*, 48(16): 9692-9701.
- Solarchem Environmental, S. 1994. *The UV/oxidation handbook*. Solarchem Environmental Systems Markham, Ont., Canada, Markham, Ont., Canada. pp. 1 volume (various pagings).
- Song, J., How, Z.T., Huang, Z., and Gamal El-Din, M. 2022. Biochar/iron oxide composite as an efficient peroxymonosulfate catalyst for the degradation of model naphthenic acids compounds. *Chemical Engineering Journal*, 429: 132220.
- Speight, J.G. 2013. Chapter 3 - Oil Sand Mining. *In Oil Sand Production Processes. Edited by J.G. Speight*. Gulf Professional Publishing, Boston. pp. 59-79.

- Suara, M.A., Ganiyu, S.O., Paul, S., Stafford, J.L., and El-Din, M.G. 2022a. Solar-activated zinc oxide photocatalytic treatment of real oil sands process water: Effect of treatment parameters on naphthenic acids, polyaromatic hydrocarbons and acute toxicity removal. *Science of the Total Environment*, 819: 153029.
- Suara, M.A., Ganiyu, S.O., Paul, S., Stafford, J.L., and Gamal El-Din, M. 2022b. Solar-activated zinc oxide photocatalytic treatment of real oil sands process water: Effect of treatment parameters on naphthenic acids, polyaromatic hydrocarbons and acute toxicity removal. *Science of the Total Environment*, 819: 153029.
- Sun, N., Chelme-Ayala, P., Klammerth, N., McPhedran, K.N., Islam, M.S., Perez-Estrada, L., Drzewicz, P., Blunt, B.J., Reichert, M., Hagen, M., Tierney, K.B., Belosevic, M., and Gamal El-Din, M. 2014. Advanced Analytical Mass Spectrometric Techniques and Bioassays to Characterize Untreated and Ozonated Oil Sands Process-Affected Water. *Environmental Science & Technology*, 48(19): 11090-11099.
- Wan, C., Shen, G.Q., and Choi, S. 2019. Waste management strategies for sustainable development. *In Encyclopedia of sustainability in higher education*. Springer. pp. 2020-2028.
- Wang, C., Alpatova, A., McPhedran, K.N., and Gamal El-Din, M. 2015a. Coagulation/flocculation process with polyaluminum chloride for the remediation of oil sands process -affected water: performance and mechanism study. *Journal of environmental management*, 160: 254-262.
- Wang, C., Klammerth, N., Huang, R., Elnakar, H., and Gamal El-Din, M. 2016. Oxidation of oil sands process-affected water by potassium ferrate (VI). *Environmental science & technology*, 50(8): 4238-4247.

- Wang, H., Zhang, L., Chen, Z., Hu, J., Li, S., Wang, Z., Liu, J., and Wang, X. 2014. Semiconductor heterojunction photocatalysts: design, construction, and photocatalytic performances. *Chemical Society Reviews*, 43(15): 5234-5244.
- Wang, H., Li, X., Zhao, X., Li, C., Song, X., Zhang, P., Huo, P., and Li, X. 2022. A review on heterogeneous photocatalysis for environmental remediation: From semiconductors to modification strategies. *Chinese Journal of Catalysis*, 43(2): 178-214.
- Wang, J., Cao, X., Huang, Y., and Tang, X. 2015b. Developmental toxicity and endocrine disruption of naphthenic acids on the early life stage of zebrafish (*Danio rerio*). *Journal of Applied Toxicology*, 35(12): 1493-1501.
- Wang, S., Zhao, M., Zhou, M., Li, Y.C., Wang, J., Gao, B., Sato, S., Feng, K., Yin, W., Igalavithana, A.D., Oleszczuk, P., Wang, X., and Ok, Y.S. 2019. Biochar-supported nZVI (nZVI/BC) for contaminant removal from soil and water: A critical review. *Journal of hazardous materials*, 373: 820-834.
- Wu, X., Yin, S., Dong, Q., Liu, B., Wang, Y., Sekino, T., Lee, S.W., and Sato, T. 2013. UV, visible and near-infrared lights induced NO<sub>x</sub> destruction activity of (Yb,Er)-NaYF<sub>4</sub>/C-TiO<sub>2</sub> composite. *Scientific Reports*, 3(1): 2918.
- Xue, J., Zhang, Y., Liu, Y., and Gamal El-Din, M. 2016. Effects of ozone pretreatment and operating conditions on membrane fouling behaviors of an anoxic-aerobic membrane bioreactor for oil sands process-affected water (OSPW) treatment. *Water research*, 105: 444-455.
- Yang, C., Wang, X., Ji, Y., Ma, T., Zhang, F., Wang, Y., Ci, M., Chen, D., Jiang, A., and Wang, W. 2019. Photocatalytic degradation of methylene blue with ZnO@C nanocomposites:

- Kinetics, mechanism, and the inhibition effect on monoamine oxidase A and B. *NanoImpact*, 15: 100174.
- Zhang, L., Zhang, Y., and Gamal El-Din, M. 2018a. Degradation of recalcitrant naphthenic acids from raw and ozonated oil sands process-affected waters by a semi-passive biofiltration process. *Water research*, 133: 310-318.
- Zhang, L., Zhang, Y., and Gamal El-Din, M. 2019. Integrated mild ozonation with biofiltration can effectively enhance the removal of naphthenic acids from hydrocarbon-contaminated water. *Science of the Total Environment*, 678: 197-206.
- Zhang, L., Zhang, Y., Patterson, J., Arslan, M., Zhang, Y., and El-Din, M.G. 2020. Biofiltration of oil sands process water in fixed-bed biofilm reactors shapes microbial community structure for enhanced degradation of naphthenic acids. *Science of the Total Environment*, 718: 137028.
- Zhang, Y., Xue, J., Liu, Y., and Gamal El-Din, M. 2016a. Treatment of oil sands process-affected water using membrane bioreactor coupled with ozonation: a comparative study. *Chemical Engineering Journal*, 302: 485-497.
- Zhang, Y., Xue, J., Liu, Y., and Gamal El-Din, M. 2018b. The role of ozone pretreatment on optimization of membrane bioreactor for treatment of oil sands process-affected water. *Journal of hazardous materials*, 347: 470-477.
- Zhang, Y., Klammerth, N., Messele, S.A., Chelme-Ayala, P., and Gamal El-Din, M. 2016b. Kinetics study on the degradation of a model naphthenic acid by ethylenediamine-N,N'-disuccinic acid-modified Fenton process. *Journal of hazardous materials*, 318: 371-378.

- Zhao, C., Wang, B., Theng, B.K.G., Wu, P., Liu, F., Wang, S., Lee, X., Chen, M., Li, L., and Zhang, X. 2021. Formation and mechanisms of nano-metal oxide-biochar composites for pollutants removal: A review. *Science of the Total Environment*, 767: 145305.
- Zhu, K., Wang, X., Chen, D., Ren, W., Lin, H., and Zhang, H. 2019. Wood-based biochar as an excellent activator of peroxydisulfate for Acid Orange 7 decolorization. *Chemosphere*, 231: 32-40.
- Zubot, W., MacKinnon, M.D., Chelme-Ayala, P., Smith, D.W., and Gamal El-Din, M. 2012. Petroleum coke adsorption as a water management option for oil sands process-affected water. *Science of the Total Environment*, 427: 364-372.

## **CHAPTER 2: Treatment of oil sands process water using petroleum coke: Field pilot.**

### **2.1 Introduction**

The production of bitumen from the mineable oil sands industry in Alberta is reliant on the use of OSPW. The major benefit of OSPW reuse and recycle are major reductions in volumes of fresh water that need to be imported from sources such as the Athabasca River. OSPW can be defined as water contained in tailings storage ponds which is used to support necessary oil production activities including bitumen extraction, process cooling, and hydro-transport of solid (Allen 2008a; Zubot et al. 2012). Generally, OSPW is a complex mixture of inorganic and organic compounds. It may contain, at varying concentrations, suspended solids, salts, organic compounds AEF, TPH, PAHs, trace elements, BTEX components (benzene, toluene, ethyl benzene, and xylenes), and phenols (Allen 2008a; Gamal El-Din et al. 2011).

OSPW has been reported to show toxicity to aquatic and other living organisms (Clemente and Fedorak 2005; Hagen et al. 2013; Li et al. 2017; MacKinnon and Boerger 1986; Rogers et al. 2002). The NAs, included in the AEF, have been recognized as a contributor to the acute toxicity found in OSPW (Clemente and Fedorak 2005; Li et al. 2017; MacKinnon and Boerger 1986; Madill et al. 2001). Since 1967, when Suncor Energy Ltd. began operating the first commercial oil sands project, there has been no operational releases of OSPW to the environment. The OSPW is stored in tailings ponds. The continuous accumulation of OSPW in tailings containment ponds poses significant challenges (Allen 2008a). Therefore, there are benefits to develop low-energy OSPW treatment technologies that could be incorporated by industry to ensure the release of treated OSPW is safe and protective of the downstream environment (Brown and Ulrich 2015).

The studies of OSPW initially focused on solid-liquid separation aimed at the enhancement of tailings settling rates and process water recovery (Allen 2008b). Recently, more research has targeted concentration reductions of AEF and NAs from OSPW. Remediation methods for OSPW are based on physical, chemical, and biological techniques. One chemical treatment method for OSPW is adsorption. According to previous research, adsorption has been shown to be an effective method to remove organic compounds from OSPW responsible for toxicity, which include AEF (Pourrezaei et al. 2014a; Zubot et al. 2012). OSPW adsorption studies have utilized different adsorbent materials, such as activated carbon (AC) (Islam et al. 2015; Islam et al. 2018), petroleum coke (PC) (Gamal El-Din et al. 2011; Pourrezaei et al. 2014a; Pourrezaei et al. 2014b; Zubot et al. 2012), carbon xerogel (CX) (Benally et al. 2019; Rashed et al. 2020), and biochar (Bhuiyan et al. 2017; Frankel et al. 2016). Other remediation methods of OSPW include coagulation and flocculation (Pourrezaei et al. 2011; Wang et al. 2015), advanced oxidation processes (AOP) (Abdalrhman et al. 2019; Abdalrhman 2019; Anderson et al. 2012; Fang et al. 2019; Fang et al. 2020; Gamal El-Din et al. 2011; Islam et al. 2014b; Klammer et al. 2015; Martin et al. 2010; Meshref et al. 2017; Qin et al. 2019; Shu et al. 2014), biofiltration (Zhang et al. 2018a, 2019; Zhang et al. 2020), anoxic aerobic membrane bioreactor (MBR) (Huang et al. 2017; Xue et al. 2016; Zhang et al. 2016, 2018b), Islam et al. 2015; Islam et al. 2014a; Islam et al. 2014b).

PC produced using a Fluid Coking Process™ is a byproduct of Syncrude's bitumen upgrading process. The carbon content of the material typically exceeds 80 wt.%(Hyndman 1981). A previous study demonstrated that PC could remove dissolved organic compounds from OSPW and produce treated OSPW that was not acutely toxic toward rainbow trout and *Vibrio fischeri*

(Zubot et al. 2012). This manuscript presents the results of a pilot-scale program that utilizes PC as an adsorbent to treat OSPW.

This study aims to examine the quality of treated OSPW as a function of residence time within placed deposits of PC under natural climatic conditions in the Fort McMurray Region. Specific objectives of the study include: 1) the assessment of the reduction of TSS that result from filtering OSPW through the PC deposit; 2) the assessment of the water chemistry of the under-drained OSPW as a function of residence time within the PC deposit to quantify changes in constituent concentration of AEF, trace elements, parent and alkylated PAHs, VOCs, major cations and anions, pH, total dissolved solids (conductivity), phenols, TPH, and DOC; 3) assessment of vanadium concentration in OSPW in contact with freshly produced PC and during storage within the coke deposit to quantify the removal efficiencies as a function of residence time; and 4) examination of the acute toxicity of PC treated OSPW with respect to standard commercial bioassays including Microtox™, Rainbow Trout, and *Daphnia magna*.

## 2.2 Materials and Methods

### 2.2.1 Pilot program

The field pilot program facilities are located in Cell 6 of the Mildred Lake Settling Basin (MLSB). The facilities consist of an inline series of reactors for the treatment of OSPW, shown in Figure 2.1. Although three reactors are shown in Figure 2.1, Reactor 3 (Polishing Pond) was not a part of the pilot program and the results presented in this manuscript. This study focuses on Reactors 1 and 2. The following is a summary of the pilot program. For more details regarding the pilot program and the reactors, please refer to Figure S1 in Appendix A.

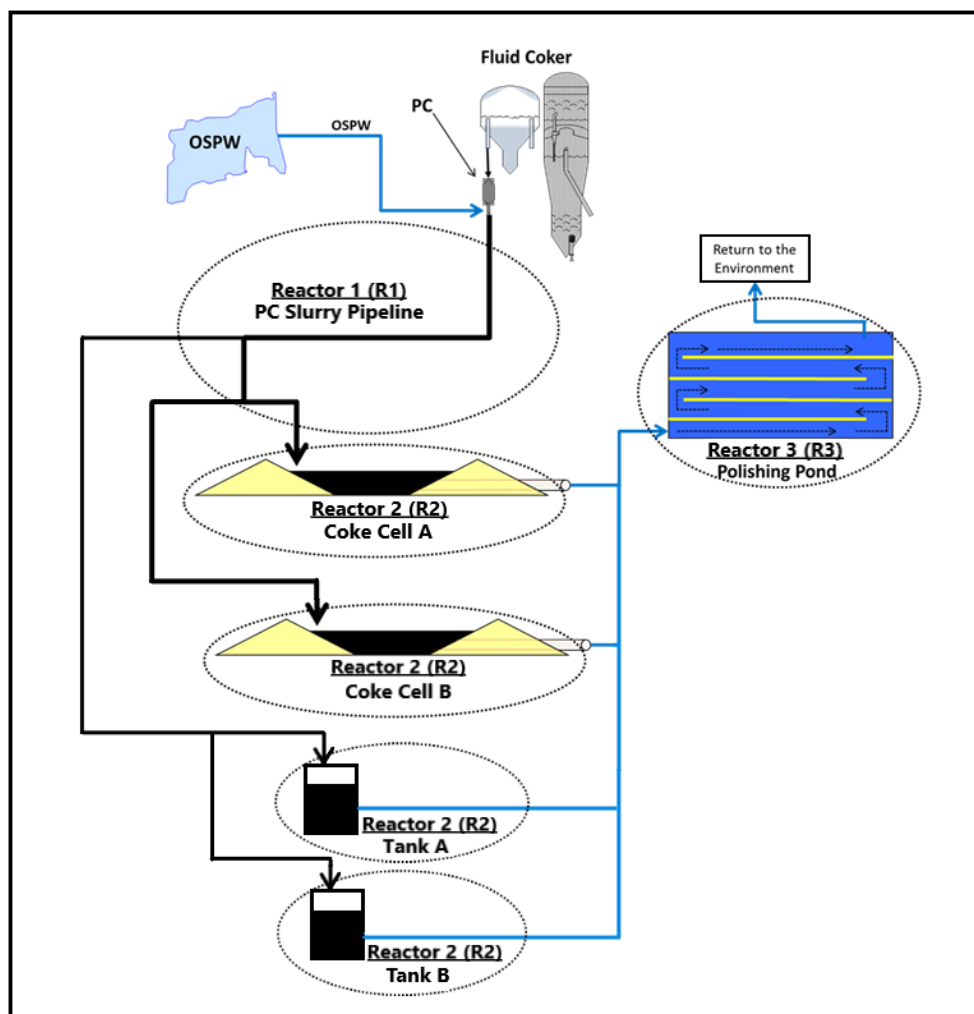


Figure 2.1: Two earthen containment cells (~600 m<sup>3</sup> each, Cell A, Cell B) and two steel tanks (~60 m<sup>3</sup> each, Tank A and Tank B) that acted as water treatment units.

Notes: Reactor 1 is represented as R1 and Reactor 2 is represented as R2. This study only focuses on R1 and R2, not R3.

Reactor 1 (R1) is a commercial scale 14-inch carbon steel pipeline that served two purposes: Firstly, it was used to transport the OSPW/PC slurry from the Fluid Coker to Reactor 2 – a distance of approximately 5 km. Secondly, this pipeline served as a plug-flow reactor in which adsorption reactions occurred. PC was obtained from Syncrude Canada Ltd (SCL) Fluid Coking unit 8-1 and

was mixed with OSPW sourced from the company's Recycle Water (RCW) pond to form a slurry that can be transported by pipeline.

Reactor 2 (R2) is a containment structure operated as a batch reactor. R2 permitted the separation of coke solids from the water by allowing the water to drain through the placed PC deposit which acted as a filter bed, and to permit kinetically slow "polishing" reactions to occur. To assess performance, there were 4 independent structures that served as R2: 2 earthen containment cells (~600 m<sup>3</sup> each) and 2 steel tanks (~60 m<sup>3</sup> each). The earthen cells were lined with a polyethylene geotextile liner (Enviro-Liner 6040™) to prevent water loss. Each cell contained an under-drain system consisting of slotted 8-inch diameter high density polyethylene (HDPE) pipe wrapped in a geotextile sock placed at the bottom of the cell to permit sampling of the treated OSPW. The dykes of the earthen cells were limited to a height of 2 m due to geotechnical constraints. These cells were filled with OSPW/PC slurry sourced from R1 between June 25 and July 9, 2012, to a PC depth of 1.5 m. The tanks were carbon-steel, skidded oil field tanks (400 BBLs, 20 ft H × 12 ft ID) which were cleaned prior to commissioning by sand blasting. They also contained an under-drain system consisting of a 6-inch slotted HDPE pipe wrapped in a geotextile sock secured to the bottom of each tank. The steel tanks were commissioned between July 23 and July 24, 2012 in a manner like the earthen cells. After being filled to a certain level with OSPW/PC slurry, the mixture was simply held in each of the reactors (R2). No mixing apparatus was used in reactor R2. Samples were withdrawn from the bottom of the reactors to assess the adsorption as a function of water contact time with the PC. No clogging issues occurred during the pilot operation. As the slurry was deposited into the cells and tanks (R2), the depth of

the coke bed increased, which decreased the clogging potential since there was more material to act as a filter bed.

Reactor 3 (R3) is a retention pond and possible future extension to R1 and R2, where aeration and final polishing steps may take place. R3 is not included as a part of the pilot project study results presented in this manuscript. Sampling was conducted upon water exiting from R1 and R2 only.

## 2.2.2 Experimental methods

### 2.2.2.1 *OSPW sampling*

Sampling of OSPW from different locations (Table S1 and Figure S1 a) was conducted to assess the water quality after treatment by different reactors. Sampling occurred from commissioning (June 2012) through August 2013, during the non-winter months. Samples were collected in 20 L PE pails. PC slurry samples collected after pipeline transport (R1) were first allowed to gravity settle and overlying water was filtered using a 0.45 µm syringe filter. A summary of samples collected and sample locations is shown in Table S1.

### 2.2.2.2 *Water analyses*

Water chemistry samples were placed into laboratory supplied containers, preserved as necessary, and submitted to Maxxam Analytics Ltd. (Edmonton, AB, now known as Bureau Veritas) within 48 h of collection. Maxxam Analytics Ltd. conducted analyses that included trace elements (dissolved and total on samples filtered using Millipore® 0.45µm syringe filter and preserved with nitric acid), major anions and cations, ammonia, alkalinity, parent and alkylated PAHs, VOCs, total dissolved solids (TDS), TSS, phenols, TPH, DOC, true color, pH, and conductivity. Please refer to Table S2 in the Appendix for the analytical methods and Tables S3 to S6 for the detailed results.

Select samples were analyzed at SCL's Research Facility (Edmonton, AB). Samples were collected from the 20 L pails using 250 mL, 500 mL or 1 L PE containers and shipped to Edmonton in an ice-chilled container within 48 h of collection. SCL Research Facility analyses included: AEF, pH, conductivity, major cations and anions, ammonium, and alkalinity. Please see Appendix A Text A1 for the analytical methods used by SCL's Research Facility.

#### 2.2.2.3 Toxicology

Select samples were collected in 20 L PE pails and sent to HydroQual Laboratories Ltd. (Calgary, AB) within 48 h of collection for completion of bioassays. Laboratory bioassays included rainbow trout, *Daphnia magna*, luminescent bacteria (Microtox™), and *Ceriodaphnia dubia*.

## 2.3 Results and discussion

### 2.3.1 Cell and tank performance

To assess changes in dissolved component concentrations resulting from dilution or concentration, measurements of chloride and electrical conductivity (EC) were completed on raw OSPW and OSPW after R1 and R2. In the source OSPW, chloride concentrations ranged between 460 and 670 mg/L (average 560 mg/L) and EC ranged between 2920 and 3900  $\mu\text{s}/\text{cm}$  (average 3510  $\mu\text{s}/\text{cm}$ ). Even though the steel tanks were considered closed systems, they were still subjected to the freeze-thaw cycle over the study period. During the 2012 field program, there was no indication of either dilution or concentration effects. Chloride concentrations and EC did not significantly change due to water ingress (e.g., rainfall) or egress (e.g., evaporation). Therefore, evaporation and precipitation were considered negligible, and the tanks were considered as closed systems.

## 2.3.2 Removal of organic compounds

### 2.3.2.1 AEF and DOC

As shown in Figure 2.2, the initial AEF concentration averaged 62 mg/L in untreated OSPW. The samples collected upon exit from R1 had an average AEF concentration of 21 mg/L which equates to a 66% reduction of AEF concentrations. The residence time within R1 is relatively short (<1 h) compared to R2 ( $\geq 4$  weeks). Zubot et al. (2012) noted that prior to the long-term adsorption experiments, the OSPW used was in contact with PC in a hydraulic transport pipeline, like R1 for the present study. The OSPW AEF concentration after the hydraulic pipeline in the previous study was 3 to 13 mg/L. This is comparable to the results upon exit from R1 for the present study. The removal efficiency of R1 is directly related to the concentration of PC in the slurry (Zubot et al. 2012). Though the pipeline was designed to transport a 20-22 wt.% PC slurry as the basis, in practice there is variation in the coke content depending on the coker operating conditions (e.g., silo operation, OSPW addition rates, etc.). Therefore, the variation of AEF concentrations at the exit of R1 can reflect the changing concentration of PC in the pipeline.

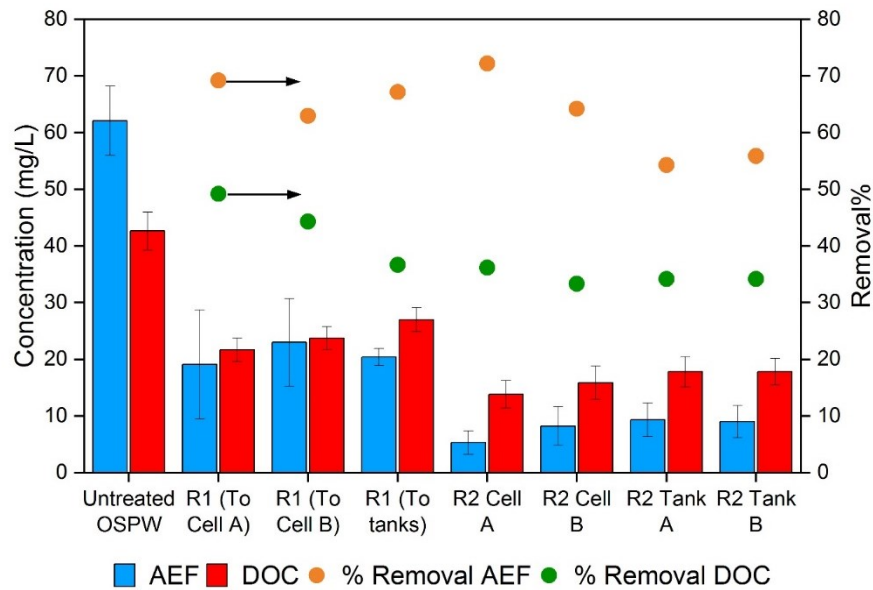
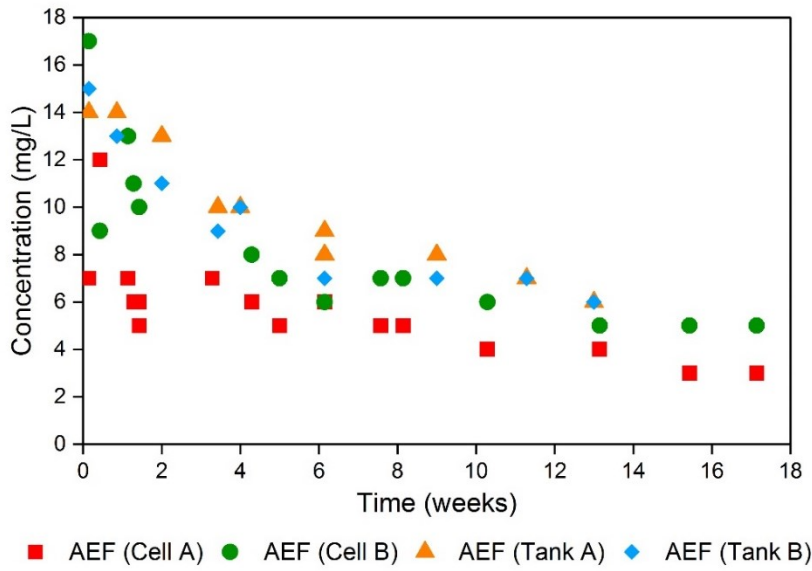


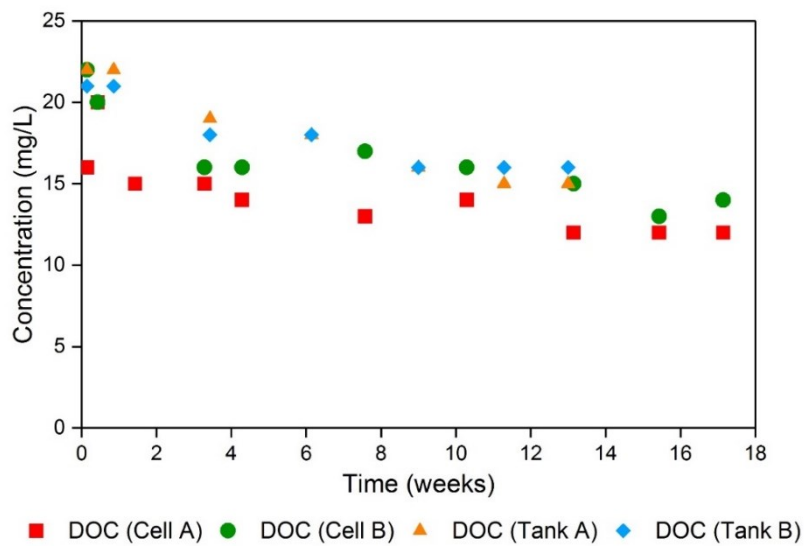
Figure 2.2: Acid extractable fraction (AEF) and dissolved organic carbon (DOC) concentrations in OSPW and after R1 and R2 (residence time: 4 weeks).

Note: The % removal of R2 was calculated based on the exit concentration from R1.

AEF concentrations further decreased (from an average of 21 mg/L) following long-term retention of the OSPW in the PC deposit (R2), as shown in Figure 2.3 (a). The decrease in AEF concentration occurred more slowly in the PC deposit. For residence time greater than or equal to 4 weeks' time, AEF concentrations in the treated OSPW did not exceed 10 mg/L, which was more than 50% removal from the starting average concentration of 21 mg/L. These results agree with results documented by Zubot et al. (2012). It was noted that enhanced AEF removal occurred at slower rates when OSPW/PC slurries were placed in columns for long residence time. In that study (Zubot et al. 2012), initial higher rates of AEF removal were followed by slower removal rates after about 3-4 months residence time, finally achieving 36 and 49% removal for residence times of 230 and 300 days, respectively.



(a)



(b)

Figure 2.3: Comparison of (a) AEF concentration and (b) DOC concentration in OSPW for residence time up to week 17.

Notes: the concentration given for each time is the average of data for Cells A and B, and Tanks A and B. The starting concentration for each reactor is from R1 effluent on specific date.

The overall combined removal efficiency of AEF by both reactors for the present study was greater than 84%. Compared to the bench-scale experimental results, when a PC concentration of 19.9 wt.% was used to treat the OSPW in short-term adsorption experiments, the removal efficiency of NAs (from UPLC/MS analysis) achieved was 82% (Zubot et al. 2012). The overall results are in agreement with another bench-scale study documented by Gamal El-Din et al. (2011). A PC dose of approximately 22 wt.% resulted in a 91% decrease of AEF (reported as total-acid extractable organics).

Higher AEF removal in R1 was followed by lower removal in R2. These observations were consistent with results from previous research, which concluded that the kinetics of AEF adsorption by PC is a biphasic process (Zubot et al. 2012). In that study, fast adsorption occurred within the pipe reactor (same pipe used for the current study, R1), and slower adsorption occurred within the column which acted as batch reactors. Examining the results shown in Figure 2.3 (a), either for cells or for tanks, the AEF concentration out of R2 decreased fast initially and then decreased slower. The AEF results from R2 are also consistent with the column studies discussed by Zubot et al. (2012). Initially, AEF removal rate is fast and is then followed by a slower adsorption phase, which is caused by the diffusion mechanisms (Zubot et al. 2012). By applying the kinetically fast reactions occurring in R1 and kinetically slow reactions in R2, this 2-reactor treatment process maximized the removal efficiency of AEF. Thus, it is reasonable that the pilot-scale results for the total removal efficiencies of AEF after two reactors (R1&R2) in the present study are greater than the bench-scale NAs removal results from Zubot et al. (2012).

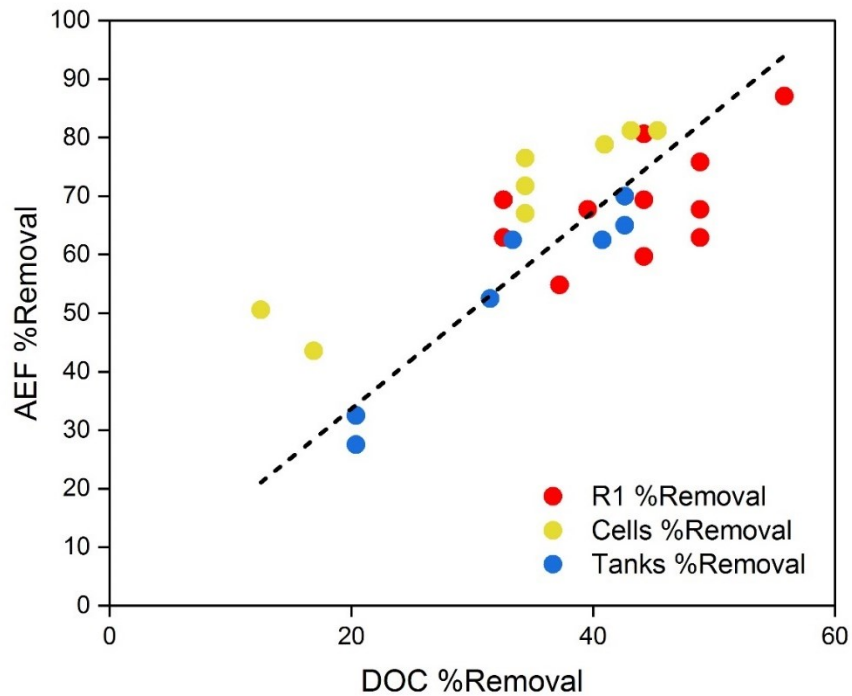


Figure 2.4: Correlation of AEF and DOC by % removal.

Notes: The % removals of AEF and DOC from cells and tanks are calculated based on the exit concentration from R1. The % removals of AEF and DOC for R1 are based on the concentration from untreated OSPW. The trend line is forced to cross the origin point.

In this study, dissolved organic carbon (DOC) was also measured to quantify the total amount of organic matter in the untreated and treated OSPW. DOC is a direct measure of the total organic content, which is not related to the oxidation state of carbon and does not measure other organically bound elements (e.g., nitrogen, hydrogen, etc.). shown in Figure 2.2, DOC in the untreated OSPW averaged 43 mg C/L. After treatment by R1, the DOC concentration averaged 27 mg C/L, representing a removal efficiency of ~37%. From Figure 2.3 (b), after retention in the PC deposit (R2) for more than 4 weeks, DOC concentrations were consistently less than 20 mg C/L, meaning more than half the organic matter in the untreated OSPW was removed. The correlation

of AEF and DOC by % removal is shown in Figure 2.4. With increasing removal of DOC, there is a corresponding increase in AEF removal. Based on this positive correlation, DOC can be seen more as a general indicator of the AEF removal in the treatment.

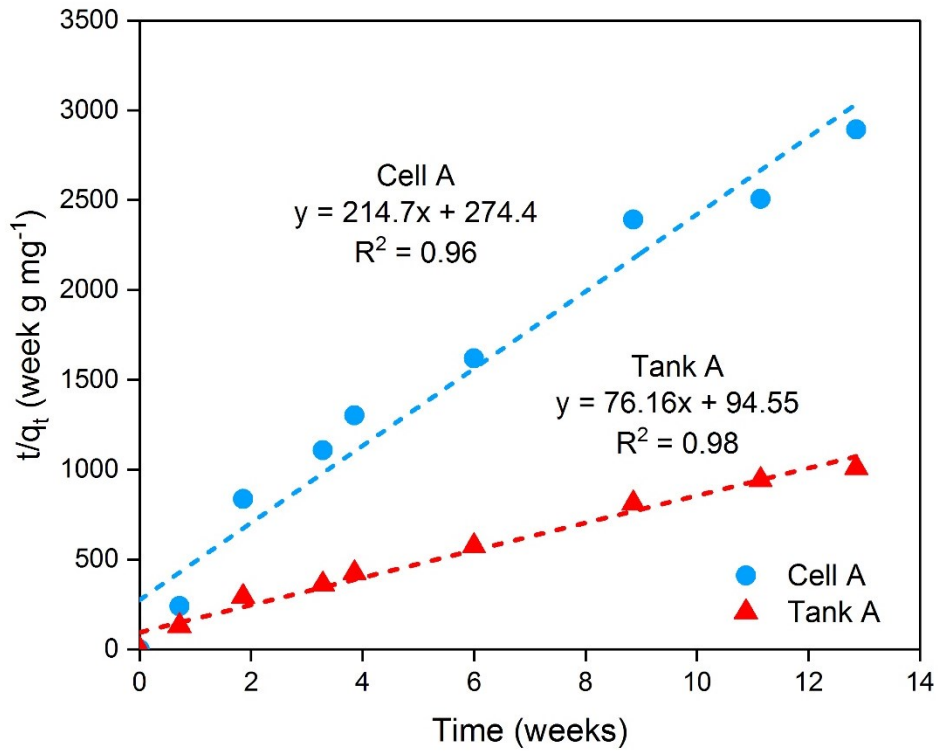


Figure 2.5: PSO model for the adsorption of AEF in OSPW treated by PC in Cell A and Tank A.

Table 2.1: PSO kinetics coefficient for AEF.

	$q_e$ (mg/g)	$k_2$ (g/mg-wk)	$R^2$
Cell A	0.0050	168.0	0.96
Cell B	0.0040	216.7	0.96
Tank A	0.013	61.34	0.98
Tank B	0.013	93.63	0.99

AEF adsorption by PC in R2 of this pilot-scale study follows PSO kinetics. This is shown in Figure 2.5 for cell A and tank A. The pseudo-second order kinetics for AEF adsorption in all R2 reactors are shown in Figure S2 with corresponding equations. Based on the four equations, the PSO rate constant ( $k_2$ ) and the equilibrium adsorption capacity ( $q_e$ ) can be directly determined. Table 2.1 summarizes the  $k_2$  and  $q_e$  results for the four R2 reactors. For example, cell A had a  $k_2$  value of 168.0 (g/mg-week) and  $q_e$  of 0.0050 mg/g ( $R^2=0.96$ ). For tank A, the resulting rate constant,  $k_2$ , was 61.34 (g/mg-week) and  $q_e$  value was 0.013 mg/g ( $R^2=0.98$ ). The kinetics results from this pilot-scale study agree with two previous bench-scale research findings, that the adsorption of AEF follows PSO kinetics Islam et al. 2018; Zubot et al. 2012). Zubot et al. (2012) used PC as the adsorbent and Islam et al. (2018) used GAC. The PSO kinetics constants determined for the different R2 reactors in the present study varied greatly depending upon whether R2 was a cell or a tank. The constants for the cells were in agreement, as were the kinetics constants for the tanks. The kinetics constants for the present study were not in agreement with the results of the bench-scale study, with  $k_2$  of 39.4 (g/mg-h) and  $q_e$  of 0.16 mg/g (Zubot et al. (2012).

Differences in  $q_e$  values may be a result of the calculations involved when using the PSO model. The value of  $q_e$  is determined by plotting  $t/q_t$  vs  $t$ . For larger masses of adsorbent used the value of  $q_t$  will decrease. A decrease of  $q_t$  will result in a higher value for  $t/q_t$ . This will lead to a higher slope in the plot of  $t/q_t$  vs.  $t$ . For PSO, the slope is equal to the reciprocal of  $q_e$ . So higher mass will lead to lower equilibrium adsorption capacity. This is one reason why the cells have the lowest resulting values for  $q_e$ , followed by the tanks. The bench-scale study has the highest value of  $q_e$ , as should be expected.

In this pilot study, the cells show faster kinetics than the tanks. Plazinski et al. (2013) determined that for the PSO model, the initial concentration ( $C_0$ ) can have a significant effect on the resulting value of  $q_e$ . Although  $C_0$  is not directly present in the calculation of  $k_2$ , it is still a significant parameter that can affect the resulting  $k_2$  since  $k_2$  is a function of  $q_e$ . An important finding is that  $k_2$  decreases with increasing  $C_0$  values because  $k_2$  is a time-scaling factor (Plazinski et al. 2013). This means that higher  $C_0$  values will take more time for the system to reach equilibrium. In this pilot study, the inlet concentration ( $C_0$ ) of AEF for cells is about 10 mg/L, and for the tanks is about 20 mg/L. Thus, the tanks need more time to reach equilibrium. This may be one explanation why the cells show faster kinetics rates.

Compared to the bench-scale study, there are several different conditions, such as the mass of PC, the volume of the water in the reactor, and the initial concentration of AEF. The mass of PC in the cells and even in the tanks was much greater than the mass used in the columns for the bench-scale study. For these reasons it is reasonable to expect that there will be differences between the kinetics results of this pilot project and the bench-scale study.

#### *2.3.2.2 TPH and Phenols*

Total Petroleum Hydrocarbons (TPH) measurements were completed by the chromatographic analysis of solvent extracts from unfiltered water samples (Table S2). As shown in Figure S3, the TPH concentration in the source OSPW (i.e., sample location 1A, 1B) ranged from 0.16 to 3 mg/L. After R1, the TPH concentrations were reduced to lower than laboratory detection limits (<0.1 mg/L). In a similar way, after R2, the TPH concentrations were also less than the laboratory detection limits. Consequently, these relatively water-insoluble contents were not mobilized from the PC deposit.

Total phenol was measured by a colorimetric method (Table S2). The changes in the total phenol concentrations are shown in Figure S4. The average total phenol concentration in the source OSPW was 0.03 mg/L, with a range between 0.02 and 0.05 mg/L. Further removal of phenols was completed by retention in the PC deposit. For retention times over 4 weeks, the phenol concentrations in the samples collected from the cells and tanks showed as less than 0.01 mg/L consistently, and the removal efficiencies exceeded 67%.

#### *2.3.2.3 Polycyclic aromatic hydrocarbons and volatile organic compounds*

PAHs present in OSPW are dominated by alkylated or substituted compounds, which represent a natural source. Figure S5 only includes the PAH components that were present in untreated and treated OSPW with the concentrations higher than laboratory detection limits. The parent PAH concentrations in untreated OSPW are commonly less than the detection limits and are therefore not represented on Figure S5. The alkylated compounds ranged between 0.5 and 8.5 µg/L. After treatment there was a significant reduction in the PAH concentration. As a result, over the approximately 3-4 months study, the concentrations of most PAH constituents in the treated OSPW were consistently lower than the detection limits. There was no evidence shown that PAHs were mobilized in either short or long-term frames. These findings are consistent with the physical and chemical properties of PAHs. In general, PAHs have very low water solubility, low vapor pressures and high octanol-water partition coefficients (Mackay 2001).

In untreated OSPW, concentrations of benzene, toluene, ethylbenzene and xylenes (BTEX) showed a range from less than laboratory detection limits to 12 µg/L. Of the total 39 VOCs that were analyzed, 37 VOCs were present at concentrations lower than laboratory detection limits. The two detected VOCs in the source OSPW were 1,2,4-trimethylbenzene and 1,3,5-

trimethylbenzene which were present at the concentrations between 0.8 and 1.4  $\mu\text{g/L}$ . Except for styrene and toluene, the concentration of BTEX and VOC components following R1 were less than laboratory detection limits. Styrene and toluene were detected in several treated OSPW samples that were collected from tanks A and B. Styrene concentrations exceeded the method detection limit (0.5  $\mu\text{g/L}$ ) slightly, ranging from 0.5 to 0.9  $\mu\text{g/L}$ . For toluene, after retention of 8 weeks, the concentrations in treated OSPW from tanks A and B were less than the method detection limits.

### 2.3.3 Removal of vanadium and changes in other trace element concentrations

Changes in vanadium concentration were observed during the pilot program. Source OSPW showed low concentration of vanadium (2.5  $\mu\text{g/L}$  to 10  $\mu\text{g/L}$ ) which increased upon exit from R1 (0.93 mg/L to 9.6 mg/L), an indication that leaching from PC had occurred. Similar leaching results were obtained during short term adsorption experiments using OSPW and PC in studies conducted by Pourrezaei et al. (2014a) and Zubot et al. (2012). For a 20 wt.% PC dose, Zubot et al. (2012) documented an increase in vanadium concentration from less than 0.05 mg/L to  $2.72 \pm 0.93$  mg/L. Pourrezaei et al. (2014a) noted that vanadium concentration increased to approximately 2.5 mg/L when using a 200 g/L dose of PC in OSPW.

The vanadium concentration in OSPW upon exit from R2 cell A and tank A over time is shown in Figure 2.6. All cells and tanks experienced an increase of vanadium concentration upon commissioning, indicating the leaching from PC had also occurred in R2. The steel tank PC deposits had lower initial spikes of vanadium than the PC deposits within the cells. Cell A had an increase of vanadium concentration up to 10.0 mg/L and tank A had an increase up to 2.1 mg/L. With increased residence time in each of R2 cells or tanks, a significant decrease of vanadium

concentration in OSPW resulted. In both cells, vanadium concentrations in OSPW decreased to less than 2 mg/L (4 weeks retention time) and to less than 1 mg/L (> 8 weeks retention time). Retention times of 4 and 8 weeks in PC tanks resulted in vanadium concentrations of less than 0.25 mg/L and 100 µg/L, respectively. In general, the results obtained are in agreement with the resulting gradual decreasing vanadium concentrations over long residence time that were documented by Zubot et al. (2012).

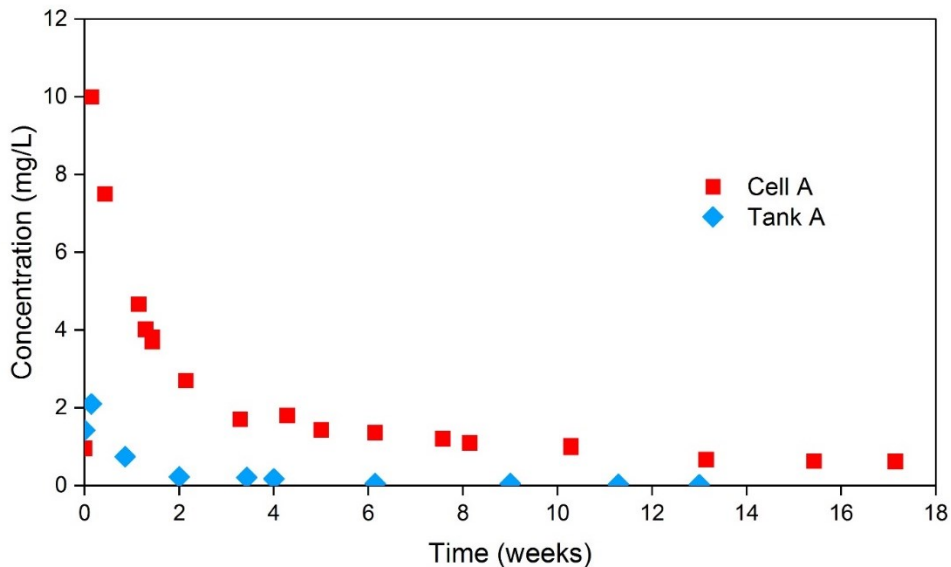


Figure 2.6: Vanadium concentrations upon exit from Cell A and Tank A with time.

Notes: The initial concentration of vanadium is from R1 exit for the cells and tanks on the day prior to the very first measurement made from R2. The incoming vanadium concentrations for Cell A and Tank A are 0.96 mg/L and 1.42 mg/L, respectively. The vanadium concentration increased due to leaching.

The bitumen utilized by SCL contains an average vanadium concentration of 225 mg/kg. There is no evidence that vanadium is solubilized into OSPW at elevated concentrations (> 10

$\mu\text{g/L}$ ) due to the hot water extraction process. This indicates that vanadium is bound as an organo-metallic complex (Moskalyk and Alfantazi 2003). During the fluid coking process, bitumen is thermally cracked, and elemental vanadium is incorporated into petroleum coke as an oxide. Production of PC in the burner vessel of the fluid coker converts metal species present in bitumen to oxidized forms that reside within the carbon PC matrix. Vanadium concentrations in the PC are reported to be approximately 1200 mg/kg (Zubot 2010).

Leaching of vanadium increases with increasing pH (Puttaswamy and Liber 2011; Wehrli and Stumm 1989). Initial vanadium leaching might be explained by the slight increase in pH of the OSPW as it passed through the reactors (section 2.3.4). A potential process improvement to accelerate vanadium removal after initial leaching may involve modest reduction in the OSPW pH using an acidification agent such as carbon dioxide (Zubot 2010).

Mechanisms likely responsible for the decrease in vanadium concentrations following long term retention in PC deposits are adsorption onto metal hydroxides within the PC matrix and/or the PC itself, as was discussed in detail by Zubot et al. (2012). The metal hydroxide adsorption mechanism may further help to explain why the observed vanadium removal rates in the OSPW collected from tanks were higher in comparison to the removal in the cells. Prior to commissioning, the tanks were hydro-tested with potable water to ensure integrity. Following a 24 h testing period, the exiting water was discolored yellow due to corrosion products (iron hydroxide) from the inside wall of the steel tanks. OSPW is an order of magnitude more saline than potable water and has a greater affinity to corrode carbon steel. After commissioning of the pilot, “rust” formed would provide media for support of additional adsorption resulting in the pronounced vanadium removal rates compared to the earthen cells.

In addition to vanadium, other elements (arsenic, cadmium, mercury, barium, manganese, molybdenum, nickel, selenium and strontium) are present in the PC matrix at elevated concentrations (Zubot et al. 2012). Changes in trace element concentrations between untreated and treated OSPW were significantly smaller than that observed with vanadium.

Arsenic concentration in source OSPW (5 and 10 µg/L) experienced no significant increases or decreases due to PC contact. Cadmium concentration in source OSPW (< 0.1 µg/L) increased after contact with R1 (0.03 to 0.23 µg/L) and after R2 (0.1 and 0.8 µg/L after 1 year). For the duration of the study (3-4 months), there were no treated OSPW samples that contained cadmium at concentrations exceeding the current Canadian Council of Ministers of the Environment (CCME) freshwater aquatic life guideline, 1 µg/L. Mercury was detected in 5 samples at concentrations between 0.0021 and 0.0033 µg/L, which just exceeded the analytical method detection limit of 0.002 µg/L. The remaining samples (source and treated OSPW) contained concentrations less than the method detection limits. Barium concentration in source OSPW (0.35 and 0.45 mg/L) decreased by about 50% after contact with R1, and further decreased with increased retention times in R2. Manganese concentrations in source OSPW (40 to 100 µg/L) remained essentially unchanged after R1 (20 µg/L to 120 µg/L) and R2 cells (30 µg/L to 110 µg/L), but showed slight increases after exit from R2 tanks (80 to 180 µg/L). This supports the field observation of internal corrosion on the inside walls of the steel tanks.

Nickel concentrations in the source OSPW (5 to 10 µg/L) increased after R1 (10 to 25 µg/L), decreased following a few weeks retention time in R2 (average ~ 10 µg/L) and did not significantly increase or decrease for the remaining monitoring period. Selenium concentrations in the source OSPW (2 to 11 µg/L) did not change significantly following contact with R1 (4 to

14 µg/L) but steady and significant decreases were observed following contact with R2. Treated OSPW contained selenium concentrations significantly reduced relative to the source OSPW. Molybdenum concentrations in source OSPW (average 0.1 mg/L) increased following R1 (0.30 to 1.60 mg/L), and slowly increased with time when in contact with R2 (1 mg/L after ~ 1-year retention time). Molybdenum concentrations exceeded CCME guideline value of 73 µg/L for source and treated OSPW. The CCME does note that molybdenum is an essential trace element for aquatic organisms and is a growth promoter for phytoplankton, periphyton and macrophytes. Concentrations less than 0.06 µg/L may be limiting to certain forms of aquatic life. Strontium concentrations in source OSPW (0.6 to 0.8mg/L) were slightly reduced following retention in R2 (0.38 to 0.71 mg/L).

#### 2.3.4 Change in major ions, conductivity, total suspended solids and pH

The pH of OSPW exiting from R2 was slightly elevated when compared with source OSPW. The average pH and pH range in the source OSPW was 7.8 and 7.55-8.10, respectively. The pH values of the OSPW drained from cells and tanks ranged from 7.79 to 8.44.

Conductivity is representative of the total dissolved solids present in OSPW. The electrical conductivity of the untreated OSPW ranged from about 3000 to 4000 µs/cm. After initial contact with PC (R1), no apparent changes were evident. Similarly, OSPW after retention in R2 (cells A, B and tanks A, B) did not exhibit any major increases or decreases in conductivity during the 2012 field project. Like EC, concentrations of sodium and chloride did not significantly increase or decrease during the 2012 program.

Major changes in water hardness (i.e.,  $\text{Ca}^{+2}$ ,  $\text{Mg}^{+2}$ ) following PC treatment were not apparent. Prior to treatment, the hardness averaged 111 mg/L as  $\text{CaCO}_3$ . Upon exit from R 2, the hardness ranged between 80 and 114 mg/L as  $\text{CaCO}_3$ .

Concentrations of sulfate in the treated OSPW upon exit from R1 increased by approximately 14% relative to source OSPW, which contained sulfate concentrations that averaged 441 mg/L. Drainage waters from cells (A & B) and tanks (A & B) contained sulfate concentrations that averaged 501, 492, 487 and 481 mg/L, respectively. Significant concentration changes between R1 and R2 were not observed even though sulphur is a major component of PC (Chung et al. 1996; Zubot 2010) and potential oxidation could lead to increased concentrations of sulfate in the treated OSPW.

Initial bicarbonate concentration in OSPW averaged 770 mg/L. Bicarbonate concentrations in the treated OSPW after R2 were reduced by approximately 31% relative to the source OSPW. Average values for the treated waters from cells (A & B) and tanks (A & B) were 590, 485, 525 and 520 mg/L, respectively. In SCL's OSPW (pH~8), the total alkalinity is primarily due to the presence of bicarbonate.

TSS concentrations in the source OSPW ranged between 30 and 94 mg/L, with an average of 63 mg/L (Figure S6). According to Figure S6, treated OSPW generally contained TSS at concentrations less than laboratory detection limits (i.e., <1 mg/L). The treatment was designed so that OSPW was retained and percolated through a deposit of PC contained in the cells and tanks. Because the grain size distribution of PC is similar to fine sand (150  $\mu\text{m}$ ) and the permeability of PC deposits is in the order of  $10^{-5}$  m/s, the system exhibited good drainage properties and acted as a filter bed to remove suspended particles present in the OSPW (Zubot 2010). Although the

particles are composed of carbon, the advantages of silica sand filtration systems appear to have been replicated (Letterman and Association 1999). As a result, the potential negative properties associated with elevated concentrations of TSS such as poor light penetration, high turbidity, undesirable aesthetics, and adsorbed organics were significantly mitigated in OSPW treated through passage in a PC deposit.

### 2.3.5 Toxicity

The toxicity of OSPW has been linked to the acid-extractable organic fraction (AEF) (Bataineh et al. 2006; Li et al. 2017; MacKinnon and Boerger 1986). In the present study, OSPW treatment using PC reduced AEF to concentrations to less than 10 mg/L in general (refer to section 2.3.2.1 and Figure 2.2) and it was expected that toxicity would decrease following treatment. Results for acute toxicity tests were conducted using a battery of standard laboratory bioassays detailed in Section 2.2.2.3. From Table 2.2, untreated OSPW displayed measurable acute toxicity based on standard fish and bacterial (i.e., Microtox™) bioassays. Toxicity is reported as lethal concentrations (LC<sub>50</sub>, LC<sub>25</sub>, % survival at 96h for fish and 48h for zooplankton), effective concentrations (EC<sub>50</sub>, EC<sub>25</sub> for zooplankton mobility at 48h) and inhibitory concentrations (IC<sub>50</sub>, IC<sub>20</sub> for suppression of bioluminescence). The more sensitive species responses to OSPW were associated with the Rainbow Trout and Microtox™ assays. The zooplankton species *Daphnia Magna* did not exhibit any acute toxicity in untreated OSPW, a result also noted by Zubot et al. (2012) in the bench-scale study.

OSPW following treatment in PC deposits exhibited significantly improved bioassay results. Lethal (LC<sub>50</sub>, mortality) and non-lethal endpoints (EC<sub>50</sub> and EC<sub>25</sub> - motility, IC<sub>50</sub> and IC<sub>25</sub> - light inhibition) for the Rainbow Trout, *Daphnia magna* (non-acute response for untreated

OSPW), and Microtox™ (bacterial) bioassays showed non acute responses. Following a retention period of 2 weeks, the treated OSPW passed all the bioassays (LC<sub>50</sub> or EC<sub>50</sub> >100%vol. and IC<sub>50</sub>>91%vol.). Most of the samples reported 100% species survival in neat samples (i.e., no dilution). In addition to significant reduction in AEF concentrations, the treatment did reduce concentrations of other organic compounds (PAHs, hydrocarbons, DOC, COD) with the net result being the production of treated OSPW that did not display an acute toxic response.

Table 2.2: Results of toxicity evaluation.

Bioassay	Description	Type	Endpoint <sup>a</sup>	Raw OSPW	Cell A	Cell B	Tank A	Tank B
Microtox	15 min	Acute	IC <sub>50</sub>	>91	>91	>91	>91	>91
			IC <sub>20</sub>	21	>91	>91	>91	>91
Rainbow trout	96 h	Acute	LC <sub>50</sub>	66	>100	>100	>100	>100
			LC <sub>25</sub>	56	>100	>100	>100	>100
Daphnia magna	48 h	Acute	LC <sub>50</sub>	>100	>100	>100	>100	>100
			LC <sub>25</sub>	>100	>100	>100	>100	>100
			EC <sub>50</sub>	>100	>100	>100	>100	>100
			EC <sub>25</sub>	>100	>100	>100	>100	>100
<i>Ceriodaphnia dubia</i>	8 days	Acute (survival)	LC <sub>50</sub>		>100	>100	>100	93
			LC <sub>25</sub>		>100	>100	>100	na
		Chronic (fecundity)	IC <sub>50</sub>		67	13	>100	70
			IC <sub>25</sub>		37	3	>100	55

<sup>a</sup>IC<sub>20</sub>, IC<sub>25</sub>, and IC<sub>50</sub> are the concentrations of an inhibitor where the response is reduced by a 20, 25, and 50%, respectively. LC<sub>25</sub> and LC<sub>50</sub> are the lethal concentrations which kill 25 and 50% of a sample population, respectively. All results are reported in vol.%, except mortality.

Water samples collected from the cells and tanks (October 2012) were assessed using the chronic bioassay based on the freshwater flea, *Ceriodaphnia dubia*. This 8-day test used acute survival (LC<sub>50</sub>) and chronic reproduction (IC<sub>50</sub>, IC<sub>25</sub>) as the toxicity endpoints. While no acute effects were observed (LC<sub>50</sub>> 100% vol.) for treated OSPW collected from cells (A & B), some

chronic effects were noted in reproduction results. A reference toxicant (NaCl) indicated inhibitory concentrations (IC) endpoints at concentrations comparable to those measured in treated OSPW (i.e., IC<sub>50</sub> for NaCl reference was 780 mg/L). Sodium chloride concentrations in OSPW ranged between 700 and 900 mg/L. Therefore, chronic toxicity observed appears to be associated with the sodium chloride present in the OSPW rather than AEF or other dissolved organic compounds. This result was also observed in chronic toxicity tests using *Ceriodaphnia dubia* for OSPW treated in smaller scale PC filled columns (Zubot et al. 2012). However, it should be noted that the increases in vanadium following contact with Reactor 1 and 2 may be partially responsible for the chronic toxicity results. Puttaswamy and Liber (2011) documented that at basic pH, vanadium leached from PC was the primary cause of toxicity to *Ceriodaphnia dubia*.

## 2.4 Conclusions

This study demonstrated that PC adsorption can be successfully used as a cost effective and efficient treatment method for OSPW. As the OSPW traversed through two reactors, the treated OSPW was assessed by looking changes in organic constituents (AEF and DOC), TPH, phenols, PAHs, VOCs, vanadium, other trace element concentrations, major ions, conductivity, total suspended solids (TSS), pH and toxicity. The key findings are summarized in the following.

The pilot-program provided additional evidence that confirmed lab-scale experimental results that the adsorption of organic constituents (i.e., AEF and DOC) is a biphasic process. Initially, the removal rate is fast and is followed by a slower diffusion-controlled process. The 2-reactor treatment process utilizes the kinetics to maximize the removal of organic compounds. The kinetically fast reactions occur within the slurry transport pipeline (R1); the kinetically slow

reactions occur within the PC deposit (R2). As well, the pilot-program confirmed that adsorption of AEF by PC followed PSO kinetics.

Based on the FT-IR method, AEF is typically present at concentrations between 50 and 80 mg/L in fresh OSPW. The field pilot program indicates porewater residence times in R2 of between 4 and 8 weeks will remove AEF to concentrations less than 10 mg/L corresponding to treatment efficiencies exceeding 80%. After retention more than 4 weeks within the PC deposit (R2), the DOC concentration consistently presented at a low level that less than 20 mg/L, which indicated that more than half of the organic constituents were removed. The positive correlation between the % removal of DOC and AEF makes DOC as a target indicator for the removal of AEF in the treatment. Laboratory results indicate that the PC water treatment performed faster in the field under natural climatic conditions as compared to the laboratory results. Scale-up appears to improve the treatment performance in terms of kinetics.

Vanadium concentrations were elevated (approximately 2-10 mg/L) after initial contact with PC in R1. Retention of OSPW in PC deposit (R2) for 8 weeks or more resulted in steady and significant reduction of vanadium (< 1 mg/L). Possible mechanism for decreasing vanadium concentrations after the initial increase due to leaching were attributed to adsorption by metal oxides in the PC or the PC itself. The use of steel tanks provided support for the adsorption of vanadium by metal oxides (e.g., rust). Two other constituents which did increase in concentrations were cadmium (treated concentrations were below CCME guideline) and molybdenum (source and untreated concentrations were above CCME guideline).

Parent and alkylated PAHs in untreated OSPW were measured at concentrations up to 8.5 µg/L. The PC treated OSPW contained PAH concentrations that were significantly reduced to concentrations less than the analytical detection limit.

Whole effluent toxicity testing using trout, zooplankton and bacteria shows PC treatment produces OSPW with no measurable acute toxicity. *Ceriodaphnia* bioassays indicated that treated OSPW still had some non-lethal chronic effects. The response to treated OSPW may be attributed to the relatively high salinity of this water and to the presence of vanadium.

Filtration of OSPW through a PC deposit significantly reduces the concentrations of total suspended solids (TSS) present. The majority of the treated OSPW samples collected from R2 contained TSS at concentrations less than laboratory detection limits. The PC deposit acted as a filter bed to remove finely suspended solid matter. Aesthetic properties of treated OSPW are significantly improved relative to untreated OSPW (i.e., reduction in color, TSS).

## 2.5 References

- Abdalrhman, A.S., Zhang, Y., and Gamal El-Din, M. 2019. Electro-oxidation by graphite anode for naphthenic acids degradation, biodegradability enhancement and toxicity reduction. *Science of the Total Environment*, 671: 270-279.
- Abdalrhman, A.S.A. 2019. Application of Electro-oxidation for the Degradation of Organics in Oil Sands Process Water (OSPW). Thesis, University of Alberta.
- Allen, E.W. 2008a. Process water treatment in Canada's oil sands industry: I. Target pollutants and treatment objectives. *Journal of Environmental Engineering and Science*, 7(2): 123-138.

- Allen, E.W. 2008b. Process water treatment in Canada's oil sands industry: II. A review of emerging technologies. *Journal of Environmental Engineering and Science*, 7(5): 499-524.
- Anderson, J., Wiseman, S., Wang, N., Moustafa, A., Perez-Estrada, L., Gamal El-Din, M., Martin, J., Liber, K., and Giesy, J.P. 2012. Effectiveness of ozonation treatment in eliminating toxicity of oil sands process-affected water to *Chironomus dilutus*. *Environmental science & technology*, 46(1): 486-493.
- Bataineh, M., Scott, A., Fedorak, P., and Martin, J. 2006. Capillary HPLC/QTOF-MS for characterizing complex naphthenic acid mixtures and their microbial transformation. *Analytical Chemistry*, 78(24): 8354-8361.
- Benally, C., Messele, S.A., and Gamal El-Din, M. 2019. Adsorption of organic matter in oil sands process water (OSPW) by carbon xerogel. *Water research*, 154: 402-411.
- Bhuiyan, T.I., Tak, J.K., Sessarego, S., Harfield, D., and Hill, J.M. 2017. Adsorption of acid-extractable organics from oil sands process-affected water onto biomass-based biochar: Metal content matters. *Chemosphere*, 168: 1337-1344.
- Brown, L.D., and Ulrich, A.C. 2015. Oil sands naphthenic acids: a review of properties, measurement, and treatment. *Chemosphere*, 127: 276-290.
- Chung, K., Janke, L., Dureau, R., and Furimsky, E. 1996. Leachability of cokes from Syncrude stockpiles. *Environmental Science and Engineering*, 9(1): 50-53.
- Clemente, J.S., and Fedorak, P.M. 2005. A review of the occurrence, analyses, toxicity, and biodegradation of naphthenic acids. *Chemosphere*, 60(5): 585-600.
- Fang, Z., Huang, R., Chelme-Ayala, P., Shi, Q., Xu, C., and Gamal El-Din, M. 2019. Comparison of UV/Persulfate and UV/H<sub>2</sub>O<sub>2</sub> for the removal of naphthenic acids and acute toxicity

- towards *Vibrio fischeri* from petroleum production process water. *Science of the Total Environment*, 694: 133686.
- Fang, Z., Huang, R., How, Z.T., Jiang, B., Chelme-Ayala, P., Shi, Q., Xu, C., and El-Din, M.G. 2020. Molecular transformation of dissolved organic matter in process water from oil and gas operation during UV/H<sub>2</sub>O<sub>2</sub>, UV/chlorine, and UV/persulfate processes. *Science of the Total Environment*, 730: 139072.
- Frankel, M.L., Bhuiyan, T.I., Veksha, A., Demeter, M.A., Layzell, D.B., Helleur, R.J., Hill, J.M., and Turner, R.J. 2016. Removal and biodegradation of naphthenic acids by biochar and attached environmental biofilms in the presence of co-contaminating metals. *Bioresource technology*, 216: 352-361.
- Gamal El-Din, M., Fu, H., Wang, N., Chelme-Ayala, P., Pérez-Estrada, L., Drzewicz, P., Martin, J.W., Zubot, W., and Smith, D.W. 2011. Naphthenic acids speciation and removal during petroleum-coke adsorption and ozonation of oil sands process-affected water. *Science of the Total Environment*, 409(23): 5119-5125.
- Hagen, M.O., Katzenback, B.A., Islam, M.D.S., Gamal El-Din, M., and Belosevic, M. 2013. The Analysis of Goldfish (*Carassius auratus* L.) Innate Immune Responses After Acute and Subchronic Exposures to Oil Sands Process-Affected Water. *Toxicological Sciences*, 138(1): 59-68.
- Huang, C., Shi, Y., Xue, J., Zhang, Y., Gamal El-Din, M., and Liu, Y. 2017. Comparison of biomass from integrated fixed-film activated sludge (IFAS), moving bed biofilm reactor (MBBR) and membrane bioreactor (MBR) treating recalcitrant organics: Importance of attached biomass. *Journal of hazardous materials*, 326: 120-129.

- Hyndman, A.W. APPLICATION OF FLUID COKING TO UPGRADING OF ATHABASCA BITUMEN. *In* 1981. McGraw Hill., New York. pp. 645-647.
- Islam, M.S., Zhang, Y., McPhedran, K.N., Liu, Y., and Gamal El-Din, M. 2015. Granular activated carbon for simultaneous adsorption and biodegradation of toxic oil sands process-affected water organic compounds. *Journal of environmental management*, 152: 49-57.
- Islam, M.S., McPhedran, K.N., Messele, S.A., Liu, Y., and Gamal El-Din, M. 2018. Isotherm and kinetic studies on adsorption of oil sands process-affected water organic compounds using granular activated carbon. *Chemosphere*, 202: 716-725.
- Islam, M.S., Dong, T., Sheng, Z., Zhang, Y., Liu, Y., and Gamal El-Din, M. 2014a. Microbial community structure and operational performance of a fluidized bed biofilm reactor treating oil sands process-affected water. *International biodeterioration & biodegradation*, 91: 111-118.
- Islam, M.S., Dong, T., McPhedran, K.N., Sheng, Z., Zhang, Y., Liu, Y., and Gamal El-Din, M. 2014b. Impact of ozonation pre-treatment of oil sands process-affected water on the operational performance of a GAC-fluidized bed biofilm reactor. *Biodegradation*, 25(6): 811-823.
- Klamerth, N., Moreira, J., Li, C., Singh, A., McPhedran, K.N., Chelme-Ayala, P., Belosevic, M., and Gamal El-Din, M. 2015. Effect of ozonation on the naphthenic acids' speciation and toxicity of pH-dependent organic extracts of oil sands process-affected water. *Science of the Total Environment*, 506: 66-75.
- Letterman, R.D., and Association, A.W.W. 1999. *Water quality and treatment: a handbook of community water supplies*. McGraw-Hill.

- Li, C., Fu, L., Stafford, J., Belosevic, M., and Gamal El-Din, M. 2017. The toxicity of oil sands process-affected water (OSPW): a critical review. *Science of the Total Environment*, 601: 1785-1802.
- Mackay, D. 2001. *Multimedia environmental models: the fugacity approach*. CRC press.
- MacKinnon, M.D., and Boerger, H. 1986. Description of two treatment methods for detoxifying oil sands tailings pond water. *Water Quality Research Journal*, 21(4): 496-512.
- Madill, R.E., Orzechowski, M.T., Chen, G., Brownlee, B.G., and Bunce, N.J. 2001. Preliminary risk assessment of the wet landscape option for reclamation of oil sands mine tailings: bioassays with mature fine tailings pore water. *Environmental Toxicology: An International Journal*, 16(3): 197-208.
- Martin, J.W., Barri, T., Han, X., Fedorak, P.M., Gamal El-Din, M., Perez, L., Scott, A.C., and Jiang, J.T. 2010. Ozonation of oil sands process-affected water accelerates microbial bioremediation. *Environmental science & technology*, 44(21): 8350-8356.
- Meshref, M.N., Chelme-Ayala, P., and Gamal El-Din, M. 2017. Fate and abundance of classical and heteroatomic naphthenic acid species after advanced oxidation processes: Insights and indicators of transformation and degradation. *Water research*, 125: 62-71.
- Moskalyk, R., and Alfantazi, A. 2003. Processing of vanadium: a review. *Minerals engineering*, 16(9): 793-805.
- Plazinski, W., Dziuba, J., and Rudzinski, W. 2013. Modeling of sorption kinetics: the pseudo-second order equation and the sorbate intraparticle diffusivity. *Adsorption*, 19(5): 1055-1064.
- Pourrezaei, P., Alpatova, A., Chelme-Ayala, P., Perez-Estrada, L., Jensen-Fontaine, M., Le, X., and Gamal El-Din, M. 2014a. Impact of petroleum coke characteristics on the adsorption

- of the organic fractions from oil sands process-affected water. *International Journal of Environmental Science and Technology*, 11(7): 2037-2050.
- Pourrezaei, P., Alpatova, A., Khosravi, K., Drzewicz, P., Chen, Y., Chelme-Ayala, P., and Gamal El-Din, M. 2014b. Removal of organic compounds and trace metals from oil sands process-affected water using zero valent iron enhanced by petroleum coke. *Journal of environmental management*, 139: 50-58.
- Pourrezaei, P., Drzewicz, P., Wang, Y., Gamal El-Din, M., Perez-Estrada, L.A., Martin, J.W., Anderson, J., Wiseman, S., Liber, K., and Giesy, J.P. 2011. The impact of metallic coagulants on the removal of organic compounds from oil sands process-affected water. *Environmental science & technology*, 45(19): 8452-8459.
- Puttaswamy, N., and Liber, K. 2011. Identifying the causes of oil sands coke leachate toxicity to aquatic invertebrates. *Environmental toxicology and chemistry*, 30(11): 2576-2585.
- Qin, R., How, Z.T., and Gamal El-Din, M. 2019. Photodegradation of naphthenic acids induced by natural photosensitizer in oil sands process water. *Water research*, 164: 114913.
- Rashed, Y., Messele, S.A., Zeng, H., and Gamal El-Din, M. 2020. Mesoporous carbon xerogel material for the adsorption of model naphthenic acids: structure effect and kinetics modelling. *Environmental technology*, 41(27): 3534-3543.
- Rogers, V.V., Wickstrom, M., Liber, K., and MacKinnon, M.D. 2002. Acute and subchronic mammalian toxicity of naphthenic acids from oil sands tailings. *Toxicological Sciences*, 66(2): 347-355.
- Shu, Z., Li, C., Belosevic, M., Bolton, J.R., and Gamal El-Din, M. 2014. Application of a solar UV/chlorine advanced oxidation process to oil sands process-affected water remediation. *Environmental science & technology*, 48(16): 9692-9701.

- Wang, C., Alpatova, A., McPhedran, K.N., and Gamal El-Din, M. 2015. Coagulation/flocculation process with polyaluminum chloride for the remediation of oil sands process-affected water: performance and mechanism study. *Journal of environmental management*, 160: 254-262.
- Wehrli, B., and Stumm, W. 1989. Vanadyl in natural waters: Adsorption and hydrolysis promote oxygenation. *Geochimica et Cosmochimica Acta*, 53(1): 69-77.
- Xue, J., Zhang, Y., Liu, Y., and Gamal El-Din, M. 2016. Effects of ozone pretreatment and operating conditions on membrane fouling behaviors of an anoxic-aerobic membrane bioreactor for oil sands process-affected water (OSPW) treatment. *Water research*, 105: 444-455.
- Zhang, L., Zhang, Y., and Gamal El-Din, M. 2018a. Degradation of recalcitrant naphthenic acids from raw and ozonated oil sands process-affected waters by a semi-passive biofiltration process. *Water research*, 133: 310-318.
- Zhang, L., Zhang, Y., and Gamal El-Din, M. 2019. Integrated mild ozonation with biofiltration can effectively enhance the removal of naphthenic acids from hydrocarbon-contaminated water. *Science of the Total Environment*, 678: 197-206.
- Zhang, L., Zhang, Y., Patterson, J., Arslan, M., Zhang, Y., and El-Din, M.G. 2020. Biofiltration of oil sands process water in fixed-bed biofilm reactors shapes microbial community structure for enhanced degradation of naphthenic acids. *Science of the Total Environment*, 718: 137028.
- Zhang, Y., Xue, J., Liu, Y., and Gamal El-Din, M. 2016. Treatment of oil sands process-affected water using membrane bioreactor coupled with ozonation: a comparative study. *Chemical Engineering Journal*, 302: 485-497.

- Zhang, Y., Xue, J., Liu, Y., and Gamal El-Din, M. 2018b. The role of ozone pretreatment on optimization of membrane bioreactor for treatment of oil sands process-affected water. *Journal of hazardous materials*, 347: 470-477.
- Zubot, W., MacKinnon, M.D., Chelme-Ayala, P., Smith, D.W., and Gamal El-Din, M. 2012. Petroleum coke adsorption as a water management option for oil sands process-affected water. *Science of the Total Environment*, 427: 364-372.
- Zubot, W.A. 2010. Removal of naphthenic acids from oil sands process water using petroleum coke. M. Sc. Eng. Thesis, Department of Civil and Environmental Engineering, University of Alberta, Edmonton, AB. Spring 2010. 179pp.

## **CHAPTER 3: Adsorption Assessment of Naphthenic Acids on Different Reclamation Materials: Coarse Sand Tailings and Peat Mineral Mix.**

### **3.1 Introduction**

Canada has the third largest oil reserves in the world and the oil sands spread in northern Alberta contains more than 166 billion barrels of crude oil (NRCAN 2020). The oil sands in Alberta are composed of approximately 85% mineral solids and 10% bitumen with 5% water (Allen 2008; Zubot et al. 2012). Due to the high content of mineral solids, Alberta oil sands industries widely apply the Clark's caustic hot water extraction process as the bitumen recovery technique. During this process, every barrel of bitumen requires about 0.2 to 2.6 barrel of fresh water, resulting in the large volume production of produced water (Canada 2020). This produced water, contained in the tailings storage ponds to support necessary oil production activities, is recognized as oil sands process water (OSPW) (Allen 2008; Zubot et al. 2012). OSPW is a complex brackish mixture solution that contains suspended solids, trace metals, inorganic compounds, and organic compounds, including recalcitrant organics such as NAs (Meng et al. 2021; Zubot et al. 2021).

NAs broadly refer to the group of saturated aliphatic and alicyclic carboxylic acids that are naturally found in oil sands or other crude oil deposits (Quinlan and Tam 2015). NAs have a general formula of  $C_nH_{2n+z}O_x$ , where  $n$  represents the carbon number ( $7 \leq n \leq 26$ ),  $z$  represents the hydrogen deficiency due to the formation of ring or double bond structures (even integer,  $0 \leq -Z \leq 18$ ), and  $x$  is the oxygen number (typically  $2 \leq x \leq 6$ ) (Huang et al. 2018). NAs can be characterized as classical NAs with an oxygen number of two and oxidized NAs (Oxy-NAs) with an oxygen number of 3 to 6 (Huang et al. 2018). NAs are one of the important concerns among all

the organic compounds in OSPW. Grewer et al. (2010) indicated that the classical and Oxy-NAs account for more than 50% of the dissolved organics. Typically, the classical NAs show higher concentration compared to other Oxy-NAs in OSPW (Huang et al. 2021; Suara et al. 2022). Many researchers have reported that OSPW is toxic to many aquatic species and other living organisms (Anderson et al. 2012; Clemente and Fedorak 2005; Hagen et al. 2013; Li et al. 2017; Sun et al. 2014). Furthermore, several studies have recognized NAs are one of the contributors to the acute and chronic toxicity of OSPW (Jones et al. 2011; Li et al. 2017; MacKinnon and Boerger 1986). Besides, NAs could cause corrosion of the equipment during the bitumen extraction process (Quinlan and Tam 2015).

With prompted concerns focusing on NAs in OSPW, different techniques have been developed to achieve NAs attenuation. To this end, adsorption is a widely researched approach for the removal of NAs from environmental matrices including OSPW. Specifically, OSPW adsorption studies have utilized different adsorbent materials, such as activated carbon (AC) (Islam et al. 2015; Islam et al. 2018), petroleum coke (PC) (Gamal El-Din et al. 2011; Pourrezaei et al. 2014; Zubot et al. 2021), carbon xerogel (CX) (Benally et al. 2019; Rashed et al. 2020), and biochar (Bhuiyan et al. 2017; Frankel et al. 2016). Besides, researchers have also used natural soils as a low-cost efficient adsorbent for the removal of organic pollutants (e.g., NAs, dye, toluene, etc.) and heavy metal ions (e.g., Cd, Zn, Pb, Cu, etc.) (Arthur et al. 2017; Janfada et al. 2006; Li et al. 2020; Lim and Lee 2015; Peng et al. 2002; Rao et al. 2020; Smaranda et al. 2017).

Coarse sand tailings (CST) are waste tailings materials from the oil sands industry. During the bitumen production process, large volumes of process water are required to generate a slurry that can be gravity-separated, where the bitumen is recovered and the coarse sand, fines, and

process water left behind. The tailings streams are poured into the tailings ponds, where the coarse sands deposit to the bottom, and the water level rises, leading to higher tailings dams (Oil Sands Magazine 2021). The general use for CST in the field is to build up the dyke to support the tailings ponds (Figure 3.1). The accumulation of tailings in the oil sands industry, coupled with land use concerns and potential environmental risks, raises concerns about the feasibility of successful tailings waste reclamation (Cossey et al. 2021; Jones and Forrest 2010). An oil sands deposit has four distinct layers as follows: the muskeg layer is the wet top layer of peatland; the overburden layer contains mostly sand and clay; the bitumen-rich oil sands ore located below the muskeg layer and overburden layer; the rock layer is the bottom layer, most commonly comprises limestone or granite (Oil Sands Magazine 2019). The surface mining process of oil sands excavates the muskeg and overburden layers to expose the oil sands ores, during which the salvaged peat-mineral mixture (PMM) is removed and stored for use as a reclamation material (Speight 2013). Peat has rich fibrous organic content which could be produced by the partial decomposition and disintegration of plants (Ali et al. 2010; Aminur et al. 2011; BBK and Prasad 2011; Zainorabidin and Mohamad 2017).

As of today, different peat materials have been studied as possible effective adsorbents in many studies. Qin et al. (2006) found that the adsorption capacity of the studied peat material followed the order  $Pb > Cu > Cd$  in a single-solute system and observed competitive adsorption at low-energy adsorption sites. Viraraghavan and de Maria Alfaro (1998) found that the adsorption of phenol on horticultural peat followed the Freundlich isotherm and reached equilibrium after 16 h. The results also showed that the studied peat adsorbed 46.1% phenol with an initial concentration of 1 mg/L. However, the adsorption performance of the reclamation material like

PMM from the oil sands industry towards OSPW-related pollutants, such as NAs, has been less researched. Similarly, studies on the properties and adsorption behavior of coarse sand tailings (CST) materials are also lacking. Therefore, more research is needed to investigate the properties and adsorption behaviour of these two different materials. The characteristics and adsorption-related results of CST and PMM are critical for helping estimate the NAs transport in the environment. Besides, developing other possible applications for CST and PMM is also a vital topic for the industry. The accumulation of CST may be mitigated based on further studies.

Therefore, the objective of the present study was to assess the adsorption potential of two reclamation materials namely CST and PMM towards NAs removal from the aqueous phase. Specifically, the study aimed to: i) investigate the characteristics of CST and PMM to help understand the adsorption behaviour; ii) study the adsorption kinetics and isotherm for targeted NAs; iii) assess the adsorption performance towards different structured NAs in a mixture by CST and PMM; iv) study the mechanisms for the adsorption process of NAs. The outcomes of this research will provide insights into the possible application of CST and PMM as reclamation materials.

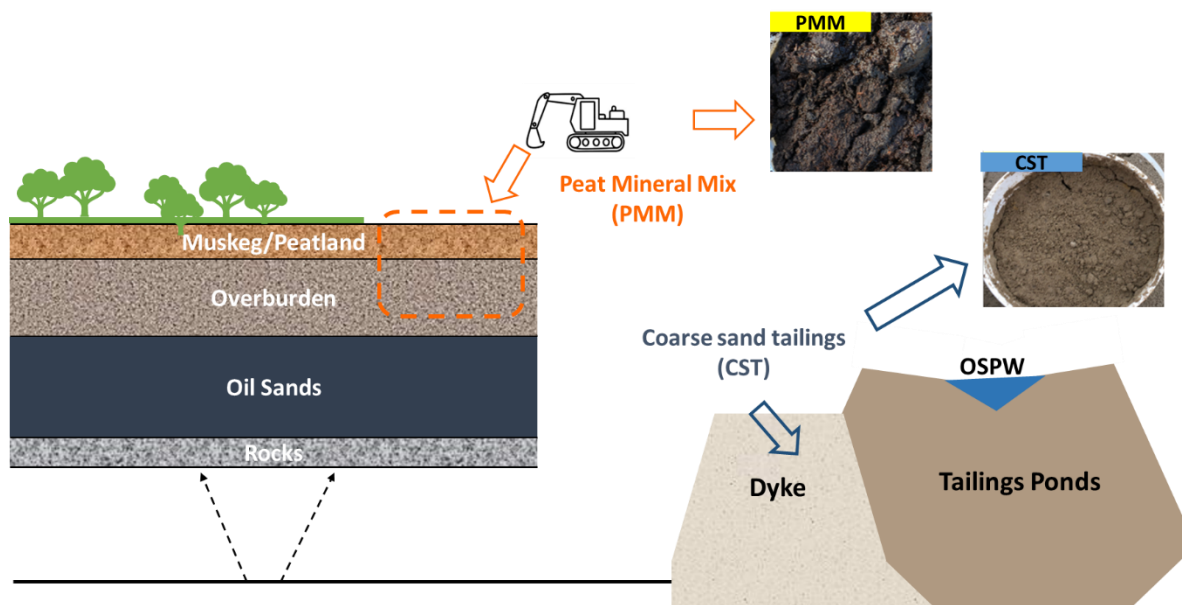


Figure 3.1: Scheme for the source of the CST and PMM.

## 3.2 Materials and methods

### 3.2.1 Reagents

NAs model compounds dodecanoic acid (DDA;  $\geq 99\%$ ), decanoic acid (DA;  $\geq 98\%$ ), 5-phenylvaleric acid (PVA; 99%), cyclohexanepentanoic acid (CHPA;  $\geq 98\%$ ), and cyclohexanecarboxylic acid (CHA;  $\geq 98\%$ ) were purchased from Sigma Aldrich (Germany). All NA solutions were prepared in buffer by 5 mM analytical grade sodium bicarbonate ( $\text{NaHCO}_3$ ;  $\geq 97.7\%$ ; Fisher Scientific) to keep the pH similar to real OSPW, around 8.5. Ultrapure water was produced using a Millipore Synergy with UV ultrapure water system.

### 3.2.2 Material preparation

The coarse sand tailings and the peat-mineral mix were obtained from an Alberta oil sands industry and stored in a cold room (at 4 °C) prior to preparation. All the raw samples were air-dried at room temperature (20 °C) until constant mass was observed. The air-dried samples were

manually grounded by mortar and pestle and passed through 2-mm mesh. Then, the well-prepared samples were stored in glass containers for experimental use (Figure S7).

### 3.2.3 Characterization of materials

The Brunauer-Emmett-Teller (BET) surface areas were determined by adsorption of nitrogen onto samples at 77 K by Autosorb iQ. The scanning electron microscopy (SEM) was conducted using Zeiss Sigma 300 VP-FESEM to observe the surface morphology of the samples. The chemical composition was investigated by the energy-dispersive X-ray spectroscopy (EDX). The phase composition was carried out at room temperature using a Rigaku X-ray diffraction spectroscopy (XRD) Ultima IV with Cobalt tube at 38 kV and 38 mA as the radiation source. The functional groups were investigated by Fourier-transform infrared spectroscopy (FTIR) using a Nicolet 8700 FTIR Spectrometer. The pH and electrical conductivity (EC) were investigated using the pH meter and EC meter following the US EPA standard method (EPA 2004) and the method by Rayment (2011). The point of zero charge (PZC) of the samples was determined by the salt addition method (Bakatula et al. 2018). The elemental analysis and cation exchange capacity (CEC) were performed by inductively coupled plasma-optical emission spectroscopy (ICP-OES) (Skinner et al. 2001). The total organic carbon (TOC) was determined by using the Thermo Flash 2000 Organic Elemental Analyzer. The clay, silt, and sand composition were investigated by LS 13320 Beckman Coulter Laser Particle Size Analyzer.

### 3.2.4 Adsorption experiments

Adsorption kinetics can help evaluate the adsorption process and viability in targeting specific pollutants. The kinetics parameters behind the mass transfer of adsorbent from the aqueous phase to the solid phase of adsorbent were evaluated based on the concentration of adsorbate at

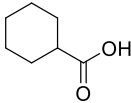
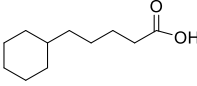
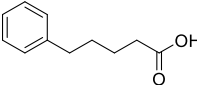
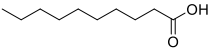
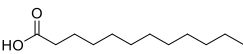
different times until equilibrium was reached (equilibrium time), which provided an insight into the rate-limiting mass transfer mechanism (Worch 2012). To evaluate the kinetics of the batch-scale adsorption process of the target organic pollutant by the reclamation materials, dodecanoic acid (Lauric Acid or DDA) was selected as the NAs model compound. The basic properties of DDA are shown in Table 3.1. The reclamation materials are very complex, thus, the single model compound as the target compound can help better understand the adsorption process. For the experiments, 30 mL of a 25 mg/L DDA solution (with 5 mM NaHCO<sub>3</sub> as buffer) was transferred into Erlenmeyer flasks and a specific mass of adsorbent materials was added to achieve the desired adsorbent dosage. The flasks were sealed with parafilm and placed on the platform shaker set at 200 rpm and room temperature, in which the contact time varied as follows: 0, 0.5, 1, 2, 4, 6, 12, 18, 24, 48, 72 and 96 h, or until equilibrium was reached. Equilibrium of organic compounds using similar natural material as adsorbent was reached between 24 and 48 h (Bošković et al. 2020; Li et al. 2019; Li et al. 2020; Rao et al. 2020). After the noted contact time, the suspension was centrifuged at 7000 rpm for 10 min and the supernatant was filtered by a 0.2 µm Nylon filter to collect the liquid. The samples were analyzed by UHPLC-SQMS to determine the DDA concentration. A schematic of the procedure is presented in Figure S8.

The adsorption isotherm plot describes the phenomenon that governs the movement of adsorbate from bulk solution to adsorbent phase at constant pH and temperature (Foo and Hameed 2010; Isiuku et al. 2021). The adsorption isotherm models also provide insight into the adsorption mechanism, adsorbate surface properties, and the affinity between adsorbate and adsorbent (Al-Ghouti and Da'ana 2020; Isiuku et al. 2021). The isotherm study applied a range of adsorbent dosages to achieve the adsorbent concentrations of 0 to 400 g/L for the CST sample and 0 to 10

g/L for the PMM sample and the contact time should be the equilibrium time determined in the kinetics study. The other experimental setting should follow the same as the kinetics study. After a certain contact time, the separation step should follow the same procedure as the other batch adsorption studies. The DDA concentration was measured by UPLC-SQMS.

Adsorption study with NAs mixture solution was also performed on batch-scale. Five NAs model compounds were selected to create the mixture solution and the basic properties are shown in Table 3.1. The concentration of each NA model compound was 10 mg/L (with 5 mM NaHCO<sub>3</sub> as buffer). 200 g/L of CST and 10 g/L of PMM were applied to the mixture adsorption experiment and contact time was from 0 to 96 h. The other experimental setup followed the same procedure as the other batch adsorption study. The concentrations of target NAs model compounds were measured by UHPLC-SQMS. All experiments were performed in triplicates.

Table 3.1: The name, formula, molecular weight and structure of selected model compounds.

Structure	Abbreviation	Name	Formula	M.W. (g/mol)	pKa at 20 °C
	CHA	Cyclohexanecarboxylic acid	C <sub>7</sub> H <sub>12</sub> O <sub>2</sub>	128.17	4.82
	CHPA	Cyclohexanepentanoic acid	C <sub>11</sub> H <sub>20</sub> O <sub>2</sub>	184.27	-
	PVA	5-phenylvaleric acid	C <sub>11</sub> H <sub>14</sub> O <sub>2</sub>	178.23	4.94
	DA	Decanoic acid	C <sub>10</sub> H <sub>20</sub> O <sub>2</sub>	172.6	4.90
	DDA	Dodecanoic Acid (Lauric Acid)	C <sub>12</sub> H <sub>24</sub> O <sub>2</sub>	200.322	5.30

### 3.2.5 Analytical methods

The concentration of the NAs model compounds was measured by an ultra-performance liquid chromatography coupled with a single quadrupole mass spectrometry (UPLC-MS) (SQ Detector 2, Waters). Chromatographic separations were performed on an ACQUITY UPLC® BEH C18 column (1.7  $\mu\text{m}$ , 2.1  $\times$  50 mm, Waters, USA) with mobile phases of 4 mM ammonium acetate and 0.1% acetic acid in water (A), and acetonitrile (B). The elution gradient was 0-0.5 min, 5% B; 0.5-3 min, increased from 5% to 95% B; then returned to the initial condition 95% B at 3.1 min and held for 1.5 min to equilibrate the column with a flow rate of 0.4 mL/min. The column was controlled at 40 °C, and the injection volume was 5  $\mu\text{L}$ . Data were acquired using MassLynx (Waters, UAS) and processed using TargetLynx (Waters, UAS). The detailed parameters of the analysis can be found in Table S7 in Appendix B.

## 3.3 Results and discussions

### 3.3.1 Material characterization

#### 3.3.1.1 Physicochemical properties

The physicochemical properties of CST and PMM are listed in Table 3.2. The pH of the target solution in all adsorption experiments was  $\sim$ 8.5, which is similar to the pH of real OSPW. CST displayed an alkaline pH (about 9), and PMM had a neutral pH of around 6.8. PZC was determined based on the method indicated by Bakatula et al. (2018). With the pH of the solution larger than the PZC of CST and PMM, the material surface should be negatively charged. Considering with the pKa of targeted NAs, repulsion forces might exist between the materials and the NAs compounds (Harrison et al. 2013). The non-saline nature of CST and PMM could be indicated by the EC values at low levels ( $< 1$  ms/cm) (Rawat et al. 2022). PMM material has higher

TOC, EC, and CEC values compared to CST material. The higher CEC could be attributed to the organic content or the clay minerals, which might lead to a better adsorption capacity (Hermosin et al. 1993; Ramachandran and D'Souza 2013). CST was identified as a sandy texture material (96% of sand), while PMM has 9.7% of clay, 41% of silt, and 49% of sand. According to the BET analysis, CST has a smaller surface area and pore volume compared to PMM (Table 3.2).

Table 3.2: Physicochemical properties of CST and PMM.

Parameter	CST	PMM
pH	9.03	6.78
PZC	6.90	6.38
EC ( $\mu\text{s}/\text{cm}$ )	97.8	115
CEC ( $\text{cmol}/\text{kg}$ )	1.64	225
TOC (%)	0.180	38.78
Al ( $\text{mg}/\text{kg}$ )	526.81	1732.4
Ca ( $\text{mg}/\text{kg}$ )	573.33	46858
Fe ( $\text{mg}/\text{kg}$ )	949.00	2107.5
Mg ( $\text{mg}/\text{kg}$ )	132.80	3335.6
Si ( $\text{mg}/\text{kg}$ )	517.91	732.57
Surface area ( $\text{m}^2/\text{g}$ )	0.51	2.0
Pore volume ( $\text{cc}/\text{g}$ )	0.0010	0.0050
Clay % ( $<5\mu\text{m}$ )	1.8	9.7
Silt % ( $5\text{-}50\mu\text{m}$ )	1.9	41
Sand % ( $>50\mu\text{m}$ )	96	49

### 3.3.1.2 SEM and EDX analysis

SEM and EDX analysis were performed to evaluate the morphology and the elemental composition of CST and PMM. The SEM images illustrated that CST and PMM have non-homogeneous shapes (Figure 3.2). CST particles showed much larger particle size compared to PMM. With increasing magnification, the heterogeneous solid surfaces of CST and PMM were

observed. Many fine particles were found dispersed on the larger CST particle surface (Figure 3.2 c), which could be small clay dishes attached to quartz (Jeong and Nousiainen 2014; Patra et al. 2020). Compared to CST, PMM showed rough and porous surfaces which were formed by irregular flake structures (Figure 3.2 d). According to Aminur et al. (2011), the soil with high organic content is usually structured with more porous space. Based on the SEM images, the different morphology properties of the two reclamation materials could lead to different adsorption behaviour. Considering the higher surface area, pore volume, and TOC, PMM material could have better adsorption capacity than CST material.

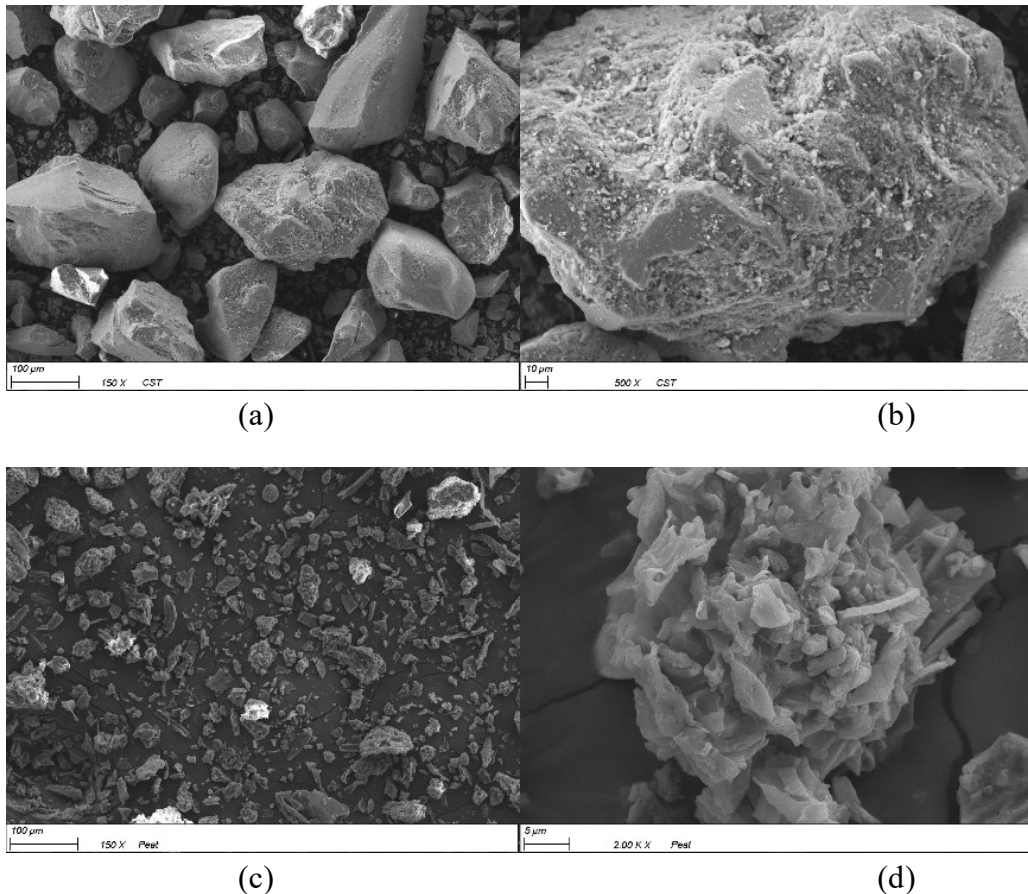


Figure 3.2: SEM images of CST (a) and (b); PMM (c) and (d)

By showing the atomic percentages, EDX outcomes indicated that CST was mainly composed of carbon, oxygen, and silicon (Figure S9). The results matched the texture analysis with the high composition of quartz. The presence of aluminum (Al) could be attributed to the presence of kaolinite. On the other hand, carbon and oxygen were the major elements identified in PMM, and small amounts of Ca, Mg, Si, P, and S were also identified.

### *3.3.1.3 FTIR and XRD analysis*

For the functional groups common to PMM and CST samples, most part of the absorbance happened at the wavenumber range from 400 to 4000  $\text{cm}^{-1}$ , which was named as mid-infrared region (Stuart 2004). It can be generally split into three parts: the “Fingerprint region” with the wavenumber from 400 to 1500  $\text{cm}^{-1}$ ; double bounded groups region between 1500 to 2500  $\text{cm}^{-1}$ , and “R-H region” between 2500 to 4000  $\text{cm}^{-1}$  (Krumins et al. 2012; Stuart 2004).

In the clay mineralogy of CST material, peaks at 3620  $\text{cm}^{-1}$  and 3697  $\text{cm}^{-1}$  correspond to the OH groups, signifying the presence of kaolinite. This was further confirmed by the XRD results shown in Figure 3.3 (a). Le Guillou et al. (2015) and Li et al. (2020) both identified kaolinite by the same absorption bands identified by FTIR spectra. Generally, the internal kaolinite-OH groups were recognized at 3620  $\text{cm}^{-1}$  and the internal surface OH groups were characterized at 3670  $\text{cm}^{-1}$  (Russell and Fraser 1994). The peak observed at 770, 796, 1080, 1799, and 1890  $\text{cm}^{-1}$  were due to quartz (Le Guillou et al. 2015; Yan et al. 2021). The band around 770  $\text{cm}^{-1}$  could be the Si-O-Al stretching vibrations and the Si-O stretching vibrations were detected at 695  $\text{cm}^{-1}$ , indicating the presence of the Si-O-Si network of quartz (Abdul Karim et al. 2020). The absorption detected from 2820 to 3000  $\text{cm}^{-1}$  could be related to organic matter (Le Guillou et al. 2015).

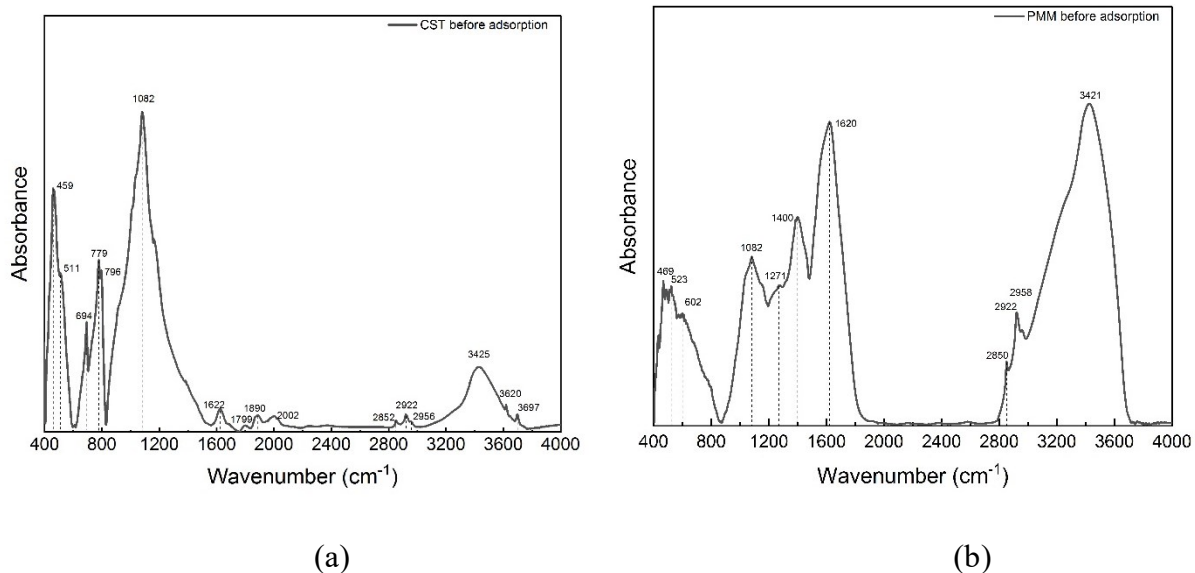


Figure 3.3: FTIR results of CST (a) and PMM (b).

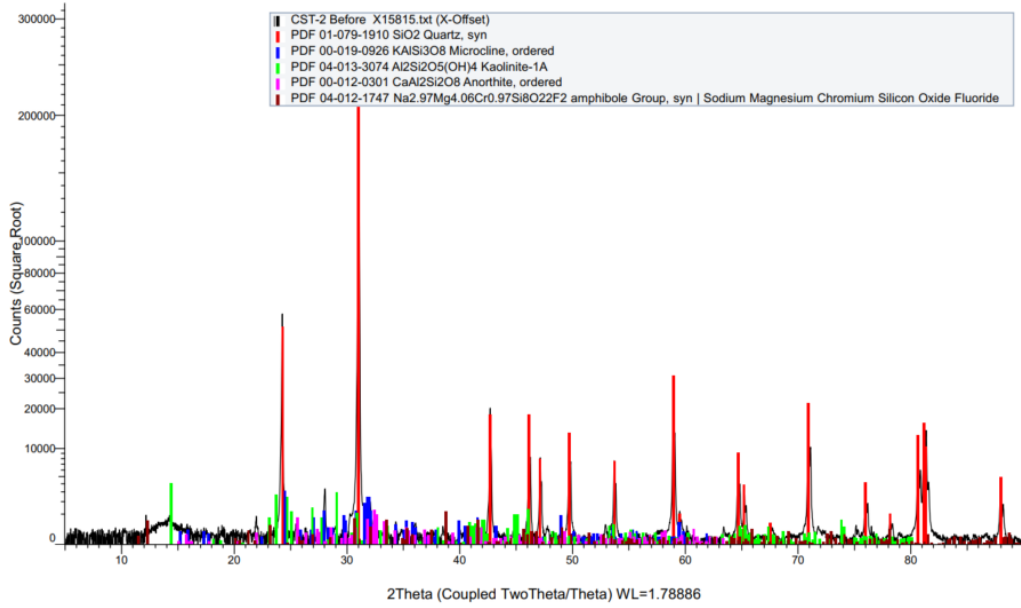
For both CST and PMM, the strong absorbance at  $3400\text{ cm}^{-1}$  was observed (Figure 3.3), representing the O-H stretching band from intermolecular hydrogen bonds formed by water molecules (Deng et al. 2022; Ryan and Huertas 2009). According to Xing et al. (2019), the absorption bands between  $2800\text{-}3000\text{ cm}^{-1}$  likely indicate hydrophobic properties, whereas the bands observed between  $1600\text{-}1800\text{ cm}^{-1}$  are correlated with hydrophilic characteristics. Similar to Drollinger et al. (2020) and Devangsari et al. (2022), aliphatic groups (C-H, C-H<sub>2</sub>, C-H<sub>3</sub>) were characterized as one of the major functional groups in both CST and PMM at  $2850$ ,  $2922\text{ cm}^{-1}$  and  $2956\text{ cm}^{-1}$ , which should contribute to the hydrophobicity of the material. The peak around  $1620\text{ cm}^{-1}$  could be attributed to various factors such as the characteristic COO<sup>-</sup> stretching frequency of the carboxylate ions, the C=C stretching of aromatic rings, the C=O vibrations of carboxylic acids/anions and amides, or N-H angular deformation (Celi et al. 1997; Fernandes et al. 2010). In addition, the CEC contents closely correspond with bands around  $1600\text{-}1800\text{ cm}^{-1}$  (Celi et al. 1997). PMM has a higher peak at  $1620\text{ cm}^{-1}$ , which meets agreement with the result of a higher

CEC value. Besides, for PMM, the stretching of C-O bonds in carboxylic groups were observed at  $1271\text{ cm}^{-1}$ , and the C-O-H bonds in carboxylic acids was detected at  $1385$  and  $1400\text{ cm}^{-1}$  (Krumins et al. 2012). The peak at  $1082\text{ cm}^{-1}$  could be the C-O stretching of the polysaccharides (Fernandes et al. 2010). For the fingerprint region of PMM, the peak around  $470\text{ cm}^{-1}$  could be assigned to the Si-O-Si bending vibration (Chapman et al. 2001), or the substituted aromatics and unsaturated aliphatic chains (Biester et al. 2014; Wei et al. 2017). Compared to CST, PMM showed stronger peaks for both regions of hydrophobic and hydrophilic functional groups, which could be beneficial for the adsorption of NAs.

To analyze the main mineral composition of CST and PMM material, the XRD spectra were carried out to identify different phases (Figure 3.4). The XRD outcomes of CST agreed with the texture analysis with the strong peak detected for quartz. Additionally, microcline, kaolinite, and anorthite were presented in CST materials. The organic amorphous peak was identified clearly in PMM (Figure 3.4 b). On the other hand, except the same mineral component as CST (quartz, microcline, and kaolinite), the presence of albite and clinocllore were also detected in PMM.

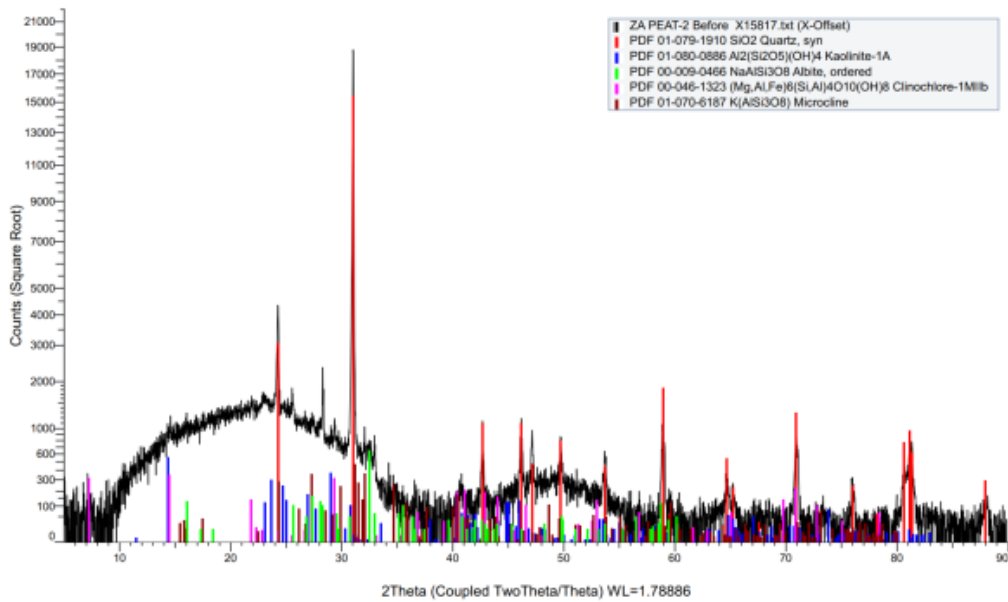
In order to study the adsorption mechanism, CST and PMM were subjected to FTIR, XRD, and SEM-EDX analysis after the adsorption process to investigate the changes in certain properties compared to the raw material. The results are shown in Section 2.3.4 and Supplementary Information.

(Coupled TwoTheta/Theta)



(a)

(Coupled TwoTheta/Theta)



(b)

Figure 3.4: XRD results of CST (a) and PMM (b)

### 3.3.2 Single NA model compound adsorption

#### 3.3.2.1 Kinetics study

The DDA concentration data for different retention times were fit to different kinetics models to obtain the best fitted model (Table 3.3). As shown in Figure S10 (a), the concentration decreased as the contact time increased from 0 to 24 h. After 24 h, the  $C/C_0$  remained constant, which means the adsorption process by CST reached the equilibrium state. The equilibrium time for the adsorption of DDA by CST materials is 24 h. According to Figure 3.5 (a) and Figure S11, the dependence of  $t/q_t$  versus  $t$  showed a clear straight-line relation, indicating the adsorption process of DDA on CST materials followed the empirical PSO kinetics. The adsorption capacity at equilibrium time was 0.05 mg/g. Additionally, the PSO rate constant,  $k_2$ , is calculated as 2.22 g/mg/h. Khan et al. (2023) studied the adsorption process of atrazine onto a sandy texture soil and the amended soil by farmyard manure and vermicompost, resulting in the adsorption efficiency at equilibrium (24 h) as 38%, 45%, and 48% respectively, meanwhile, the kinetics data best fitted to the PSO model. Rauf et al. (2008) investigated the adsorption behaviour of coomassie blue, malachite green, and safranin orange on locally available sand in the south-eastern region of UAE, reporting that the kinetics for the three dyes all followed the PSO model.

Based on the kinetics parameters shown in Table 3.3, the adsorption process of DDA on PMM could be described by the empirical PFO kinetics and IPD model. Compared to the PFO model, the calculated adsorption capacity using the IPD model,  $q_{e\_IPD}$ , matched more closely with the results obtained from experiments ( $q_{e\_exp} = 2.37$  mg/g), indicating that the adsorption process of DDA onto PMM was more appropriately fitted with the IPD model. As seen in Figure 3.5 (b), the points were not linear over the whole time range, indicating that more than one processes

affected the adsorption process. Weber and Huang (1996) reported a three-domain model to describe the adsorption process of the hydrophobic organic contaminants on soils and sediments, which include the exposed mineral domain, the amorphous soil organic matter domain, and the condensed soil organic matter domain. It was also supported that the humic and fulvic materials (generally present in peat materials) tend to form monolayer on the mineral surfaces of soils and the hydrophobic organic contaminant need to penetrate the hydrophilic shells and be trapped in the hydrophobic core of the macromolecular organic aggregates (Murphy et al. 1990; Weber and Huang 1996). Similarly, the DDA adsorption process on PMM could be represented by two stages (Figure 3.5 b), where the first stage has a slower rate constant,  $K_{p1}$ , equals to  $0.24 \text{ mg/g/min}^{0.5}$  and that of the second phase,  $K_{p2}$ , is  $0.54 \text{ mg/g/min}^{0.5}$ .

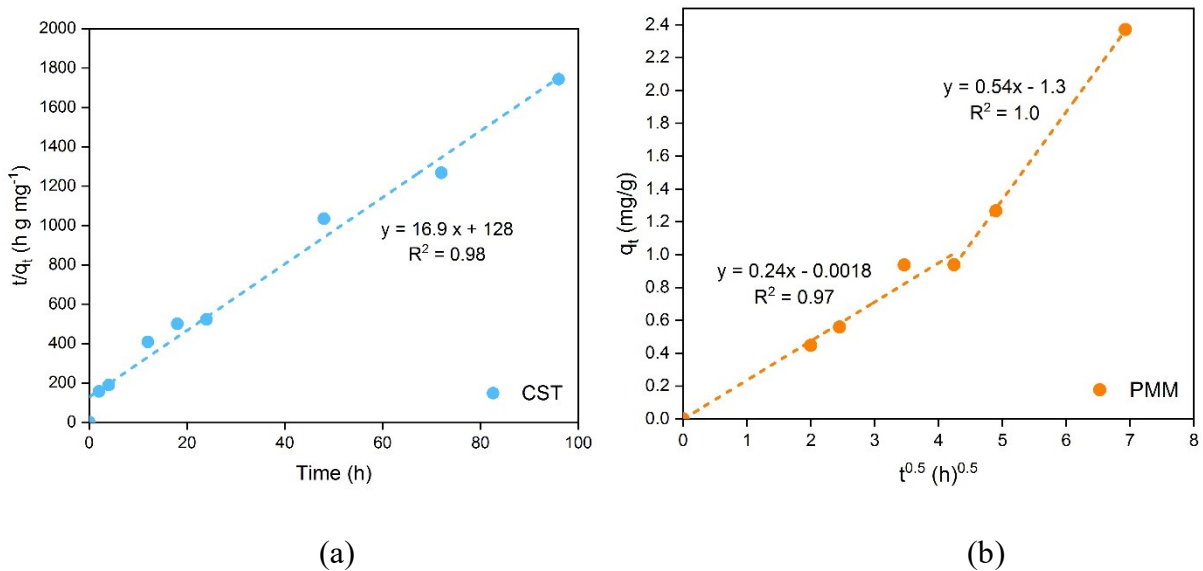


Figure 3.5: Kinetics of DDA adsorption by CST (a) and PMM (b).

Table 3.3: Kinetics models and parameters for DDA adsorption by CST and PMM.

Models		Parameters	DDA adsorption by CST	DDA adsorption by PMM
Empirical kinetics	Pseudo-first order (PFO)	$q_{e\_PFO}$ (mg/g)	0.038	2.1
		$k_1$ (h <sup>-1</sup> )	0.032	0.025
		$R^2$	0.75	0.94
	Pseudo-second order (PSO)	$q_{e\_PSO}$ (mg/g)	0.059	2.4
		$k_2$ (h <sup>-1</sup> )	2.2	0.031
		$R^2$	0.98	0.70
Equilibrium isotherm kinetics	Langmuir	$q_{max}$ (mg/g)	-0.021	6.73
		$K_L$ (L/mg)	-0.039	0.40
		$R^2$	0.83	0.88
	Freundlich	$K_f$ [(mg/g)(mg/L) <sup>1/n</sup> ]	$1.1 \times 10^{-7}$	2.7
		$1/n$	4.5	0.31
		$R^2$	0.98	0.90
Transport kinetics	Intra-particle diffusion (IPD)	$q_{e\_IPD}$ (mg/g)	0.037	2.4
		$k_p$ ((mg/g/h <sup>0.5</sup> ))	0.0050	0.24 ( $k_{p1}$ ); 0.54 ( $K_{p2}$ )
		$R^2$	0.84	0.97 (Phase 1); 1.00 (Phase 2)
	Elovich	$q_{e\_Elovich}$ (mg/g)	0.042	2.0
		$\alpha$ (mg/g/h)	1.5	2.0
		$\beta$ (g/mg)	57	1.4
	$R^2$	0.80	0.84	

### 3.3.2.2 Isotherm study

In the isotherm analysis, adsorption data were evaluated using both the Langmuir and the Freundlich equilibrium models (Figure S13 and Table 3.3). The isotherm of DDA adsorption by CST and PMM both fitted with the Freundlich model, with the  $R^2$  as 0.98 and 0.90, respectively (Figure 3.6). In contrast, the simulation results of the Langmuir isotherm model were not satisfactory, suggesting that the adsorption sites were not limited for monolayer adsorption and the adsorption energy was not distributed homogeneously (Chen et al. 2021). Considering the complex

and heterogeneous surfaces shown by the SEM images of CST and PMM, the adsorption process of DDA could be adequately explained by the Freundlich model. The adsorption of DDA on CST and PMM should be considered as a multilayer adsorption process, which means that the adsorbates could accumulate on the surface of the adsorbents in multilayers. Moreover, higher value of  $K_f$  were observed with DDA adsorption onto PMM, implying a greater adsorption tendency toward the PMM compared to CST, while the corresponding  $1/n$  value is 0.31, indicating the favorable adsorption. The isotherm results of CST and PMM agreed with several adsorption studies using natural soils with a heterogenous nature as adsorbent. For instance, Pateiro-Moure et al. (2009) reported the adsorption process of three herbicides on natural and processed soils with Freundlich isotherm as the best fitted model. Previously, Wei et al. (2017) investigated the adsorption behaviour of perfluorooctane sulfonate by different soils, and the adsorption isotherm followed the Freundlich model with relatively high correlation coefficients for all soils, which make sense considering the heterogeneous and complex nature of the studied soils.

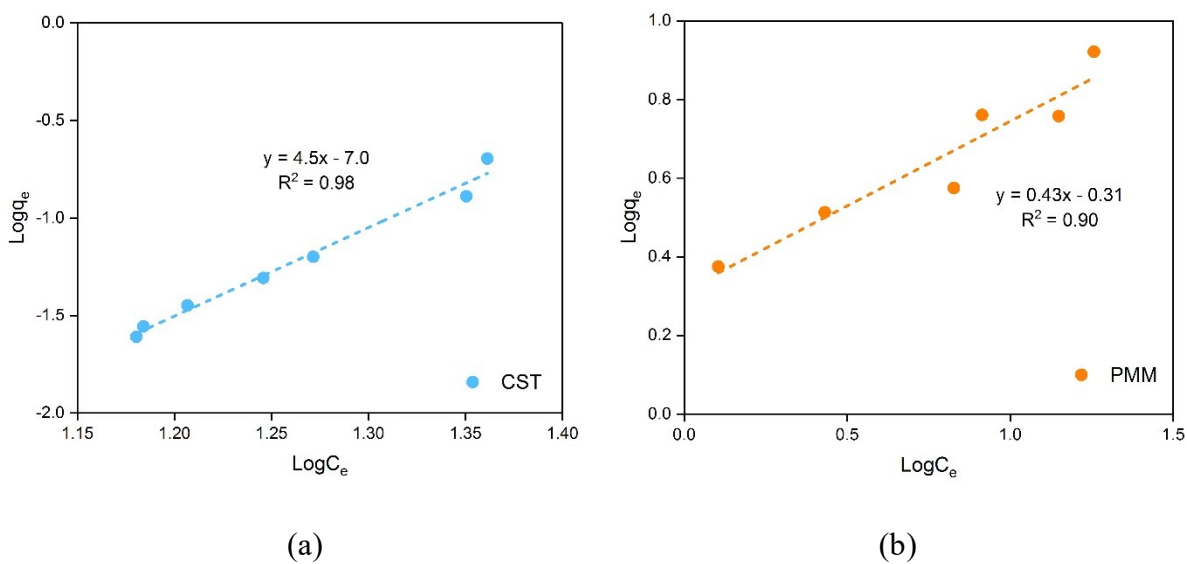


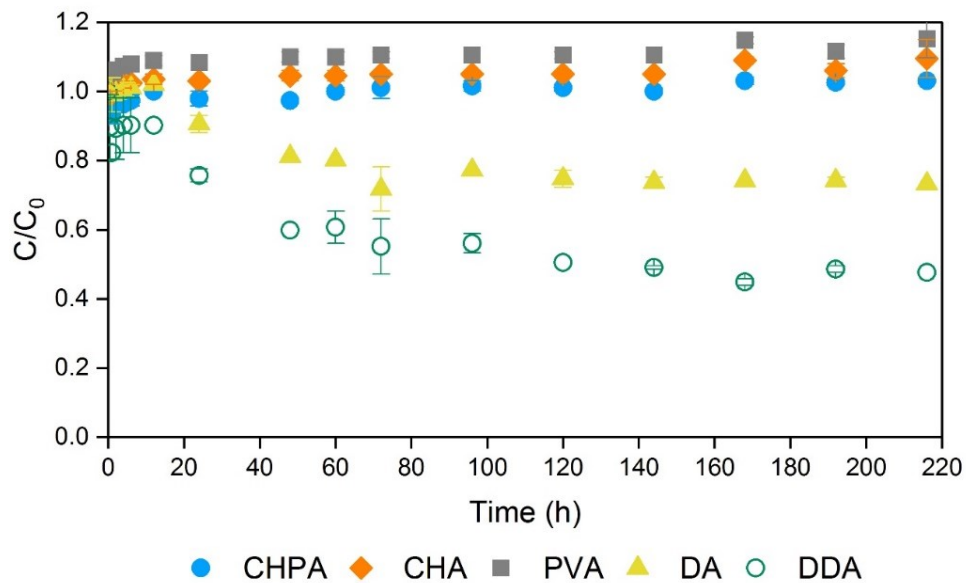
Figure 3.6: The linearized Freundlich models for DDA adsorption by CST (a) and PMM (b).

### 3.3.3 Adsorption behavior towards NAs model compound mixture solution

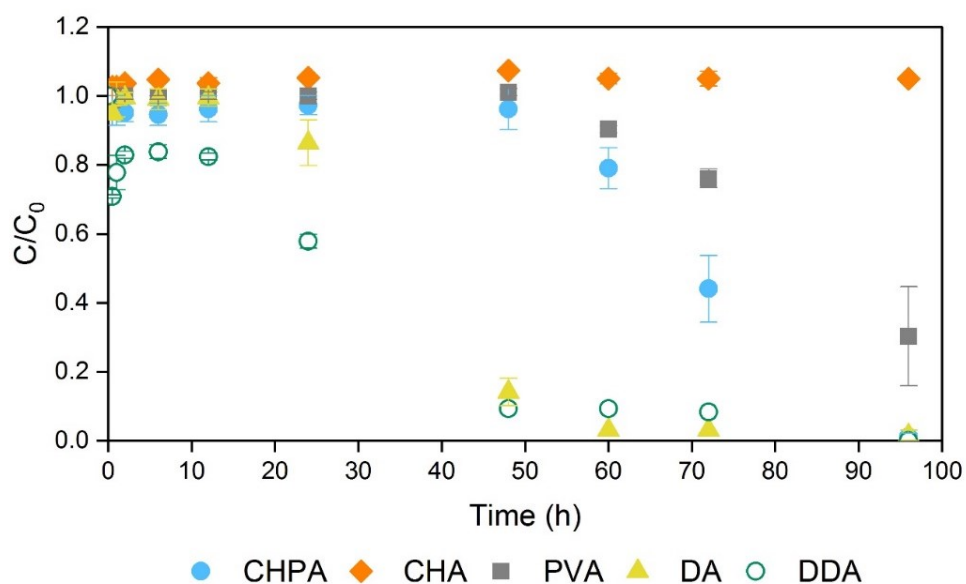
In order to investigate the adsorption performance of CST and PMM towards different NAs, a mixture solution of five NAs was applied in the experiment. Five NAs have different structures: CHA has a saturated carbon ring and a carboxylic group; CHPA also has a saturated carbon ring and a branched-chain on the ring with a carboxylic group; PVA has a very similar structure to CHPA but with an aromatic ring; DA is a straight-chain saturated NAs compound with 10-carbon atom and the carboxylic group is at one end of the chain; DDA has a longer chain with 12-carbon atom.

After 24 h adsorption by 200 g/L CST, the concentrations of CHA, CHPA, and PVA have no significant change. However, the removals of DA and DDA finally reached about 25% and 50% (Figure 3.7 a). The adsorption of DA and DDA by CST followed the PSO kinetics (Figure S14). The adsorption equilibrium time of DA and DDA was 120 h. Figure 7 (a) shows the CST adsorption capacity ( $q_e$ ) of DA at equilibrium is 0.01 mg/L and the  $q_e$  of DDA is 0.03 mg/g. Compared to the mono-compound adsorption experiment in the kinetics study, the equilibrium adsorption capacity of DDA by CST was decreased, and the time to reach the equilibrium stage was increased (Table S8). The reason may be explained by two aspects: for the NAs solution, adsorption competition likely occurred between DA and DDA, and the initial concentration of DDA in the mixture (10 mg/L) was less than that in the mono-compound adsorption experiment (25 mg/L). Previously, the initial concentration of target pollutants had an obvious influence on the adsorption capacity (Moustafa et al. 2014). Considering the straight-chain structure of DA and DDA, the results indicated that the straight-chain structure is easier to adsorb onto the CST material. Besides, DA and DDA are nonpolar molecules, and the hydrophobic interactions likely

made DA and DDA easy to remove (Sun 2022). By comparing DA and DDA, DDA achieved a better removal by CST. This may demonstrate that adsorption on CST increases with increasing the alkyl chain length. Zhanget al. (2013) previously found that for perfluoroalkyl surfactants with C5 to C15, the adsorption on sludge increases with increasing alkyl chain length. Besides, Wang et al. (1999) concluded that the chain length of adsorbates could be a major influence on the adsorption behavior as the longer chain length of the adsorbate promotes the adsorption onto Na-kaolinite by enhancing both hydrophobic interaction and the cation exchange. Li and Gallus (2007) also reported that longer chain length strengthens the hydrophobic interaction during the adsorption process.



(a)



(b)

Figure 3.7: NAs mixture adsorption (a) by CST (b) by PMM.

After 96 h adsorption by 10 g/L PMM,  $C/C_0$  of each of the NAs model compounds decreased significantly, except for CHA (Figure 3.7 b). CHPA, DA, and DDA achieved 100% removal at 96 h by PMM, while PVA achieved 70% removal at 96 h. Figure 3.8 (b) shows that the adsorption equilibrium was reached for DA and DDA, and the kinetics followed the IPD model (Figure S15). The adsorption of DA by PMM reached equilibrium at 60 h with the equilibrium capacity of 0.96 mg/g. For DDA adsorption by PMM, the equilibrium time was 48 h with  $q_e$  as 1 mg/L. For PVA and CHPA, the equilibrium was not reached until 96 h. Compared to the mono-compound adsorption experiment in the kinetics study, the equilibrium adsorption capacity of DDA by PMM decreased as well, and the time to reach the equilibrium stage was the same. This might be caused by the adsorption competition in the mixture solution and the change in the initial concentration of DDA (Ju and Young 2005). On the other hand, the fast adsorption of DA and

DDA by PMM was mainly observed from 12 to 48 h. The fast removal of PVA and CHPA mainly occurred from 48 to 96 h. This may also demonstrate that straight-chain structure compounds were more competitive for adsorption compared to the compounds with other structures. Moreover, the adsorption capacity by PMM at 96 h for CHPA (0.92 mg/g) is larger than that of PVA (0.66 mg/g). Paredes-Doig et al. (2014) found that the adsorption process on activated carbon depends not only on the porosity and functional groups of the adsorbent but also on the properties of adsorbate including the formula weight of the aromatic compound, solubility, number and type of substituting groups in the aromatic ring, acidity (pKa), and the adsorbate-adsorbent interaction. It is assumed that the adsorption performance of different NAs may also depend on the molecular weight, solubility, pKa, and the interaction with certain functional groups on different materials.

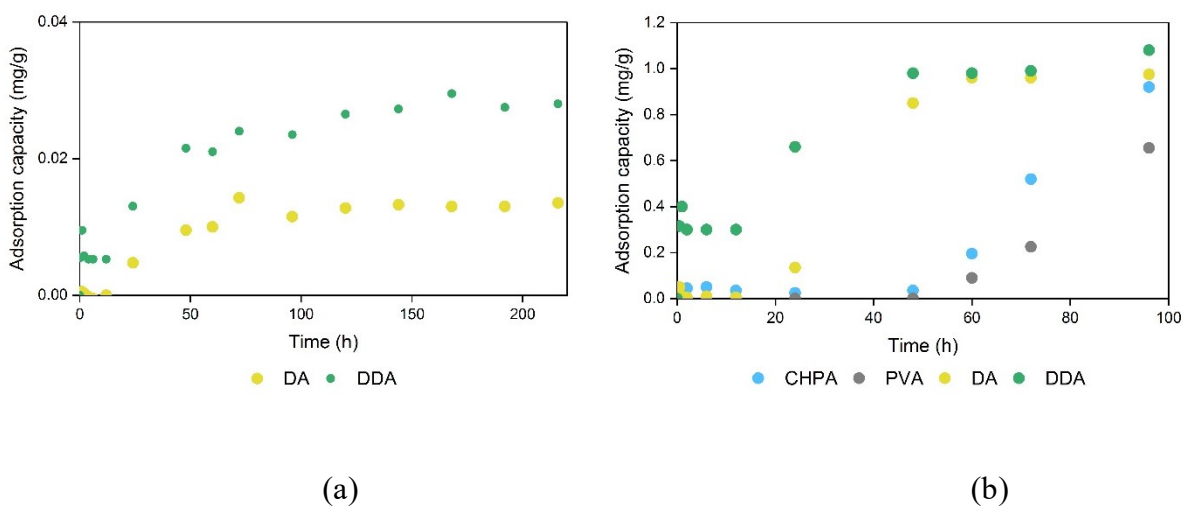


Figure 3.8: NAs mixture adsorption capacity (a) by CST (b) by PMM.

### 3.3.4 Mechanism insight

For both CST and PMM, possible adsorption mechanism could be discussed from several aspects, including the kinetics and isotherm models, and the characteristics changes of adsorbate

materials after the adsorption process.

Based on the adsorption performance towards NAs mixture by CST and PMM, both of them showed preferential removal of hydrophobic compounds. CST only showed removal to DDA and DA, while PMM first showed fast adsorption of DDA and DA, then followed by other more hydrophilic compounds as CHPA and PVA. The hydrophobic fraction of adsorbent showed affinity with hydrophobic compounds in aqueous solution (Zhou et al. 2011). Tang et al. (2010) indicated that high hydrophobic contaminants could be effectively removed by adsorbent with low surface polarity. Herein, it could be assumed that the hydrophobic fraction of CST and PMM primarily contribute to the adsorption process of the NAs. Figure S16 shows the changes in FTIR spectra after the adsorption process by shifted peaks. The CH<sub>3</sub> stretching peak at 2956 cm<sup>-1</sup> shifted to 2960 cm<sup>-1</sup> for the post-adsorption CST material. For PMM, the peak of aliphatic groups (at 2850, 2922, and 2958 cm<sup>-1</sup>) shifted to 2852, 2920, and 2960 cm<sup>-1</sup> after the adsorption of NAs. The shifted peaks of hydrophobic groups supported that the hydrophobic interaction should be one of the important mechanisms involved in the adsorption process. Moreover, Figure S17 showed the overlaid XRD results of before and after adsorption materials, in which decreased intensity of quartz and several mineral compositions such as kaolinite and microcline were observed in post-adsorption CST and PMM. It could be evidence that the mineral composition in CST and PMM contributed to the adsorption process (Shen 1999). It was found that the presence of the hydrophobic siloxane groups on kaolinite and other clay minerals in soils could help retain the hydrophobic organic chemicals even if with a low concentration of organic carbon (Li and Wei 2022; Moyo et al. 2014). Similarly, Li et al. (2020) indicated that hydrophobic surfaces in clayey minerals mainly contribute to the adsorption of toluene on soils by hydrophobic interaction.

The adsorption performance of CST and PMM towards DDA and DA in the mixture solution could be further explained by the hydrophobic interaction. Based on the results shown in Figure 3.8, the adsorption of DDA and DA showed two stages. The first stage showed higher adsorption rates, which could be attributed to the abundance of free adsorption sites at the beginning. The free sites and the target compounds formed hydrophobic interaction rapidly. Then, the second stage showed a slower increase in the adsorption capacity, during which the adsorbate needed to encounter more resistance and transport deeper to reach the available free sites. Zhou et al. (2011) reported a similar two-phase adsorption process of bisphenol A (BPA) on peat by hydrophobic interaction as the main driving force.

Furthermore, the absorption peak around  $3400\text{ cm}^{-1}$  shifted for both CST and PMM after adsorption (Figure S16), which could indicate that weak hydrogen bonding might also contribute to the adsorption process of NAs (Li et al. 2020). Therefore, the adsorption mechanism of DDA onto CST and PMM should include both hydrophobic interaction and hydrogen bonding (Figure 3.9). Additionally, the low surface area and porosity of CST implied that physisorption is not likely the key mechanism. Due to the fact that all adsorption processes occurred on CST material followed PSO kinetics models, the adsorption of NAs on CST followed the chemisorption process (Al-Smadi et al. 2019). The best fit for the PSO kinetics model might also indicate that the adsorption rates of NAs on CST were more dependent on the accessible adsorption site than the concentration of the target contaminant in the solution (Khan et al. 2023). On the other hand, the IPD model appropriately described the selected NAs compounds onto PMM (Figure S15). The multilinear plot showed two clear regions, suggesting that the interparticle diffusion step governed the adsorption of NAs on PMM (George William et al. 2018).

PMM showed much better adsorption potential compared to CST, which could be explained by the surface properties. The abundant hydrophobic and hydrophilic functional groups of PMM make it desirable for the removal of a diverse range of NAs with different structures, which matched the results from the adsorption of NAs mixture. Additionally, the relatively higher surface area and porous structure could lead to a better adsorption performance. Besides, the texture results and XRD analysis showed that PMM material has more clay (9.7%) and organic composition (TOC as 38.8%) compared to CST. It was reported that the soils containing higher clayey minerals resulted in higher adsorption capacity, while the organic carbon in soils played a key role in the adsorption of hydrophobic organic chemicals (Li et al. 2020; Moyo et al. 2014).

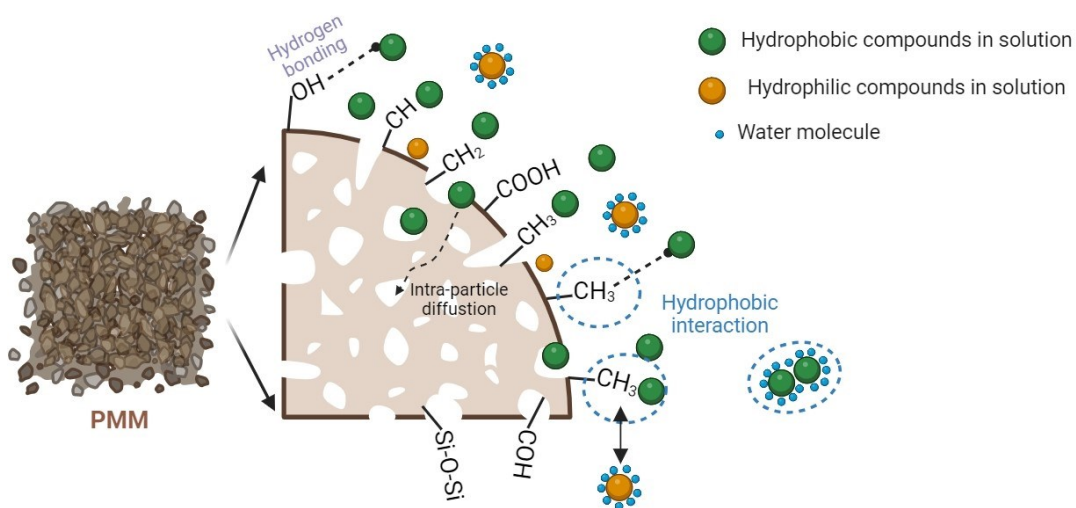


Figure 3.9: Possible adsorption mechanism.

### 3.4 Conclusions

In this study, the adsorption behavior of NAs onto two different reclamation materials was assessed. CST was characterized as a sandy texture material with heterogeneous surfaces and less porous structures. Compared to CST, PMM was identified as an organic-rich reclamation material

with a relatively high surface area and pore volume as well as more clay composition. Additionally, PMM exhibited significant portions of hydrophobic functional groups, leading to a better adsorption potential. According to the adsorption study of DDA, PMM had a stronger adsorption capacity of 2.4 mg/g at equilibrium and nearly 100% removal of DDA was achieved by 10g/L PMM at 48 h. The adsorption kinetics of DDA on CST and PMM best fitted the PSO and the IPD models, respectively. The adsorption isotherm of DDA on CST and PMM could be appropriately explained by the Freundlich model, indicating the occurrence of multilayer adsorption. Only DDA and DA were partially removed by CST from the five NAs mixture solution, while PMM showed more effective adsorption capacity by achieving 100% removal of DDA, DA, and CHPA and 70% removal of PVA in 96 h. NAs like DA and DDA with longer chain structures were more competitive during the adsorption process. Hydrophobic interaction was identified as the predominant adsorption mechanism for NAs on CST and PMM.

Based on the outcomes of this study, PMM material showed great adsorption potential towards NAs related to OSPW. Herein, the reclamation material, PMM, could be suggested as a potential alternative adsorbent for NAs removal from real OSPW as a future application. For instance, wetlands built by PMM could be one possible effective treatment for OSPW. On the other hand, CST also showed some adsorption capacity, especially for the hydrophobic NAs that had long chain structures, it is possible to develop some future applications by CST in combination with other treatment steps. Another potential option is to mix the CST with some other materials like soil amendments to enhance the adsorption capacity.

### 3.5 References

Abdul Karim, M.R., Ul Haq, E., Hussain, M.A., Khan, K.I., Nadeem, M., Atif, M., Ul Haq, A.,

- Naveed, M., and Alam, M.M. 2020. Experimental evaluation of sustainable geopolymer mortars developed from loam natural soil. *Journal of Asian Architecture and Building Engineering*, 19(6): 637-646.
- Al-Ghouti, M.A., and Da'ana, D.A. 2020. Guidelines for the use and interpretation of adsorption isotherm models: A review. *Journal of hazardous materials*, 393: 122383.
- Al-Smadi, B.M., Al Oran, E.H., and Abu Hajar, H.A. 2019. Adsorption-desorption of cypermethrin and chlorfenapyr on Jordanian soils. *Arabian Journal of Geosciences*, 12(15): 465.
- Ali, F.H., Sing, W.L., and Hashim, R. 2010. Engineering properties of improved fibrous peat. *Scientific Research and Essay*, 5(2): 154-169.
- Allen, E.W. 2008. Process water treatment in Canada's oil sands industry: I. Target pollutants and treatment objectives. *Journal of Environmental Engineering and Science*, 7(2): 123-138.
- Aminur, M., Kolay, P., Taib, S., Mohd Zain, M., and Kamal, A. 2011. Physical, geotechnical and morphological characteristics of peat soils from Sarawak. *Inst. Eng. Malaysia*, 72(4): 5.
- Anderson, J., Wiseman, S.B., Moustafa, A., El-Din, M.G., Liber, K., and Giesy, J.P. 2012. Effects of exposure to oil sands process-affected water from experimental reclamation ponds on *Chironomus dilutus*. *Water research*, 46(6): 1662-1672.
- Arthur, J.D., Mark, N.W., Taylor, S., Šimunek, J., Brusseau, M.L., and Dontsova, K.M. 2017. Batch soil adsorption and column transport studies of 2, 4-dinitroanisole (DNAN) in soils. *Journal of contaminant hydrology*, 199: 14-23.
- Bakatula, E.N., Richard, D., Neculita, C.M., and Zagury, G.J. 2018. Determination of point of zero charge of natural organic materials. *Environmental Science and Pollution Research*, 25(8): 7823-7833.
- BBK, K.S.H., and Prasad, A. 2011. Study of Peat Media on Stabilization of Peat by Traditional

- Binders. *Int. J. Phys. Sci*, 6(3): 476-481.
- Benally, C., Messele, S.A., and Gamal El-Din, M. 2019. Adsorption of organic matter in oil sands process water (OSPW) by carbon xerogel. *Water research*, 154: 402-411.
- Bhuiyan, T.I., Tak, J.K., Sessarego, S., Harfield, D., and Hill, J.M. 2017. Adsorption of acid-extractable organics from oil sands process-affected water onto biomass-based biochar: Metal content matters. *Chemosphere*, 168: 1337-1344.
- Biester, H., Knorr, K.-H., Schellekens, J., Basler, A., and Hermanns, Y.-M. 2014. Comparison of different methods to determine the degree of peat decomposition in peat bogs. *Biogeosciences*, 11(10): 2691-2707.
- Bošković, N., Brandstätter-Scherr, K., Sedláček, P., Bílková, Z., Bielská, L., and Hofman, J. 2020. Adsorption of epoxiconazole and tebuconazole in twenty different agricultural soils in relation to their properties. *Chemosphere*, 261: 127637.
- Canada, N.R. 2020. Crude oil facts.
- Celi, L., Schnitzer, M., and Nègre, M. 1997. ANALYSIS OF CARBOXYL GROUPS IN SOIL HUMIC ACIDS BY A WET CHEMICAL METHOD, FOURIER-TRANSFORM INFRARED SPECTROPHOTOMETRY, AND SOLUTION-STATE CARBON-13 NUCLEAR MAGNETIC RESONANCE. A COMPARATIVE STUDY. *Soil Science*, 162(3): 189-197.
- Chapman, S., Campbell, C., Fraser, A., and Puri, G. 2001. FTIR spectroscopy of peat in and bordering Scots pine woodland: relationship with chemical and biological properties. *Soil Biology and Biochemistry*, 33(9): 1193-1200.
- Chen, X., Gu, X., Bao, L., Ma, S., and Mu, Y. 2021. Comparison of adsorption and desorption of triclosan between microplastics and soil particles. *Chemosphere*, 263: 127947.

- Clemente, J.S., and Fedorak, P.M. 2005. A review of the occurrence, analyses, toxicity, and biodegradation of naphthenic acids. *Chemosphere*, 60(5): 585-600.
- Cossey, H.L., Batycky, A.E., Kaminsky, H., and Ulrich, A.C. 2021. Geochemical stability of oil sands tailings in mine closure landforms. *Minerals*, 11(8): 830.
- Deng, X., Jiang, Y., Zhang, M.a., Nan, Z., Liang, X., and Wang, G. 2022. Sorption properties and mechanisms of erythromycin and ampicillin in loess soil: Roles of pH, ionic strength, and temperature. *Chemical Engineering Journal*, 434: 134694.
- Devangsari, I., Nurudin, M., Sartohadi, J., and Karmila, Y. Characteristics of peat functional group in Padang Island, Indonesia. *In IOP Conference Series: Earth and Environmental Science*. 2022. IOP Publishing. p. 012022.
- Drollinger, S., Knorr, K.-H., Knierzinger, W., and Glatzel, S. 2020. Peat decomposition proxies of Alpine bogs along a degradation gradient. *Geoderma*, 369: 114331.
- EPA, U. 2004. SW-846 test method 9045D: soil and waste pH. US EPA, Washington DC.
- Fernandes, A.N., Giovanela, M., Esteves, V.I., and Sierra, M.M.d.S. 2010. Elemental and spectral properties of peat and soil samples and their respective humic substances. *Journal of Molecular Structure*, 971(1): 33-38.
- Foo, K.Y., and Hameed, B.H. 2010. Insights into the modeling of adsorption isotherm systems. *Chemical Engineering Journal*, 156(1): 2-10.
- Frankel, M.L., Bhuiyan, T.I., Veksha, A., Demeter, M.A., Layzell, D.B., Helleur, R.J., Hill, J.M., and Turner, R.J. 2016. Removal and biodegradation of naphthenic acids by biochar and attached environmental biofilms in the presence of co-contaminating metals. *Bioresource technology*, 216: 352-361.
- Gamal El-Din, M., Fu, H., Wang, N., Chelme-Ayala, P., Pérez-Estrada, L., Drzewicz, P., Martin,

- J.W., Zubot, W., and Smith, D.W. 2011. Naphthenic acids speciation and removal during petroleum-coke adsorption and ozonation of oil sands process-affected water. *Science of the Total Environment*, 409(23): 5119-5125.
- George William, K., Serkan, E., Atakan, Ö., Özcan, H.K., and Serdar, A. 2018. Modelling of Adsorption Kinetic Processes—Errors, Theory and Application. *In* Advanced sorption process applications. *Edited by* E. Serpil. IntechOpen, Rijeka. p. Ch. 10.
- Grewer, D.M., Young, R.F., Whittal, R.M., and Fedorak, P.M. 2010. Naphthenic acids and other acid-extractables in water samples from Alberta: what is being measured? *Science of the Total Environment*, 408(23): 5997-6010.
- Hagen, M.O., Katzenback, B.A., Islam, M.D.S., Gamal El-Din, M., and Belosevic, M. 2013. The Analysis of Goldfish (*Carassius auratus* L.) Innate Immune Responses After Acute and Subchronic Exposures to Oil Sands Process-Affected Water. *Toxicological Sciences*, 138(1): 59-68.
- Harrison, J.S., Higgins, C.D., O'Meara, M.J., Koellhoffer, J.F., Kuhlman, B.A., and Lai, J.R. 2013. Role of electrostatic repulsion in controlling pH-dependent conformational changes of viral fusion proteins. *Structure*, 21(7): 1085-1096.
- Hermosin, M.C., Martin, P., and Cornejo, J. 1993. Adsorption mechanisms of monobutyltin in clay minerals. *Environmental science & technology*, 27(12): 2606-2611.
- Huang, R., Yang, L., How, Z.T., Fang, Z., Bekele, A., Letinski, D.J., Redman, A.D., and El-Din, M.G. 2021. Characterization of raw and ozonated oil sands process water utilizing atmospheric pressure gas chromatography time-of-flight mass spectrometry combined with solid phase microextraction. *Chemosphere*, 266: 129017.
- Huang, R., Chen, Y., Meshref, M.N.A., Chelme-Ayala, P., Dong, S., Ibrahim, M.D., Wang, C.,

- Klamerth, N., Hughes, S.A., Headley, J.V., Peru, K.M., Brown, C., Mahaffey, A., and Gamal El-Din, M. 2018. Characterization and determination of naphthenic acids species in oil sands process-affected water and groundwater from oil sands development area of Alberta, Canada. *Water research*, 128: 129-137.
- Isiuku, B.O., Okonkwo, P.C., and Emeagwara, C.D. 2021. Batch adsorption isotherm models applied in single and multicomponent adsorption systems – a review. *Journal of Dispersion Science and Technology*, 42(12): 1879-1897.
- Islam, M.S., Zhang, Y., McPhedran, K.N., Liu, Y., and Gamal El-Din, M. 2015. Granular activated carbon for simultaneous adsorption and biodegradation of toxic oil sands process-affected water organic compounds. *Journal of environmental management*, 152: 49-57.
- Islam, M.S., McPhedran, K.N., Messele, S.A., Liu, Y., and Gamal El-Din, M. 2018. Isotherm and kinetic studies on adsorption of oil sands process-affected water organic compounds using granular activated carbon. *Chemosphere*, 202: 716-725.
- Janfada, A., Headley, J.V., Peru, K.M., and Barbour, S. 2006. A laboratory evaluation of the sorption of oil sands naphthenic acids on organic rich soils. *Journal of Environmental Science and Health, Part A*, 41(6): 985-997.
- Jeong, G., and Nousiainen, T. 2014. TEM analysis of the internal structures and mineralogy of Asian dust particles and the implications for optical modeling. *Atmospheric Chemistry and Physics*, 14(14): 7233-7254.
- Jones, D., Scarlett, A.G., West, C.E., and Rowland, S.J. 2011. Toxicity of individual naphthenic acids to *Vibrio fischeri*. *Environmental science & technology*, 45(22): 9776-9782.
- Jones, R., and Forrest, D. 2010. Oil Sands Mining Reclamation Challenge Dialogue–Report and Appendices.

- Ju, D., and Young, T.M. 2005. The Influence of Natural Organic Matter Rigidity on the Sorption, Desorption, and Competitive Displacement Rates of 1,2-Dichlorobenzene. *Environmental science & technology*, 39(20): 7956-7963.
- Khan, S.U., Kumar, A., Prasad, M., Upadhyay, D., Mehta, B.K., Shashikumara, P., and Tamboli, P. 2023. Effect of soil amendments on the sorption behavior of atrazine in sandy loam soil. *Environmental Monitoring and Assessment*, 195(6): 686.
- Krumins, J., Klavins, M., Seglins, V., and Kaup, E. 2012. Comparative study of peat composition by using FT-IR spectroscopy. *Rigas Tehniskas Universitates Zinatniskie Raksti*, 26: 106.
- Le Guillou, F., Wetterlind, W., Rossel, R.V., Hicks, W., Grundy, M., and Tuomi, S. 2015. How does grinding affect the mid-infrared spectra of soil and their multivariate calibrations to texture and organic carbon? *Soil Research*, 53(8): 913-921.
- Li, C., Fu, L., Stafford, J., Belosevic, M., and Gamal El-Din, M. 2017. The toxicity of oil sands process-affected water (OSPW): a critical review. *Science of the Total Environment*, 601: 1785-1802.
- Li, F., Fang, X., Zhou, Z., Liao, X., Zou, J., Yuan, B., and Sun, W. 2019. Adsorption of perfluorinated acids onto soils: Kinetics, isotherms, and influences of soil properties. *Science of the Total Environment*, 649: 504-514.
- Li, Y., and Wei, M. 2022. Evaluation on adsorption capacity of low organic matter soil for hydrophobic organic pollutant. *Journal of Environmental Chemical Engineering*, 10(3): 107561.
- Li, Y., Wei, M., Liu, L., Xue, Q., and Yu, B. 2020. Adsorption of toluene on various natural soils: Influences of soil properties, mechanisms, and model. *Science of the Total Environment*: 140104.

- Li, Z., and Gallus, L. 2007. Adsorption of dodecyl trimethylammonium and hexadecyl trimethylammonium onto kaolinite — Competitive adsorption and chain length effect. *Applied Clay Science*, 35(3): 250-257.
- Lim, S.-F., and Lee, A.Y.W. 2015. Kinetic study on removal of heavy metal ions from aqueous solution by using soil. *Environmental Science and Pollution Research*, 22(13): 10144-10158.
- MacKinnon, M.D., and Boerger, H. 1986. Description of two treatment methods for detoxifying oil sands tailings pond water. *Water Quality Research Journal*, 21(4): 496-512.
- Meng, L., How, Z.T., Ganiyu, S.O., and Gamal El-Din, M. 2021. Solar photocatalytic treatment of model and real oil sands process water naphthenic acids by bismuth tungstate: Effect of catalyst morphology and cations on the degradation kinetics and pathways. *Journal of hazardous materials*, 413: 125396.
- Moustafa, A.M.A., McPhedran, K.N., Moreira, J., and Gamal El-Din, M. 2014. Investigation of Mono/Competitive Adsorption of Environmentally Relevant Ionized Weak Acids on Graphite: Impact of Molecular Properties and Thermodynamics. *Environmental science & technology*, 48(24): 14472-14480.
- Moyo, F., Tandlich, R., Wilhelmi, B.S., and Balaz, S. 2014. Sorption of Hydrophobic Organic Compounds on Natural Sorbents and Organoclays from Aqueous and Non-Aqueous Solutions: A Mini-Review. *International journal of environmental research and public health*, 11(5): 5020-5048.
- Murphy, E.M., Zachara, J.M., and Smith, S.C. 1990. Influence of mineral-bound humic substances on the sorption of hydrophobic organic compounds. *Environmental science & technology*, 24(10): 1507-1516.

- NRCAN. 2020. Natural Resources Canada Water Management in oil sands. Available from <https://natural-resources.canada.ca/our-natural-resources/energy-sources-distribution/fossil-fuels/crude-oil/what-are-oil-sands/18089>.
- Oil Sands Magazine. 2019. Surface mining techniques used in the oil sands. *In* Online (<https://www.oilsandsmagazine.com/technical/mining/surface-mining>, Diunduh 18 Maret 2019), Oil Sands Magazine.
- Oil Sands Magazine. 2021. Tailing Ponds 101. *In* Online (<https://www.oilsandsmagazine.com/technical/mining/tailings-ponds>, Updated on March 3, 2021), Oil Sands Magazine.
- Paredes-Doig, A.L., Sun-Kou, M.d.R., Picasso-Escobar, G., and Cannata, J.L. 2014. A study of the adsorption of aromatic compounds using activated carbons prepared from chestnut shell. *Adsorption Science & Technology*, 32(2-3): 165-180.
- Pateiro-Moure, M., Pérez-Novo, C., Arias-Estévez, M., Rial-Otero, R., and Simal-Gándara, J. 2009. Effect of organic matter and iron oxides on quaternary herbicide sorption–desorption in vineyard-devoted soils. *Journal of colloid and interface science*, 333(2): 431-438.
- Patra, B., Pal, R., Paulraj, R., Pradhan, S.N., and Meena, R. 2020. Mineralogical composition and C/N contents in soil and water among betel vineyards of coastal Odisha, India. *SN Applied Sciences*, 2(6): 998.
- Peng, J., Headley, J., and Barbour, S. 2002. Adsorption of single-ring model naphthenic acids on soils. *Canadian geotechnical journal*, 39(6): 1419-1426.
- Pourrezaei, P., Alpatova, A., Khosravi, K., Drzewicz, P., Chen, Y., Chelme-Ayala, P., and El-Din, M.G. 2014. Removal of organic compounds and trace metals from oil sands process-affected water using zero valent iron enhanced by petroleum coke. *Journal of*

- environmental management, 139: 50-58.
- Qin, F., Wen, B., Shan, X.-Q., Xie, Y.-N., Liu, T., Zhang, S.-Z., and Khan, S.U. 2006. Mechanisms of competitive adsorption of Pb, Cu, and Cd on peat. *Environmental Pollution*, 144(2): 669-680.
- Quinlan, P.J., and Tam, K.C. 2015. Water treatment technologies for the remediation of naphthenic acids in oil sands process-affected water. *Chemical Engineering Journal*, 279: 696-714.
- Ramachandran, V., and D'Souza, S. 2013. Adsorption of nickel by Indian soils. *Journal of soil science and plant nutrition*, 13(1): 165-173.
- Rao, L., Luo, J., Zhou, W., Zou, Z., Tang, L., and Li, B. 2020. Adsorption–desorption behavior of benzobicyclon hydrolysate in different agricultural soils in China. *Ecotoxicology and Environmental Safety*, 202: 110915.
- Rashed, Y., Messele, S.A., Zeng, H., and Gamal El-Din, M. 2020. Mesoporous carbon xerogel material for the adsorption of model naphthenic acids: structure effect and kinetics modelling. *Environmental technology*, 41(27): 3534-3543.
- Rauf, M.A., Bukallah, S.B., Hamour, F.A., and Nasir, A.S. 2008. Adsorption of dyes from aqueous solutions onto sand and their kinetic behavior. *Chemical Engineering Journal*, 137(2): 238-243.
- Rawat, A.P., Kumar, V., Singh, P., Shukla, A.C., and Singh, D.P. 2022. Kinetic Behavior and Mechanism of Arsenate Adsorption by Loam and Sandy Loam Soil. *Soil and sediment contamination: An international journal*, 31(1): 15-39.
- Rayment, G.E. 2011. *Soil chemical methods : Australasia. Edited by D.J. Lyons.* CSIRO Publishing, Collingwood, Vic. .:
- Russell, J., and Fraser, A. 1994. Infrared methods. *In Clay Mineralogy: Spectroscopic and*

- chemical determinative methods. Springer. pp. 11-67.
- Ryan, P.C., and Huertas, F.J. 2009. The temporal evolution of pedogenic Fe–smectite to Fe–kaolin via interstratified kaolin–smectite in a moist tropical soil chronosequence. *Geoderma*, 151(1): 1-15.
- Shen, Y.-H. 1999. Sorption of humic acid to soil: the role of soil mineral composition. *Chemosphere*, 38(11): 2489-2499.
- Skinner, M.F., Zabowski, D., Harrison, R., Lowe, A., and Xue, D. 2001. Measuring the cation exchange capacity of forest soils. *Communications in Soil Science and Plant Analysis*, 32(11-12): 1751-1764.
- Smaranda, C., Popescu, M.-C., Bulgariu, D., Măluțan, T., and Gavrilescu, M. 2017. Adsorption of organic pollutants onto a Romanian soil: Column dynamics and transport. *Process Safety and Environmental Protection*, 108: 108-120.
- Speight, J.G. 2013. Chapter 3 - Oil Sand Mining. *In Oil Sand Production Processes. Edited by J.G. Speight.* Gulf Professional Publishing, Boston. pp. 59-79.
- Stuart, B.H. 2004. *Infrared spectroscopy: fundamentals and applications.* John Wiley & Sons.
- Suara, M.A., Ganiyu, S.O., Paul, S., Stafford, J.L., and El-Din, M.G. 2022. Solar-activated zinc oxide photocatalytic treatment of real oil sands process water: Effect of treatment parameters on naphthenic acids, polyaromatic hydrocarbons and acute toxicity removal. *Science of the Total Environment*, 819: 153029.
- Sun, N., Chelme-Ayala, P., Klammerth, N., McPhedran, K.N., Islam, M.S., Perez-Estrada, L., Drzewicz, P., Blunt, B.J., Reichert, M., and Hagen, M. 2014. Advanced analytical mass spectrometric techniques and bioassays to characterize untreated and ozonated oil sands process-affected water. *Environmental science & technology*, 48(19): 11090-11099.

- Sun, Q. 2022. The Hydrophobic Effects: Our Current Understanding. *Molecules*, 27(20).
- Tang, X., Zhou, Y., Xu, Y., Zhao, Q., Zhou, X., and Lu, J. 2010. Sorption of polycyclic aromatic hydrocarbons from aqueous solution by hexadecyltrimethylammonium bromide modified fibric peat. *Journal of chemical technology & biotechnology*, 85(8): 1084-1091.
- Viraraghavan, T., and de Maria Alfaro, F. 1998. Adsorption of phenol from wastewater by peat, fly ash and bentonite. *Journal of hazardous materials*, 57(1): 59-70.
- Wang, J., Han, B., Dai, M., Yan, H., Li, Z., and Thomas, R. 1999. Effects of chain length and structure of cationic surfactants on the adsorption onto Na-Kaolinite. *Journal of colloid and interface science*, 213(2): 596-601.
- Weber, W.J., and Huang, W. 1996. A Distributed Reactivity Model for Sorption by Soils and Sediments. 4. Intraparticle Heterogeneity and Phase-Distribution Relationships under Nonequilibrium Conditions. *Environmental science & technology*, 30(3): 881-888.
- Wei, C., Song, X., Wang, Q., and Hu, Z. 2017. Sorption kinetics, isotherms and mechanisms of PFOS on soils with different physicochemical properties. *Ecotoxicology and Environmental Safety*, 142: 40-50.
- Worch, E. 2012. Adsorption technology in water treatment: fundamentals, processes, and modeling. Walter de Gruyter.
- Xing, Z., Tian, K., Du, C., Li, C., Zhou, J., and Chen, Z. 2019. Agricultural soil characterization by FTIR spectroscopy at micrometer scales: Depth profiling by photoacoustic spectroscopy. *Geoderma*, 335: 94-103.
- Yan, B., Liu, S., Chastain, M.L., Yang, S., and Chen, J. 2021. A new FTIR method for estimating the firing temperature of ceramic bronze-casting moulds from early China. *Scientific Reports*, 11(1): 3316.

- Zainorabidin, A., and Mohamad, H.M. 2017. Engineering properties of integrated tropical peat soil in Malaysia. *Electronic Journal of Geotechnical Engineering*, 22(02): 457-466.
- Zhang, C., Yan, H., Li, F., Hu, X., and Zhou, Q. 2013. Sorption of short- and long-chain perfluoroalkyl surfactants on sewage sludges. *Journal of hazardous materials*, 260: 689-699.
- Zhou, Y., Chen, L., Lu, P., Tang, X., and Lu, J. 2011. Removal of bisphenol A from aqueous solution using modified fibric peat as a novel biosorbent. *Separation and Purification Technology*, 81(2): 184-190.
- Zubot, W., An, Z., Benally, C., and Gamal El-Din, M. 2021. Treatment of oil sands process water using petroleum coke: Field pilot. *Journal of environmental management*, 289: 112407.
- Zubot, W., MacKinnon, M.D., Chelme-Ayala, P., Smith, D.W., and Gamal El-Din, M. 2012. Petroleum coke adsorption as a water management option for oil sands process-affected water. *Science of the Total Environment*, 427: 364-372.

## **CHAPTER 4: Efficient Degradation of Naphthenic Acids in Water Using a Sustainable Engineered Biochar/ZnO Composite Under Solar Light.**

### **4.1 Introduction**

NAs are recognized as a family of saturated aliphatic and alicyclic carboxylic acids that are naturally present in the oil sands in Northern Alberta and other oil reserves (Quinlan and Tam 2015; Whitby 2010). During the bitumen extraction process, NAs are concentrated in OSPW, which is a complex brackish mixture commonly stored in tailings ponds awaiting suitable treatment (Allen 2008; Jones et al. 2012; Quinlan and Tam 2015). The NAs in OSPW have brought important environmental concerns. For instance, several studies have reported that NAs could cause acute and chronic toxicity to aquatic and mammalian species (Clemente and Fedorak 2005; Frank et al. 2009; Hagen et al. 2013; Li et al. 2017; MacKinnon and Boerger 1986).

NAs can be represented by the general formula  $C_nH_{2n+z}O_x$ , where “n” means the carbon number ( $7 \leq n \leq 26$ ), “z” indicates the hydrogen deficiency due to the ring or double bond in the chemical structure of the acids (even integer,  $0 \leq -Z \leq 18$ ), and “x” the oxygen number (typically  $2 \leq x \leq 6$ ) (Huang et al. 2018). Classical NAs could be typically characterized with an oxygen number equal to 2, and the oxidized NAs (Oxy-NAs) have an oxygen number ranging from 3 to 6. Furthermore, heteroatomic NAs could be represented by  $C_nH_{2n+z}SO_x$  and  $C_nH_{2n+z}NO_x$  (Huang et al. 2018). In general, most studies have focused on the removal of classical NAs oxy-NAs from OSPW; however, studying the degradation of heteroatomic NAs is also important and worth further investigation (Meng et al. 2021).

AOPs are promising treatment methods for the remediation of various matrices, including

OSPW. Different AOPs have been applied for the degradation of natural and synthetic NAs, such as, ozonation (Pérez-Estrada et al. 2011; Qin et al. 2020), sulfate radical-based processes (Arslan et al. 2023), Fenton and Fenton-like systems, (Wang et al. 2016; Zhang et al. 2016), UV-based AOPs (Fang et al. 2020), among others. The degradation mechanism of these AOPs is directly based on the generation of highly reactive radicals, mainly hydroxyl ( $\cdot\text{OH}$ ), sulfate ( $\text{SO}_4^{\cdot-}$ ), and superoxide ( $\text{O}_2^{\cdot-}$ ) radicals, which can oxidize organic matter into shorter chain by-products. However, the drawbacks of high energy and consumable chemicals limit the application of these AOPs (Meng et al. 2021).

Among various AOPs, semiconductor-assisted photocatalysis has attracted increasing attention since the potential utilization of recyclable material and solar energy, and different semiconductors have been developed as photocatalysts (Xu et al. 2020; Yang et al. 2019). Due to its effectiveness and low cost, ZnO has recently been proposed as a promising photocatalyst for water treatment; however, some important drawbacks have limited its application. For instance, due to the relatively wide band gap (3.37 eV) and high exciton binding energy (60 meV), it is difficult to excite ZnO under visible radiation (or under solar light) (Cai et al. 2022). Furthermore, the photocorrosion effect and the high recombination rate of photogenerated electron-hole ( $e^-h^+$  pairs) limit the application of ZnO (Mohamed et al. 2023; Yang et al. 2019).

Recently, biochar-supported photocatalysis has emerged as a new strategy to overcome the limitations of individual photocatalytic materials (Kahkeci and Gamal El-Din 2023). Loaded photocatalyst on biochar (BC) surfaces can produce composites with greater adsorption capacities, higher chemical stability, and enhanced photocatalytic degradation compared to bare semiconductor photocatalysts (Kahkeci and Gamal El-Din 2023). Cai et al. (2022) prepared a

novel ZnO/Pic photocatalyst using pine as the carbon source and achieved effective degradation of metronidazole under visible light irradiation. Gonçalves et al. (2022) synthesized ZnO/BC composites using biowaste from brewed coffee and chitosan. In that study, the photocatalytic performance of the composite for degrading solutions containing phenol was found to be superior to that of pristine ZnO. Chen et al. (2019) and Yang et al. (2019) reported that composites are beneficial to obtain better photocatalytic performance by multi-scale fine structures and excellent characteristics, more reactive sites, and the inhibition ability of the recombination rate of the photoinduced  $e^-h^+$  pairs.

Despite this, the effectiveness and feasibility of degrading OSPW-related NAs using biochar/ZnO composites remained a research gap. Furthermore, only a few studies have investigated the correlation between the molecular structure of NAs with the degradation performance of different AOPs (Afzal et al. 2012; Pérez-Estrada et al. 2011). However, the fact is that the OSPW generally contains hundreds if not thousands of different NAs with different structures (de Oliveira Livera et al. 2018). Herein, it is an essential step to investigate the photocatalytic performance of biochar/ZnO composite for the degradation of a complex blends of NAs with different structures prior to the application into real OSPW remediation.

Therefore, this study aimed to develop sustainable wood-waste based biochar/ZnO composites and use them in combination with solar light for the effective photocatalytic degradation of model NAs. The photocatalytic performance of prepared BC/ZnO composites was studied through: 1) the effect of the ZnO content and the dosage of the composite on the degradation of a single model NA (CHA), 2) the kinetics of the degradation of CHA, 3) the investigation of the main reactive oxygen species generated photocatalytic process, and 4) the

assessment of the reusability of the BC/ZnO composite in the best experimental conditions. Moreover, the composite with the optimal ZnO content was applied for the degradation of a mixture of NAs with significant differences in their chemical structures. This study performed the first attempt to assess the degradation efficiency and competition kinetics towards different NAs in a mixture using biochar/ZnO composite as photocatalyst under solar irradiation, which should be an important insight for its further application in the treatment of real OSPW.

## 4.2 Materials and methods

### 4.2.1 Material and reagents

Hardwood forestry waste was used as biomass to prepare the pristine and biochar/ZnO composites. The samples were provided by Inno Tech Alberta. The following chemicals were used without any further purification: zinc nitrate hexahydrate ( $\text{Zn}(\text{NO}_3)_2 \cdot 6\text{H}_2\text{O}$ ;  $\geq 99.0\%$ ; Sigma Aldrich), anhydrous sodium carbonate ( $\text{Na}_2\text{CO}_3$ ;  $\geq 99.5\%$ ; Fisher Scientific), 5,5-dimethyl-1-pyrroline *N*-oxide (DMPO;  $\geq 99.0\%$ ; Dojindo Laboratories), 5-tert-butoxycarbonyl 5-methyl-1-pyrroline *N*-oxide (BMPO;  $\geq 98.0\%$ ; Dojindo Laboratories), 2,2,6,6-tetramethylpiperidine (TEMP;  $\geq 99.0\%$ ; Fisher Scientific), and NAs models (cyclohexanecarboxylic acid (CHA;  $\geq 98.0\%$ ), isonipecotic acid (IA;  $\geq 97.0\%$ ), tetrahydro-2H-thiopyran-4-carboxylic acid (T-2H-T4CA;  $\geq 97.0\%$ ), tetrahydropyran-4-carboxylic acid (T4CA;  $\geq 97.0\%$ ), cyclohexanepentanoic acid (CHPA;  $\geq 98.0\%$ ), hexanoic acid (HA;  $\geq 99.0\%$ ), 4-methylheptanoic acid (4-MHA;  $\geq 97.0\%$ ), and decanoic acid (DA;  $\geq 98.0\%$ ); Sigma Aldrich). To simulate a similar pH to real OSPW (around 8.5), all NA solutions were prepared in the buffer using 5 mM of sodium bicarbonate ( $\text{NaHCO}_3$ ;  $\geq 97.7\%$ ; Fisher Scientific). Ultrapure water (Millipore Synergy UV,  $\rho \geq 18.2 \text{ M}\Omega \text{ cm}$ ) was used to prepare all solutions.

## 4.2.2 Experimental methods

### 4.2.2.1 Synthesis of BC and BC/ZnO

First, hardwood wastes were dried in an oven at 105 °C overnight to remove the water content. Then, the dried raw material was submitted to pyrolysis using a muffle furnace at 600 °C (10 °C/min heating rate) for 2 h under N<sub>2</sub> atmosphere. The obtained material was then cooled to room temperature and rinsed three times with ultrapure water, followed by a drying step at 105 °C. The product was finally sieved evenly and stored in dark glass bottles for future use. In this work, pristine biochar is referred to as BC.

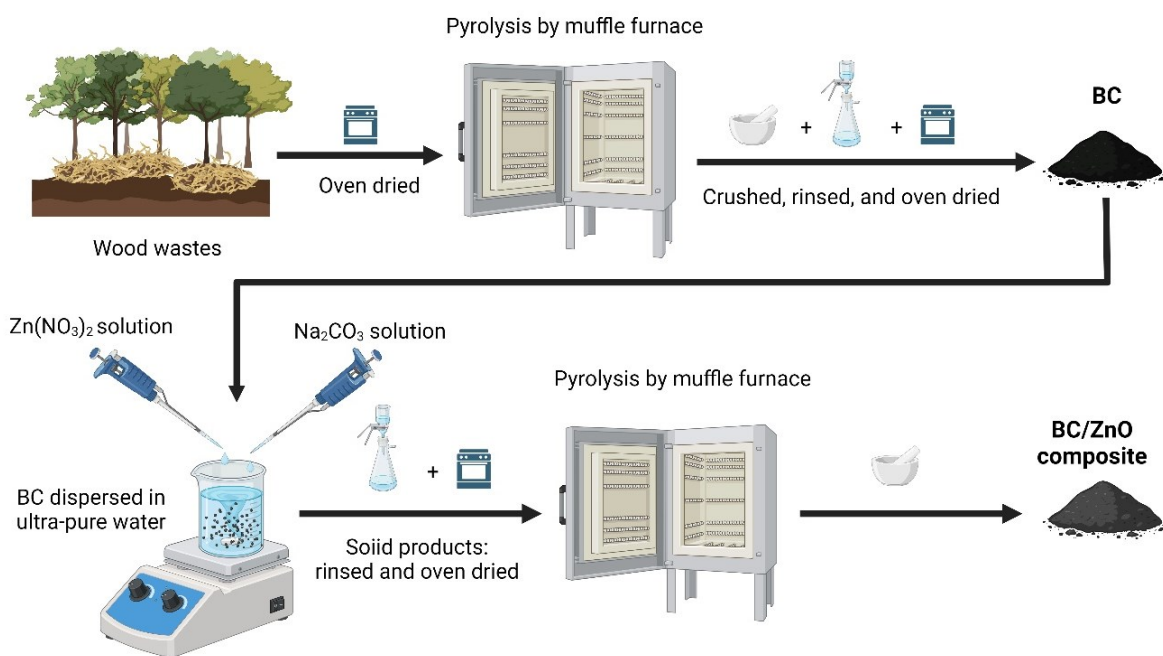


Figure 4.1: The scheme of the synthesis steps of BC/ZnO composites.

The composites, i.e., BC/ZnO, were synthesized by impregnation method with the designed ZnO contents as 10, 20, 30, and 50% wt. A certain amount of biochar was dispersed in a certain volume of ultrapure water. Subsequently, a corresponding volume of Zn(NO<sub>3</sub>)<sub>2</sub> stock

solution (0.5 M) was added to the previous dispersion under continuous stirring. After 5 min, a certain volume of Na<sub>2</sub>CO<sub>3</sub> stock solution (1 M) was added to the solution drop wisely under constant stirring. The final dispersion should reach 30 mL and the solution was stirred at room temperature for 1 h for the precipitation of zinc carbonate. Next, the solution was transferred to 50 mL flacon tubes, and the solid product were separated by centrifugation, washed with ultrapure water, and dried overnight at 80 °C. Finally, the dried material was calcined at 600 °C for 2 h (in N<sub>2</sub> environment) to yield the biochar/ZnO. For comparison purpose, synthesized ZnO (Syn-ZnO) was produced by the same method without adding biochar. A scheme of the steps involved in the fabrication of the BC/ZnO composites can be seen in Figure 4.1.

#### 4.2.2.2 Characterization of BC/ZnO

Various techniques were employed to characterize the best BC/ZnO composite: 1) the morphology and the chemical composition of the composite photocatalyst were investigated by scanning electron microscopy and energy-dispersive X-ray spectroscopy (SEM-EDX, Zeiss Sigma 300 VP-FESEM equipped with a Bruker EDX system); 2) the phase composition was identified by X-ray diffraction spectroscopy (XRD, Ultima IV, Rigaku, from 5° to 90°, CuK $\alpha$ <sub>1</sub> 1.5406 Å, CuK $\alpha$ <sub>2</sub> 1.5444, CuK $\beta$  1.3922); 3) the surface chemical composition and chemical states analysis were conducted by X-ray photoelectron spectroscopy (XPS, Kratos AXIS 165, Kratos Analytical); 4) the elemental analysis was performed by inductively coupled plasma-optical emission spectroscopy (ICP-OES, iCAP6300 Duo, Thermo); 5) the band gap and optical properties were analyzed by UV-Vis diffuse reflectance spectra (UV-VIS-NIR Cary 5000 with a DRA-CA-50M accessory, Agilent) and photoluminescence (PL, Fluorimeter QM-8075-11, HORIBA-PTI) measurements, respectively.

### 4.2.3 Photocatalytic degradation experiments

The photocatalytic performance of the BC/ZnO composites with different ZnO content was first investigated for the degradation of CHA (25 mg/L), a classical NA. 0.5 g/L of BC/ZnO composite was added to a cylindrical glass reactor containing 60 mL solution of the targeted NA. Before irradiation, the suspension was stirred steadily at dark condition for 60 min to reach the adsorption-equilibrium process. Subsequently, the system was exposed to solar irradiation (SS200AAA, Photon Emission Tech; 1000 W ozone-free arc lamp) under continuous stirring. A fixed irradiance of 100 mW/cm<sup>2</sup> was used for all the experiments. At certain intervals, samples were withdrawn from the reacting solution and filtered using 0.2 μm Nylon filters (Thermo Scientific). The filtered samples were stored in the fridge at 4 °C until further analyses. All experiments were conducted in duplicate. The setup used in the photocatalytic experiments is shown in Figures 4.2.

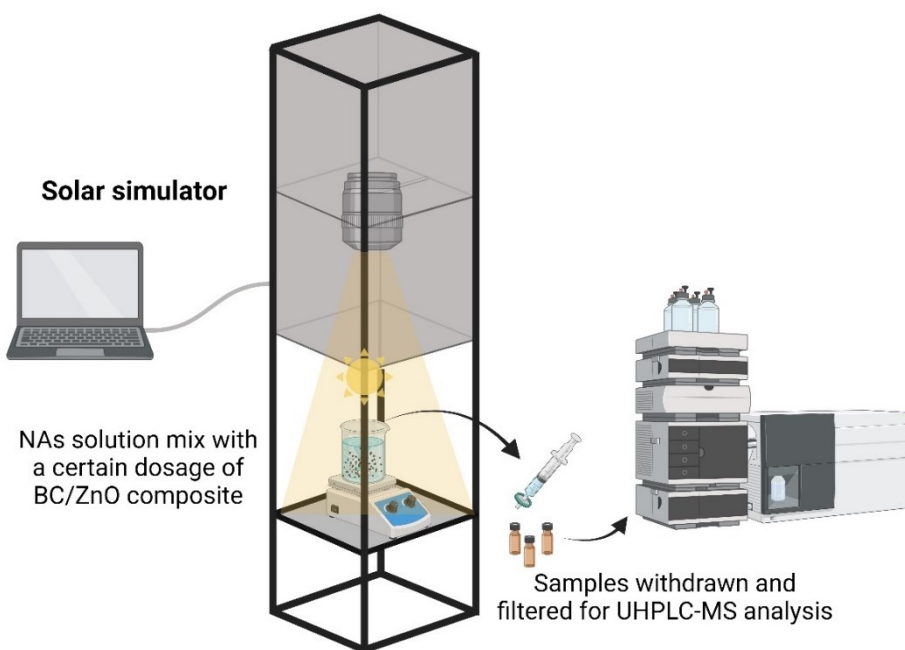


Figure 4.2: Setup of the photocatalytic experiments using BC/ZnO composites.

#### 4.2.4 Reactive oxygen species (ROS) and reusability tests

Electron paramagnetic resonance (EPR) analyses were employed to identify the main ROS that drive the degradation of CHA by BC/ZnO composite under solar light. The analyses were conducted using an EPR spectrometer (ELEXSYS-II, Bruker E-500) with a center field and resonance frequency of 3897 G and 9.81 GHz, respectively. The EPR spectra were collected based on the set-up of magnetic field modulation, amplitude, and microwave power of 100 kHz, 1.0 G, and 20 mW, with the sweep time of 60 s. The EPR experiments were performed in a 5 mL reactor using a 1 mL solution following the same experimental set-up mentioned in Section 4.2.3. To load sampled into the EPR assembly for analysis, 200  $\mu$ L aliquot was withdrawn from the system and transferred to a Suprasil<sup>®</sup> quartz tube with one end sealed and placed in tripe tube cell. DMPO (50 mM) and BMPO (3 mM) were applied as spin-trap reagents to detect  $\cdot$ OH and  $O_2^{\cdot-}$ , while TEMP (200 mM) was employed to detect the presence of singlet oxygen ( $^1O_2$ ).

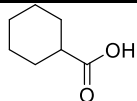
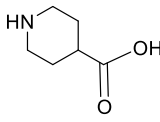
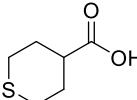
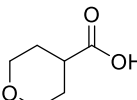
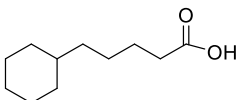
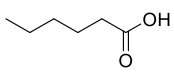
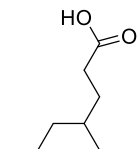
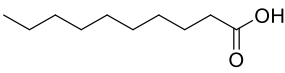
The stability and reusability of the BC/ZnO composite was investigated for the best ZnO content. For that, photocatalytic experiments for the degradation of CHA were repeated for four cycles. After each cycle, the used photocatalyst was separated from the treated solution by vacuum filtration. Then, the material was washed with ultrapure water three times and dried at 60  $^{\circ}$ C overnight for next cycle use.

#### 4.2.5 Performance of the BC/ZnO in the degradation of a mixture of NAs

The photocatalytic degradation performance of the best BC/ZnO composite was investigated for the simultaneous degradation of eight NAs model compounds with significant differences in their chemical structures. The general properties of the NAs compounds are listed in Table 4.1. All experiments were performed in duplicate. This is the first work that evaluated the

degradation efficiency and the competition kinetics towards NAs mixture using BC/ZnO composite with solar irradiation, which could give an essential insight into the complicated relationship between the structure and the preferential degradation phenomenon of NAs. Considering the complex composition of NAs in real OSPW, the outcomes of this experiment would serve as proof of concept for the potential implementation of this composite in the remediation of real OSPW.

Table 4.1: NAs models investigated in this study.

Chemical structure	Abbreviation	Name	Formula	M.W. (g/mol)
	CHA	Cyclohexanecarboxylic acid	C <sub>7</sub> H <sub>12</sub> O <sub>2</sub>	128.17
	IA	Isonipecotic acid	C <sub>6</sub> H <sub>11</sub> NO <sub>2</sub>	129.16
	T-2 H-T4CA	Tetrahydro-2 H-thiopyran-4-carboxylic acid	C <sub>6</sub> H <sub>10</sub> O <sub>2</sub> S	146.21
	T4CA	Tetrahydropyran-4-carboxylic acid	C <sub>6</sub> H <sub>10</sub> O <sub>3</sub>	130.14
	CHPA	Cyclohexanepentanoic acid	C <sub>11</sub> H <sub>20</sub> O <sub>2</sub>	184.27
	HA	n-caproic acid/ Hexanoic acid	C <sub>6</sub> H <sub>12</sub> O <sub>2</sub>	116.16
	4-MHA	4-methylheptanoic acid	C <sub>8</sub> H <sub>16</sub> O <sub>2</sub>	144.21
	DA	Decanoic acid	C <sub>10</sub> H <sub>20</sub> O <sub>2</sub>	172.26

#### 4.2.6 Analytical methods

The concentration of CHA during the photocatalytic experiments was monitored by an ultra-high performance liquid chromatography (UHPLC; Acquity H Class, Waters) coupled to a single quadrupole mass spectrometry (SQ Detector 2, Waters). Since the concentration of the NAs in the mixture was in a lower range, the concentration of each NA was measured by ultra-high-performance liquid chromatography (UHPLC; Agilent 1290 Infinity II) coupled to a triple quadrupole mass spectrometer (QQMS; Agilent 6495). Further details of both analysis methods can be found in Appendix C Text C1 and Table S9.

### 4.3 Results and discussions

#### 4.3.1 Characterization of BC/ZnO

##### 4.3.1.1 SEM and EDX analysis

SEM and EDX analysis were performed to evaluate the morphology and the elemental composition of the prepared BC/ZnO composite. Figure 4.3 shows the SEM images of the synthesized BC/30%ZnO composite. A clearly porous structure and roughened surface of the biochar material can be seen in Figure 4.3 (a). Additionally, Figures 4.3 (b to d) showcased that the ZnO particles are irregular spherical shapes, and most of them were in the form of aggregates on the biochar. The inhomogeneous structural properties of biochar prove its ability to be a good platform for the ZnO particles to disperse and attach. The presence of Zn was also confirmed from the EDX mapping results shown in Figure 4.3 (i). In addition, other elements were detected, such as K and Ca, which should be considered plant ingredients. The results obtained from SEM and EDX analysis confirm the presence of ZnO in the wood waste-based biochar and similar results were observed by Kamal et al. (2022) and Pang et al. (2021).

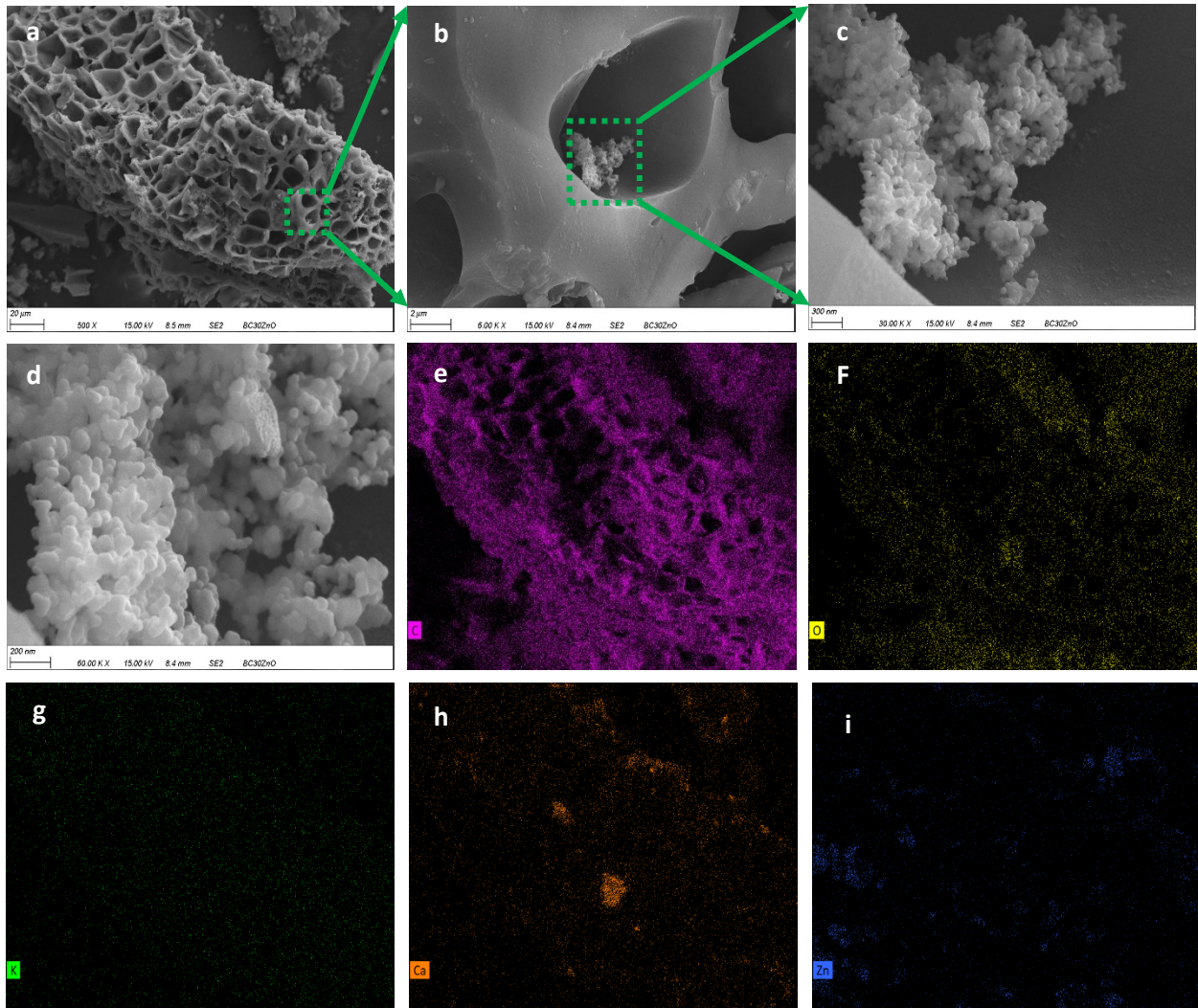


Figure 4.3: SEM images of the BC/30%ZnO composite.

#### 4.3.1.2 XRD and XPS analysis

Figure 4.4 shows the XRD pattern of the BC/ZnO composite. According to the PDF pattern 04-003-2106 (Zincite, ZnO), the XRD peaks of the composite well matched with the characteristic peaks of hexagonal ZnO system, where the angles of strong and sharp peaks were  $31.78^\circ$ ,  $34.44^\circ$ ,  $36.27^\circ$ ,  $47.54^\circ$ ,  $56.61^\circ$ ,  $62.89^\circ$ ,  $66.41^\circ$ ,  $67.99^\circ$ ,  $69.13^\circ$ , and  $72.59^\circ$ , indicating good crystallinity and purity, and the biochar did not influence the structure of the ZnO particles (Amir et al. 2022; Choi

et al. 2022; Yang et al. 2019). Besides, the broad peaks at 11.33, 18.14 and 22.64 were recognized as the amorphous phase in the composite, which were attribute to the carbon structure of biochar. The XRD results confirmed the successful synthesis of BC/ZnO composite.

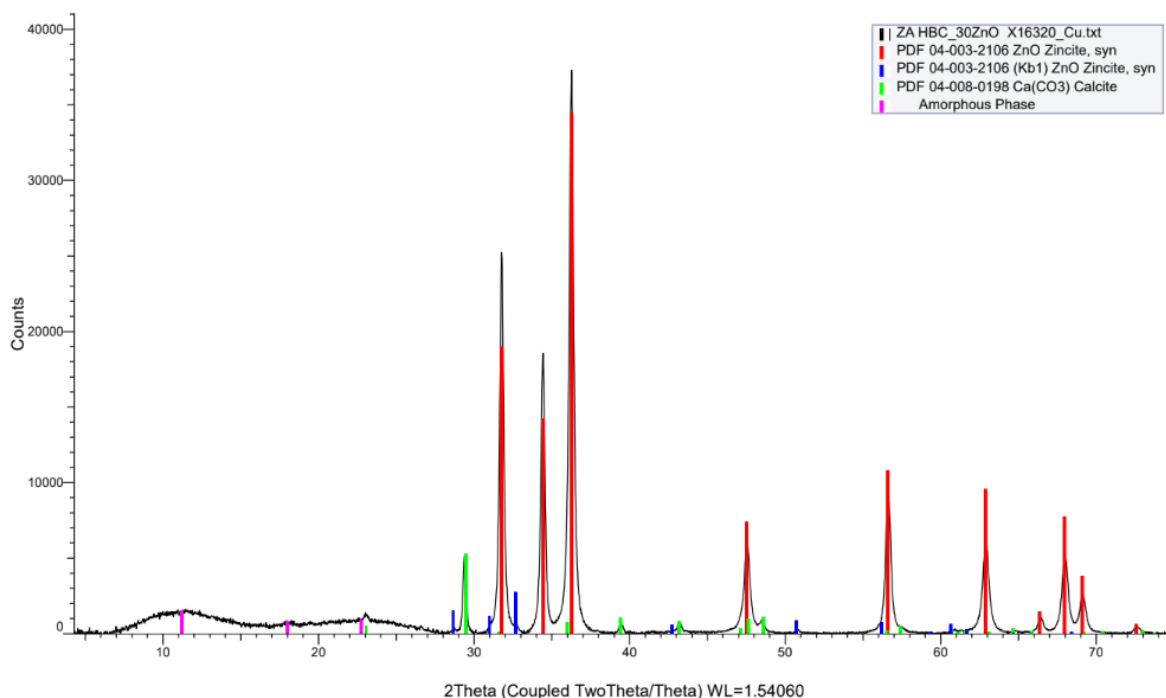


Figure 4.4: XRD results of the BC/30%ZnO composite.

As a strong surface technique, the XPS analysis was employed to characterize the chemical states and surface composition of the BC/ZnO composite. Figure 4.5 shows the XPS spectra of the BC/30%ZnO composite. The survey scan results shown in Figure 4.5 (a) revealed the existence of carbon (C 1s), oxygen (O 1s), and zinc (Zn) as major constituents in the composite. In addition, high-resolution spectra of C 1s, O 1s, and Zn 2p were performed to obtain more information. Figure 4.5 (b) showed the C 1s spectra and the three prominent peaks at 284.8 eV, 286.2 eV, and 287.4 eV were attributed to C-C/C=C, C-O, and C=O, respectively (Cai et al. 2022; Park et al. 2019). According to Figure 4.5 (c), the O 1s peak could be decomposed into two peaks at 531.4

eV and 532.7 eV. The peak with a lower binding energy phase corresponded to the oxygen lattice ( $O_L$ ), which could be attributed to the Zn-O bond in the ZnO networks. The 532.7 eV peak indicated the oxygen vacancies ( $O_V$ ) on the surface of the BC/ZnO composite, usually related to surface hydroxyl groups ( $-OH$ ) (Jing et al. 2021; Kim and Kim 2015). Furthermore, the oxygen vacancies can serve as active site that trigger the adsorption of  $O_2$  on the surface of the composite, while the adsorbed or chemisorbed  $O_2$ ,  $H_2O$  or C-O-Zn bond could cause the peak at 532.7 eV (He et al. 2021b; Mankomal and Kaur 2022). Two symmetric peaks were detected at 1022.7 eV and 1045.8 eV in the Zn 2p spectra shown in Figure 4.5 (d), which were associated with the Zn  $2p_{3/2}$  and Zn  $2p_{1/2}$ , respectively. The binding energy separation between the two peaks is 23.1 eV, which confirmed the presence of the normal  $Zn^{2+}$  valence state in the synthesized BC/ZnO composite by showing highly coincident with the reference value of ZnO wurtzite ( $\sim 23.0$  eV) (Cai et al. 2022; Chen et al. 2019; Kim and Kim 2015). Therefore, all the results from the XPS analysis confirmed the formation of ZnO on the surface of the hard wood-based biochar.

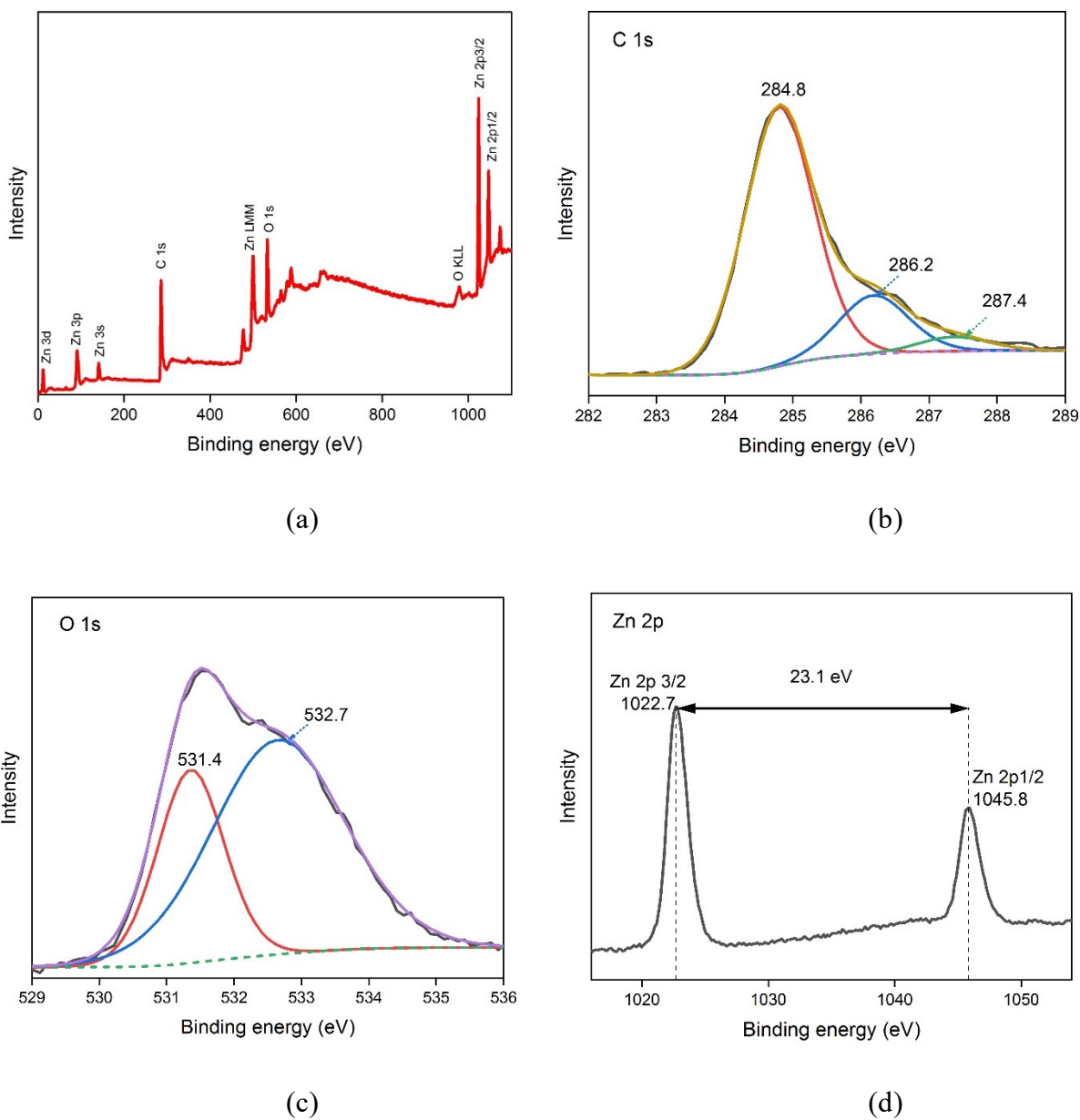


Figure 4.5: (a) XPS survey scan spectrum of the BC/30%ZnO composite and high-resolution XPS spectra of (b) C 1s (c) O 1s and (d) Zn 2p.

#### 4.3.1.3 Optical properties

Photoluminescence spectroscopy (PL) was employed to study the optical properties of BC/30%ZnO composite. The PL spectrum could provide useful information regarding the charge

carriers transfer at interfaces and photogenerated electron-hole efficiency, which is related with photocatalytic performance of the composite (Amir et al. 2022). Figure 4.6 (a) shows PL spectra of BC/30%ZnO composite and Syn-ZnO. The decreased PL intensity indicates a lower recombination rate of photogenerated electrons and holes (Li et al. 2019). It can be seen from Figure 4.6 (a) that the composite showed lower fluorescence intensity compared to ZnO, which means that the biochar inhibited the recombination of photoinduced electron-hole pairs from ZnO and improved the photocatalytic performance.

Figure 4.6 (b) shows the UV-vis DRA reflectance spectra of the BC/30%ZnO composite and Syn-ZnO. From the spectra, both the composite and syn-ZnO showed a characteristic peak at the wavelength of 372 nm. The band gap is the distance between the valence band and the lowest empty conduction band, which could determine the amount of photon energy needed to be absorbed by the semiconductor to cause photo-generation of photogenerated electrons and holes (Ekennia et al. 2021). Based on the Tauc method, the band gap of the composite and syn-ZnO was calculated from the UV-vis DRA reflectance spectra. The Tauc method has the assumption that the energy-dependent absorption coefficient  $\alpha$  can be expressed by equation (1), where  $h$  is the Plank constant,  $\nu$  is the frequency of photon,  $E_g$  is the band gap energy, and  $B$  is a constant. Furthermore, in combination with the Kubelka-Munk function (equation 2), the Tauc equation could be transformed into equation 3, where  $R_\infty$  is the reflectance obtained from the UV-vis reflectance spectra, and  $K$  and  $S$  are the absorption and scattering coefficients, respectively. According to equation 2, the absorbance response could be calculated from the reflectance, and the results were presented in Figure 4.6 (c). It is obvious that both BC/30%ZnO composite and Syn-ZnO had strong responses below 400 nm, which mainly assigned to the intrinsic band

absorption of ZnO as a semiconductor (Jing et al. 2021). Moreover, the composite showed stronger responses to visible light than Syn-ZnO. Yang et al. (2019) reported similar UV-vis DRS results that the ZnO@C composite showed a stronger response to visible light than Syn-ZnO.

In general, the  $\gamma$  factor in equation 3 is equal to 1/2 or 2 for the direct and indirect transition band gaps, respectively (Makula et al. 2018). As shown in Figures 4.6 (d) and (e), using the Tauc method, the band gap of BC/30%ZnO and Syn-ZnO were determined as 3.21 eV and 3.26 eV, respectively. Several studies have observed similar results in the slightly decreased band gap of the biochar/ZnO composite compared to pure ZnO. It could be explained by the electronic interaction between carbon and metal oxide, which could absorb more photons and be utilized in photocatalytic reactions, resulting in a higher photocatalytic activity than pure ZnO (Cai et al. 2022; Yang et al. 2019). Furthermore, Mankomal and Kaur (2022) explained that the narrowed band gap of the composite was possibly caused by the formation of the Zn-O-C bond, which allowed the electrons to transfer from ZnO to the surface of the biochar.

$$(\alpha \cdot hv)^{1/\gamma} = B(hv - E_g) \quad (1)$$

$$F(R_\infty) = \frac{K}{S} = \frac{(1 - R_\infty)^2}{2R_\infty} \quad (2)$$

$$(F(R_\infty) \cdot hv)^{1/\gamma} = B(hv - E_g) \quad (3)$$

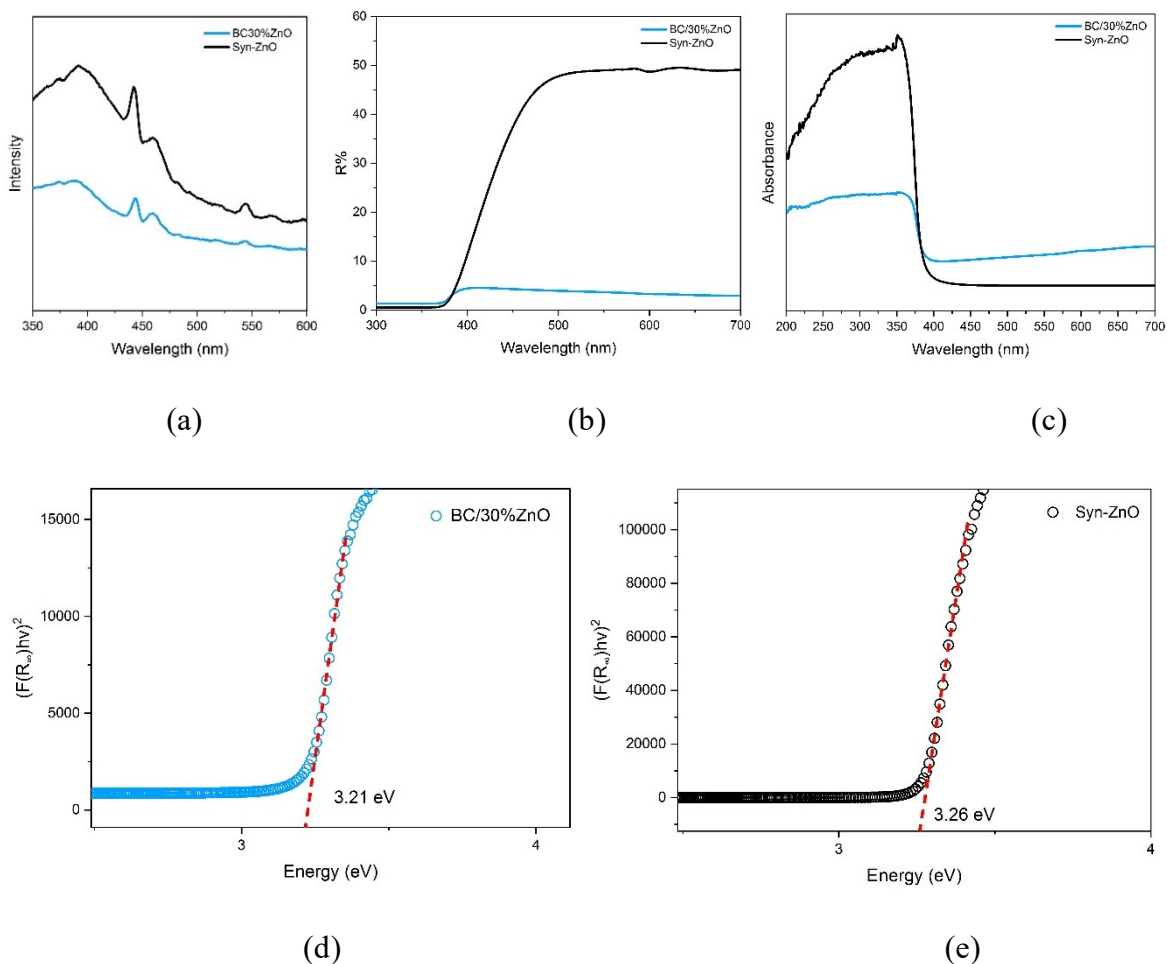


Figure 4.6 (a) PL spectrum; (b) UV-vis DRA reflectance; (c) Absorbance response plot spectrum of the BC/30%ZnO composite and Syn-ZnO; Tauc plot of (d) BC/30%ZnO and (e) Syn-ZnO were obtained with diffusion reflectance spectroscopy.

#### 4.3.2 Effect of ZnO content and catalyst dosage on CHA degradation

As a cyclic aliphatic carboxylic acid, CHA is one of the typical classical NAs widely used to study the degradation of model NAs (Afzal et al. 2015; Meng et al. 2021). In this study, CHA was selected to evaluate the photocatalytic performance of BC/ZnO composites under simulated solar light. 25 mg/L CHA was prepared with carbonate buffer to keep the pH stable around 8.5. Before the photocatalytic experiments, control experiments were conducted at dark conditions

using BC, Syn-ZnO, and BC/30%ZnO to evaluate the adsorption capacity of the individual materials and the prepared composite. Experiments using only CHA under solar irradiation were also performed (photolysis control). Figures 4.7 (a-c) showed that no removal of CHA was found by adsorption under dark conditions in 120 min. In addition, Figure 4.7 (d) indicates that in the absence of the composite, simulated solar light did not result in any CHA removal, even after 360 min of irradiation time.

To understand the effect of ZnO content on the photocatalytic performance of the composite, different composites with 10, 20, 30, and 50 wt.% of ZnO were designed and synthesized. Figure 4.8 (a) describes the photocatalytic degradation profile of CHA using different BC/ZnO composites with the same dosage (0.5 mg/L). According to Figure 4.8 (b), in 4 h of solar irradiation, the total degradation efficiency of CHA was 61.2% and 85.4% using BC/10%ZnO and BC/20%ZnO, respectively. However, a 93.7% CHA degradation efficiency was found when the composite with 30 wt.% ZnO was tested. With increasing the ZnO content to 50 wt.%, there was a slight decreasing effect on the degradation of CHA. He et al. (2021b) also observed similar results in the photocatalytic degradation of methylene blue by BC/ZnO under UV-visible light, reporting a moderate decrease in the degradation efficiency (98.7% to 83.0%) while increasing the biochar/ZnO molar ratio from 1:0.5 to 1:2. This is probably associated with the higher generation of radical species, which can result in a faster rate of recombination reactions and a decrease in the performance of the degradation process. Based on the results described above, the BC/30%ZnO composite was selected as the best material for the following experiments in this study.

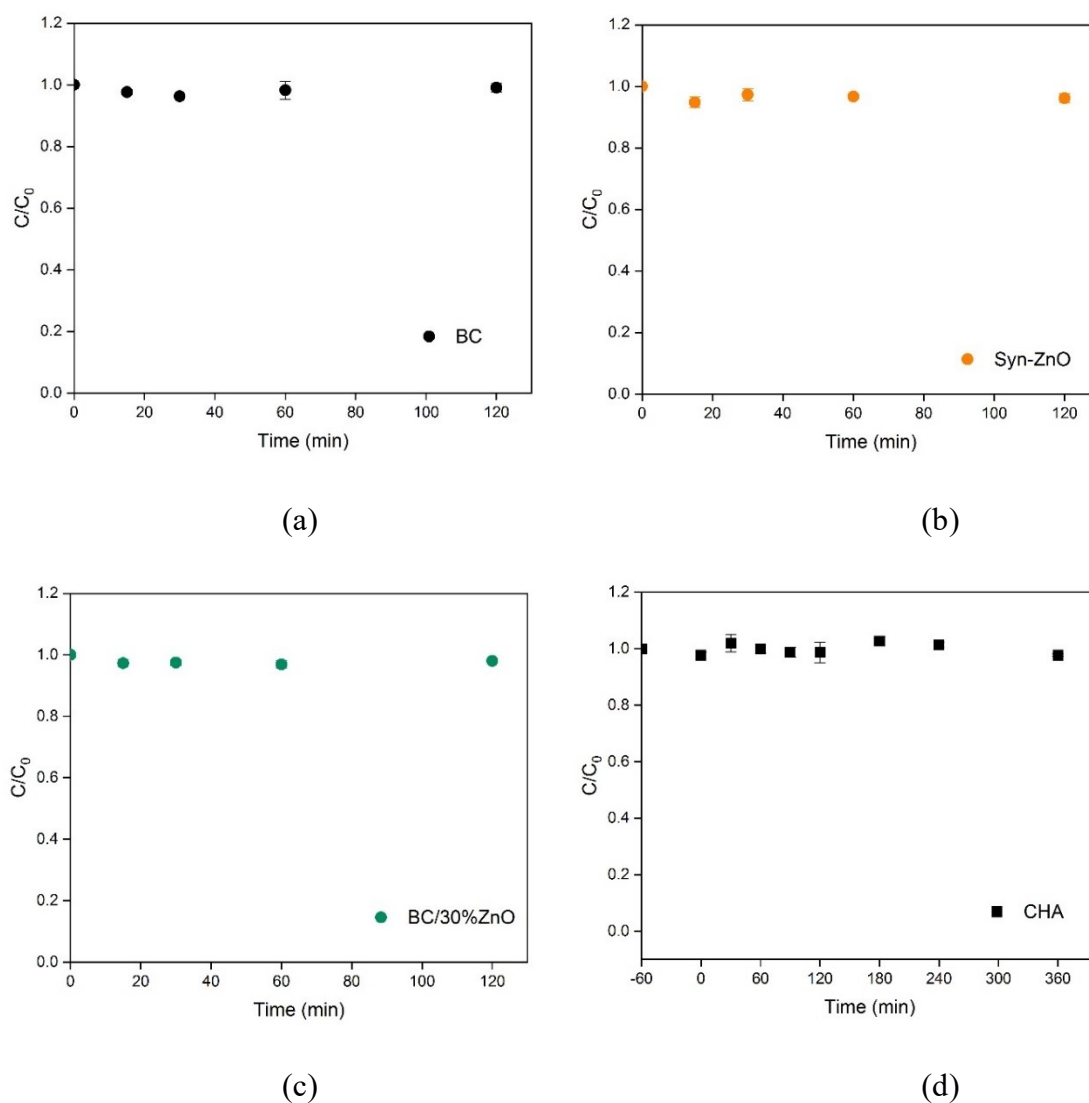


Figure 4.7: Dark adsorption control of (a) BC; (b) Syn-ZnO; and (c) BC/ZnO composite; and (d) CHA photolysis control. The dosage of BC, Syn-ZnO, and BC/ZnO is 0.5 g/L.  $[CHA]_0 = 25$  mg/L.

Figure 4.9 shows the effect of different BC/30%ZnO dosages (0.1, 0.25, 0.5, 1.0, and 2.0 g/L) and solar irradiation times on CHA degradation. The degradation of CHA by BC/30%ZnO followed the PFO kinetics model, and the rate constant were summarized in Table 4.2. The degradation efficiency of CHA showed a rapid increase in the kinetics rates ( $k_{PFO}$ ) from 0.179 to 0.732  $h^{-1}$ , when the composite dose increased from 0.1 g/L to 0.5 g/L. Then, the increase slowed

down with the composite dosage from 0.5 g/L to 2 g/L ( $0.830 \text{ h}^{-1}$ ). While increasing the concentration of the composite, more photocatalytic active sites were available to absorb more photons and generate more reactive species that could quickly degrade the target contaminant (Meng et al. 2021). However, increasing the composite dosage above the optimum concentration could lead to the occurrence of the scattering effect and a reduction in solar light penetration depth, resulting in less increase in the degradation efficiency of CHA (Gonçalves et al. 2022; Makama et al. 2020).

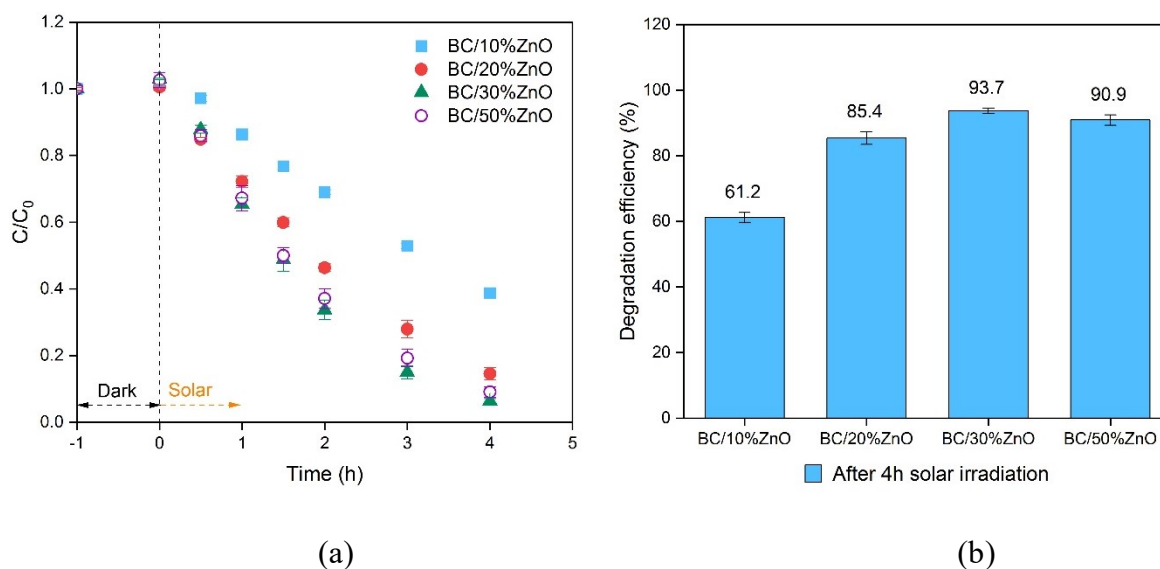


Figure 4.8: CHA degradation using different BC/ZnO composites under solar irradiation: (a)  $C/C_0$  vs. Time; (b) Comparison of different content of ZnO.

In addition, Figure 4.9 (b) shows no significant differences in the degradation percentage, increasing the irradiation time from 4 to 6 h. Considering both the cost and effectiveness, the best experimental conditions for the following experiments were 0.5 g/L BC/30%ZnO and 4 h of solar irradiation. To compare the photocatalytic performance, Syn-ZnO were applied at the same dosage as the ZnO content in 0.5 g/L BC/30%ZnO composite for CHA degradation, resulting in a

degradation efficiency of 48.3% (Figure 4.10). Therefore, the photocatalytic performance of BC/30%ZnO has been enhanced to approximately twice that of the Syn-ZnO.

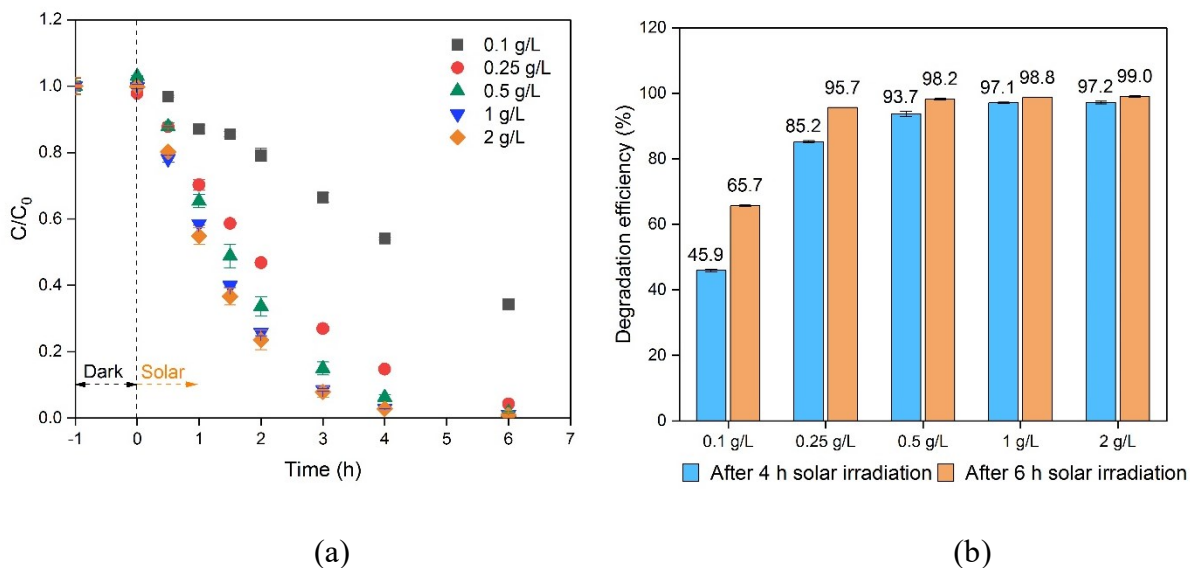


Figure 4.9: CHA degradation using different dosages of BC/30%ZnO under solar irradiation: (a)  $C/C_0$  vs. Time; (b) Comparison on solar irradiation time.

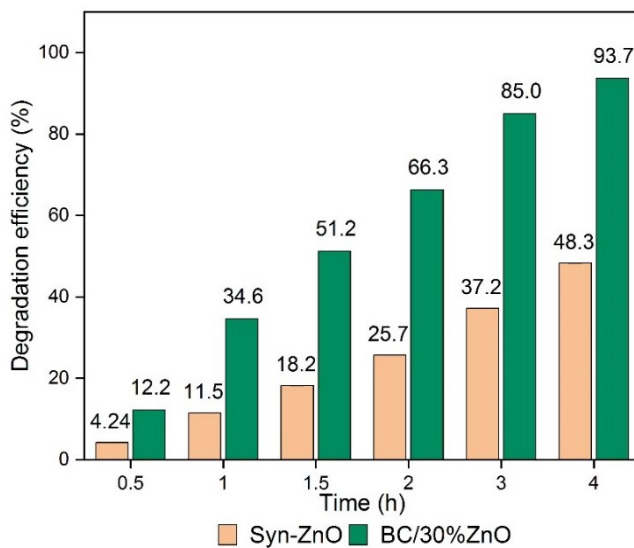


Figure 4.10: CHA degradation using same ZnO content of the BC/30%ZnO composite and Syn-ZnO.

Table 4.2: PFO kinetics parameters of BC/30%ZnO composite.

Dosage of BC/30%ZnO (g/L)	$k_{\text{PFO}}$ ( $\text{h}^{-1}$ )	$R^2$
0.1	0.179	0.980
0.25	0.530	0.988
0.5	0.732	0.997
1	0.807	0.980
2	0.830	0.985

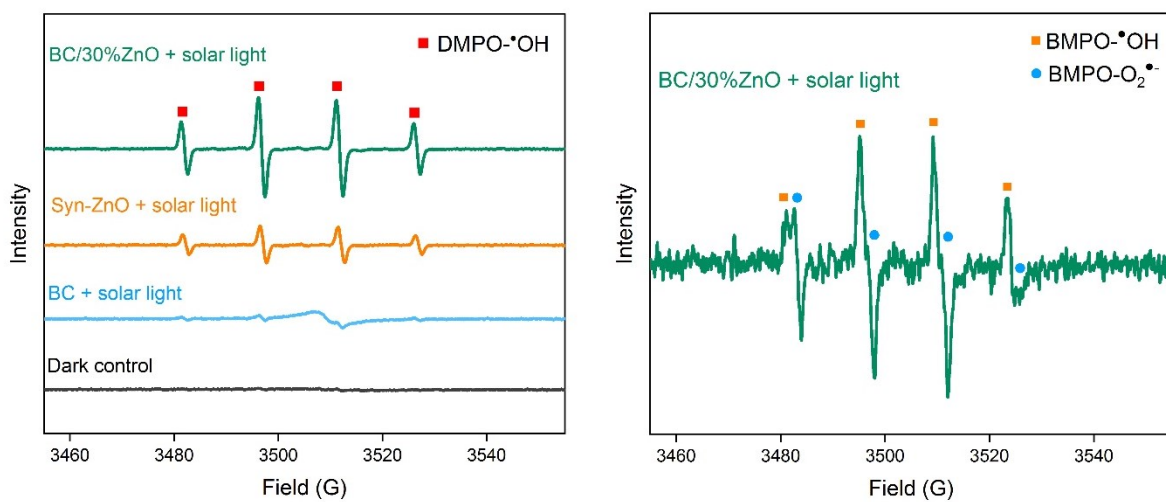
#### 4.3.3 ROS and possible mechanism of BC/ZnO under solar irradiation

To identify the main ROS involved in the degradation mechanism of CHA, EPR analysis was conducted with different trapping reagents. DMPO and BMPO were used to identify  $\cdot\text{OH}$  and  $\text{O}_2^{\cdot-}$  species, respectively. As shown in the EPR spectra (Figure 4.11 a), no signal of DMPO-derived adduct was detected using the composite at dark conditions. However, after 5 min under simulated solar light, the peaks of the adduct DMPO- $\cdot\text{OH}$  were identified for both the BC/30%ZnO composite and Syn-ZnO, showing a typically pattern signals with an approximately intensity ratio of 1:2:2:1 (Ganiyu et al. 2022). Although the results confirmed that the BC/30%ZnO composite and syn-ZnO generated  $\cdot\text{OH}$ , the DMPO- $\cdot\text{OH}$  peaks were much more intense using the BC/30%ZnO system. This may suggest that loading ZnO on the BC surface results in a higher generation of  $\cdot\text{OH}$  species during the CHA photodegradation process, i.e., better photocatalytic properties.

The formation of  $\text{O}_2^{\cdot-}$  species was also investigated by EPR measurements using BMPO as trapping agent. EPR spectra was collected in 2.5 min of solar irradiation using the composite. The appearance of strong peaks for BMPO- $\cdot\text{OH}$  spin adducts is shown in Figure 4.11 (b), which complement the results obtained with DMPO. Additionally, it was also found the formation of four

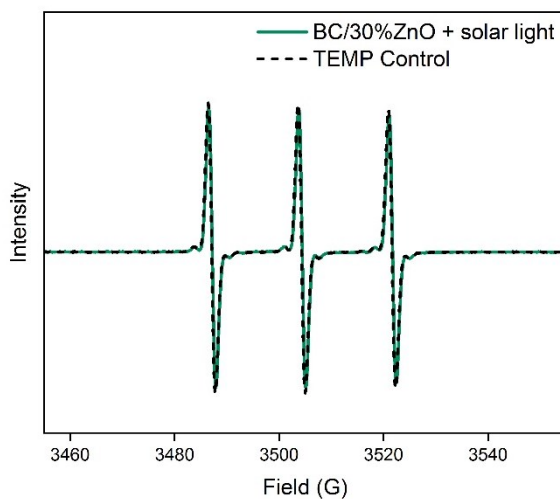
low-intensity peaks next to the BMPO- $\cdot\text{OH}$  peaks. Antonopoulou et al. (2023) obtained similar peaks by EPR spectra with BMPO, and the four tiny peaks could possibly be attributed to the BMPO adducts with  $\text{O}_2^{\cdot-}$ . In this sense, the observed signals prove the simultaneous generation of both  $\cdot\text{OH}$  and  $\text{O}_2^{\cdot-}$  species. In addition, TEMP was applied as another probe chemical to identify the presence of  $^1\text{O}_2$  species. According to the EPR spectra shown in Figure 4.11 (c), no signals of  $^1\text{O}_2$  were detected. Considering all the observations from EPR spectra, it appears that  $\cdot\text{OH}$  species play an important role in the degradation mechanism of CHA, while  $\text{O}_2^{\cdot-}$  may have a low contribution.

Combined with the results from EPR analysis and the characteristics of the composite, the mechanism is similar to the results reported by other published studies (He et al. 2021b; Lee et al. 2016; Li et al. 2023; Mankomal and Kaur 2022). With narrow band gaps, by acquiring photon energy from solar irradiation, the photogenerated  $e^-$  transferred from the gap band phase to the conduction phase while  $h^+$  were generated on the surface of BC/30%ZnO composite, and the biochar inhibited the recombination of the  $e^-h^+$  pairs (equation 4 to 6). The production of  $\cdot\text{OH}$  species could be mainly attributed to the reaction of the generated  $h^+$  with water molecules and hydroxyl groups (equations 7 and 8). Besides, electrons could react with oxygen and generate  $\text{O}_2^{\cdot-}$ , which could directly attend to the degradation process of CHA. On the other hand,  $\text{O}_2^{\cdot-}$  could also convert to  $\cdot\text{OH}$  by reactions shown in equations 9 to 12. With  $\cdot\text{OH}$  playing the dominant role, the CHA was eventually degraded with high efficiency using BC/30%ZnO composite under solar light.



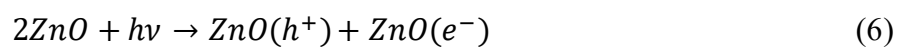
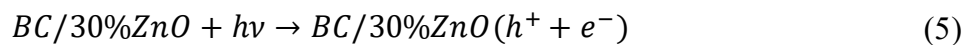
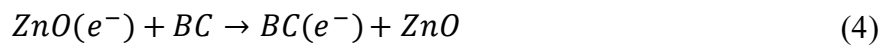
(a)

(b)



(c)

Figure 4.11: EPR spectra using (a) DMPO; (b) BMPO, and (c) TEMP as trapping agents.



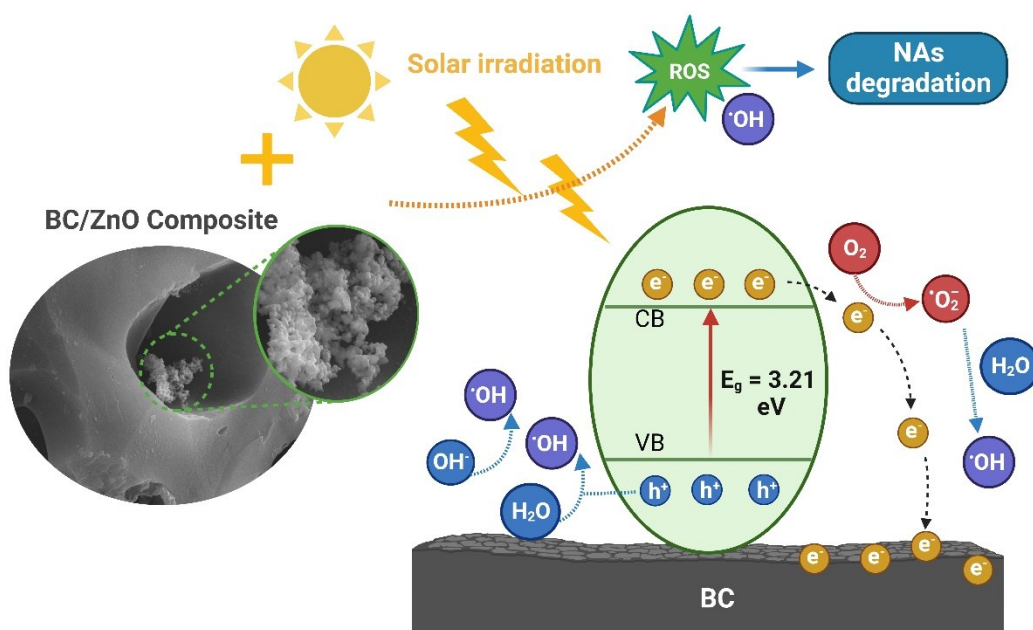
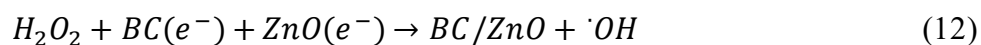
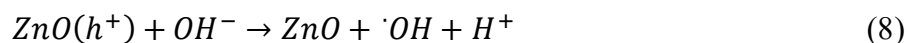


Figure 4.12: Schematic representation of photocatalytic mechanism for the degradation of NAs using BC/ZnO composite under solar irradiation.

#### 4.3.4 Reusability of BC/ZnO

The reusability and stability of photocatalysts are critical considerations that could affect the practical application of these materials. Therefore, the photocatalytic performance of the

BC/30%ZnO composite was investigated through successive cycles of use. The degradation efficiency was calculated after each cycle and shown in the bar chart in Figure 4.13. After 4 cycles of use, the efficiency of the composite for CHA degradation was still up to 92.9%, which clearly indicated that the composite showed good stability and reusability. Additionally, after 4 times use, SEM images of the composite were captured to identify possible changes in the morphology of the material. Comparing the SEM images of the composite before and after use (see Figure 4.14), no significant differences were observed for the porous structure biochar platform and the attached ZnO particles. Therefore, the BC/30%ZnO composite proposed in this study performed high photocatalytic degradation performance while maintaining notable chemical and physical stability over repeated cycles.

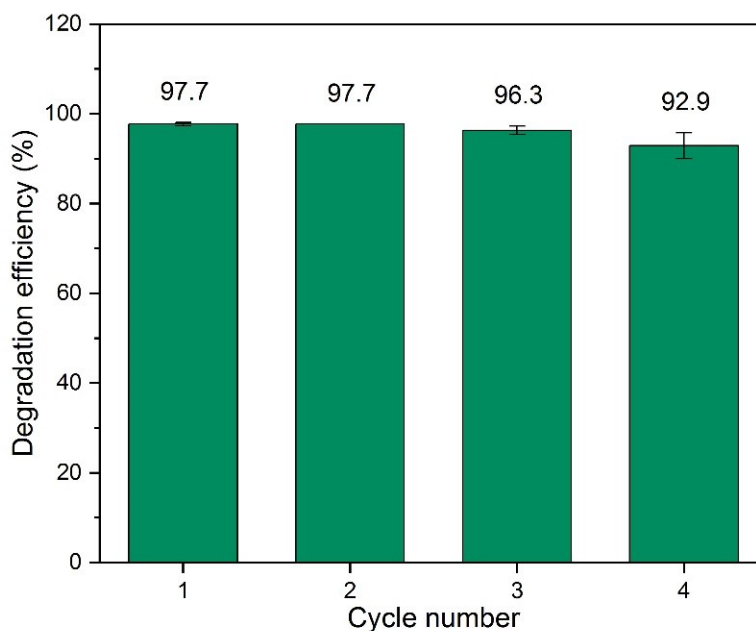


Figure 4.13: Reusability tests for the BC/30%ZnO composite.

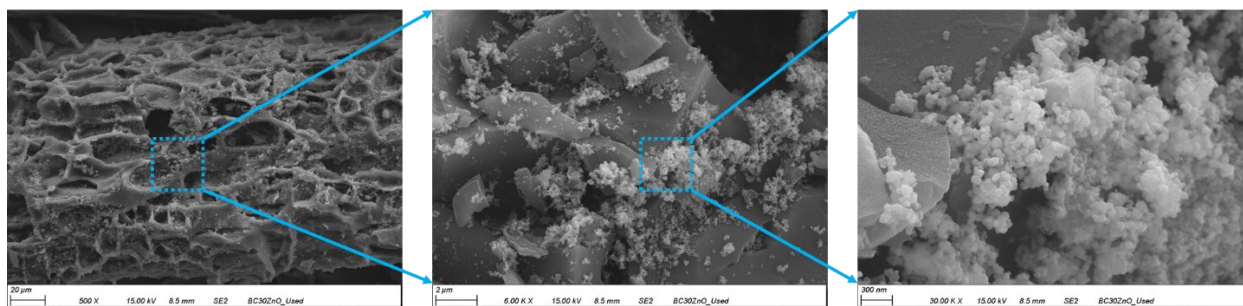


Figure 4.14: SEM images of BC/30%ZnO after 4 cycles of use.

#### 4.3.5 Degradation performance of BC/30%ZnO towards NAs mixture

To further evaluate the photocatalytic performance of the BC/30%ZnO composite, a complex mixture containing 8 different classes of NAs was used as the target contaminated solution. The total initial concentration of NAs was 40 mg/L (i.e., 5 mg/L of each NA), similar to the classical NAs concentration in real OSPW. Considering the increased initial total concentration of the target contaminant, the solar irradiation time was increased to 6 h accordingly with 0.5 g/L of BC/30%ZnO composite results obtained for the CHA. Before the solar irradiation started, the photodegradation and dark adsorption control were conducted for the mixture solution. No degradation of all NAs was found without the presence of composite at dark conditions (Figure 4.15), which confirmed the degradation of the target NAs was due to the simultaneous presence of the composite and the solar light.

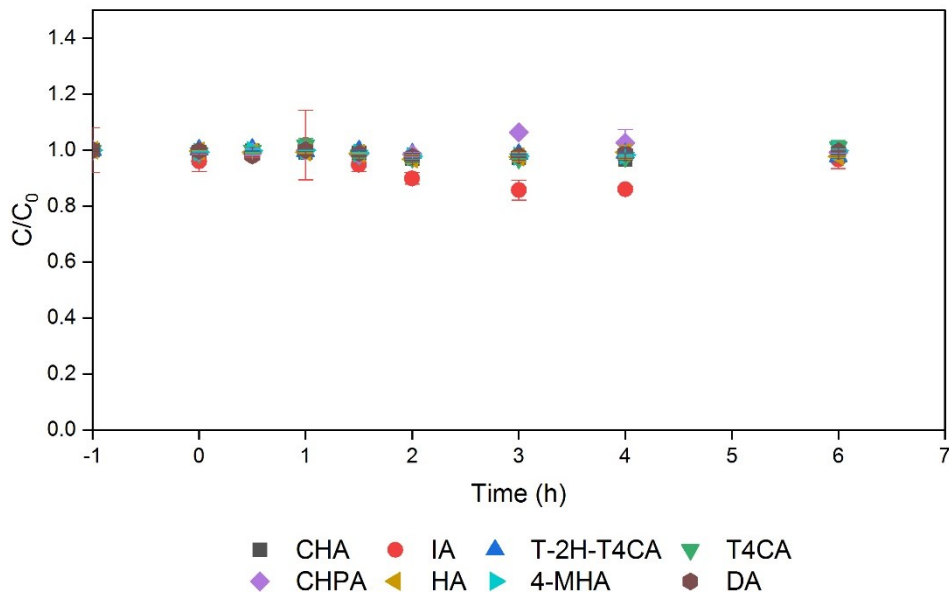
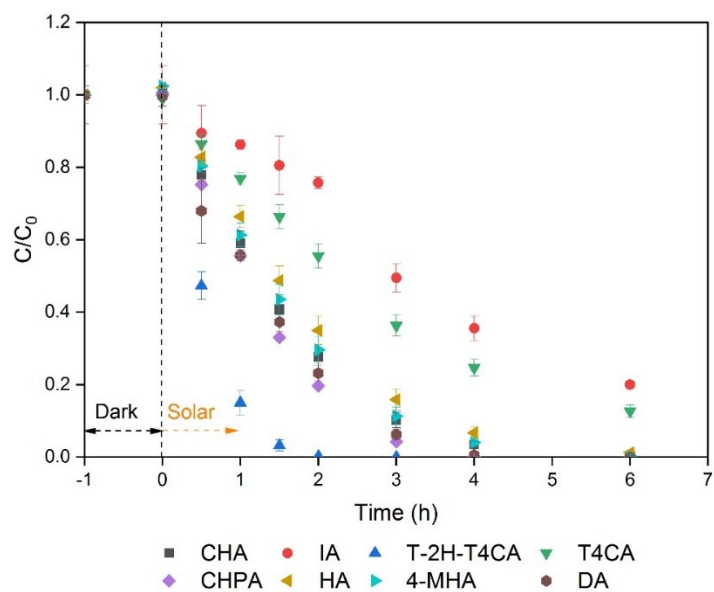
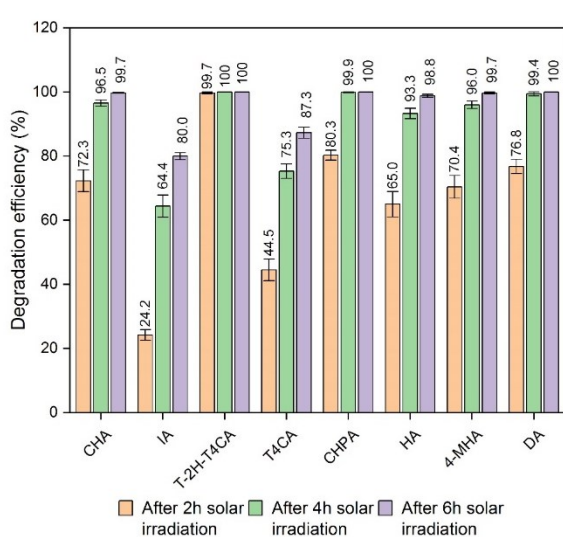


Figure 4.15: Control experiment: photodegradation of the NAs in the mixture in the absence of the composite.

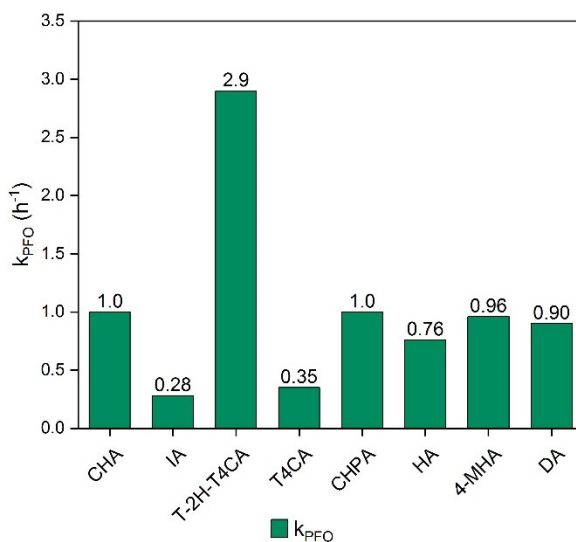
The degradation process of each individual NAs in the mixture is described in Figures 4.16 (a-b). All NAs achieved an efficient degradation rate by the composite under solar irradiation, while different degradation efficiencies were observed. For example, the T-2H-T4CA was fully degraded by BC/30%ZnO composite in 2 h but only after 4 h solar most of the NAs in the mixture reached nearly 100% degradation, including CHA (99.7%), CHPA (>99%), HA (98.8%), 4-MHA (99.68%), and DA (>99%). In contrast, the degradation efficiency of IA and T4CA was lower than other NAs at the same time of irradiation; however, the final degradation efficiency of these NAs was over 80% in 6 h of treatment. Eventually, the total degradation efficiency of the NAs in the mixture achieved 95.5% using the composite under 6 h of solar irradiation.



(a)



(b)



(c)

Figure 4.16: Simultaneous degradation of a mixture of NAs using the BC/30%ZnO composite under solar irradiation: (a)  $C/C_0$  vs. Time; (b) Degradation efficiency of different NAs after 2, 4, and 6 h solar irradiation; (c) PFO rate constants of different NAs.

The preferential degradation of specific NA compounds implied the occurrence of competition between the different structured NAs. The degradation process of the different NAs all fitted with PFO kinetics, and the corresponding degradation rates are shown in Figure 4.16 (c). T-2H-T4CA had the fastest degradation rate ( $2.90 \text{ h}^{-1}$ ) among all NAs, which was 2.90 times the reaction rate of CHA in the mixture. It could be explained by the structure of T-2H-T4CA, where the non-bonding electrons of S atoms could enhance its overall reactivity towards oxidizing species. de Oliveira Livera et al. (2018) investigated the structure-reactivity relationship of NAs in the photocatalytic degradation process using  $0.5 \text{ g/L TiO}_2$  as photocatalyst under UV irradiation and it was reported that the degradation rate for T-2H-T4CA was 2.67 times of that for CHA.

In the mixture, the degradation rate for the eight model NAs follows the order: T-2H-T4CA > CHPA > CHA > 4-MHA > DA > HA > T4CA > IA. According to these results, the NAs with saturated rings such as CHPA and CHA showed higher reaction rates than the linear chain structured NAs (4-MHA, DA, and HA), indicating that the single saturated ring could increase the reactivity of the compound. Similar tendencies were also proved by de Oliveira Livera et al. (2018) that 4-pentylcyclohexanoic acid (4pnCHA) photocatalytic degradation rate was 1.38 times of the rate of the linear dodecanoic acid (DDA). Besides, Afzal et al. (2012) found that compared to small, linear, and acyclic NAs, reactivity favored large, branched, and cyclic NAs, leading to a better oxidization performance by the UV/H<sub>2</sub>O<sub>2</sub> process, in which  $\cdot\text{OH}$  also have the main role in the degradation mechanism. The preferential degradation observed in this study also supported this finding. Compared to CHA, CHPA has a longer branch attached to the saturated ring and showed a faster degradation rate. In addition, among the linear chain structured NAs in the mixture, DA has a carbon number of 10, and the reaction rate was 1.18 times the rate of HA, which has a

carbon number of 6. Furthermore, 4-MHA showcased a faster reaction rate with less carbon number compared to DA, which could be attributed to the introduction of the tertiary carbon by the alkyl branching-point. The tertiary carbon-centered radicals have higher stability than primary and secondary radicals, which could increase the rate (Afzal et al. 2012). Similarly, Meng et al. (2021) evaluated the photocatalytic activity of  $\text{Bi}_2\text{WO}_6$  (1 g/L) with simulated solar light by applying 4 different NAs (individually) as the target pollutants, and the degradation rates were reported in the following order: T-2H-T4CA > CHA > IA > T4CA. Compared to that work, the BC/30%ZnO composite in our study showed better photocatalytic degradation performance for the IA and T4CA degradation.

#### 4.3.6 Leaching test

A leaching test was conducted to investigate the potential released of Zn from the composite material into the solution. For that, 0.5 g/L of the BC/30%ZnO composite were dispersed into 60 mL of buffer solution (5 mM  $\text{NaHCO}_3$ ) and mixed continuously for 24 h under dark condition. Then, the liquid samples were collected by a 0.2  $\mu\text{m}$  filter and analyzed by ICP-OES. A small concentration of Zn (38  $\mu\text{g/L}$ ) was measured in the liquid sample after 24 h of mixing, which means approximately only 0.05% of the total content of Zn in the composite. This also confirms the good stability of the composite material, even after 24 h of contact with the solution. Jusoh et al. (2013) developed mesostructured silica nanoparticles loaded with ZnO (ZnO/MSN) as photocatalyst, and they reported 2.97% (equivalent to 148.5  $\mu\text{g/L}$ ) of Zn leaching after 8 h UV irradiation with 1 g/L of ZnO/MSN. Based on the risk management scope for Zn and soluble Zn compounds by Environment and Climate Change Canada (ECCC), the Code of Practice for base metal smelting and refining lists an effluent limit for Zn at a maximum monthly mean

concentration of 500  $\mu\text{g/L}$  (ECCC 2019). Therefore, the measured leached Zn concentration in our study is more than 13 times lower than the recommended limit. The United States Environmental Protection Agency (US EPA) published an acute and chronic criterion of 120  $\mu\text{g/L}$  as the limits of Zn for the protection of freshwater aquatic life (USEPA 2007).

#### 4.4 Conclusions and future perspectives

This study successfully synthesized BC/ZnO composites with different ZnO content using wood wastes as biomass. Based on the degradation of CHA, the best experimental conditions were determined as 0.5 g/L BC/30%ZnO and 4 h of solar irradiation time, achieving 93.7% degradation efficiency of CHA following the PFO kinetics. By using different techniques, we confirmed that the porous structure and roughened surface of the biochar make it an excellent platform to support ZnO particles. In addition, BC played an important role as an electron reservoir that could reduce the recombination rate of photogenerated  $e^-h^+$  pairs, as well as providing more reactive sites in the BC/30%ZnO composite.  $\cdot\text{OH}$  species detected by EPR measurements were found to have an important role in CHA degradation, and the composite showed a good reusability and stability after 4 successive cycles of use. As the essential pre-step prior to successful implementation on real OSPW, this is the first study that applied BC/30%ZnO composite as the photocatalyst, while the simulated solar light as the energy source, for the simultaneous degradation of a complex mixture of 8 NAs with significantly different structures. The competition phenomenon was observed for different structured NAs with the degradation rate following the order of T-2H-T4CA > CHPA > CHA > 4-MHA > DA > HA > T4CA > IA. After 6 h solar irradiation, the total degradation efficiency of NAs in the mixture was up to 95.5%.

Considering the excellent photocatalytic performance of the BC/30%ZnO composite for

NAs degradation, as well as its good reusability and stability, this photocatalyst is a sustainable approach for the treatment of real OSPW. In scale-up applications, a lower catalyst dosage can be applied, and solar natural light can be used as irradiation source. By combining wood waste-based biochar containing a low ZnO content, solar radiation as a green energy source, and low composite dosage, the outcomes of this research constitute an eco-friendly and cost-effective approach for industrial wastewater remediation.

#### 4.5 References

- Afzal, A., Chelme-Ayala, P., Drzewicz, P., Martin, J.W., and Gamal El-Din, M. 2015. Effects of Ozone and Ozone/Hydrogen Peroxide on the Degradation of Model and Real Oil-Sands-Process-Affected-Water Naphthenic Acids. *Ozone: Science & Engineering*, 37(1): 45-54.
- Afzal, A., Drzewicz, P., Pérez-Estrada, L.A., Chen, Y., Martin, J.W., and Gamal El-Din, M. 2012. Effect of Molecular Structure on the Relative Reactivity of Naphthenic Acids in the UV/H<sub>2</sub>O<sub>2</sub> Advanced Oxidation Process. *Environmental science & technology*, 46(19): 10727-10734.
- Allen, E.W. 2008. Process water treatment in Canada's oil sands industry: I. Target pollutants and treatment objectives. *Journal of Environmental Engineering and Science*, 7(2): 123-138.
- Amir, M., Fazal, T., Iqbal, J., Din, A.A., Ahmed, A., Ali, A., Razzaq, A., Ali, Z., Rehman, M.S.U., and Park, Y.-K. 2022. Integrated adsorptive and photocatalytic degradation of pharmaceutical micropollutant, ciprofloxacin employing biochar-ZnO composite photocatalysts. *Journal of Industrial and Engineering Chemistry*, 115: 171-182.
- Antonopoulou, M., Bika, P., Papailias, I., Zervou, S.-K., Vrettou, A., Efthimiou, I., Mitrikas, G., Ioannidis, N., Trapalis, C., Dallas, P., Vlastos, D., and Hiskia, A. 2023. Photocatalytic

- degradation of organic micropollutants under UV-A and visible light irradiation by exfoliated g-C<sub>3</sub>N<sub>4</sub> catalysts. *Science of the Total Environment*, 892: 164218.
- Arslan, M., Ganiyu, S.O., Lillico, D.M.E., Stafford, J.L., and Gamal El-Din, M. 2023. Fate of dissolved organics and generated sulfate ions during biofiltration of oil sands process water pretreated with sulfate radical advanced oxidation process. *Chemical Engineering Journal*, 458: 141390.
- Boguta, P., Sokołowska, Z., Skic, K., and Tomczyk, A. 2019. Chemically engineered biochar – Effect of concentration and type of modifier on sorption and structural properties of biochar from wood waste. *Fuel*, 256: 115893.
- Cai, H., Zhang, D., Ma, X., and Ma, Z. 2022. A novel ZnO/biochar composite catalysts for visible light degradation of metronidazole. *Separation and Purification Technology*, 288: 120633.
- Chen, M., Bao, C., Hu, D., Jin, X., and Huang, Q. 2019. Facile and low-cost fabrication of ZnO/biochar nanocomposites from jute fibers for efficient and stable photodegradation of methylene blue dye. *Journal of Analytical and Applied Pyrolysis*, 139: 319-332.
- Choi, M., Brabec, C., and Hayakawa, T. 2022. X-ray Diffraction, Micro-Raman and X-ray Photoemission Spectroscopic Investigations for Hydrothermally Obtained Hybrid Compounds of Delafossite CuGaO<sub>2</sub> and Wurtzite ZnO. *Ceramics*, 5(4): 655-672.
- Clemente, J.S., and Fedorak, P.M. 2005. A review of the occurrence, analyses, toxicity, and biodegradation of naphthenic acids. *Chemosphere*, 60(5): 585-600.
- de Oliveira Livera, D., Leshuk, T., Peru, K.M., Headley, J.V., and Gu, F. 2018. Structure-reactivity relationship of naphthenic acids in the photocatalytic degradation process. *Chemosphere*, 200: 180-190.

ECCC. 2019. Risk Management Scope for Zinc and Soluble Zinc Compounds under the Zinc and its Compounds grouping. *Edited by* H. Canada.

Ekennia, A.C., Uduagwu, D.N., Nwaji, N.N., Oje, O.O., Emma-Uba, C.O., Mgbii, S.I., Olowo, O.J., and Nwanji, O.L. 2021. Green Synthesis of Biogenic Zinc Oxide Nanoflower as Dual Agent for Photodegradation of an Organic Dye and Tyrosinase Inhibitor. *Journal of Inorganic and Organometallic Polymers and Materials*, 31(2): 886-897.

Fang, Z., Huang, R., How, Z.T., Jiang, B., Chelme-Ayala, P., Shi, Q., Xu, C., and El-Din, M.G. 2020. Molecular transformation of dissolved organic matter in process water from oil and gas operation during UV/H<sub>2</sub>O<sub>2</sub>, UV/chlorine, and UV/persulfate processes. *Science of the Total Environment*, 730: 139072.

Frank, R.A., Fischer, K., Kavanagh, R., Burnison, B.K., Arsenault, G., Headley, J.V., Peru, K.M., Kraak, G.V.D., and Solomon, K.R. 2009. Effect of Carboxylic Acid Content on the Acute Toxicity of Oil Sands Naphthenic Acids. *Environmental science & technology*, 43(2): 266-271.

Ganiyu, S.O., Arslan, M., and Gamal El-Din, M. 2022. Combined solar activated sulfate radical-based advanced oxidation processes (SR-AOPs) and biofiltration for the remediation of dissolved organics in oil sands produced water. *Chemical Engineering Journal*, 433: 134579.

Gonçalves, N.P.F., Lourenço, M.A.O., Baleuri, S.R., Bianco, S., Jagdale, P., and Calza, P. 2022. Biochar waste-based ZnO materials as highly efficient photocatalysts for water treatment. *Journal of Environmental Chemical Engineering*, 10(2): 107256.

Hagen, M.O., Katzenback, B.A., Islam, M.D.S., Gamal El-Din, M., and Belosevic, M. 2013. The Analysis of Goldfish (*Carassius auratus* L.) Innate Immune Responses After Acute and

- Subchronic Exposures to Oil Sands Process-Affected Water. *Toxicological Sciences*, 138(1): 59-68.
- He, M., Xu, Z., Sun, Y., Chan, P.S., Lui, I., and Tsang, D.C.W. 2021a. Critical impacts of pyrolysis conditions and activation methods on application-oriented production of wood waste-derived biochar. *Bioresource technology*, 341: 125811.
- He, Y., Wang, Y., Hu, J., Wang, K., Zhai, Y., Chen, Y., Duan, Y., Wang, Y., and Zhang, W. 2021b. Photocatalytic property correlated with microstructural evolution of the biochar/ZnO composites. *Journal of Materials Research and Technology*, 11: 1308-1321.
- Huang, R., Chen, Y., Meshref, M.N.A., Chelme-Ayala, P., Dong, S., Ibrahim, M.D., Wang, C., Klammerth, N., Hughes, S.A., Headley, J.V., Peru, K.M., Brown, C., Mahaffey, A., and Gamal El-Din, M. 2018. Characterization and determination of naphthenic acids species in oil sands process-affected water and groundwater from oil sands development area of Alberta, Canada. *Water research*, 128: 129-137.
- Jing, H., Ji, L., Wang, Z., Guo, J., Lu, S., Sun, J., Cai, L., and Wang, Y. 2021. Synthesis of ZnO Nanoparticles Loaded on Biochar Derived from *Spartina alterniflora* with Superior Photocatalytic Degradation Performance. *Nanomaterials*, 11(10): 2479.
- Jones, D., West, C.E., Scarlett, A.G., Frank, R.A., and Rowland, S.J. 2012. Isolation and estimation of the 'aromatic' naphthenic acid content of an oil sands process-affected water extract. *Journal of Chromatography A*, 1247: 171-175.
- Jusoh, N.W.C., Jalil, A.A., Triwahyono, S., Setiabudi, H.D., Sapawe, N., Satar, M.A.H., Karim, A.H., Kamarudin, N.H.N., Jusoh, R., Jaafar, N.F., Salamun, N., and Efendi, J. 2013. Sequential desilication–isomorphous substitution route to prepare mesostructured silica

- nanoparticles loaded with ZnO and their photocatalytic activity. *Applied Catalysis A: General*, 468: 276-287.
- Kahkeci, J., and Gamal El-Din, M. 2023. Biochar-supported photocatalysts: Performance optimization and applications in emerging contaminant removal from wastewater. *Chemical Engineering Journal*, 476: 146530.
- Kamal, A., Saleem, M.H., Alshaya, H., Okla, M.K., Chaudhary, H.J., and Munis, M.F.H. 2022. Ball-milled synthesis of maize biochar-ZnO nanocomposite (MB-ZnO) and estimation of its photocatalytic ability against different organic and inorganic pollutants. *Journal of Saudi Chemical Society*, 26(3): 101445.
- Kim, C.H., and Kim, B.-H. 2015. Zinc oxide/activated carbon nanofiber composites for high-performance supercapacitor electrodes. *Journal of Power Sources*, 274: 512-520.
- Lee, K.M., Lai, C.W., Ngai, K.S., and Juan, J.C. 2016. Recent developments of zinc oxide based photocatalyst in water treatment technology: A review. *Water research*, 88: 428-448.
- Li, C., Fu, L., Stafford, J., Belosevic, M., and Gamal El-Din, M. 2017. The toxicity of oil sands process-affected water (OSPW): a critical review. *Science of the Total Environment*, 601: 1785-1802.
- Li, L., Liu, L., Li, Z., Hu, D., Gao, C., Xiong, J., and Li, W. 2019. The synthesis of CB[8]/ZnO composites materials with enhanced photocatalytic activities. *Heliyon*, 5(5): e01714.
- Li, Y., Lu, Q., Gamal Ei-Din, M., and Zhang, X. 2023. Immobilization of Photocatalytic ZnO Nanocaps on Planar and Curved Surfaces for the Photodegradation of Organic Contaminants in Water. *ACS ES&T Water*, 3(8): 2740-2752.
- MacKinnon, M.D., and Boerger, H. 1986. Description of two treatment methods for detoxifying oil sands tailings pond water. *Water Quality Research Journal*, 21(4): 496-512.

- Makama, A.B., Salmiaton, A., Choong, T.S.Y., Hamid, M.R.A., Abdullah, N., and Saion, E. 2020. Influence of parameters and radical scavengers on the visible-light-induced degradation of ciprofloxacin in ZnO/SnS<sub>2</sub> nanocomposite suspension: Identification of transformation products. *Chemosphere*, 253: 126689.
- Makula, P., Pacia, M., and Macyk, W. 2018. How To Correctly Determine the Band Gap Energy of Modified Semiconductor Photocatalysts Based on UV–Vis Spectra. *The Journal of Physical Chemistry Letters*, 9(23): 6814-6817.
- Mankomal, and Kaur, H. 2022. Synergistic effect of biochar impregnated with ZnO nano-flowers for effective removal of organic pollutants from wastewater. *Applied Surface Science Advances*, 12: 100339.
- Meng, L., How, Z.T., Ganiyu, S.O., and Gamal El-Din, M. 2021. Solar photocatalytic treatment of model and real oil sands process water naphthenic acids by bismuth tungstate: Effect of catalyst morphology and cations on the degradation kinetics and pathways. *Journal of hazardous materials*, 413: 125396.
- Mohamed, K.M., Benitto, J.J., Vijaya, J.J., and Bououdina, M. 2023. Recent Advances in ZnO-Based Nanostructures for the Photocatalytic Degradation of Hazardous, Non-Biodegradable Medicines. *Crystals*, 13(2): 329.
- Pang, Y.L., Law, Z.X., Lim, S., Chan, Y.Y., Shuit, S.H., Chong, W.C., and Lai, C.W. 2021. Enhanced photocatalytic degradation of methyl orange by coconut shell-derived biochar composites under visible LED light irradiation. *Environmental Science and Pollution Research*, 28(21): 27457-27473.
- Park, S.J., Das, G.S., Schütt, F., Adelung, R., Mishra, Y.K., Tripathi, K.M., and Kim, T. 2019. Visible-light photocatalysis by carbon-nano-onion-functionalized ZnO tetrapods:

- degradation of 2,4-dinitrophenol and a plant-model-based ecological assessment. *NPG Asia Materials*, 11(1): 8.
- Pérez-Estrada, L.A., Han, X., Drzewicz, P., Gamal El-Din, M., Fedorak, P.M., and Martin, J.W. 2011. Structure–reactivity of naphthenic acids in the ozonation process. *Environmental science & technology*, 45(17): 7431-7437.
- Qin, R., Chelme-Ayala, P., and Gamal El-Din, M. 2020. The impact of oil sands process water matrix on the ozonation of naphthenic acids: from a model compound to a natural mixture. *Canadian Journal of Civil Engineering*, 47(10): 1166-1174.
- Quinlan, P.J., and Tam, K.C. 2015. Water treatment technologies for the remediation of naphthenic acids in oil sands process-affected water. *Chemical Engineering Journal*, 279: 696-714.
- Shaheen, S.M., Niazi, N.K., Hassan, N.E.E., Bibi, I., Wang, H., Tsang, Daniel C.W., Ok, Y.S., Bolan, N., and Rinklebe, J. 2019. Wood-based biochar for the removal of potentially toxic elements in water and wastewater: a critical review. *International Materials Reviews*, 64(4): 216-247.
- USEPA. 2007. National Recommended Water Quality Criteria - Aquatic Life Criteria Table. *Edited by U.S.E.P. Agency*.
- Wang, C., Klammerth, N., Huang, R., Elnakar, H., and Gamal El-Din, M. 2016. Oxidation of oil sands process-affected water by potassium ferrate (VI). *Environmental science & technology*, 50(8): 4238-4247.
- Whitby, C. 2010. Chapter 3 - Microbial Naphthenic Acid Degradation. *In Advances in Applied Microbiology*. Academic Press. pp. 93-125.
- Xu, X., Meng, L., Dai, Y., Zhang, M., Sun, C., Yang, S., He, H., Wang, S., and Li, H. 2020. Bi-spheres SPR-coupled Cu<sub>2</sub>O/Bi<sub>2</sub>MoO<sub>6</sub> with hollow spheres forming Z-scheme

Cu<sub>2</sub>O/Bi/Bi<sub>2</sub>MoO<sub>6</sub> heterostructure for simultaneous photocatalytic decontamination of sulfadiazine and Ni(II). *Journal of hazardous materials*, 381: 120953.

Yang, C., Wang, X., Ji, Y., Ma, T., Zhang, F., Wang, Y., Ci, M., Chen, D., Jiang, A., and Wang, W. 2019. Photocatalytic degradation of methylene blue with ZnO@C nanocomposites: Kinetics, mechanism, and the inhibition effect on monoamine oxidase A and B. *NanoImpact*, 15: 100174.

Zhang, Y., Klammerth, N., Messele, S.A., Chelme-Ayala, P., and Gamal El-Din, M. 2016. Kinetics study on the degradation of a model naphthenic acid by ethylenediamine-N,N'-disuccinic acid-modified Fenton process. *Journal of hazardous materials*, 318: 371-378.

## CHAPTER 5. GENERAL CONCLUSIONS AND RECOMMENDATIONS

### 5.1 Thesis overview

Each year, large volumes of OSPW are generated from the bitumen extraction process by the oil sands industry in Alberta. The accumulation issue and the environmental concerns of the OSPW attracted increasing attention for developing remediation methods. Previous studies have reported that NAs are one of the main contributors that cause the toxicity of OSPW and remain structurally stable through natural attenuation processes such as biodegradation, photolysis, and hydrolysis. Therefore, the removal of NAs from OSPW has become a crucial research topic, during which various physical, chemical, biological, and combined technologies have been developed and evaluated over the years. Among all the developed technologies, adsorption was considered an effective and practical method to remove organic compounds from OSPW responsible for toxicity. So far, several adsorbents have been developed and evaluated for the adsorption performance of NAs or AEF from OSPW on bench-scale studies. On the other hand, AOPs are considered an efficient treatment for removing NAs from OSPW. Particularly, the photocatalysis process can be an eco-friendly and sustainable route since it can both use solar light as renewable green energy and environmentally friendly materials as catalysts. To date, it has been confirmed that ZnO can be used for the oxidative decomposition of NAs. Unfortunately, several specified drawbacks hinder the practical application of this semiconductor as photocatalyst, such as short photogenerated  $e^-h^+$  pairs lifetimes, limited visible light absorption, difficulties in recycling from reaction solutions, and potential leaching risks.

Additionally, according to the current situation of large amounts of waste production, waste prevention, recycling, reuse, and recovery are important strategies for waste material management

that can help achieve sustainable development goals. Due to the continuous accumulation issue of waste materials and the necessity for cost-effective and practical treatment methods for OSPW, the development of eco-friendly waste-derived materials became a crucial research topic and gained increasing attention due to its great potential. Therefore, this thesis addressed the development and application of different waste-derived materials and evaluated the effectiveness and feasibility for removing NAs related to OSPW.

As an undervalued by-product of the oil refining process, PC has been proved as an undervalued by-product that could be an efficient adsorbent alternative for the removal of AEF from OSPW. As a following upgraded scale-up study, Chapter 2 addressed the first large-scale field pilot study using the Fluid Coking Process Produced PC as an adsorbent for OSPW treatment.

Besides, the characteristics and adsorption potential of reclamation materials from oil sands industry, CST and PMM materials, have been less investigated. Additionally, it is essential to develop possible applications to help mitigate the accumulation issue of these materials. Chapter 3 presented the outcomes for the properties and adsorption behavior of NAs by these materials, simultaneously providing suggestions for the in-field management and the possible future application.

On the other hand, wood wastes from forestry could be used as cost-effective feedstock to produce biochar. More importantly, as a sustainable, cost-effective, and eco-friendly carbon material with various advantages, biochar was considered an excellent alternative to generate composite with semiconductors to achieve enhanced photocatalytic performance. However, the effectiveness and feasibility of degrading OSPW-related NAs using biochar/ZnO composite remained a research gap. Therefore, the BC/ZnO composites were designed and prepared in

Chapter 4. This novel study applied the BC/ZnO composite for the solar photocatalytic degradation of both single NA model and a complex NAs mixture. The findings of this study provided a crucial insight into the feasibility of using BC/ZnO composite towards real OSPW.

## 5.2 Conclusions

The results obtained from this research indicated that different waste-derived materials were successfully developed and showed great potential for the remediation of OSPW. Based on the experimental results, the main outcomes from each chapter are as follows:

### **Chapter 2 – Treatment of oil sands process water using petroleum coke: Field pilot**

In this study, for the first time, the feasibility and effectiveness of PC adsorption treatment for OSPW was assessed by a large-scale field pilot study. The water quality of treated OSPW was evaluated by looking changes in organic constituents (AEF and DOC), TPH, phenols, PAHs, VOCs, vanadium, other trace element concentrations, major ions, conductivity, TSS, pH, and toxicity. The key findings are summarized in the following:

- AEF adsorption by PC followed PSO kinetics, and the overall combined removal efficiency of AEF was greater than 80%.
- Reactor 1 showed higher AEF removal than Reactor 2. DOC decreased about 50% after 4 weeks of retention in the PC deposit.
- An increase in vanadium concentration after PC contact indicated that vanadium leaching occurred. However, with increased residence time in the PC deposit, vanadium concentration decreased in the cells and tanks by 42% and 98%, respectively.

- Filtration through the PC deposit reduced the TSS in OSPW to less than laboratory-detectable limits.
- Unlike untreated OSPW, treated OSPW did not show an acute toxic response based on whole effluent toxicity testing using trout, zooplankton, and bacteria.

All the findings from this study finally lead to the conclusion that PC adsorption is a potentially commercially viable technology for efficient remediation of OSPW.

### **Chapter 3 – Adsorption Assessment of Naphthenic Acids on Reclamation Materials: Coarse Sand Tailings and Peat mineral Mix**

In this study, the adsorption behavior of NAs on two reclamation materials from the oil sands industry was detailed investigated. The main outcomes are summarized in the following:

- CST was characterized as a sandy texture material with heterogeneous surfaces and less porous structures. PMM was identified as an organic-rich material with a relatively high surface area and pore volume as well as more clay composition. The exhibited significant portions of hydrophobic functional groups in PMM led to a better adsorption potential.
- The adsorption of DDA on CST and PMM followed a PSO kinetics and IPD model separately. The Freundlich model provided the best description for the DDA adsorption on these materials.
- The adsorption capacity of DDA at equilibrium for PMM (2.4 mg/g) is much higher than CST (0.05 mg/g).

- Hydrophobic interaction was identified as the predominant adsorption mechanism for NAs on CST and PMM.
- Only DDA and DA were partially removed by CST from the NAs mixture solution. PMM showed more effective adsorption capacity by achieving around 100% removal of DDA, DA, and CHPA and 70% removal of PVA in 96 h.

Based on the outcomes of this study, PMM material showed great adsorption potential towards NAs. It was highlighted that PMM could be suggested as a potential alternative adsorbent for NAs removal from real OSPW as a future application.

#### **Chapter 4 – Efficient Degradation of Naphthenic Acids in Water Using a Sustainable Engineered Biochar/ZnO Composite Under Solar Light**

In this study, BC/ZnO composites were successfully developed and synthesized using wood wastes as a sustainable biochar source and applied under simulated solar light for the photocatalytic degradation of NAs. The main outcomes are summarized in the following:

- The porous structure and roughened surface of the biochar make it an excellent platform to support ZnO particles. Moreover, the biochar served as an electron sink that could inhibit the recombination of photogenerated  $e^-$ - $h^+$  pairs and provided more reactive sites.
- The effect of different ZnO content, different dosages of the composite, and different solar irradiation times was investigated. The best experimental conditions were determined as 0.5 g/L BC/30%ZnO with 4 h solar irradiation, reaching 93.7% of CHA degradation efficiency following PFO kinetics.

- •OH species were the main ROS involved in the degradation process of CHA using the composite under solar radiation.
- The composite presented a good reusability after 4 cycles of use, maintaining a degradation efficiency over 90%.
- This was the first study using BC/30%ZnO composite as a photocatalyst for the degradation of a NAs mixture under solar irradiation. A competition tendency of different NAs during the degradation process was observed: NAs with S atom, as well as large, branched, and cyclic NAs showed a better degradation performance.
- After 6 h solar irradiation, the total degradation efficiency of NAs in the mixture using 0.5 g/L BC/30%ZnO composite was up to 95.5%.

Considering the excellent photocatalytic performance of the BC/30%ZnO composite for NAs degradation, as well as its good reusability and stability, this photocatalyst is a sustainable approach for the remediation of OSPW.

In sum, the outcomes from the thesis provided valuable insights into developing sustainable and cost-effective remediation approaches for OSPW. In the meantime, all the findings enhanced the understanding of different waste-derived materials and highlighted the possible application for them in the future. Among these studies with different waste materials, it was suggested that the *in-situ* PC adsorption is most likely to be practically applied for OSPW remediation with the current supporting data from the large-scale study. More importantly, this research offered meaningful guidance for pursuing a “win-win” sustainable development by further promoting economically feasible waste management and environmental remediation at the same time.

### 5.3 Recommendations for future studies

From the wastewater management and waste material management perspective, addressing the remediation of OSPW and recycling waste materials is essential. Based on the results from the research, further research is required to advance this pursuit. The recommendations are proposed accordingly as follows:

- For the petroleum adsorption treatment of OSPW, current 4-month pilot-program results supported the conclusion from previous bench-scale studies, which indicated that PC can be used as a cost-effective and efficient adsorbent material for the *in-situ* treatment of OSPW. As the next stage, a full-scale program is suggested for another upgraded scale-up attempt, which can be designed to run for a longer term. Besides, another concern is the internal corrosion inside the walls of the steel tank reactors, which is related to changes in the trace metal concentration of the treated OSPW. Future studies should pay attention to this matter.
- PMM can be applied as a good adsorbent material for future study. The current results showed that PMM removed different structured NAs model compounds. As a further suggestion, real OSPW should be introduced to study the removal efficiency of organic and inorganic constituents by PMM. Furthermore, the adsorption process can be evaluated by fixed-bed columns and passive treatments such as wetlands and pit lakes to achieve the scale-up study. Moreover, considering the accumulation issue of CST and the selective removal results of long-chain structured hydrophobic NAs model compounds, a fixed bed column filled by different layers containing both CST and

- other sorbents can be built up for further study. On the other hand, soil amendments can be another option to be assessed.
- The BC/ZnO composites significantly degraded the NAs mixture under solar light. One important future work is to investigate the reaction pathway of NAs model compounds degradation. Furthermore, the photocatalytic degradation performance of NAs from real OSPW should be investigated, more importantly, the treated OSPW needs to be assessed for toxicity. In the meantime, the optimization of lower dosage of the composite and longer solar irradiation time needs to be conducted.
  - Although the performance of this BC/ZnO photocatalysis system was adequate for all the parameters investigated, the results of this study are limited to lab-scale application and batch conditions. Future studies should be focused on understanding and applying this system at pilot and full scale, aiming at its application in combination with known OSPW treatments, such as wetlands, and pit lakes.
  - The BC/ZnO composite outcomes provide a great insight into the potential of waste-derived biochar-supported semiconductor photocatalysts for the degradation of NAs related to OSPW using solar light. ZnO is not the only choice as the semiconductor photocatalyst that can be combined with biochar. At the same time, the feedstock of biochar can be changed to other waste materials, such as wheat straw from agricultural activities or food waste from local human activities, etc.
  - Finally, as an important concern, economic cost analysis and life cycle assessment should be involved as parts of future work for *in-situ* PC adsorption, PMM or CST

adsorption as well as the BC/ZnO photocatalysis, which can give important guidance for the practical implementation of the OSPW remediation.

## BIBLIOGRAPHY

- Abdalrhman, A.S., Zhang, Y., and Gamal El-Din, M. 2019. Electro-oxidation by graphite anode for naphthenic acids degradation, biodegradability enhancement and toxicity reduction. *Science of the Total Environment*, 671: 270-279.
- Abdalrhman, A.S.A. 2019. Application of Electro-oxidation for the Degradation of Organics in Oil Sands Process Water (OSPW). Thesis, University of Alberta.
- Abdul Karim, M.R., Ul Haq, E., Hussain, M.A., Khan, K.I., Nadeem, M., Atif, M., Ul Haq, A., Naveed, M., and Alam, M.M. 2020. Experimental evaluation of sustainable geopolymer mortars developed from loam natural soil. *Journal of Asian Architecture and Building Engineering*, 19(6): 637-646.
- Afzal, A., Chelme-Ayala, P., Drzewicz, P., Martin, J.W., and Gamal El-Din, M. 2015. Effects of Ozone and Ozone/Hydrogen Peroxide on the Degradation of Model and Real Oil-Sands-Process-Affected-Water Naphthenic Acids. *Ozone: Science & Engineering*, 37(1): 45-54.
- Afzal, A., Drzewicz, P., Pérez-Estrada, L.A., Chen, Y., Martin, J.W., and Gamal El-Din, M. 2012. Effect of Molecular Structure on the Relative Reactivity of Naphthenic Acids in the UV/H<sub>2</sub>O<sub>2</sub> Advanced Oxidation Process. *Environmental science & technology*, 46(19): 10727-10734.
- Ahmad, I., Zou, Y., Yan, J., Liu, Y., Shukrullah, S., Naz, M.Y., Hussain, H., Khan, W.Q., and Khalid, N.R. 2023. Semiconductor photocatalysts: A critical review highlighting the various strategies to boost the photocatalytic performances for diverse applications. *Advances in Colloid and Interface Science*, 311: 102830.

- Al-Ghouti, M.A., and Da'ana, D.A. 2020. Guidelines for the use and interpretation of adsorption isotherm models: A review. *Journal of hazardous materials*, 393: 122383.
- Al-Smadi, B.M., Al Oran, E.H., and Abu Hajar, H.A. 2019. Adsorption-desorption of cypermethrin and chlorfenapyr on Jordanian soils. *Arabian Journal of Geosciences*, 12(15): 465.
- Alberta Energy Regulator. 2023. State of Fluid Tailings Management for Mineable Oil Sands, 2022. Alberta Energy Regulator: Calgary, AB, Canada.
- Ali, F.H., Sing, W.L., and Hashim, R. 2010. Engineering properties of improved fibrous peat. *Scientific Research and Essay*, 5(2): 154-169.
- Allen, E.W. 2008a. Process water treatment in Canada's oil sands industry: I. Target pollutants and treatment objectives. *Journal of Environmental Engineering and Science*, 7(2): 123-138.
- Allen, E.W. 2008b. Process water treatment in Canada's oil sands industry: II. A review of emerging technologies. *Journal of Environmental Engineering and Science*, 7(5): 499-524.
- Aminur, M., Kolay, P., Taib, S., Mohd Zain, M., and Kamal, A. 2011. Physical, geotechnical and morphological characteristics of peat soils from Sarawak. *Inst. Eng. Malaysia*, 72(4): 5.
- Amir, M., Fazal, T., Iqbal, J., Din, A.A., Ahmed, A., Ali, A., Razzaq, A., Ali, Z., Rehman, M.S.U., and Park, Y.-K. 2022. Integrated adsorptive and photocatalytic degradation of pharmaceutical micropollutant, ciprofloxacin employing biochar-ZnO composite photocatalysts. *Journal of Industrial and Engineering Chemistry*, 115: 171-182.
- Anderson, J., Wiseman, S.B., Moustafa, A., El-Din, M.G., Liber, K., and Giesy, J.P. 2012a. Effects of exposure to oil sands process-affected water from experimental reclamation ponds on *Chironomus dilutus*. *Water research*, 46(6): 1662-1672.
- Anderson, J., Wiseman, S., Wang, N., Moustafa, A., Perez-Estrada, L., Gamal El-Din, M., Martin, J., Liber, K., and Giesy, J.P. 2012b. Effectiveness of ozonation treatment in eliminating

- toxicity of oil sands process-affected water to *Chironomus dilutus*. *Environmental science & technology*, 46(1): 486-493.
- Antonopoulou, M., Bika, P., Papailias, I., Zervou, S.-K., Vrettou, A., Efthimiou, I., Mitrikas, G., Ioannidis, N., Trapalis, C., Dallas, P., Vlastos, D., and Hiskia, A. 2023. Photocatalytic degradation of organic micropollutants under UV-A and visible light irradiation by exfoliated g-C<sub>3</sub>N<sub>4</sub> catalysts. *Science of the Total Environment*, 892: 164218.
- Arslan, M., Ganiyu, S.O., Lillico, D.M.E., Stafford, J.L., and Gamal El-Din, M. 2023. Fate of dissolved organics and generated sulfate ions during biofiltration of oil sands process water pretreated with sulfate radical advanced oxidation process. *Chemical Engineering Journal*, 458: 141390.
- Arthur, J.D., Mark, N.W., Taylor, S., Šimunek, J., Brusseau, M.L., and Dontsova, K.M. 2017. Batch soil adsorption and column transport studies of 2, 4-dinitroanisole (DNAN) in soils. *Journal of contaminant hydrology*, 199: 14-23.
- Bakatula, E.N., Richard, D., Neculita, C.M., and Zagury, G.J. 2018. Determination of point of zero charge of natural organic materials. *Environmental Science and Pollution Research*, 25(8): 7823-7833.
- Barrette, J., Paré, D., Manka, F., Guindon, L., Bernier, P., and Titus, B. 2018. Forecasting the spatial distribution of logging residues across the Canadian managed forest. *Canadian Journal of Forest Research*, 48(12): 1470-1481.
- Bataineh, M., Scott, A., Fedorak, P., and Martin, J. 2006. Capillary HPLC/QTOF-MS for characterizing complex naphthenic acid mixtures and their microbial transformation. *Analytical Chemistry*, 78(24): 8354-8361.

- BBK, K.S.H., and Prasad, A. 2011. Study of Peat Media on Stabilization of Peat by Traditional Binders. *Int. J. Phys. Sci*, 6(3): 476-481.
- Benally, C., Messele, S.A., and Gamal El-Din, M. 2019. Adsorption of organic matter in oil sands process water (OSPW) by carbon xerogel. *Water research*, 154: 402-411.
- Bhavani, P., Hussain, M., and Park, Y.-K. 2022. Recent advancements on the sustainable biochar based semiconducting materials for photocatalytic applications: A state of the art review. *Journal of cleaner production*, 330: 129899.
- Bhuiyan, T.I., Tak, J.K., Sessarego, S., Harfield, D., and Hill, J.M. 2017. Adsorption of acid-extractable organics from oil sands process-affected water onto biomass-based biochar: Metal content matters. *Chemosphere*, 168: 1337-1344.
- Biester, H., Knorr, K.-H., Schellekens, J., Basler, A., and Hermanns, Y.-M. 2014. Comparison of different methods to determine the degree of peat decomposition in peat bogs. *Biogeosciences*, 11(10): 2691-2707.
- Boguta, P., Sokołowska, Z., Skic, K., and Tomczyk, A. 2019. Chemically engineered biochar – Effect of concentration and type of modifier on sorption and structural properties of biochar from wood waste. *Fuel*, 256: 115893.
- Bošković, N., Brandstätter-Scherr, K., Sedláček, P., Bílková, Z., Bielská, L., and Hofman, J. 2020. Adsorption of epoxiconazole and tebuconazole in twenty different agricultural soils in relation to their properties. *Chemosphere*, 261: 127637.
- Brown, L.D., and Ulrich, A.C. 2015. Oil sands naphthenic acids: a review of properties, measurement, and treatment. *Chemosphere*, 127: 276-290.
- Cai, H., Zhang, D., Ma, X., and Ma, Z. 2022. A novel ZnO/biochar composite catalysts for visible light degradation of metronidazole. *Separation and Purification Technology*, 288: 120633.

Canada, N.R. 2020. Crude oil facts.

Celi, L., Schnitzer, M., and Nègre, M. 1997. ANALYSIS OF CARBOXYL GROUPS IN SOIL HUMIC ACIDS BY A WET CHEMICAL METHOD, FOURIER-TRANSFORM INFRARED SPECTROPHOTOMETRY, AND SOLUTION-STATE CARBON-13 NUCLEAR MAGNETIC RESONANCE. A COMPARATIVE STUDY. *Soil Science*, 162(3): 189-197.

Chapman, S., Campbell, C., Fraser, A., and Puri, G. 2001. FTIR spectroscopy of peat in and bordering Scots pine woodland: relationship with chemical and biological properties. *Soil Biology and Biochemistry*, 33(9): 1193-1200.

Chen, M., Bao, C., Hu, D., Jin, X., and Huang, Q. 2019. Facile and low-cost fabrication of ZnO/biochar nanocomposites from jute fibers for efficient and stable photodegradation of methylene blue dye. *Journal of Analytical and Applied Pyrolysis*, 139: 319-332.

Chen, X., Gu, X., Bao, L., Ma, S., and Mu, Y. 2021. Comparison of adsorption and desorption of triclosan between microplastics and soil particles. *Chemosphere*, 263: 127947.

Choi, M., Brabec, C., and Hayakawa, T. 2022. X-ray Diffraction, Micro-Raman and X-ray Photoemission Spectroscopic Investigations for Hydrothermally Obtained Hybrid Compounds of Delafossite CuGaO<sub>2</sub> and Wurtzite ZnO. *Ceramics*, 5(4): 655-672.

Chung, K., Janke, L., Dureau, R., and Furimsky, E. 1996. Leachability of cokes from Syncrude stockpiles. *Environmental Science and Engineering*, 9(1): 50-53.

Clemente, J.S., and Fedorak, P.M. 2005. A review of the occurrence, analyses, toxicity, and biodegradation of naphthenic acids. *Chemosphere*, 60(5): 585-600.

COSIA. 2012. Guide for Fluid Fine Tailings Management. Online (Available from <https://cosia.ca/node/57>, accessed 23 May 2023).

- Cossey, H.L., Batycky, A.E., Kaminsky, H., and Ulrich, A.C. 2021. Geochemical stability of oil sands tailings in mine closure landforms. *Minerals*, 11(8): 830.
- Cui, J., Zhang, F., Li, H., Cui, J., Ren, Y., and Yu, X. 2020. Recent Progress in Biochar-Based Photocatalysts for Wastewater Treatment: Synthesis, Mechanisms, and Applications. *Applied Sciences* 10(3) [cited].
- de Oliveira Livera, D., Leshuk, T., Peru, K.M., Headley, J.V., and Gu, F. 2018. Structure-reactivity relationship of naphthenic acids in the photocatalytic degradation process. *Chemosphere*, 200: 180-190.
- Deng, X., Jiang, Y., Zhang, M.a., Nan, Z., Liang, X., and Wang, G. 2022. Sorption properties and mechanisms of erythromycin and ampicillin in loess soil: Roles of pH, ionic strength, and temperature. *Chemical Engineering Journal*, 434: 134694.
- Deng, Y., and Zhao, R. 2015. Advanced Oxidation Processes (AOPs) in Wastewater Treatment. *Current Pollution Reports*, 1(3): 167-176.
- Devangsari, I., Nurudin, M., Sartohadi, J., and Karmila, Y. Characteristics of peat functional group in Padang Island, Indonesia. *In IOP Conference Series: Earth and Environmental Science*. 2022. IOP Publishing. p. 012022.
- Drollinger, S., Knorr, K.-H., Knierzinger, W., and Glatzel, S. 2020. Peat decomposition proxies of Alpine bogs along a degradation gradient. *Geoderma*, 369: 114331.
- ECCC. 2019. Risk Management Scope for Zinc and Soluble Zinc Compounds under the Zinc and its Compounds grouping. *Edited by H. Canada*.
- Ekennia, A.C., Uduagwu, D.N., Nwaji, N.N., Oje, O.O., Emma-Uba, C.O., Mgbii, S.I., Olowo, O.J., and Nwanji, O.L. 2021. Green Synthesis of Biogenic Zinc Oxide Nanoflower as Dual

- Agent for Photodegradation of an Organic Dye and Tyrosinase Inhibitor. *Journal of Inorganic and Organometallic Polymers and Materials*, 31(2): 886-897.
- EPA, U. 2004. SW-846 test method 9045D: soil and waste pH. US EPA, Washington DC.
- Fan, T.P. 1991. Characterization of naphthenic acids in petroleum by fast atom bombardment mass spectrometry. *Energy & Fuels*, 5(3): 371-375.
- Fang, Z., Huang, R., Chelme-Ayala, P., Shi, Q., Xu, C., and Gamal El-Din, M. 2019. Comparison of UV/Persulfate and UV/H<sub>2</sub>O<sub>2</sub> for the removal of naphthenic acids and acute toxicity towards *Vibrio fischeri* from petroleum production process water. *Science of the Total Environment*, 694: 133686.
- Fang, Z., Huang, R., How, Z.T., Jiang, B., Chelme-Ayala, P., Shi, Q., Xu, C., and El-Din, M.G. 2020. Molecular transformation of dissolved organic matter in process water from oil and gas operation during UV/H<sub>2</sub>O<sub>2</sub>, UV/chlorine, and UV/persulfate processes. *Science of the Total Environment*, 730: 139072.
- Fernandes, A.N., Giovanela, M., Esteves, V.I., and Sierra, M.M.d.S. 2010. Elemental and spectral properties of peat and soil samples and their respective humic substances. *Journal of Molecular Structure*, 971(1): 33-38.
- Foo, K.Y., and Hameed, B.H. 2010. Insights into the modeling of adsorption isotherm systems. *Chemical Engineering Journal*, 156(1): 2-10.
- Frank, R.A., Fischer, K., Kavanagh, R., Burnison, B.K., Arsenault, G., Headley, J.V., Peru, K.M., Kraak, G.V.D., and Solomon, K.R. 2009. Effect of Carboxylic Acid Content on the Acute Toxicity of Oil Sands Naphthenic Acids. *Environmental science & technology*, 43(2): 266-271.

- Frankel, M.L., Bhuiyan, T.I., Veksha, A., Demeter, M.A., Layzell, D.B., Helleur, R.J., Hill, J.M., and Turner, R.J. 2016. Removal and biodegradation of naphthenic acids by biochar and attached environmental biofilms in the presence of co-contaminating metals. *Bioresource technology*, 216: 352-361.
- Gamal El-Din, M., Fu, H., Wang, N., Chelme-Ayala, P., Pérez-Estrada, L., Drzewicz, P., Martin, J.W., Zubot, W., and Smith, D.W. 2011. Naphthenic acids speciation and removal during petroleum-coke adsorption and ozonation of oil sands process-affected water. *Science of the Total Environment*, 409(23): 5119-5125.
- Ganiyu, S.O., Arslan, M., and Gamal El-Din, M. 2022. Combined solar activated sulfate radical-based advanced oxidation processes (SR-AOPs) and biofiltration for the remediation of dissolved organics in oil sands produced water. *Chemical Engineering Journal*, 433: 134579.
- Garcia-Garcia, E., Ge, J.Q., Oladiran, A., Montgomery, B., El-Din, M.G., Perez-Estrada, L.C., Stafford, J.L., Martin, J.W., and Belosevic, M. 2011. Ozone treatment ameliorates oil sands process water toxicity to the mammalian immune system. *Water research*, 45(18): 5849-5857.
- George William, K., Serkan, E., Atakan, Ö., Özcan, H.K., and Serdar, A. 2018. Modelling of Adsorption Kinetic Processes—Errors, Theory and Application. *In* Advanced sorption process applications. *Edited by* E. Serpil. IntechOpen, Rijeka. p. Ch. 10.
- Gonçalves, N.P.F., Lourenço, M.A.O., Baleuri, S.R., Bianco, S., Jagdale, P., and Calza, P. 2022. Biochar waste-based ZnO materials as highly efficient photocatalysts for water treatment. *Journal of Environmental Chemical Engineering*, 10(2): 107256.

- Grewer, D.M., Young, R.F., Whittal, R.M., and Fedorak, P.M. 2010. Naphthenic acids and other acid-extractables in water samples from Alberta: what is being measured? *Science of the Total Environment*, 408(23): 5997-6010.
- Hagen, M.O., Katzenback, B.A., Islam, M.D.S., Gamal El-Din, M., and Belosevic, M. 2013. The Analysis of Goldfish (*Carassius auratus* L.) Innate Immune Responses After Acute and Subchronic Exposures to Oil Sands Process-Affected Water. *Toxicological Sciences*, 138(1): 59-68.
- Harrison, J.S., Higgins, C.D., O'Meara, M.J., Koellhoffer, J.F., Kuhlman, B.A., and Lai, J.R. 2013. Role of electrostatic repulsion in controlling pH-dependent conformational changes of viral fusion proteins. *Structure*, 21(7): 1085-1096.
- He, M., Xu, Z., Sun, Y., Chan, P.S., Lui, I., and Tsang, D.C.W. 2021a. Critical impacts of pyrolysis conditions and activation methods on application-oriented production of wood waste-derived biochar. *Bioresource technology*, 341: 125811.
- He, Y., Wang, Y., Hu, J., Wang, K., Zhai, Y., Chen, Y., Duan, Y., Wang, Y., and Zhang, W. 2021b. Photocatalytic property correlated with microstructural evolution of the biochar/ZnO composites. *Journal of Materials Research and Technology*, 11: 1308-1321.
- Hermosin, M.C., Martin, P., and Cornejo, J. 1993. Adsorption mechanisms of monobutyltin in clay minerals. *Environmental science & technology*, 27(12): 2606-2611.
- Herrmann, J.-M. 1999. Heterogeneous photocatalysis: fundamentals and applications to the removal of various types of aqueous pollutants. *Catalysis Today*, 53(1): 115-129.
- Hossain, N., Bhuiyan, M.A., Pramanik, B.K., Nizamuddin, S., and Griffin, G. 2020. Waste materials for wastewater treatment and waste adsorbents for biofuel and cement supplement applications: A critical review. *Journal of cleaner production*, 255: 120261.

- Huang, C., Shi, Y., Xue, J., Zhang, Y., Gamal El-Din, M., and Liu, Y. 2017. Comparison of biomass from integrated fixed-film activated sludge (IFAS), moving bed biofilm reactor (MBBR) and membrane bioreactor (MBR) treating recalcitrant organics: Importance of attached biomass. *Journal of hazardous materials*, 326: 120-129.
- Huang, C.P., Dong, C., and Tang, Z. 1993. Advanced chemical oxidation: Its present role and potential future in hazardous waste treatment. *Waste Management*, 13(5): 361-377.
- Huang, R., Yang, L., How, Z.T., Fang, Z., Bekele, A., Letinski, D.J., Redman, A.D., and El-Din, M.G. 2021. Characterization of raw and ozonated oil sands process water utilizing atmospheric pressure gas chromatography time-of-flight mass spectrometry combined with solid phase microextraction. *Chemosphere*, 266: 129017.
- Huang, R., Chen, Y., Meshref, M.N.A., Chelme-Ayala, P., Dong, S., Ibrahim, M.D., Wang, C., Klammerth, N., Hughes, S.A., Headley, J.V., Peru, K.M., Brown, C., Mahaffey, A., and Gamal El-Din, M. 2018. Characterization and determination of naphthenic acids species in oil sands process-affected water and groundwater from oil sands development area of Alberta, Canada. *Water research*, 128: 129-137.
- Hyndman, A.W. APPLICATION OF FLUID COKING TO UPGRADING OF ATHABASCA BITUMEN. *In* 1981. McGraw Hill., New York. pp. 645-647.
- Ibhadon, A.O., and Fitzpatrick, P. 2013. Heterogeneous Photocatalysis: Recent Advances and Applications. *Catalysts*, 3(1): 189-218.
- Ippolito, J.A., Cui, L., Kammann, C., Wrage-Mönnig, N., Estavillo, J.M., Fuertes-Mendizabal, T., Cayuela, M.L., Sigua, G., Novak, J., Spokas, K., and Borchard, N. 2020. Feedstock choice, pyrolysis temperature and type influence biochar characteristics: a comprehensive meta-data analysis review. *Biochar*, 2(4): 421-438.

- Isiuku, B.O., Okonkwo, P.C., and Emeagwara, C.D. 2021. Batch adsorption isotherm models applied in single and multicomponent adsorption systems – a review. *Journal of Dispersion Science and Technology*, 42(12): 1879-1897.
- Islam, M.S., Zhang, Y., McPhedran, K.N., Liu, Y., and Gamal El-Din, M. 2015. Granular activated carbon for simultaneous adsorption and biodegradation of toxic oil sands process-affected water organic compounds. *Journal of environmental management*, 152: 49-57.
- Islam, M.S., McPhedran, K.N., Messele, S.A., Liu, Y., and Gamal El-Din, M. 2018. Isotherm and kinetic studies on adsorption of oil sands process-affected water organic compounds using granular activated carbon. *Chemosphere*, 202: 716-725.
- Islam, M.S., Dong, T., Sheng, Z., Zhang, Y., Liu, Y., and Gamal El-Din, M. 2014a. Microbial community structure and operational performance of a fluidized bed biofilm reactor treating oil sands process-affected water. *International biodeterioration & biodegradation*, 91: 111-118.
- Islam, M.S., Dong, T., McPhedran, K.N., Sheng, Z., Zhang, Y., Liu, Y., and Gamal El-Din, M. 2014b. Impact of ozonation pre-treatment of oil sands process-affected water on the operational performance of a GAC-fluidized bed biofilm reactor. *Biodegradation*, 25(6): 811-823.
- Janfada, A., Headley, J.V., Peru, K.M., and Barbour, S. 2006. A laboratory evaluation of the sorption of oil sands naphthenic acids on organic rich soils. *Journal of Environmental Science and Health, Part A*, 41(6): 985-997.
- Jeong, G., and Nousiainen, T. 2014. TEM analysis of the internal structures and mineralogy of Asian dust particles and the implications for optical modeling. *Atmospheric Chemistry and Physics*, 14(14): 7233-7254.

- Jing, H., Ji, L., Wang, Z., Guo, J., Lu, S., Sun, J., Cai, L., and Wang, Y. 2021. Synthesis of ZnO Nanoparticles Loaded on Biochar Derived from *Spartina alterniflora* with Superior Photocatalytic Degradation Performance. *Nanomaterials*, 11(10): 2479.
- Jones, D., Scarlett, A.G., West, C.E., and Rowland, S.J. 2011. Toxicity of individual naphthenic acids to *Vibrio fischeri*. *Environmental science & technology*, 45(22): 9776-9782.
- Jones, D., West, C.E., Scarlett, A.G., Frank, R.A., and Rowland, S.J. 2012. Isolation and estimation of the 'aromatic' naphthenic acid content of an oil sands process-affected water extract. *Journal of Chromatography A*, 1247: 171-175.
- Jones, R., and Forrest, D. 2010. Oil Sands Mining Reclamation Challenge Dialogue—Report and Appendices.
- Ju, D., and Young, T.M. 2005. The Influence of Natural Organic Matter Rigidity on the Sorption, Desorption, and Competitive Displacement Rates of 1,2-Dichlorobenzene. *Environmental science & technology*, 39(20): 7956-7963.
- Jusoh, N.W.C., Jalil, A.A., Triwahyono, S., Setiabudi, H.D., Sapawe, N., Satar, M.A.H., Karim, A.H., Kamarudin, N.H.N., Jusoh, R., Jaafar, N.F., Salamun, N., and Efendi, J. 2013. Sequential desilication–isomorphous substitution route to prepare mesostructured silica nanoparticles loaded with ZnO and their photocatalytic activity. *Applied Catalysis A: General*, 468: 276-287.
- Kahkeci, J., and Gamal El-Din, M. 2023. Biochar-supported photocatalysts: Performance optimization and applications in emerging contaminant removal from wastewater. *Chemical Engineering Journal*, 476: 146530.
- Kamal, A., Saleem, M.H., Alshaya, H., Okla, M.K., Chaudhary, H.J., and Munis, M.F.H. 2022. Ball-milled synthesis of maize biochar-ZnO nanocomposite (MB-ZnO) and estimation of

- its photocatalytic ability against different organic and inorganic pollutants. *Journal of Saudi Chemical Society*, 26(3): 101445.
- Khan, S.U., Kumar, A., Prasad, M., Upadhyay, D., Mehta, B.K., Shashikumara, P., and Tamboli, P. 2023. Effect of soil amendments on the sorption behavior of atrazine in sandy loam soil. *Environmental Monitoring and Assessment*, 195(6): 686.
- Kim, C.H., and Kim, B.-H. 2015. Zinc oxide/activated carbon nanofiber composites for high-performance supercapacitor electrodes. *Journal of Power Sources*, 274: 512-520.
- Klamerth, N., Moreira, J., Li, C., Singh, A., McPhedran, K.N., Chelme-Ayala, P., Belosevic, M., and Gamal El-Din, M. 2015. Effect of ozonation on the naphthenic acids' speciation and toxicity of pH-dependent organic extracts of oil sands process-affected water. *Science of the Total Environment*, 506: 66-75.
- Krumins, J., Klavins, M., Seglins, V., and Kaup, E. 2012. Comparative study of peat composition by using FT-IR spectroscopy. *Rigas Tehniskas Universitates Zinatniskie Raksti*, 26: 106.
- Le Guillou, F., Wetterlind, W., Rossel, R.V., Hicks, W., Grundy, M., and Tuomi, S. 2015. How does grinding affect the mid-infrared spectra of soil and their multivariate calibrations to texture and organic carbon? *Soil Research*, 53(8): 913-921.
- Lee, K.M., Lai, C.W., Ngai, K.S., and Juan, J.C. 2016. Recent developments of zinc oxide based photocatalyst in water treatment technology: A review. *Water research*, 88: 428-448.
- Leshuk, T., Wong, T., Linley, S., Peru, K.M., Headley, J.V., and Gu, F. 2016. Solar photocatalytic degradation of naphthenic acids in oil sands process-affected water. *Chemosphere*, 144: 1854-1861.
- Letterman, R.D., and Association, A.W.W. 1999. *Water quality and treatment: a handbook of community water supplies*. McGraw-Hill.

- Li, C., Fu, L., Stafford, J., Belosevic, M., and Gamal El-Din, M. 2017. The toxicity of oil sands process-affected water (OSPW): a critical review. *Science of the Total Environment*, 601: 1785-1802.
- Li, F., Fang, X., Zhou, Z., Liao, X., Zou, J., Yuan, B., and Sun, W. 2019a. Adsorption of perfluorinated acids onto soils: Kinetics, isotherms, and influences of soil properties. *Science of the Total Environment*, 649: 504-514.
- Li, L., Liu, L., Li, Z., Hu, D., Gao, C., Xiong, J., and Li, W. 2019b. The synthesis of CB[8]/ZnO composites materials with enhanced photocatalytic activities. *Heliyon*, 5(5): e01714.
- Li, Y., Lu, Q., Gamal Ei-Din, M., and Zhang, X. 2023. Immobilization of Photocatalytic ZnO Nanocaps on Planar and Curved Surfaces for the Photodegradation of Organic Contaminants in Water. *ACS ES&T Water*, 3(8): 2740-2752.
- Li, Y., Wei, M., Liu, L., Xue, Q., and Yu, B. 2020. Adsorption of toluene on various natural soils: Influences of soil properties, mechanisms, and model. *Science of the Total Environment*: 140104.
- Li, Z., and Gallus, L. 2007. Adsorption of dodecyl trimethylammonium and hexadecyl trimethylammonium onto kaolinite — Competitive adsorption and chain length effect. *Applied Clay Science*, 35(3): 250-257.
- Liang, S., Xiao, K., Mo, Y., and Huang, X. 2012. A novel ZnO nanoparticle blended polyvinylidene fluoride membrane for anti-irreversible fouling. *Journal of Membrane Science*, 394-395: 184-192.
- Lim, S.-F., and Lee, A.Y.W. 2015. Kinetic study on removal of heavy metal ions from aqueous solution by using soil. *Environmental Science and Pollution Research*, 22(13): 10144-10158.

- Mackay, D. 2001. Multimedia environmental models: the fugacity approach. CRC press.
- MacKinnon, M.D., and Boerger, H. 1986. Description of two treatment methods for detoxifying oil sands tailings pond water. *Water Quality Research Journal*, 21(4): 496-512.
- Madill, R.E., Orzechowski, M.T., Chen, G., Brownlee, B.G., and Bunce, N.J. 2001. Preliminary risk assessment of the wet landscape option for reclamation of oil sands mine tailings: bioassays with mature fine tailings pore water. *Environmental Toxicology: An International Journal*, 16(3): 197-208.
- Makama, A.B., Salmiaton, A., Choong, T.S.Y., Hamid, M.R.A., Abdullah, N., and Saion, E. 2020. Influence of parameters and radical scavengers on the visible-light-induced degradation of ciprofloxacin in ZnO/SnS<sub>2</sub> nanocomposite suspension: Identification of transformation products. *Chemosphere*, 253: 126689.
- Makula, P., Pacia, M., and Macyk, W. 2018. How To Correctly Determine the Band Gap Energy of Modified Semiconductor Photocatalysts Based on UV–Vis Spectra. *The Journal of Physical Chemistry Letters*, 9(23): 6814-6817.
- Mankomal, and Kaur, H. 2022. Synergistic effect of biochar impregnated with ZnO nano-flowers for effective removal of organic pollutants from wastewater. *Applied Surface Science Advances*, 12: 100339.
- Martin, J.W., Barri, T., Han, X., Fedorak, P.M., Gamal El-Din, M., Perez, L., Scott, A.C., and Jiang, J.T. 2010. Ozonation of oil sands process-affected water accelerates microbial bioremediation. *Environmental science & technology*, 44(21): 8350-8356.
- Meng, L., How, Z.T., Ganiyu, S.O., and Gamal El-Din, M. 2021. Solar photocatalytic treatment of model and real oil sands process water naphthenic acids by bismuth tungstate: Effect of

- catalyst morphology and cations on the degradation kinetics and pathways. *Journal of hazardous materials*, 413: 125396.
- Meshref, M.N., Chelme-Ayala, P., and Gamal El-Din, M. 2017. Fate and abundance of classical and heteroatomic naphthenic acid species after advanced oxidation processes: Insights and indicators of transformation and degradation. *Water research*, 125: 62-71.
- Mian, M.M., and Liu, G. 2018. Recent progress in biochar-supported photocatalysts: synthesis, role of biochar, and applications. *RSC advances*, 8(26): 14237-14248.
- Miklos, D.B., Remy, C., Jekel, M., Linden, K.G., Drewes, J.E., and Hübner, U. 2018. Evaluation of advanced oxidation processes for water and wastewater treatment—A critical review. *Water research*, 139: 118-131.
- Mohamed, K.M., Benitto, J.J., Vijaya, J.J., and Bououdina, M. 2023. Recent Advances in ZnO-Based Nanostructures for the Photocatalytic Degradation of Hazardous, Non-Biodegradable Medicines. *Crystals*, 13(2): 329.
- Moskalyk, R., and Alfantazi, A. 2003. Processing of vanadium: a review. *Minerals engineering*, 16(9): 793-805.
- Moustafa, A.M.A., McPhedran, K.N., Moreira, J., and Gamal El-Din, M. 2014. Investigation of Mono/Competitive Adsorption of Environmentally Relevant Ionized Weak Acids on Graphite: Impact of Molecular Properties and Thermodynamics. *Environmental science & technology*, 48(24): 14472-14480.
- Murphy, E.M., Zachara, J.M., and Smith, S.C. 1990. Influence of mineral-bound humic substances on the sorption of hydrophobic organic compounds. *Environmental science & technology*, 24(10): 1507-1516.

- NRCAN. 2020. Natural Resources Canada Water Management in oil sands. Available from <https://natural-resources.canada.ca/our-natural-resources/energy-sources-distribution/fossil-fuels/crude-oil/what-are-oil-sands/18089>.
- Nyakas, A., Han, J., Peru, K.M., Headley, J.V., and Borchers, C.H. 2013. Comprehensive analysis of oil sands processed water by direct-infusion Fourier-transform ion cyclotron resonance mass spectrometry with and without offline UHPLC sample prefractionation. *Environmental science & technology*, 47(9): 4471-4479.
- Oil Sands Magazine. 2019. Surface mining techniques used in the oil sands. *In* Online (<https://www.oilsandsmagazine.com/technical/mining/surface-mining>, Diunduh 18 Maret 2019), Oil Sands Magazine.
- Oil Sands Magazine. 2021. Tailing Ponds 101. *In* Online (<https://www.oilsandsmagazine.com/technical/mining/tailings-ponds>, Updated on March 3, 2021), Oil Sands Magazine.
- Ong, C.B., Ng, L.Y., and Mohammad, A.W. 2018. A review of ZnO nanoparticles as solar photocatalysts: Synthesis, mechanisms and applications. *Renewable and Sustainable Energy Reviews*, 81: 536-551.
- Pang, Y.L., Law, Z.X., Lim, S., Chan, Y.Y., Shuit, S.H., Chong, W.C., and Lai, C.W. 2021. Enhanced photocatalytic degradation of methyl orange by coconut shell-derived biochar composites under visible LED light irradiation. *Environmental Science and Pollution Research*, 28(21): 27457-27473.
- Paredes-Doig, A.L., Sun-Kou, M.d.R., Picasso-Escobar, G., and Cannata, J.L. 2014. A study of the adsorption of aromatic compounds using activated carbons prepared from chestnut shell. *Adsorption Science & Technology*, 32(2-3): 165-180.

- Park, S.J., Das, G.S., Schütt, F., Adelong, R., Mishra, Y.K., Tripathi, K.M., and Kim, T. 2019. Visible-light photocatalysis by carbon-nano-onion-functionalized ZnO tetrapods: degradation of 2,4-dinitrophenol and a plant-model-based ecological assessment. *NPG Asia Materials*, 11(1): 8.
- Pateiro-Moure, M., Pérez-Novo, C., Arias-Estévez, M., Rial-Otero, R., and Simal-Gándara, J. 2009. Effect of organic matter and iron oxides on quaternary herbicide sorption–desorption in vineyard-devoted soils. *Journal of colloid and interface science*, 333(2): 431-438.
- Patra, B., Pal, R., Paulraj, R., Pradhan, S.N., and Meena, R. 2020. Mineralogical composition and C/N contents in soil and water among betel vineyards of coastal Odisha, India. *SN Applied Sciences*, 2(6): 998.
- Peng, J., Headley, J., and Barbour, S. 2002. Adsorption of single-ring model naphthenic acids on soils. *Canadian geotechnical journal*, 39(6): 1419-1426.
- Pérez-Estrada, L.A., Han, X., Drzewicz, P., Gamal El-Din, M., Fedorak, P.M., and Martin, J.W. 2011. Structure–reactivity of naphthenic acids in the ozonation process. *Environmental science & technology*, 45(17): 7431-7437.
- Plazinski, W., Dziuba, J., and Rudzinski, W. 2013. Modeling of sorption kinetics: the pseudo-second order equation and the sorbate intraparticle diffusivity. *Adsorption*, 19(5): 1055-1064.
- Pourrezaei, P., Alpatova, A., Khosravi, K., Drzewicz, P., Chen, Y., Chelme-Ayala, P., and El-Din, M.G. 2014a. Removal of organic compounds and trace metals from oil sands process-affected water using zero valent iron enhanced by petroleum coke. *Journal of environmental management*, 139: 50-58.

- Pourrezaei, P., Alpatova, A., Chelme-Ayala, P., Perez-Estrada, L., Jensen-Fontaine, M., Le, X., and El-Din, M.G. 2014b. Impact of petroleum coke characteristics on the adsorption of the organic fractions from oil sands process-affected water. *International Journal of Environmental Science and Technology*, 11(7): 2037-2050.
- Pourrezaei, P., Drzewicz, P., Wang, Y., Gamal El-Din, M., Perez-Estrada, L.A., Martin, J.W., Anderson, J., Wiseman, S., Liber, K., and Giesy, J.P. 2011. The impact of metallic coagulants on the removal of organic compounds from oil sands process-affected water. *Environmental science & technology*, 45(19): 8452-8459.
- Puttaswamy, N., and Liber, K. 2011. Identifying the causes of oil sands coke leachate toxicity to aquatic invertebrates. *Environmental toxicology and chemistry*, 30(11): 2576-2585.
- Qin, F., Wen, B., Shan, X.-Q., Xie, Y.-N., Liu, T., Zhang, S.-Z., and Khan, S.U. 2006. Mechanisms of competitive adsorption of Pb, Cu, and Cd on peat. *Environmental Pollution*, 144(2): 669-680.
- Qin, R., How, Z.T., and Gamal El-Din, M. 2019. Photodegradation of naphthenic acids induced by natural photosensitizer in oil sands process water. *Water research*, 164: 114913.
- Qin, R., Chelme-Ayala, P., and Gamal El-Din, M. 2020. The impact of oil sands process water matrix on the ozonation of naphthenic acids: from a model compound to a natural mixture. *Canadian Journal of Civil Engineering*, 47(10): 1166-1174.
- Quinlan, P.J., and Tam, K.C. 2015. Water treatment technologies for the remediation of naphthenic acids in oil sands process-affected water. *Chemical Engineering Journal*, 279: 696-714.
- Ramachandran, V., and D'Souza, S. 2013. Adsorption of nickel by Indian soils. *Journal of soil science and plant nutrition*, 13(1): 165-173.

- Rao, L., Luo, J., Zhou, W., Zou, Z., Tang, L., and Li, B. 2020. Adsorption–desorption behavior of benzobicyclon hydrolysate in different agricultural soils in China. *Ecotoxicology and Environmental Safety*, 202: 110915.
- Rashed, Y., Messele, S.A., Zeng, H., and Gamal El-Din, M. 2020. Mesoporous carbon xerogel material for the adsorption of model naphthenic acids: structure effect and kinetics modelling. *Environmental technology*, 41(27): 3534-3543.
- Rauf, M.A., Bukallah, S.B., Hamour, F.A., and Nasir, A.S. 2008. Adsorption of dyes from aqueous solutions onto sand and their kinetic behavior. *Chemical Engineering Journal*, 137(2): 238-243.
- Rawat, A.P., Kumar, V., Singh, P., Shukla, A.C., and Singh, D.P. 2022. Kinetic Behavior and Mechanism of Arsenate Adsorption by Loam and Sandy Loam Soil. *Soil and sediment contamination: An international journal*, 31(1): 15-39.
- Rayment, G.E. 2011. *Soil chemical methods : Australasia. Edited by D.J. Lyons.* CSIRO Publishing, Collingwood, Vic. .:
- Rodríguez-Padrón, D., Luque, R., and Muñoz-Batista, M.J. 2020. Waste-derived materials: opportunities in photocatalysis. *Heterogeneous Photocatalysis: Recent Advances*: 1-28.
- Rogers, V.V., Wickstrom, M., Liber, K., and MacKinnon, M.D. 2002. Acute and subchronic mammalian toxicity of naphthenic acids from oil sands tailings. *Toxicological Sciences*, 66(2): 347-355.
- Rowland, S.J., West, C.E., Jones, D., Scarlett, A.G., Frank, R.A., and Hewitt, L.M. 2011. Steroidal Aromatic ‘Naphthenic Acids’ in Oil Sands Process-Affected Water: Structural Comparisons with Environmental Estrogens. *Environmental science & technology*, 45 (22): 9806-9815.

- Russell, J., and Fraser, A. 1994. Infrared methods. *In Clay Mineralogy: Spectroscopic and chemical determinative methods*. Springer. pp. 11-67.
- Ryan, P.C., and Huertas, F.J. 2009. The temporal evolution of pedogenic Fe–smectite to Fe–kaolin via interstratified kaolin–smectite in a moist tropical soil chronosequence. *Geoderma*, 151(1): 1-15.
- S, R., and P, B. 2019. The potential of lignocellulosic biomass precursors for biochar production: Performance, mechanism and wastewater application—A review. *Industrial Crops and Products*, 128: 405-423.
- Scarlett, A.G., West, C.E., Jones, D., Galloway, T.S., and Rowland, S.J. 2012. Predicted toxicity of naphthenic acids present in oil sands process-affected waters to a range of environmental and human endpoints. *Science of the Total Environment*, 425: 119-127.
- Scarlett, A.G., Reinardy, H.C., Henry, T., West, C.E., Frank, R.A., Hewitt, L.M., and Rowland, S.J. 2013. Acute toxicity of aromatic and non-aromatic fractions of naphthenic acids extracted from oil sands process-affected water to larval zebrafish. *Chemosphere*, 93(2): 415-420.
- Shaheen, S.M., Niazi, N.K., Hassan, N.E.E., Bibi, I., Wang, H., Tsang, Daniel C.W., Ok, Y.S., Bolan, N., and Rinklebe, J. 2019. Wood-based biochar for the removal of potentially toxic elements in water and wastewater: a critical review. *International Materials Reviews*, 64(4): 216-247.
- Shan, R., Han, J., Gu, J., Yuan, H., Luo, B., and Chen, Y. 2020. A review of recent developments in catalytic applications of biochar-based materials. *Resources, Conservation and Recycling*, 162: 105036.
- Shen, Y.-H. 1999. Sorption of humic acid to soil: the role of soil mineral composition. *Chemosphere*, 38(11): 2489-2499.

- Shu, Z., Li, C., Belosevic, M., Bolton, J.R., and Gamal El-Din, M. 2014. Application of a solar UV/chlorine advanced oxidation process to oil sands process-affected water remediation. *Environmental science & technology*, 48(16): 9692-9701.
- Skinner, M.F., Zabowski, D., Harrison, R., Lowe, A., and Xue, D. 2001. Measuring the cation exchange capacity of forest soils. *Communications in Soil Science and Plant Analysis*, 32(11-12): 1751-1764.
- Smaranda, C., Popescu, M.-C., Bulgariu, D., Măluțan, T., and Gavrilescu, M. 2017. Adsorption of organic pollutants onto a Romanian soil: Column dynamics and transport. *Process Safety and Environmental Protection*, 108: 108-120.
- Solarchem Environmental, S. 1994. *The UV/oxidation handbook*. Solarchem Environmental Systems Markham, Ont., Canada, Markham, Ont., Canada. pp. 1 volume (various pagings).
- Song, J., How, Z.T., Huang, Z., and Gamal El-Din, M. 2022. Biochar/iron oxide composite as an efficient peroxymonosulfate catalyst for the degradation of model naphthenic acids compounds. *Chemical Engineering Journal*, 429: 132220.
- Speight, J.G. 2013. Chapter 3 - Oil Sand Mining. *In Oil Sand Production Processes. Edited by J.G. Speight*. Gulf Professional Publishing, Boston. pp. 59-79.
- Stuart, B.H. 2004. *Infrared spectroscopy: fundamentals and applications*. John Wiley & Sons.
- Suara, M.A., Ganiyu, S.O., Paul, S., Stafford, J.L., and El-Din, M.G. 2022. Solar-activated zinc oxide photocatalytic treatment of real oil sands process water: Effect of treatment parameters on naphthenic acids, polyaromatic hydrocarbons and acute toxicity removal. *Science of the Total Environment*, 819: 153029.
- Sun, N., Chelme-Ayala, P., Klamerth, N., McPhedran, K.N., Islam, M.S., Perez-Estrada, L., Drzewicz, P., Blunt, B.J., Reichert, M., and Hagen, M. 2014. Advanced analytical mass

- spectrometric techniques and bioassays to characterize untreated and ozonated oil sands process-affected water. *Environmental science & technology*, 48(19): 11090-11099.
- Sun, Q. 2022. The Hydrophobic Effects: Our Current Understanding. *Molecules*, 27(20).
- Tang, X., Zhou, Y., Xu, Y., Zhao, Q., Zhou, X., and Lu, J. 2010. Sorption of polycyclic aromatic hydrocarbons from aqueous solution by hexadecyltrimethylammonium bromide modified fibric peat. *Journal of chemical technology & biotechnology*, 85(8): 1084-1091.
- USEPA. 2007. National Recommended Water Quality Criteria - Aquatic Life Criteria Table. *Edited by U.S.E.P. Agency*.
- Viraraghavan, T., and de Maria Alfaro, F. 1998. Adsorption of phenol from wastewater by peat, fly ash and bentonite. *Journal of hazardous materials*, 57(1): 59-70.
- Wan, C., Shen, G.Q., and Choi, S. 2019. Waste management strategies for sustainable development. *In Encyclopedia of sustainability in higher education*. Springer. pp. 2020-2028.
- Wang, C., Alpatova, A., McPhedran, K.N., and Gamal El-Din, M. 2015a. Coagulation/flocculation process with polyaluminum chloride for the remediation of oil sands process-affected water: performance and mechanism study. *Journal of environmental management*, 160: 254-262.
- Wang, C., Klammerth, N., Huang, R., Elnakar, H., and Gamal El-Din, M. 2016. Oxidation of oil sands process-affected water by potassium ferrate (VI). *Environmental science & technology*, 50(8): 4238-4247.
- Wang, H., Zhang, L., Chen, Z., Hu, J., Li, S., Wang, Z., Liu, J., and Wang, X. 2014. Semiconductor heterojunction photocatalysts: design, construction, and photocatalytic performances. *Chemical Society Reviews*, 43(15): 5234-5244.

- Wang, H., Li, X., Zhao, X., Li, C., Song, X., Zhang, P., Huo, P., and Li, X. 2022. A review on heterogeneous photocatalysis for environmental remediation: From semiconductors to modification strategies. *Chinese Journal of Catalysis*, 43(2): 178-214.
- Wang, J., Cao, X., Huang, Y., and Tang, X. 2015b. Developmental toxicity and endocrine disruption of naphthenic acids on the early life stage of zebrafish (*Danio rerio*). *Journal of Applied Toxicology*, 35(12): 1493-1501.
- Wang, J., Han, B., Dai, M., Yan, H., Li, Z., and Thomas, R. 1999. Effects of chain length and structure of cationic surfactants on the adsorption onto Na-Kaolinite. *Journal of colloid and interface science*, 213(2): 596-601.
- Wang, S., Zhao, M., Zhou, M., Li, Y.C., Wang, J., Gao, B., Sato, S., Feng, K., Yin, W., Igalavithana, A.D., Oleszczuk, P., Wang, X., and Ok, Y.S. 2019. Biochar-supported nZVI (nZVI/BC) for contaminant removal from soil and water: A critical review. *Journal of hazardous materials*, 373: 820-834.
- Weber, W.J., and Huang, W. 1996. A Distributed Reactivity Model for Sorption by Soils and Sediments. 4. Intraparticle Heterogeneity and Phase-Distribution Relationships under Nonequilibrium Conditions. *Environmental science & technology*, 30(3): 881-888.
- Wehrli, B., and Stumm, W. 1989. Vanadyl in natural waters: Adsorption and hydrolysis promote oxygenation. *Geochimica et Cosmochimica Acta*, 53(1): 69-77.
- Wei, C., Song, X., Wang, Q., and Hu, Z. 2017. Sorption kinetics, isotherms and mechanisms of PFOS on soils with different physicochemical properties. *Ecotoxicology and Environmental Safety*, 142: 40-50.
- Whitby, C. 2010. Chapter 3 - Microbial Naphthenic Acid Degradation. *In Advances in Applied Microbiology*. Academic Press. pp. 93-125.

- Worch, E. 2012. Adsorption technology in water treatment: fundamentals, processes, and modeling. Walter de Gruyter.
- Wu, X., Yin, S., Dong, Q., Liu, B., Wang, Y., Sekino, T., Lee, S.W., and Sato, T. 2013. UV, visible and near-infrared lights induced NO<sub>x</sub> destruction activity of (Yb,Er)-NaYF<sub>4</sub>/C-TiO<sub>2</sub> composite. *Scientific Reports*, 3(1): 2918.
- Xing, Z., Tian, K., Du, C., Li, C., Zhou, J., and Chen, Z. 2019. Agricultural soil characterization by FTIR spectroscopy at micrometer scales: Depth profiling by photoacoustic spectroscopy. *Geoderma*, 335: 94-103.
- Xu, X., Meng, L., Dai, Y., Zhang, M., Sun, C., Yang, S., He, H., Wang, S., and Li, H. 2020. Bi-spheres SPR-coupled Cu<sub>2</sub>O/Bi<sub>2</sub>MoO<sub>6</sub> with hollow spheres forming Z-scheme Cu<sub>2</sub>O/Bi/Bi<sub>2</sub>MoO<sub>6</sub> heterostructure for simultaneous photocatalytic decontamination of sulfadiazine and Ni(II). *Journal of hazardous materials*, 381: 120953.
- Xue, J., Zhang, Y., Liu, Y., and Gamal El-Din, M. 2016. Effects of ozone pretreatment and operating conditions on membrane fouling behaviors of an anoxic-aerobic membrane bioreactor for oil sands process-affected water (OSPW) treatment. *Water research*, 105: 444-455.
- Yan, B., Liu, S., Chastain, M.L., Yang, S., and Chen, J. 2021. A new FTIR method for estimating the firing temperature of ceramic bronze-casting moulds from early China. *Scientific Reports*, 11(1): 3316.
- Yang, C., Wang, X., Ji, Y., Ma, T., Zhang, F., Wang, Y., Ci, M., Chen, D., Jiang, A., and Wang, W. 2019. Photocatalytic degradation of methylene blue with ZnO@C nanocomposites: Kinetics, mechanism, and the inhibition effect on monoamine oxidase A and B. *NanoImpact*, 15: 100174.

- Zainorabidin, A., and Mohamad, H.M. 2017. Engineering properties of integrated tropical peat soil in Malaysia. *Electronic Journal of Geotechnical Engineering*, 22(02): 457-466.
- Zhang, C., Yan, H., Li, F., Hu, X., and Zhou, Q. 2013. Sorption of short- and long-chain perfluoroalkyl surfactants on sewage sludges. *Journal of hazardous materials*, 260: 689-699.
- Zhang, L., Zhang, Y., and Gamal El-Din, M. 2018a. Degradation of recalcitrant naphthenic acids from raw and ozonated oil sands process-affected waters by a semi-passive biofiltration process. *Water research*, 133: 310-318.
- Zhang, L., Zhang, Y., and Gamal El-Din, M. 2019. Integrated mild ozonation with biofiltration can effectively enhance the removal of naphthenic acids from hydrocarbon-contaminated water. *Science of the Total Environment*, 678: 197-206.
- Zhang, L., Zhang, Y., Patterson, J., Arslan, M., Zhang, Y., and El-Din, M.G. 2020. Biofiltration of oil sands process water in fixed-bed biofilm reactors shapes microbial community structure for enhanced degradation of naphthenic acids. *Science of the Total Environment*, 718: 137028.
- Zhang, Y., Xue, J., Liu, Y., and Gamal El-Din, M. 2016a. Treatment of oil sands process-affected water using membrane bioreactor coupled with ozonation: a comparative study. *Chemical Engineering Journal*, 302: 485-497.
- Zhang, Y., Xue, J., Liu, Y., and Gamal El-Din, M. 2018b. The role of ozone pretreatment on optimization of membrane bioreactor for treatment of oil sands process-affected water. *Journal of hazardous materials*, 347: 470-477.

- Zhang, Y., Klammerth, N., Messele, S.A., Chelme-Ayala, P., and Gamal El-Din, M. 2016b. Kinetics study on the degradation of a model naphthenic acid by ethylenediamine-N,N'-disuccinic acid-modified Fenton process. *Journal of hazardous materials*, 318: 371-378.
- Zhao, C., Wang, B., Theng, B.K.G., Wu, P., Liu, F., Wang, S., Lee, X., Chen, M., Li, L., and Zhang, X. 2021. Formation and mechanisms of nano-metal oxide-biochar composites for pollutants removal: A review. *Science of the Total Environment*, 767: 145305.
- Zhou, Y., Chen, L., Lu, P., Tang, X., and Lu, J. 2011. Removal of bisphenol A from aqueous solution using modified fibric peat as a novel biosorbent. *Separation and Purification Technology*, 81(2): 184-190.
- Zhu, K., Wang, X., Chen, D., Ren, W., Lin, H., and Zhang, H. 2019. Wood-based biochar as an excellent activator of peroxydisulfate for Acid Orange 7 decolorization. *Chemosphere*, 231: 32-40.
- Zubot, W., An, Z., Benally, C., and Gamal El-Din, M. 2021. Treatment of oil sands process water using petroleum coke: Field pilot. *Journal of environmental management*, 289: 112407.
- Zubot, W., MacKinnon, M.D., Chelme-Ayala, P., Smith, D.W., and Gamal El-Din, M. 2012. Petroleum coke adsorption as a water management option for oil sands process-affected water. *Science of the Total Environment*, 427: 364-372.
- Zubot, W.A. 2010. Removal of naphthenic acids from oil sands process water using petroleum coke. M. Sc. Eng. Thesis, Department of Civil and Environmental Engineering, University of Alberta, Edmonton, AB. Spring 2010. 179pp.

## APPENDIX A

**Appendix A contains 1 Text, 1 copyright permission, 6 Figures, and 6 Tables.**

### *Text A1: Water chemistry analyses*

Table S2 gives a summary of the analytical methods used by Maxxam Analytics Ltd. to perform the different types of water analyses. SCL's Research facility also performed different types of analyses for select water samples. Each of the water analyses methods is briefly described in the following.

AEF in OSPW were quantified using Fourier-Transform Infrared Spectroscopy (FT-IR) method described by Jivraj et al. (1996). In brief, the OSPW sample (50-80 mL) was acidified using HCl to pH of 2. The sample was then extracted using 30 mL of dichloromethane (DCM), three different times. The extracted DCM with acidified organics from the OSPW water sample were then combined and evaporated to dryness (leaving behind the organics). The dried organics were reconstituted with a known amount of DCM and injected in a KBr cell. A Nicolet model 8700 FT-IR spectrometer manufactured by Thermo Electron Corporation was used to quantify the infrared light adsorption at two wavenumbers ( $1703\text{ cm}^{-1}$  and  $1740\text{ cm}^{-1}$ ). The concentration of AEF in the solvent was determined by comparing the total peak height of the samples to a standard calibration curve. Prior to analyses, a five-point calibration curve was established using commercially purchased naphthenic acid standard (Fluka #70340) with a method of detection limit of 1 mg/L.

Major cations and trace elements were measured using a Varian Vista-RL inductively coupled plasma atomic emission spectrometer (ICP-AES) equipped with radial mounted torch,

Sturman-Masters V-groove nebulizer and Sturman-Masters spray chamber. Prior to analyses, samples were filtered using a 0.45  $\mu\text{m}$  syringe filter and then acidified with 5 wt. % nitric acid.

Anion concentrations ( $\text{Cl}^-$ ,  $\text{SO}_4^{2-}$ ,  $\text{F}^-$ ,  $\text{Br}^-$ ,  $\text{PO}_4^{3-}$ ,  $\text{NO}_3^-$ ,  $\text{NO}_2^-$ ) were determined using filtered water samples (0.45  $\mu\text{m}$ ) and a Dionex-DX 600 series ion chromatograph fitted with an Ion-Pac AS4A-SC analytical column (4x250 mm). A 3 mM sodium bicarbonate/2.4 mM sodium carbonate eluent was used at a flowrate of 2 mL/min to effect separation at a constant temperature of 30°C. An Atlas electrolyte suppressor and conductivity detector was used to quantify anion concentrations.

Alkalinity ( $\text{HCO}_3^-$ ,  $\text{CO}_3^{2-}$  and total alkalinity as  $\text{CaCO}_3$  equivalents) was measured with a Metrohm Alkalinity 855 Robotic Titrator with flat membrane electrode. A 10 mL sample aliquot was titrated with 0.1 N hydrochloric acid to reach the bicarbonate endpoint ( $\sim\text{pH}$  4.3), determined using an inflection point method. This measured volume was used to calculate the sample's Total Alkalinity in "mg/L as  $\text{CaCO}_3$  equivalents" from which the carbonate and bicarbonate ion concentrations are calculated and reported based on the laboratory measured pH. To minimize interferences from atmospheric carbon dioxide, samples were degassed with argon.

Ammonium ion ( $\text{NH}_4^+$ ) concentrations were determined using ion chromatography on a Dionex ICS-5000 series chromatographic system with a self-regenerating suppressor and conductivity detection. An Ion-Pac CS16 analytical column (3 x 250 mm) held at 30°C was used with gradient elution from 10 to 52 mM of methanesulfonic acid at 0.4 mL/min to separate the ammonium from the other cations in the sample, in particular sodium ( $\text{Na}^+$ ).

## Permission of copyright of Chapter 2:

**CCC** RightsLink Sign in/Register ? 🔗



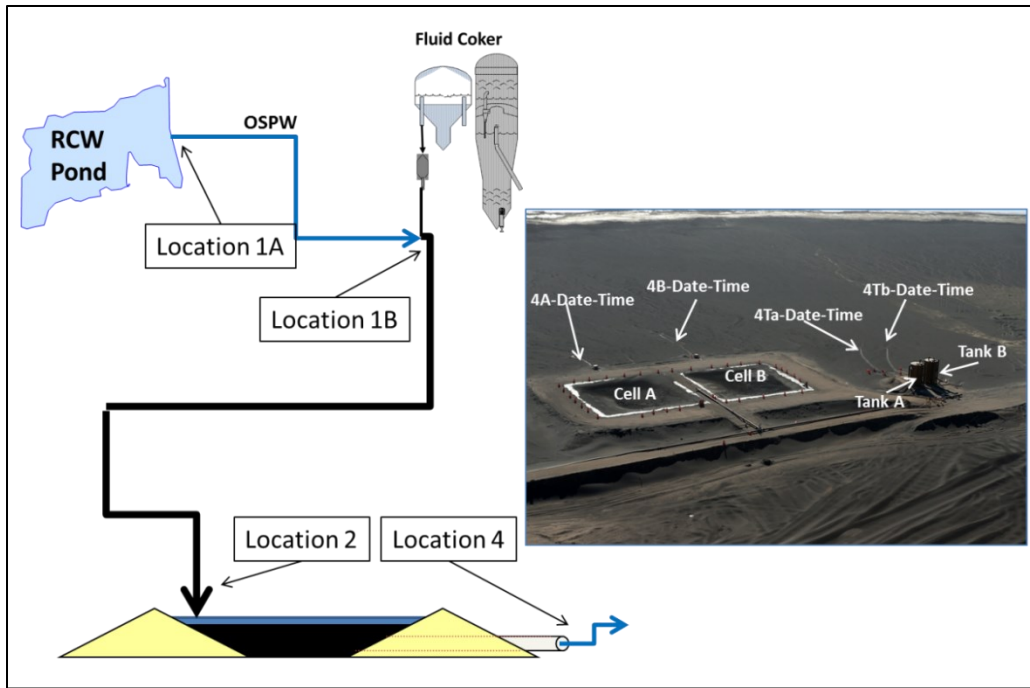
**Treatment of oil sands process water using petroleum coke: Field pilot**  
Author: Warren Zubot,Zhexuan An,Chelsea Benally,Mohamed Gamal El-Din  
Publication: Journal of Environmental Management  
Publisher: Elsevier  
Date: 1 July 2021  
© 2021 Elsevier Ltd. All rights reserved.

**Journal Author Rights**

Please note that, as the author of this Elsevier article, you retain the right to include it in a thesis or dissertation, provided it is not published commercially. Permission is not required, but please ensure that you reference the journal as the original source. For more information on this and on your other retained rights, please visit: <https://www.elsevier.com/about/our-business/policies/copyright#Author-rights>

BACK CLOSE WINDOW

© 2024 Copyright - All Rights Reserved | Copyright Clearance Center, Inc. | Privacy statement | Data Security and Privacy | For California Residents | Terms and Conditions  
Comments? We would like to hear from you. E-mail us at [customercare@copyright.com](mailto:customercare@copyright.com)



(a)



(b)



(c)



(d)

Figure S1: (a) Field pilot study sample locations; (b) Under-drain system prior to PC deposition: Cells and Tanks; (c) Tanks on pad being filled with PC/OSPW slurry; d) Top view Tank B showing Tee-distributor (10”) and under-drain manifold (insets).

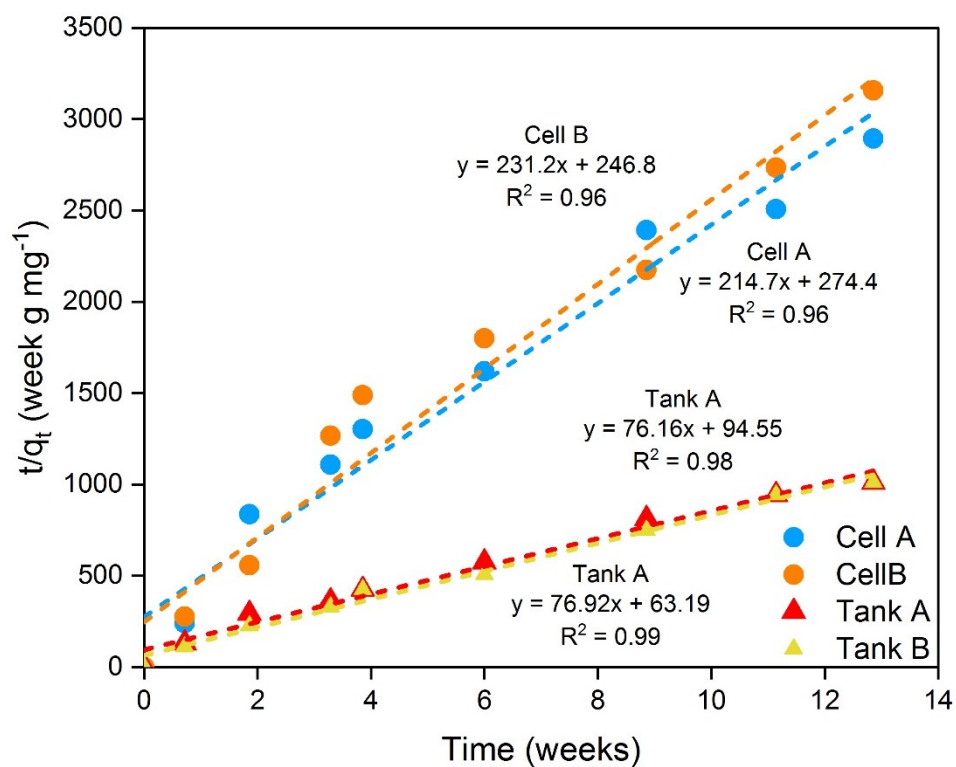


Figure S2: PSO model for the adsorption of AEF in OSPW treated by PC in different R2 reactors.

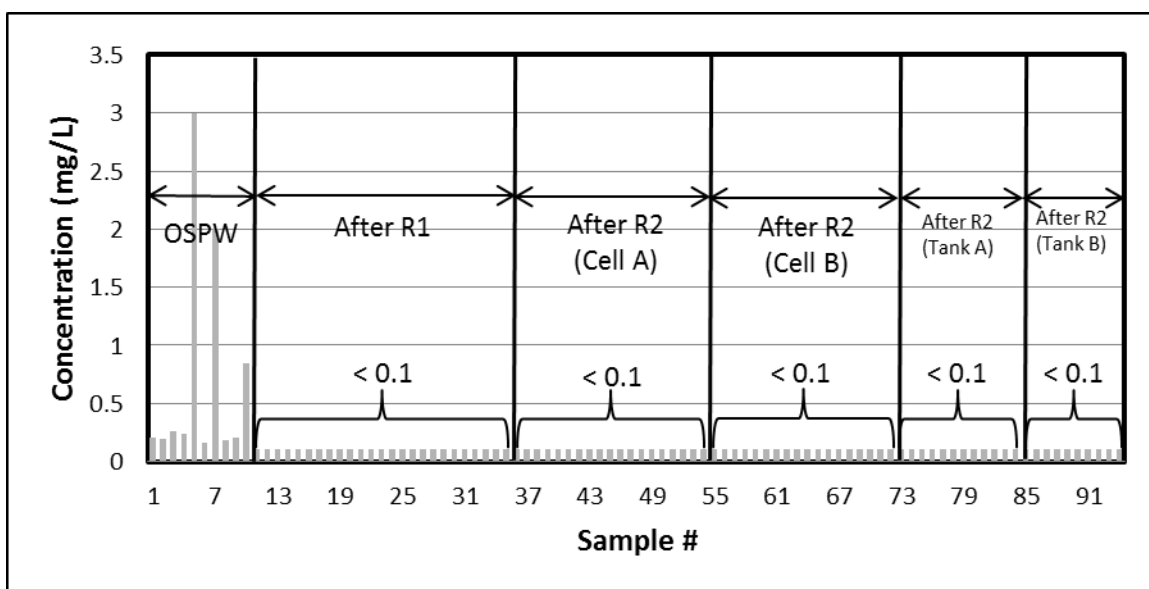


Figure S3: Change in TPH concentrations for different reactors at different residence times.

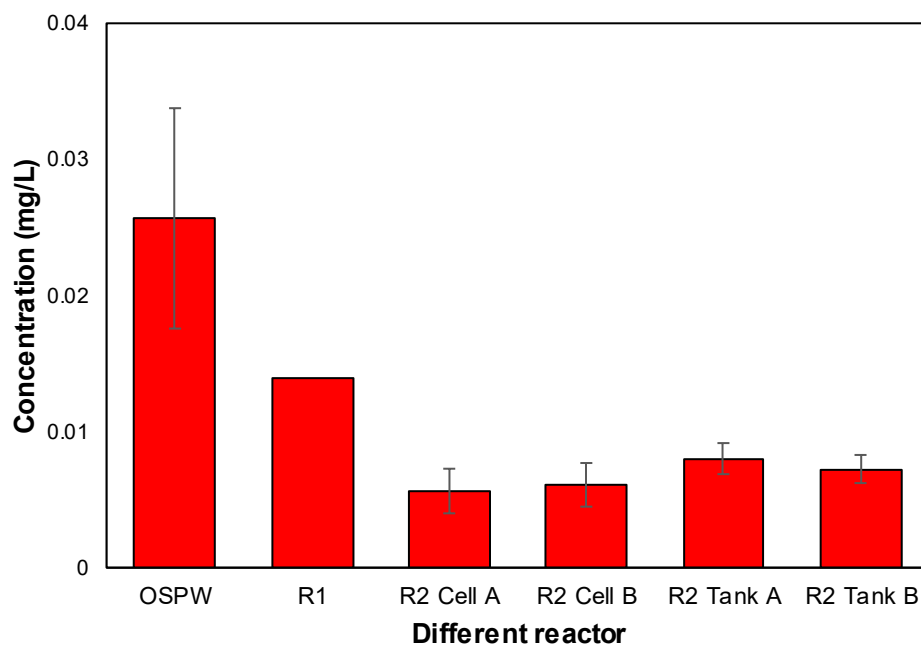


Figure S4: Average phenol concentration in source OSPW and in OSPW after treatment by R1, R2 cells, and R2 tanks over the entire sampling period (OSPW-4 weeks, R1-4weeks, R2 cells - 59 weeks, R2 tanks – 55 weeks).



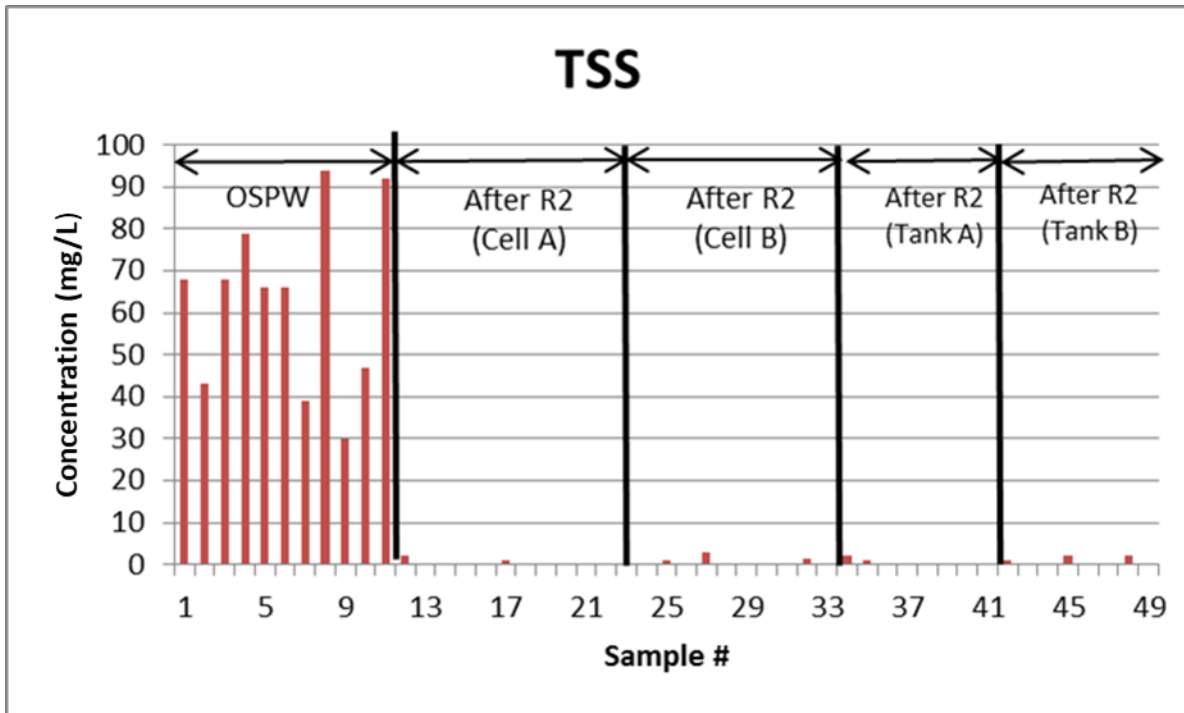


Figure S6: Change in TSS concentrations for different reactors at different residence times.

Table S1: Summary of OSPW samples collected and sample locations.

Samples collected	Sample location(s)
<u>Source OSPW</u>	
	Location 1A: OSPW at RCW pond
	Location 1B: OSPW prior to entry into the coke sluice tanks
<u>Treated OSPW after pipeline transport (from reactor 1)</u>	
	Location 2A: Sluice OSPW discharged into cell A
	Location 2B: Sluice OSPW discharged into cell B
	Location 2: Sluice OSPW discharged into tanks A/B
<u>Treated OSPW after drainage through PC deposit (from reactor 2)</u>	
	Location 4A: Cell A under-drain
	Location 4B: Cell B under-drain
	Location 4Ta: Tank A under-drain
	Location 4Tb: Tank B under-drain

Table S2: Analytical methods used.

Analyte	Method
<i>General Properties</i>	
pH at 25°C	SM 4500 – H+B
Conductivity at 25°C	SM 2510-B
True Colour	SM 2120 C
Total Dissolved Solids (TDS)	SM 1030E
Total Suspended Solids (TSS)	SM 2540-D
<i>Inorganics</i>	
Elements by ICP	EPA 200.7
Elements by ICPMS	EPA 200.8
Chloride	EPA 325.2
Sulfate	EPA 375.4
Alkalinity	SM 2320-B
Hardness	SM 2340B
Ion Balance	SM 1030E
Cadmium-low level	EPA 200.8
Mercury-low level	EPA 1631/1631B
Nitrate/Nitrite	SM 4110-B
<i>Organics</i>	
Dissolved Organic Carbon (DOC)	MMCW 119
Biochemical Oxygen Demand (BOD)	SM 5210B
Chemical Oxygen Demand (COD)	SM5220D
Phenols	EPA 420.2
TPH (BTEX/F1/F2)	EPA 8260C,3510C/CCME PHCCWS
Parent and Alkylated PAHs	EPA 3540C/8270D
VOCs	EPA 8260 C

Tables S3: General water chemistry of OSPW

Table S3 (a): General water chemistry – OSPW prior to treatment.

Sample ID.	Date	pH	Cond-activity uS/cm	TDS mg/L	TSS mg/L	Nap. Acids mg/L	DOC mg/L	TPH mg/L	NH <sub>4</sub> mg/L	NO <sub>2</sub> mg/L	NO <sub>3</sub> mg/L	NO <sub>2</sub> + NO <sub>3</sub> mg/L	BOD <sub>5</sub> mg/L	COD mg/L	Phenols mg/L	Color units	Na mg/L	K mg/L	Mg mg/L	Ca mg/L	Cl mg/L	SO <sub>4</sub> mg/L	HCO <sub>3</sub> mg/L	CO <sub>3</sub> mg/L	Alkal- inity mg/L	Ion Bal. mg/mg	Hardness as CaCO <sub>3</sub> mg/L
1A-20120626-1045	26-Jun-12	7.56	3900	2500	68	69	44	0.21	0.49	<0.10	<0.10	<0.03	5	230	0.02	24	860	14	12	23.0	670	500	820	0	672	0.93	108
1A-20120703-1155	3-Jul-12	7.55	3380	2100	43	56	46	0.19	0.13	<0.050	<0.10	<0.015	7	280	0.025	28	710	14	13	26.0	550	440	760	0	623	0.91	119
1B-20120625-1115	25-Jun-12	7.76	3830	2300	68	64	41	0.26	0.42	<0.10	<0.10	<0.03	5	220	0.022		810	14.0	13.0	26.0	610	490	790	0	648	0.94	119
1B-20120626-1120	26-Jun-12	7.91	3900	2500	79	71	43	0.24	0.66	<0.10	<0.10	<0.03	5	240	0.02	24	840	14.0	12.0	23.0	650	500	840	0	689	0.92	108
1B-20120627-1240	27-Jun-12	7.61	3680	2300	66	69	42	3	0.05	<0.050	0.16	0.035	9	200			820	13.0	12.0	23.8	570	470	800	0	656	0.98	110
1B-20120627-1240	27-Jun-12	7.62	3680			56											840	13.8	12.4	23.4		468					
1B-20120628-1010	28-Jun-12	7.80	3870	2300	66	69	42		0.10	<0.050	0.16	0.035	9	200		25	820	13.4	12.0	21.9	570	470	800	0	656	0.98	105
1B-20120628-1010	28-Jun-12	7.78	3870			64											911	14.2	11.7	22.0		459					
1B-20120703-1330	3-Jul-12	7.78	3360	2200	39	64	44	0.18	0.05	<0.050	<0.10	<0.015	7	250	0.026	28	760	14.0	13.0	25.0	550	440	770	0	631	0.96	117
1B-20120709-1050	9-Jul-12	7.77	3140	1900	94	57	33		0.34	<0.010	0.17	0.039	8	220	0.029	29	660	13.0	13.0	29.0	460	420	650	0	533	0.98	127
1B-2012-0709-1050	9-Jul-12	7.83	3130			53		2									666	13.4	14.7	30.7		438					
1B-20120723-0850	23-Jul-12	8.03	3290	2100	30	57	44		0.05	0.053	0.15	0.049	6	260	0.022	31	760	13.0	11.0	24.0	510	370	740	0	607	1.04	106
1B-20120723-1630	23-Jul-12	7.93	3420	2100	47	66	45	0.18	0.05	<0.010	0.08	0.018	6	270	0.02	29	800	12.0	11.0	22.0	540	350	790	0	648	1.05	101
1B20120724-0950	24-Jul-12	8.00	2920	2000	92	64	45	0.2	14.5	<0.010	0.12	0.028	9	330	0.047	31	750	13.0	11.0	24.0	510	360	740	0	607	1.03	106
1B20120724-0950	24-Jul-12	8.10	3290			52		0.85									690	13.1	11.5	23.4							
<b>Average</b>		<b>7.80</b>	<b>3511</b>	<b>2209</b>	<b>63</b>	<b>62</b>	<b>43</b>	<b>0.73</b>	<b>1.53</b>	<b>0.05</b>	<b>0.14</b>	<b>0.03</b>	<b>7</b>	<b>245</b>	<b>0.03</b>	<b>28</b>	<b>780</b>	<b>13.5</b>	<b>12.2</b>	<b>24.5</b>	<b>563</b>	<b>441</b>	<b>773</b>	<b>0</b>	<b>633</b>	<b>0.97</b>	<b>111</b>

Note: Analyses by Maxxam Labs and Syncrude Research

Table S3 (b): General water chemistry – OSPW treatment after R1.

Sample ID.	Date	pH	Cond-activity uS/cm	TDS mg/L	TSS mg/L	Nap. Acids mg/L	DOC mg/L	TPH mg/L	NH <sub>4</sub> mg/L	NO <sub>2</sub> mg/L	NO <sub>3</sub> mg/L	NO <sub>2</sub> + NO <sub>3</sub> mg/L	BOD <sub>5</sub> mg/L	COD mg/L	Phenols mg/L	Color units	Na mg/L	K mg/L	Mg mg/L	Ca mg/L	Cl mg/L	SO <sub>4</sub> mg/L	HCO <sub>3</sub> mg/L	CO <sub>3</sub> mg/L	Alkal- inity mg/L	Ion Bal. mg/mg	Hardness as CaCO <sub>3</sub> mg/L		
<b>OSPW in Petroleum Coke Slurry Input to Cell A</b>																													
2A-20120625-1530	25-Jun-12	8.14	3690			25		<0.10	0.20								744	13.5	13.4	26.1		480					121		
2A-20120625-1530	25-Jun-12	8.22	3700			30		<0.10									856	15.2	14.1	27.0		534					128		
2A-20120626-0900	26-Jun-12	8.28	3990			8	19	<0.10	3.91					92			850	21.0	9.8	17.0		690					84		
2A-20120626-1500	26-Jun-12	8.24	3960	2500	8	20	22	<0.10	0.13	<0.10	<0.10	<0.03	3	110	0.014	13	900	16.6	10.9	17.5	650	610	680	12	577	0.97	89		
2A-20120627-1009	27-Jun-12	8.41	3900			12	24	<0.10	4.12					110			862	18.5	9.5	18.7		570					86		
2A-20120628-1035	28-Jun-12	8.32	3900			36		<0.10	0.05								836	14.5	11.5	21.3		450					101		
2A-20120703-1025	3-Jul-12	8.14	3390			23		<0.10	0.05								726	14.2	11.9	21.9		420					104		
2A-20120709-0925	9-Jul-12	8.31	3090			10		<0.10	7.60								674	15.1	14.5	28.0		450					130		
2A-2012-0710-0835	10-Jul-12	8.31	3850			8		<0.10	0.05								889	15.7	11.4	17.0		525					90		
<b>Average</b>		<b>8.26</b>	<b>3719</b>	<b>2500</b>	<b>8</b>	<b>19</b>	<b>22</b>	<b>0.10</b>	<b>2.01</b>				<b>3</b>	<b>104</b>	<b>0.014</b>	<b>13</b>	<b>815</b>	<b>16.0</b>	<b>11.9</b>	<b>21.6</b>	<b>650</b>	<b>525</b>	<b>680</b>	<b>12</b>	<b>577</b>		<b>104</b>		
<b>OSPW in Petroleum Coke Slurry Input to Cell B</b>																													
2B-20120625-1430	25-Jun-12	8.21	3710			28	27	<0.10	0.46					140			760	15.0	14.0	26.0		540					121		
2B-20120626-1200	26-Jun-12	8.19	3890			23	22	<0.10	0.39					130			830	16.0	12.0	19.0		540					97		
2B-20120626-1500	26-Jun-12	8.42	3940			25	24	<0.10	0.52					120			890	15.0	11.0	18.0		510					92		
2B-20120627-0924	27-Jun-12	8.37	3950			15	22	<0.10	3.63					110			880	18.0	9.3	17.0		540					83		
2B-20120628-1031	28-Jun-12	8.31	3860			33		<0.10	0.05								841	15.0	11.7	21.5		468					103		
2B-20120626-1200	26-Jun-12	8.25	3930			28		<0.10									898	15.4	11.7	19.4		534					97		
2B-20120703-1035	3-Jul-12	8.14	3490			23		<0.10	7.20					750			750	16.0	13.0	23.0		480					109		
2B-20120705-1015	5-Jul-12	7.49	2930			34		<0.10	0.05								631	13.0	16.3	40.8		561					170		
2B-20120703-1035	3-Jul-12	8.22	3460			23		<0.10						800			800	16.3	12.3	21.4		468					105		
2B-20120709-0902	9-Jul-12	8.37	3130			12		<0.10	10.1					660			660	15.0	13.0	27.0		450					134		
2B-2012-0710-0830	10-Jul-12	8.24	3040			9		<0.10	0.05					675			675	13.6	13.0	22.8		477					111		
<b>Average</b>		<b>8.20</b>	<b>3575</b>			<b>23</b>	<b>24</b>	<b>0.10</b>	<b>2.49</b>				<b>125</b>				<b>783</b>	<b>15.3</b>	<b>12.5</b>	<b>23.3</b>		<b>506</b>					<b>111</b>		
<b>OSPW in Petroleum Coke Slurry Input to Tanks A and B</b>																													
2-20120723-1220	23-Jul-12	8.17	3290			23	29	<0.10	0.05					130			703	15.1	11.8	21.4		450					103		
2-20120723-1510	23-Jul-12	8.42	3320			19	29	<0.10	10.4					140			720	14.8	11.2	21.8		420					101		
2-20120724-0910	24-Jul-12	8.27	3280			19	24	<0.10	0.05					170			702	15.3	12.3	23.8		450					111		
2-2012724-1630	24-Jul-12	8.22	3380			20	26	<0.10	13.4					130			716	15.9	12.8	24.0		480					113		
2-2012724-1630	24-Jul-12	8.22	3400			21		<0.10						703			703	15.4	12.3	22.9		462					109		
<b>Average</b>		<b>8.26</b>	<b>3334</b>			<b>20</b>	<b>27</b>	<b>0.10</b>	<b>5.98</b>				<b>143</b>				<b>709</b>	<b>15.3</b>	<b>12.1</b>	<b>22.8</b>		<b>452</b>					<b>107</b>		

Note: Analyses by Maxxam Labs and Syncrude Research

Table S3 (c): General water chemistry – Treated OSPW after Reactor 2 (cells).

Sample I.D.	Date	pH	Cond-activity uS/cm	TDS mg/L	TSS mg/L	Nap. Acids mg/L	DOC mg/L	TPH mg/L	NH <sub>4</sub> mg/L	NO <sub>2</sub> mg/L	NO <sub>3</sub> mg/L	NO <sub>3</sub> mg/L	BOD <sub>5</sub> mg/L	COD mg/L	Phenols mg/L	Color units	Na mg/L	K mg/L	Mg mg/L	Ca mg/L	Cl mg/L	SO <sub>4</sub> mg/L	HCO <sub>3</sub> mg/L	CO <sub>2</sub> mg/L	Alkalinity mg/L	Ion Bal. mg/L	Hardness as CaCO <sub>3</sub> mg/L
<b>Treated OSPW from Cell A</b>																											
4A-20120628-1300	28-Jun-12	8.14	3980	2500	2	7	16	<0.10	3.25	<0.05	0.66	0.15	4	76			920	20.6	9.8	16.1	650	690	480	2.3	397.276	1.0374	81
4A-20120628-0900	28-Jun-12	8.32	3740		<1.0	12	20	<0.10	0.05				90		16	860	16.2	10.6	17.7	610	570	610			500	1.01323	88
4A-20120703-1004	3-Jul-12	8.28	3850			7		<0.10	2.19							863	15.9	9.9	15.6	615	549	800			491.803	1.02421	80
4A-20120704-1540	4-Jul-12	8.44	3850			6		<0.10	0.05							862	15.4	10.2	15.5	615	510	610			500	1.04082	81
4A-20120705-0920	5-Jul-12	8.38	3930	2500	<1.0	6	15	<0.10	0.42	<0.05	<0.066	<0.015	<2	75	0.009	8.4	920	16.0	10.7	15.6	660	590	670	25	590.847	0.98552	84
4A-20120705-0920	5-Jul-12	8.40	3940			5		<0.10								952	16.4	10.6	15.3	690	534	680			557.377	1.04198	82
4A-20120710-0835	10-Jul-12	8.30	3800	2500	<1.0		15			<0.01	0.39	0.088	<2	87	0.0061	7.3	870	15.0	10.0	16.0	700	510	700	16	600.437	0.94078	82
4A-20120718-0910	18-Jul-12	8.29	3880	2300	<1.0	7	15	<0.10	0.05	<0.01	<0.013	<0.003	<2	100	0.005	6	809	14.6	9.9	14.2	600	450	850	28	579.454	0.97941	77
4A-20120725-1015	25-Jul-12	8.34	3680	2100	1	6	14	<0.10	0.05	<0.01	<0.013	<0.003	<2	84	0.006	5.7	792	14.3	9.6	13.7	500	520	640	14	547.923	1.01143	74
4A-20120730-1435	30-Jul-12	8.13	3520			5		<0.10	0.05							853	14.7	9.9	14.3	570	489	625			512.295	1.0689	77
4A-20120807-1025	7-Aug-12	8.09	3410			6		<0.10	1.13							753	13.4	9.7	14.2	500	450	580			475.41	1.04957	76
4A-20120817-1033	17-Aug-12	8.11	3300	2000	<1.0	5	13	<0.10	1.45	<0.01	0.04	0.009	<2.0	65	0.0067	4.9	706	12.8	10.1	14.7	520	430	590	13	505.273	0.96704	79
4A-20120821-1027	21-Aug-12	8.12	3170			5		<0.10	1.44							697	12.7	10.4	15.3	480	416	593	7	497.732	1.00371	82	
4A-20120905-1135	5-Sep-12	8.17	3140			4	14	<0.10	0.25				57			632	12.3	10.1	14.5	480	416	513	6	430.492	0.95333	78	
4A-20120905-1135	5-Sep-12	8.26	3180			4		<0.10	0.31							642	12.4	9.9	14.1	470	415	574	8	483.825	0.943	77	
4A-20120925-1055	25-Sep-12	7.94	3210	1900	<1.0	4	12	<0.10	1.50	<0.01	0.071	<0.016	<2.0	53	0.0039	4.2	668	12.7	10.3	14.7	480	430	550	13	472.486	0.96972	80
4A-20121011-1345	11-Oct-12	8.38	3180	1800	<1.0	3	12	<0.10	0.81	<0.017	0.033	<0.013	59	0.0065	3	671	12.1	11.0	15.9	480	400	520	15	451.23	1.01026	86	
4A-20121023-1335	23-Oct-12	8.26	3440	2000	<1.0	3	12	<0.10	1.10	<0.01	0.084	<0.019	67		4	749	13.2	11.9	17.3	540	420	550	7.8	463.82	1.04581	93	
4A-20130614-1057	14-Jun-13	8.46	4000	2400	<1.0	3	9.8	<0.10	0.50	<0.01	0.47	0.47	<2.0	57	0.0035	3.9	855	12.7	13.8	19.5	620	580	540	11	460.956	1.02211	106
4A-20130815-1010	15-Aug-13	8.14	3960	2500	<1.0	3	12	<0.10	<0.01	2.6	0.82	3.42	5.4	72	0.004	6.1	830	13.0	14.0	19.0	650	660	540	5	450.956	0.93812	106
<b>Average</b>		<b>8.25</b>	<b>3598</b>	<b>2227</b>		<b>5</b>	<b>14</b>		<b>0.9</b>	<b>2.60</b>	<b>0.32</b>	<b>0.83</b>	<b>4.70</b>	<b>72</b>	<b>0.0056</b>	<b>6.3</b>	<b>795</b>	<b>14.3</b>	<b>10.6</b>	<b>15.7</b>	<b>572</b>	<b>501</b>	<b>591</b>	<b>12</b>	<b>498</b>		<b>83</b>
<b>Treated OSPW from Cell B</b>																											
4B-20120628-1345	28-Jun-12	8.35	3890			17	22	<0.10	0.57				110			875	15.3	11.4	18.9	600	510	625			512	1	95
4B-20120628-0900	28-Jun-12	8.21	3900	2300	<1.0	9	20	<0.10	3.36	<0.01	0.44	0.1	2	88	0.0088	12	867	17.4	9.0	15.2	590	490	590	34	540	1	75
4B-20120703-1013	3-Jul-12	8.43	3820			13		<0.10	0.05							861	15.4	11.4	17.8	580	516	595			488	1	92
4B-20120703-1515	3-Jul-12	8.35	3810			12		<0.10	0.05							863	15.6	11.2	17.8	580	516	610			500	1	91
4B-20120704-1540	4-Jul-12	8.39	3550			11		<0.10	0.05							809	14.8	10.4	16.3	545	471	590			484	1	84
4B-20120705-0935	5-Jul-12	8.43	3480			10		<0.10	0.05							802	14.5	10.6	16.5	540	468	580			475	1	85
4B-20120710-830	10-Jul-12	8.30	3150	1900	1.0		16			0.085	0.28	0.09	<2	80	0.0073	8	700	13.0	12.0	21.0	480	450	510	8.6	432	1	103
4B-20120718-0931	18-Jul-12	8.29	3070	1900	<1.0		16			6.7	2.6	2.6	7	87	0.0057	7	685	13.0	13.0	22.0	470	460	500	3.6	416	1	109
4B-20120725-1025	25-Jul-12	8.29	3070	1900	3.0	8	16	<0.10	0.05	1	0.56	0.43	5	72	0.0053	6	663	13.7	13.1	21.9	450	510	470	7.9	398	1	109
4B-20120730-1440	30-Jul-12	7.79	3120			7		<0.10	0.15							717	14.3	13.7	22.8	490	528	470	5	394	1	114	
4B-20120807-1030	7-Aug-12	7.88	3200			6		<0.10	0.11							692	14.1	14.3	23.2	480	537	475			389	1	118
4B-20120817-1010	17-Aug-12	8.17	3370	2100	<1.0	7	17	<0.10		0.4	0.17	0.16	3.8	65	0.0068	6	715	14.7	15.4	24.1	520	560	470	13	407	1	124
4B-20120821-1028	21-Aug-12	8.33	3450			7		<0.10								746	15.4	16.3	24.9	520	568	495	8	419	1	130	
4B-20120905-1140	5-Sep-12	8.11	3460			6	16	<0.10	0.21				73			682	14.8	15.3	22.7	520	573	488	5	408	1	121	
4B-20120925-1103	25-Sep-12	7.86	3220	1900	<1.0	5	15	<0.10	0.05	0.2	0.2	0.11	5.6	59	0.0037	5	647	12.8	14.3	22.4	480	550	430	10	369	1	116
4B-20121011-1350	11-Oct-12	8.29	3080	1700	<1.0	5	13	<0.10	0.05	0.067	8.3	1.9	57	0.0070	4	580	11.4	13.7	21.8	420	440	380	7.2	323	1	112	
4B-20121023-1340	23-Oct-12	8.34	3220	1900	<1.0	5	14	<0.10	1.48	0.095	0.43	0.13	58		5	669	12.6	14.6	24.0	490	480	410	6.4	347	1	121	
4B-20130614-1105	14-Jun-13	8.27	2200	1300	1.3	3	10	<0.10	0.31	0.83	0.27	0.32	5	41	0.0041	3	446	8.4	12.0	26.7	290	360	290	2	241	1	117
4B-20130815-1015	15-Aug-13	7.95	2010	1200	<1.0	9	15	<0.10	<0.01	2.8	0.16	0.9	6.4	47	<0.002	4	370	8.0	13.0	31.0	270	360	260	2	216	1	132
<b>Average</b>		<b>8.21</b>	<b>3287</b>	<b>1810</b>		<b>8</b>	<b>16</b>		<b>0.47</b>	<b>1.35</b>	<b>1.34</b>	<b>0.67</b>	<b>4.97</b>	<b>70</b>	<b>0.0061</b>	<b>6.0</b>	<b>705</b>	<b>13.6</b>	<b>12.9</b>	<b>21.6</b>	<b>490</b>	<b>492</b>	<b>486</b>	<b>9</b>	<b>408</b>		<b>108</b>

Note: Analyses by Maxxam Labs and Syncrude Research

Table S3 (d): General water chemistry – Treated OSPW after Reactor 2 (tanks).

Sample I.D.	Date	pH	Cond-activity uS/cm	TDS mg/L	TSS mg/L	Nap. Acids mg/L	DOC mg/L	TPH mg/L	NH <sub>4</sub> mg/L	NO <sub>2</sub> mg/L	NO <sub>3</sub> mg/L	NO <sub>3</sub> mg/L	BOD <sub>5</sub> mg/L	COD mg/L	Phenols mg/L	Color units	Na mg/L	K mg/L	Mg mg/L	Ca mg/L	Cl mg/L	SO <sub>4</sub> mg/L	HCO <sub>3</sub> mg/L	CO <sub>2</sub> mg/L	Alkalinity mg/L	Ion Bal. mg/L	Hardness as CaCO <sub>3</sub> mg/L
<b>Treated OSPW from Tank A</b>																											
4TA-20120725-0940	25-Jul-12	8.32	3220	1900	2	14	22	<0.10	0.05	<0.01	0.084	<0.019	4	100	0.0095	12	680	14.3	11.7	21.4	450	490	600	7	503.47	0.97853	102
4TA-20120730-1455	30-Jul-12	8.06	3240	1900	1	14																					

Tables S4: Trace Elements (Dissolved) in OSPW

Table S4 (a): Trace Elements (Dissolved) – OSPW prior to Treatment.

Sample ID	Date	Sb	As	Cd	Hg	Al	Ba	Be	B	Cr	Co	Cu	Fe	Pb	Li	Mn	Mo	Ni	P	Se	Si	Ag	Sr	S	Ti	Sn	Tl	U	V	Zn
		mg/L	mg/L	ug/L	ug/L	mg/L	mg/L	mg/L	mg/L	mg/L	mg/L	mg/L	mg/L	mg/L	mg/L	mg/L	mg/L	mg/L	mg/L	mg/L	mg/L	mg/L	mg/L	mg/L	mg/L	mg/L	mg/L	mg/L	mg/L	mg/L
1A-20120626-1045	26-Jun-12	0.0019	0.0048	0.031	<0.002	0.11	0.38	<0.0025	2.40	<0.0025	0.001	<0.0005	<0.060	<0.0005	0.19	0.065	0.1	0.009	<0.10	0.0022	2.8	<0.0002	0.68	160	<0.0005	<0.0025	0.0031	0.0073	<0.0025	<0.0075
1A-20120703-1155	3-Jul-12	<0.0015	0.0079	0.033		0.6	0.46	<0.0025	2.10	<0.0025	0.001	0.0005	<0.060	<0.0005	0.17	0.057	0.1	0.0099	<0.10	0.011	3	<0.0002	0.77	140	<0.0005	<0.0025	0.014	0.0056	0.007	<0.0075
1B-20120625-1115	25-Jun-12	<0.0015	0.0042	0.024	<0.002	0.13	0.38	<0.0025	2.40	<0.0025	0.0016	0.0005	<0.060	<0.0005	0.19	0.097	0.1	0.01	<0.10	0.0032	2.8	<0.0002	0.7	160	<0.0005	<0.0025	0.004	0.0067	0.010	<0.0075
1B-20120626-1120	26-Jun-12	0.0017	0.0054	0.047	<0.002	0.14	0.38	<0.0025	2.50	0.0026	0.0011	0.0014	<0.060	<0.0005	0.19	0.064	0.1	0.0097	<0.10	0.0022	2.8	<0.0002	0.69	160	<0.0005	<0.0025	<0.0025	0.0073	0.010	<0.0075
1B-20120627-1240	27-Jun-12								2.24				<0.060											145						0.010
1B-20120627-1240	27-Jun-12								2.34															156						0.010
1B-20120628-1010	28-Jun-12								2.41				<0.060			0.067								141						0.010
1B-20120628-1010	28-Jun-12								2.51															153						0.010
1B-20120703-1330	3-Jul-12	0.0011	0.0078	0.040		0.07	0.46	<0.0010	2.10	<0.0010	0.0010	0.0005	0.18	<0.0002	0.17	0.048	0.1	0.0096	<0.10	0.011	4.0	<0.0001	0.77	140	<0.0002	<0.0010	<0.0010	0.0052	0.010	0.014
1B-20120709-1050	9-Jul-12	<0.0015	0.0061	0.026		0.56	0.38	<0.0025	1.70	<0.0025	0.0011	<0.0005	0.14	<0.0005	0.14	0.07	0.059	0.01	<0.10	0.0096	3.2	<0.0002	0.73	130	<0.0005	<0.0025	0.0075	0.0049	0.010	<0.0075
1B-2012-0709-1050	9-Jul-12								1.86															146						0.010
1B-20120723-0850	23-Jul-12	<0.0015	0.0070	0.030	<0.002	0.24	0.45	<0.0025	2.00	<0.0025	<0.0008	0.0010	<0.060	<0.0005	0.16	0.043	0.091	0.0089	<0.10	0.0066	2.6	<0.0002	0.75	130	<0.0005	<0.0025	0.003	0.005	0.010	0.0076
1B-20120723-1630	23-Jul-12	<0.0015	0.0070	0.023	<0.002	0.23	0.43	<0.0025	2.10	<0.0025	0.0008	0.0009	<0.060	<0.0005	0.17	0.043	0.09	0.0091	0.11	0.0052	2.6	<0.0002	0.72	130	<0.0005	<0.0025	0.0028	0.0054	0.008	0.011
1B20120724-0950	24-Jul-12	<0.0015	0.0075	0.019	<0.002	0.19	0.45	<0.0025	2.00	<0.0025	<0.0008	0.0009	<0.060	<0.0005	0.16	0.045	0.089	0.0081	<0.10	0.0078	2.6	<0.0002	0.75	130	<0.0005	<0.0025	0.0035	0.0049	0.009	0.012
1B20120724-0950	24-Jul-12								1.99															126						
<b>Average</b>		<b>0.0016</b>	<b>0.006</b>	<b>0.030</b>		<b>0.25</b>	<b>0.42</b>		<b>2.18</b>	<b>0.0026</b>	<b>0.0011</b>	<b>0.0008</b>	<b>0.160</b>		<b>0.17</b>	<b>0.061</b>	<b>0.10</b>	<b>0.009</b>	<b>0.11</b>	<b>0.0065</b>	<b>2.9</b>		<b>0.73</b>	<b>143</b>		<b>0.0054</b>	<b>0.0058</b>	<b>0.009</b>	<b>0.011</b>	

Note: Samples field filtered (0.45 um). Analyses by Maxxam Labs.

Table S4 (b): Trace Elements (Dissolved) – OSPW Treatment after Reactor 1.

Sample ID	Date	Sb	As	Cd	Hg	Al	Ba	Be	B	Cr	Co	Cu	Fe	Pb	Li	Mn	Mo	Ni	P	Se	Si	Ag	Sr	S	Ti	Sn	Tl	U	V	Zn	
		mg/L	mg/L	ug/L	ug/L	mg/L	mg/L	mg/L	mg/L	mg/L	mg/L	mg/L	mg/L	mg/L	mg/L	mg/L	mg/L	mg/L	mg/L	mg/L	mg/L	mg/L	mg/L	mg/L	mg/L	mg/L	mg/L	mg/L	mg/L	mg/L	
<b>OSPW in Petroleum Coke Slurry Input to Cell A</b>																															
2A-20120625-1530	25-Jun-12								2.20															160						0.93	
2A-20120625-1530	25-Jun-12								2.38															178						0.98	
2A-20120626-0900	26-Jun-12	0.0036	0.0180	0.230		1.9	0.07	<0.0010	2.80	<0.0010	0.0006	0.0009	<0.060	<0.0002	0.31	0.072	1.5	0.018	0.19	0.0097	5.3	<0.0001	0.49	230	<0.0002	<0.0010	0.0029	0.0042	0.60	0.011	
2A-20120626-1500	26-Jun-12	0.0027	0.0088	0.100	<0.002	0.87	0.097	<0.0025	2.60	<0.0025	<0.0008	<0.0005	<0.060	<0.0005	0.24	0.056	0.59	0.018	<0.10	0.005	3.3	<0.0002	0.50	190	<0.0005	<0.0025	0.0028	0.0075	3.50	<0.0075	
2A-20120627-1009	27-Jun-12	0.0042	0.0220	0.220		2.6	0.1	<0.0010	2.80	<0.0010	0.0005	0.0004	<0.060	<0.0002	0.3	0.03	1.6	0.012	0.25	0.011	5.1	<0.0001	0.61	190	<0.0002	<0.0010	0.0025	0.0066	8.70	0.005	
2A-20120628-1035	28-Jun-12	0.0024	0.0065	0.061		0.44	0.17	<0.0010	2.40	<0.0010	0.0009	0.0003	<0.060	<0.0002	0.22	0.084	0.36	0.021	<0.10	0.0041	2.6	<0.0001	0.59	150	<0.0002	<0.0010	0.0032	0.0070	1.10	<0.003	
2A-20120703-1025	3-Jul-12	0.0018	0.0097	0.110		0.42	0.21	<0.0010	2.20	<0.0010	0.0007	0.0002	0.064	<0.0002	0.18	0.063	0.33	0.015	<0.10	0.01	3.4	<0.0001	0.67	140	<0.0002	<0.0010	0.0060	0.0060	1.50	<0.003	
2A-20120709-0925	9-Jul-12	0.0023	0.0110	0.068		0.88	0.19	<0.0025	1.80	<0.0025	<0.0008	<0.0005	<0.060	<0.0005	0.16	0.056	0.57	0.016	0.14	0.014	3.4	<0.0002	0.69	150	<0.0005	<0.0025	0.0029	0.0056	3.10	<0.0075	
2A-2012-0710-0835	10-Jul-12								2.54															175						2.61	
<b>Average</b>		<b>0.0028</b>	<b>0.0127</b>	<b>0.132</b>		<b>1.19</b>	<b>0.14</b>		<b>2.41</b>	<b>0.0007</b>	<b>0.0004</b>	<b>0.004</b>	<b>0.064</b>		<b>0.24</b>	<b>0.062</b>	<b>0.83</b>	<b>0.02</b>	<b>0.19</b>	<b>0.01</b>	<b>3.9</b>		<b>0.59</b>	<b>174</b>		<b>0.0034</b>	<b>0.0062</b>	<b>0.56</b>	<b>0.01</b>		
<b>OSPW in Petroleum Coke Slurry Input to Cell B</b>																															
2B-20120625-1430	25-Jun-12	0.0019	0.0045	0.065		0.24	0.21	<0.0010	2.30	<0.0010	0.00094	0.0003	<0.060	<0.0002	0.2	0.12	0.33	0.018	<0.10	0.0059	2.7	<0.0001	0.66	180	<0.0002	<0.0010	0.0014	0.0069	0.98	0.003	
2B-20120626-1200	26-Jun-12	0.0024	0.0072	0.085		0.71	0.13	<0.0010	2.50	<0.0010	0.00069	0.0016	<0.060	<0.0002	0.22	0.065	0.41	0.019	<0.10	0.0049	3	<0.0001	0.55	180	<0.0002	<0.0010	0.0020	0.0077	2.20	0.012	
2B-20120626-1500	26-Jun-12	0.0022	0.0072	0.067		0.67	0.11	<0.0010	2.50	<0.0010	0.00071	0.0009	<0.060	<0.0002	0.22	0.061	0.4	0.02	<0.10	0.0047	3.1	<0.0001	0.52	170	<0.0002	<0.0010	0.0021	0.0073	2.20	0.006	
2B-20120627-0924	27-Jun-12	0.0041	0.0200	0.180		2.1	0.096	<0.0010	2.80	<0.0010	0.00046	0.0008	<0.060	<0.0002	0.28	0.035	1.3	0.012	0.17	0.0091	4.7	<0.0001	0.58	180	<0.0002	<0.0010	0.0023	0.007	7.30	0.011	
2B-20120628-1031	28-Jun-12								2.48															156						1.48	
2B-20120628-1200	28-Jun-12								2.57															178						2.23	
2B-20120703-1035	3-Jul-12	0.0021	0.0073	0.120		0.35	0.17	<0.0010	2.20	<0.0010	0.00088	0.0004	<0.060	<0.0002	0.2	0.09	0.46	0.019	<0.10	0.011	3.1	<0.0001	0.65	160	<0.0002	<0.0010	0.0035	0.0067	1.10	0.004	
2B-20120705-1015	5-Jul-12								1.62															187						1.55	
2B-20120703-1035	3-Jul-12								2.12															156						1.11	
2B-20120709-0902	9-Jul-12	0.0023	0.0110	0.068		0.94	0.19	<0.0025	1.80	<0.0025	<0.0008	<0.0005	<0.060																		

Table S4 (c): Trace Elements (Dissolved) – OSPW Treatment after Reactor 2 (cells).

Sample ID	Date	Sb	As	Cd	Hg	Al	Ba	Be	B	Cr	Co	Cu	Fe	Pb	Li	Mn	Mo	Ni	P	Se	Si	Ag	Sr	S	Ti	Sn	Tl	U	V	Zn	
		mg/L	mg/L	ug/L	ug/L	mg/L	mg/L	mg/L	mg/L	mg/L	mg/L	mg/L	mg/L	mg/L	mg/L	mg/L	mg/L	mg/L	mg/L	mg/L	mg/L	mg/L	mg/L	mg/L	mg/L	mg/L	mg/L	mg/L	mg/L	mg/L	
<b>Treated OSPW from Cell A</b>																															
4A-20120626-1300	26-Jun-12	0.0037	0.019	0.24	<0.002	1.2	0.09	<0.0025	2.90	<0.0025	<0.0008	<0.0005	<0.060	<0.0005	0.3	0.05	1.7	0.011	0.27	0.0098	6.1	<0.0002	0.49	220	<0.0005	<0.0025	<0.0025	0.0039	10.00	<0.0075	
4A-20120628-0900	28-Jun-12	0.004	0.017	0.24	0.97	0.065	<0.0025	2.30	<0.0025	<0.0008	<0.0005	<0.060	<0.0005	0.27	0.05	1.8	0.012	0.26	0.0091	5.5	<0.0002	0.46	190	<0.0005	<0.0025	0.0036	0.0053	7.50	0.009		
4A-20120703-1004	3-Jul-12								2.74																						
4A-20120704-1540	4-Jul-12								2.57																						
4A-20120705-0920	5-Jul-12	0.0027	0.011	0.18	0.37	0.043	<0.0025	2.60	<0.0025	<0.0008	<0.0005	<0.060	<0.0005	0.23	0.05	0.79	0.0082	0.34	0.0053	3.6	<0.0002	0.46	180	<0.0005	<0.0025	<0.0025	0.01	3.70	<0.0075		
4A-20120705-0920	5-Jul-12								2.51																						
4A-20120710-0835	10-Jul-12	0.0025	0.012	0.08	0.41	0.041	<0.0025	2.30	<0.0025	<0.0008	<0.0005	<0.060	<0.0005	0.2	0.06	0.75	0.0085	0.24	0.0025	3.4	<0.0002	0.44	160	<0.0005	<0.0025	<0.0025	0.01	2.70	0.023		
4A-20120718-0910	18-Jul-12	<0.0015	0.012	0.07	<0.002	0.31	0.041	<0.0025	2.50	<0.0025	<0.0008	0.00073	<0.060	<0.0005	0.21	0.05	0.87	0.0094	0.19	0.0018	3.5	<0.0002	0.45	160	<0.0005	<0.0025	<0.0025	0.0091	1.70	0.011	
4A-20120725-1015	25-Jul-12	<0.003	0.012	0.40	<0.002	0.33	0.036	<0.005	2.40	<0.005	<0.0015	<0.010	<0.060	<0.0010	0.18	0.06	0.79	0.0083	0.24	0.0011	3.6	<0.0005	0.42	150	<0.0010	<0.005	<0.005	0.01	1.80	0.020	
4A-20120730-1435	30-Jul-12								2.61																						
4A-20120807-1025	7-Aug-12								2.49																						
4A-20120817-1003	17-Aug-12	<0.0015	0.012	0.11	0.0027	0.22	0.031	<0.0025	2.30	<0.0025	<0.0008	<0.0005	0.066	<0.0005	0.17	0.07	0.72	0.0072	0.21	0.00081	3.6	<0.0002	0.4	140	<0.0005	<0.0025	<0.0025	0.007	1.20	<0.0075	
4A-20120821-1027	21-Aug-12	0.0011	0.011	0.08	0.22	0.03	<0.0010	2.10	<0.0010	<0.0003	<0.0002	<0.060	<0.0002	0.15	0.06	0.72	0.0069	0.2	0.0008	3.5	<0.0001	0.38	130	<0.0002	<0.0010	0.0017	0.0064	1.10	<0.003		
4A-20120905-1135	5-Sep-12								2.32																						
4A-20120905-1135	5-Sep-12								2.33																						
4A-20120925-1055	25-Sep-12	<0.0015	0.0093	0.07	0.0028	0.16	0.033	<0.0025	2.30	<0.0025	<0.0008	<0.0005	<0.060	<0.0005	0.16	0.07	0.74	0.0062	0.24	<0.0005	3.7	<0.0002	0.42	140	<0.0005	<0.0025	<0.0025	0.0063	0.67	<0.0075	
4A-20121011-1345	11-Oct-12	<0.003	0.01	0.32	0.15	0.033	<0.005	2.30	<0.005	<0.0015	<0.010	0.064	<0.0010	0.16	0.08	0.89	0.0066	0.3	<0.0010	3.7	<0.0005	0.45	150	<0.0010	<0.005	<0.005	0.0067	0.63	<0.015		
4A-20121023-1335	23-Oct-12	<0.0030	0.012	0.40	0.0021	0.18	0.031	<0.0050	2.20	<0.005	<0.0015	0.0013	<0.060	<0.0010	0.16	0.07	0.96	0.0064	0.21	<0.0010	3.2	<0.0005	0.43	150	<0.0010	<0.0050	<0.0050	0.008	0.62	<0.015	
4A-20130614-1057	14-Jun-13	<0.0030	0.01	0.39	<0.002	0.14	0.029	<0.0050	2.20	<0.005	<0.0015	0.0025	0.22	<0.0010	0.17	0.11	1.2	0.0063	0.23	<0.0010	2.7	<0.0005	0.52	200	<0.0005	<0.0050	0.0096	0.35	<0.015		
4A-20130615-1010	15-Aug-13	0.00082	0.012	0.78	<0.0020	0.1	0.032	<0.0010	2.40	<0.0010	<0.0003	0.00028	<0.060	<0.0002	0.18	0.10	1.2	0.0067	0.18	0.00027	2.9	<0.00010	0.51	210	<0.0002	<0.0010	<0.0010	0.0097	0.79	<0.003	
<b>Average</b>		<b>0.002</b>	<b>0.012</b>	<b>0.26</b>	<b>0.37</b>	<b>0.04</b>		<b>2.45</b>		<b>0.002</b>		<b>0.0012</b>	<b>0.20</b>	<b>0.07</b>	<b>0.99</b>	<b>0.008</b>	<b>0.24</b>	<b>0.0035</b>	<b>3.8</b>		<b>0.45</b>	<b>165</b>				<b>0.0027</b>	<b>0.0078</b>	<b>2.80</b>	<b>0.02</b>		
<b>Treated OSPW from Cell B</b>																															
4B-20120626-1345	26-Jun-12	0.0023	0.0077	0.076	0.57	0.12	<0.0010	2.40	<0.0010	0.00067	<0.0002	<0.060	<0.0002	0.22	0.06	0.51	0.019	0.12	0.0058	3.3	<0.0001	0.53	170	<0.0002	<0.0010	0.0017	0.0076	2.80	0.004		
4B-20120628-0900	28-Jun-12	0.003	0.0140	0.140	<0.002	0.63	0.079	<0.0025	2.50	<0.0025	<0.0008	<0.0005	<0.060	<0.0005	0.24	0.052	0.96	0.013	0.18	0.0091	3.9	<0.0002	0.54	170	<0.0005	<0.0025	0.0027	0.0071	4.80	0.008	
4B-20120703-1013	3-Jul-12								2.54																						
4B-20120703-1515	3-Jul-12								2.58																						
4B-20120704-1540	4-Jul-12								2.37																						
4B-20120705-0935	5-Jul-12								2.34																						
4B-20120710-830	10-Jul-12	0.0018	0.0087	0.074	0.33	0.064	<0.0025	1.80	<0.0025	<0.0008	0.0010	<0.060	<0.0005	0.16	0.057	0.52	0.013	0.11	0.0051	2.9	<0.0002	0.56	150	<0.0005	<0.0025	<0.0025	0.0051	1.50	<0.0075		
4B-20120718-0931	18-Jul-12	0.0015	0.0074	0.081	<0.002	0.23	0.089	<0.0025	2.00	<0.0025	<0.0008	<0.0005	<0.060	<0.0005	0.18	0.036	0.51	0.012	<0.10	0.0038	3.1	<0.0002	0.66	160	<0.0005	<0.0025	<0.0025	0.0047	1.30	0.016	
4B-20120725-1025	25-Jul-12	0.0032	0.0079	0.290	<0.002	0.23	0.078	<0.005	1.90	<0.005	<0.0015	<0.010	<0.060	<0.0010	0.15	0.053	0.6	0.012	0.12	0.0042	3.1	0.0011	0.61	160	<0.0010	<0.005	<0.005	0.005	1.30	0.017	
4B-20120730-1440	30-Jul-12								2.16																						
4B-20120807-1030	7-Aug-12								2.22																						
4B-20120817-1010	17-Aug-12	<0.0015	0.0094	0.120	<0.002	0.18	0.07	<0.0025	2.20	<0.0025	<0.0008	0.0005	<0.060	<0.0005	0.17	0.063	0.74	0.012	0.16	0.003	3.1	<0.0002	0.66	180	<0.0005	<0.0025	<0.0025	0.0049	1.00	<0.0075	
4B-20120821-1028	21-Aug-12	0.0015	0.0093	0.087	0.2	0.07	<0.0010	2.10	<0.0010	<0.0003	<0.0002	<0.060	<0.0002	0.17	0.051	0.74	0.012	0.1	0.0031	2.9	<0.0001	0.64	180	<0.0002	<0.0010	0.0017	0.005	1.10	<0.003		
4B-20120905-1140	5-Sep-12								2.33																						
4B-20120925-1103	25-Sep-12	<0.0015	0.0076	0.050	<0.002	0.14	0.059	<0.0025	2.10	<0.0025	<0.0008	<0.0005	<0.060	<0.0005	0.16	0.06	0.74	0.01	0.19	0.00088	2.9	<0.0002	0.62	200	<0.0005	<0.0025	<0.0025	0.0048	0.62	<0.0075	
4B-20121011-1350	11-Oct-12	0.0012	0.0076	0.250	0.12	0.056	<0.0010	1.90	<0.0010	<0.0003	<0.0002	<0.060	<0.0002	0.15	0.056	0.74	0.0087	0.18	0.001	2.4	<0.0001	0.63	160	<0.0002	<0.0010	<0.0010	0.0045	0.54	<0.003		
4B-20121023-1340	23-Oct-12	<0.003	0.0079	0.340	<0.002	0.12	0.05	<0.0050	1.80	<0.0050	<0.0015	0.0011	0.068	<0.0010	0.15	0.063	0.85	0.009	0.13	<0.0010	2.3	<0.0005	0.56	160	<0.0010	<0.0050	<0.0050	0.0055	0.50	<0.015	
4B-20130614-1105	14-Jun-13	<0.0006	0.0050	0.180																											

Tables S5: PAH concentrations in OSPW

Table S5 (a): PAH concentrations in OSPW (pre-treatment).

PAH		Sample Location									
		1A 26-Jun-12	1A 3-Jul-12	1B 25-Jun-12	1B 26-Jun-12	1B 27-Jun-12	1B 3-Jul-12	1B 9-Jul-12	1B 23-Jul-12	1B 23-Jul-12	1B 24-Jul-12
Naphthalene	ug/L	<0.10	<0.10	<0.20	<0.20	<0.10	<0.10	<0.10	<0.10	<0.10	<0.10
2-Methylnaphthalene	ug/L	<0.10	<0.10	<0.20	<0.20	<0.10	<0.10	<0.10	<0.10	<0.10	<0.10
C1-Naphthalene	ug/L	<0.10	<0.10	<0.20	<0.20	<0.10	<0.10	<0.10	<0.10	<0.10	0.31
C2-Naphthalene	ug/L	<0.10	<0.10	<0.20	<0.20	<0.10	<0.10	<0.10	<0.10	<0.10	2.6
C3-Naphthalene	ug/L	<0.10	0.22	<0.20	<0.20	0.41	0.21	0.24	0.17	0.18	3.8
C4-Naphthalene	ug/L	<0.10	0.43	<0.20	<0.20	1.5	0.37	0.74	0.23	0.29	5.8
Acenaphthylene	ug/L	<0.10	<0.10	<0.20	<0.20	<0.10	<0.10	<0.10	<0.10	<0.10	<0.10
Acenaphthene	ug/L	<0.10	<0.10	<0.20	<0.20	<0.10	<0.10	<0.10	<0.10	<0.10	0.53
Acridine	ug/L	<0.20	<0.20	<0.40	<0.40	<0.20	<0.20	<0.20	<0.20	<0.20	<0.20
Fluorene	ug/L	<0.050	<0.050	<0.10	<0.10	<0.050	<0.050	<0.050	<0.050	<0.050	0.19
C1-fluorene	ug/L	<0.050	<0.050	<0.10	<0.10	0.15	<0.050	0.11	<0.050	<0.050	0.53
C2-fluorene	ug/L	<0.050	0.19	<0.10	<0.10	0.37	0.22	0.25	<0.050	0.12	2.4
C3-fluorene	ug/L	<0.050	0.59	<0.10	<0.10	1.2	0.5	0.7	<0.050	0.36	5.7
Biphenyl	ug/L	<0.020	<0.020	<0.040	<0.040	<0.020	<0.020	<0.020	<0.020	<0.020	<0.020
C1-biphenyl	ug/L	<0.020	0.067	0.061	<0.040	<0.020	0.046	0.038	0.066	0.043	0.15
C2-biphenyl	ug/L	<0.020	0.17	<0.040	<0.040	<0.020	0.11	0.13	0.11	0.10	1.00
Phenanthrene	ug/L	<0.050	<0.050	<0.10	<0.10	<0.050	<0.050	<0.050	<0.050	<0.050	0.33
C1-phenanthrene	ug/L	<0.050	0.092	<0.10	<0.10	0.29	0.078	0.12	0.074	0.08	2.9
C2-phenanthrene	ug/L	0.1	0.18	<0.10	<0.10	1	0.15	0.42	0.22	0.19	5.4
C3-phenanthrene	ug/L	0.13	0.19	<0.10	<0.10	1.2	0.16	0.67	0.28	0.24	5.9
C4-phenanthrene	ug/L	<0.050	0.18	<0.10	<0.10	0.43	0.1	0.4	0.22	0.22	3
Anthracene	ug/L	<0.010	<0.010	<0.020	<0.020	<0.015	<0.010	<0.014	<0.010	<0.010	<0.12
Retene	ug/L	<0.050	<0.050	<0.10	<0.10	<0.050	<0.050	<0.050	<0.050	<0.050	0.28
Dibenzothiophene	ug/L	<0.020	<0.020	<0.040	<0.040	<0.020	<0.020	<0.020	<0.020	<0.020	0.17
C1-dibenzothiophene	ug/L	0.029	<0.020	<0.040	<0.040	0.13	<0.020	<0.020	<0.020	<0.020	1.4
C2-dibenzothiophene	ug/L	0.13	0.18	<0.040	<0.040	1.6	0.12	0.63	0.21	0.22	8.5
C3-dibenzothiophene	ug/L	0.13	0.15	<0.040	<0.040	1.3	0.14	0.65	0.28	0.23	5.7
C4-dibenzothiophene	ug/L	<0.020	0.21	<0.040	<0.040	0.7	<0.020	0.42	0.3	0.27	4.2
Fluoranthene	ug/L	<0.040	<0.040	<0.080	<0.080	<0.040	<0.040	<0.040	<0.040	<0.040	0.097
Pyrene	ug/L	0.038	0.052	<0.040	<0.040	0.098	0.037	0.08	0.074	0.058	0.33
C1-pyrene	ug/L	0.074	0.17	<0.040	<0.040	0.31	0.14	0.22	0.15	0.15	1
C2-pyrene	ug/L	0.1	0.34	<0.040	<0.040	0.51	0.26	0.38	0.27	0.29	2
C3-pyrene	ug/L	<0.020	0.55	<0.040	<0.040	0.79	0.46	0.76	0.52	0.54	4.4
C4-pyrene	ug/L	<0.020	0.18	<0.040	<0.040	0.16	<0.020	0.29	0.21	0.18	1.8
Benzo(a)anthracene	ug/L	<0.009	<0.009	<0.017	<0.017	<0.009	<0.009	<0.009	<0.009	<0.009	<0.009
Chrysene	ug/L	<0.009	<0.009	<0.017	<0.017	0.018	<0.009	<0.009	<0.009	<0.009	0.082
C1-chrysene	ug/L	0.025	0.088	<0.017	<0.017	0.14	0.071	0.12	0.093	0.085	0.72
C2-chrysene	ug/L	0.07	0.25	<0.017	<0.017	0.37	0.21	0.4	0.27	0.22	2.7
C3-chrysene	ug/L	<0.009	0.087	<0.017	<0.017	0.097	0.061	0.12	0.12	0.1	0.93
C4-chrysene	ug/L	<0.009	<0.009	<0.017	<0.017	<0.009	<0.009	<0.009	<0.009	<0.009	0.15
Benzo[e]pyrene	ug/L	<0.050	<0.050	<0.10	<0.10	<0.050	<0.050	<0.050	<0.050	<0.050	0.058
Benzo(b&j)fluoranthene	ug/L	<0.009	0.018	<0.017	<0.017	<0.009	0.015	0.014	0.015	0.011	0.06
Benzo(k)fluoranthene	ug/L	<0.009	<0.009	<0.017	<0.017	<0.009	<0.009	<0.009	<0.009	<0.009	<0.009
Benzo(c)phenanthrene	ug/L	<0.050	<0.050	<0.10	<0.10	<0.050	<0.050	<0.050	<0.050	<0.050	<0.050
Benzo(a)pyrene	ug/L	<0.0075	<0.0075	<0.015	<0.015	<0.0075	<0.0075	<0.0075	<0.0075	<0.0075	0.028
Benzo[a]pyrene	ug/L	<0.010	0.011	0.019	0.019	<0.010	0.01	0.01	0.01	0.01	0.054
C1-benzo(a)pyrene	ug/L	<0.0075	0.038	<0.015	<0.015	0.036	<0.0075	0.045	0.042	<0.0075	0.29
C2-benzo(a)pyrene	ug/L	<0.0075	0.025	<0.015	<0.015	<0.0075	<0.0075	<0.0075	<0.0075	<0.0075	0.25
Indeno(1,2,3-cd)pyrene	ug/L	<0.009	0.0095	<0.017	<0.017	<0.009	<0.009	<0.009	<0.009	<0.009	0.017
Dibenz(a,h)anthracene	ug/L	<0.0075	<0.0075	<0.015	<0.015	<0.0075	<0.0075	<0.0075	<0.0075	<0.0075	0.016
Perylene	ug/L	<0.050	<0.050	<0.10	<0.10	<0.050	<0.050	<0.050	<0.050	<0.050	0.053
Benzo(g,h,i)perylene	ug/L	<0.009	<0.009	<0.017	<0.017	<0.009	<0.009	<0.009	<0.009	<0.009	0.024
Quinoline	ug/L	<0.20	0.28	<0.40	<0.40	<0.20	0.4	0.38	0.56	0.51	1.7

PAH (Polycyclic Aromatics Hydrocarbons) in water by GC/MS analyses conducted by Maxxam Labs, Calgary using EPA Method EPA 3540C/8270D

Table S5 (b): PAH concentrations after R1.

PAH		Sample Location	
		2A 25-Jun-12	2A 26-Jun-12
<b>Naphthalene</b>	ug/L	<0.10	<0.10
2-Methylnaphthalene	ug/L	<0.10	<0.10
C1-Naphthalene	ug/L	<0.10	<0.10
C2-Naphthalene	ug/L	<0.10	<0.10
C3-Naphthalene	ug/L	<0.10	<0.10
C4-Naphthalene	ug/L	<0.10	<0.10
<b>Acenaphthylene</b>	ug/L	<0.10	<0.10
<b>Acenaphthene</b>	ug/L	<0.10	<0.10
<b>Acridine</b>	ug/L	<0.20	<0.20
<b>Fluorene</b>	ug/L	<0.050	<0.050
C1-fluorene	ug/L	<0.050	<0.050
C2-fluorene	ug/L	<0.050	<0.050
C3-fluorene	ug/L	<0.050	<0.050
<b>Biphenyl</b>	ug/L	<0.020	<0.020
C1-biphenyl	ug/L	0.047	<0.020
C2-biphenyl	ug/L	<0.020	<0.020
<b>Phenanthrene</b>	ug/L	<0.050	<0.050
C1-phenanthrene	ug/L	<0.050	<0.050
C2-phenanthrene	ug/L	<0.050	<0.050
C3-phenanthrene	ug/L	<0.050	<0.050
C4-phenanthrene	ug/L	<0.050	<0.050
<b>Anthracene</b>	ug/L	<0.010	<0.010
<b>Retene</b>	ug/L	<0.050	<0.050
<b>Dibenzothiophene</b>	ug/L	<0.020	<0.020
C1-dibenzothiophene	ug/L	<0.020	<0.020
C2-dibenzothiophene	ug/L	<0.020	<0.020
C3-dibenzothiophene	ug/L	<0.020	<0.020
C4-dibenzothiophene	ug/L	<0.020	<0.020
<b>Fluoranthene</b>	ug/L	<0.040	<0.040
<b>Pyrene</b>	ug/L	<0.020	<0.020
C1-pyrene	ug/L	<0.020	<0.020
C2-pyrene	ug/L	<0.020	<0.020
C3-pyrene	ug/L	<0.020	<0.020
C4-pyrene	ug/L	<0.020	<0.020
<b>Benzo(a)anthracene</b>	ug/L	<0.009	<0.009
<b>Chrysene</b>	ug/L	<0.009	<0.009
C1-chrysene	ug/L	<0.009	<0.009
C2-chrysene	ug/L	<0.009	<0.009
C3-chrysene	ug/L	<0.009	<0.009
C4-chrysene	ug/L	<0.009	<0.009
<b>Benzo[e]pyrene</b>	ug/L	<0.050	<0.050
<b>Benzo(b&amp;j)fluoranthene</b>	ug/L	<0.009	<0.009
<b>Benzo(k)fluoranthene</b>	ug/L	<0.009	<0.009
<b>Benzo(c)phenanthrene</b>	ug/L	<0.050	<0.050
<b>Benzo(a)pyrene</b>	ug/L	<0.0075	<0.0075
<b>Benzo[a]pyrene</b>	ug/L	<0.010	<0.010
C1-benzo(a)pyrene	ug/L	<0.0075	<0.0075
C2-benzo(a)pyrene	ug/L	<0.0075	<0.0075
<b>Indeno(1,2,3-cd)pyrene</b>	ug/L	<0.009	<0.009
<b>Dibenz(a,h)anthracene</b>	ug/L	<0.0075	<0.0075
<b>Perylene</b>	ug/L	<0.050	<0.050
<b>Benzo(g,h,i)perylene</b>	ug/L	<0.009	<0.009
<b>Quinoline</b>	ug/L	<0.20	<0.20

PAH (Polycyclic Aromatics Hydrocarbons) in water by GC/MS analyses conducted by Maxxam Labs, Calgary using EPA Method EPA 3540C/8270D



Table S5 (d): PAH concentrations in OSPW after R2 (tanks).

PAH		Sample Location											
		4Ta 25-Jul-12	4Ta 17-Aug-12	4Ta 30-Jul-12	4Ta 25-Sep-12	4Ta 14-Jun-13	4Ta 15-Aug-13	4Tb 25-Jul-12	4Tb 17-Aug-12	4Tb 30-Jul-12	4Tb 25-Sep-12	4Tb 14-Jun-13	4Tb 15-Aug-13
<b>Naphthalene</b>	ug/L	<0.10	<0.10	<0.10	<0.10	<0.10	<0.10	<0.10	<0.10	<0.10	<0.10	<0.10	<0.10
1-Methylnaphthalene	ug/L	<0.10	<0.10	<0.10	<0.10	<0.10	<0.10	<0.10	<0.10	<0.10	<0.10	<0.10	<0.10
2-Methylnaphthalene	ug/L	<0.10	<0.10	<0.10	<0.10	<0.10	<0.10	<0.10	<0.10	<0.10	<0.10	<0.10	<0.10
C1-Naphthalene	ug/L	<0.10	<0.10	<0.10	<0.10	<0.10	<0.10	<0.10	<0.10	<0.10	<0.10	<0.10	<0.10
C2-Naphthalene	ug/L	<0.10	<0.10	<0.10	<0.10	<0.10	<0.10	<0.10	<0.10	<0.10	<0.10	<0.10	<0.10
C3-Naphthalene	ug/L	<0.10	<0.10	<0.10	<0.10	<0.10	<0.10	<0.10	<0.10	<0.10	<0.10	<0.10	<0.10
C4-Naphthalene	ug/L	<0.10	<0.10	<0.10	<0.10	<0.10	<0.10	<0.10	<0.10	<0.10	<0.10	<0.10	<0.10
<b>Acenaphthylene</b>	ug/L	<0.10	<0.10	<0.10	<0.10	<0.10	<0.10	<0.10	<0.10	<0.10	<0.10	<0.10	<0.10
<b>Acenaphthene</b>	ug/L	<0.10	<0.10	<0.10	<0.10	<0.10	<0.10	<0.10	<0.10	<0.10	<0.10	<0.10	<0.10
C1-Acenaphthene	ug/L	<0.10	<0.10	<0.10	<0.10	<0.10	<0.10	<0.10	<0.10	<0.10	<0.10	<0.10	<0.10
<b>Acridine</b>	ug/L	<0.20	<0.20	<0.20	<0.20	<0.20	<0.20	<0.20	<0.20	<0.20	<0.20	<0.20	<0.20
<b>Fluorene</b>	ug/L	<0.050	<0.050	<0.050	<0.050	<0.050	<0.050	<0.050	<0.050	<0.050	<0.050	<0.050	<0.050
C1-fluorene	ug/L	<0.050	<0.050	<0.050	<0.050	0.055	0.055	<0.050	<0.050	<0.050	<0.050	<0.050	<0.050
C2-fluorene	ug/L	<0.050	<0.050	<0.050	<0.050	<0.050	<0.13	<0.050	<0.050	<0.050	<0.050	0.057	<0.13
C3-fluorene	ug/L	<0.050	<0.050	<0.050	<0.050	<0.050	<0.17	<0.050	<0.050	<0.050	<0.050	<0.050	<0.17
<b>Biphenyl</b>	ug/L	<0.020	<0.020	<0.020	<0.020	0.02	<0.055	<0.020	<0.020	<0.020	<0.020	<0.020	<0.055
C1-biphenyl	ug/L	<0.020	<0.020	<0.020	<0.020	<0.16	<0.18	<0.020	<0.020	<0.020	<0.020	<0.16	0.18
C2-biphenyl	ug/L	<0.020	<0.020	<0.020	<0.020	<0.085	<0.11	<0.020	<0.020	<0.020	<0.020	<0.085	0.12
<b>Phenanthrene</b>	ug/L	<0.050	<0.050	<0.050	<0.050	<0.050	0.061	<0.050	<0.050	<0.050	<0.050	<0.050	0.059
C1-phenanthrene	ug/L	<0.050	<0.050	<0.050	<0.050	<0.050	<0.050	<0.050	<0.050	<0.050	<0.050	<0.050	<0.050
C2-phenanthrene	ug/L	<0.050	<0.050	<0.050	<0.050	<0.050	0.055	<0.050	<0.050	<0.050	<0.050	<0.050	<0.050
C3-phenanthrene	ug/L	<0.050	<0.050	<0.050	<0.050	<0.050	<0.050	<0.050	<0.050	<0.050	<0.050	<0.050	<0.050
C4-phenanthrene	ug/L	<0.050	<0.050	<0.050	<0.050	<0.050	<0.050	<0.050	<0.050	<0.050	<0.050	<0.050	<0.050
<b>Anthracene</b>	ug/L	<0.010	<0.010	<0.010	<0.010	<0.010	<0.010	<0.010	<0.010	<0.010	<0.010	<0.010	<0.010
<b>Retene</b>	ug/L	<0.050	<0.050	<0.050	<0.050	<0.050	<0.050	<0.050	<0.050	<0.050	<0.050	<0.050	<0.050
<b>Dibenzothiophene</b>	ug/L	<0.020	<0.020	<0.020	<0.020	<0.020	<0.020	<0.020	<0.020	<0.020	<0.020	<0.020	<0.020
C1-dibenzothiophene	ug/L	<0.020	<0.020	<0.020	<0.020	<0.020	<0.020	<0.020	<0.020	<0.020	<0.020	<0.020	<0.020
C2-dibenzothiophene	ug/L	<0.020	<0.020	<0.020	<0.020	<0.020	0.028	<0.020	<0.020	<0.020	<0.020	<0.020	0.034
C3-dibenzothiophene	ug/L	<0.020	<0.020	<0.020	<0.020	<0.020	<0.020	<0.020	<0.020	<0.020	<0.020	<0.020	0.027
C4-dibenzothiophene	ug/L	<0.020	<0.020	<0.020	<0.020	<0.020	<0.020	<0.020	<0.020	<0.020	<0.020	<0.020	<0.020
<b>Fluoranthene</b>	ug/L	<0.040	<0.040	<0.040	<0.040	<0.040	<0.040	<0.040	<0.040	<0.040	<0.040	<0.040	<0.040
<b>Pyrene</b>	ug/L	<0.020	<0.020	<0.020	<0.020	<0.020	<0.020	<0.020	<0.020	<0.020	<0.020	<0.020	<0.020
C1-pyrene	ug/L	<0.020	<0.020	<0.020	<0.020	<0.020	<0.020	<0.020	<0.020	<0.020	<0.020	<0.020	<0.020
C2-pyrene	ug/L	<0.020	<0.020	<0.020	<0.020	<0.020	<0.020	<0.020	<0.020	<0.020	<0.020	<0.020	<0.020
C3-pyrene	ug/L	<0.020	<0.020	<0.020	<0.020	<0.020	<0.020	<0.020	<0.020	<0.020	<0.020	<0.020	<0.020
C4-pyrene	ug/L	<0.020	<0.020	<0.020	<0.020	<0.020	<0.020	<0.020	<0.020	<0.020	<0.020	<0.020	<0.020
<b>Benzo(a)anthracene</b>	ug/L	<0.009	<0.009	<0.009	<0.009	<0.009	<0.009	<0.009	<0.009	<0.009	<0.009	<0.009	<0.009
<b>Chrysene</b>	ug/L	<0.009	<0.009	<0.009	<0.009	<0.009	<0.009	<0.009	<0.009	<0.009	<0.009	<0.009	<0.009
C1-chrysene	ug/L	<0.009	<0.009	<0.009	<0.009	<0.009	<0.009	<0.009	<0.009	<0.009	<0.009	0.011	<0.009
C2-chrysene	ug/L	<0.009	<0.009	<0.009	<0.009	<0.009	<0.009	<0.009	<0.009	<0.009	<0.009	0.038	<0.009
C3-chrysene	ug/L	<0.009	<0.009	<0.009	<0.009	<0.009	<0.009	<0.009	<0.009	<0.009	<0.009	<0.009	<0.009
C4-chrysene	ug/L	<0.009	<0.009	<0.009	<0.009	<0.009	<0.009	<0.009	<0.009	<0.009	<0.009	<0.009	<0.009
<b>Benzo[e]pyrene</b>	ug/L	<0.050	<0.050	<0.050	<0.050	<0.050	<0.050	<0.050	<0.050	<0.050	<0.050	<0.050	<0.050
<b>Benzo(b&amp;j)fluoranthene</b>	ug/L	<0.009	<0.009	<0.009	<0.009	<0.009	<0.009	<0.009	<0.009	<0.009	<0.009	<0.009	<0.009
<b>Benzo(k)fluoranthene</b>	ug/L	<0.009	<0.009	<0.009	<0.009	<0.009	<0.009	<0.009	<0.009	<0.009	<0.009	<0.009	<0.009
<b>Benzo(c)phenanthrene</b>	ug/L	<0.050	<0.050	<0.050	<0.050	<0.050	<0.050	<0.050	<0.050	<0.050	<0.050	<0.050	<0.050
<b>Benzo(a)pyrene</b>	ug/L	<0.008	<0.008	<0.008	<0.008	<0.008	<0.008	<0.008	<0.008	<0.008	<0.008	<0.008	<0.008
<b>Benzo[a]pyrene (equival)</b>	ug/L	<0.010	<0.010	<0.010	<0.010	0.021	<0.010	<0.010	<0.010	<0.010	<0.010	0.021	<0.010
C1-benzo(a)pyrene	ug/L	<0.008	<0.008	<0.008	<0.008	<0.008	<0.008	<0.008	<0.008	<0.008	<0.008	<0.008	<0.008
C2-benzo(a)pyrene	ug/L	<0.008	<0.008	<0.008	<0.008	<0.008	<0.008	<0.008	<0.008	<0.008	<0.008	<0.008	<0.008
<b>Indeno(1,2,3-cd)pyrene</b>	ug/L	<0.009	<0.009	<0.009	<0.009	<0.009	<0.009	<0.009	<0.009	<0.009	<0.009	<0.009	<0.009
<b>Dibenz(a,h)anthracene</b>	ug/L	<0.008	<0.008	<0.008	<0.008	<0.031	<0.031	<0.008	<0.008	<0.008	<0.008	<0.031	<0.008
<b>Perylene</b>	ug/L	<0.050	<0.050	<0.050	<0.050	<0.050	<0.050	<0.050	<0.050	<0.050	<0.050	<0.050	<0.050
<b>Benzo(g,h,i)perylene</b>	ug/L	<0.009	<0.009	<0.009	<0.009	<0.009	<0.009	<0.009	<0.009	<0.009	<0.009	<0.009	<0.009
<b>Quinoline</b>	ug/L	<0.20	<0.20	<0.20	<0.20	<0.20	<0.20	<0.20	<0.20	<0.20	<0.20	<0.20	0.26

PAH (Polycyclic Aromatics) in water by GC/MS analyses conducted by Maxxam Labs, Calgary using EPA Method EPA 3540C/8270D

Tables S6: VOC concentration in OSPW

Table S6 (a): VOC concentrations in OSPW (pre-treatment).

VOLATILES		Sample Location									
		1A 26-Jun-12	1A 3-Jul-12	1B 25-Jun-12	1B 26-Jun-12	1B 27-Jun-12	1B 3-Jul-12	1B 9-Jul-12	1B 23-Jul-12	1B 23-Jul-12	1B 24-Jul-12
<b>TPH</b>											
F1 (C6-C10)	mg/L	<0.10	<0.10	<0.10	<0.10	<0.10	<0.10	<0.10	<0.10	<0.10	<0.10
F2 (C10-C16)	mg/L	0.21	0.19	0.26	0.24	3	0.16	2	0.18	0.2	0.85
<b>BTEX</b>											
Benzene	ug/L	<0.40	<0.40	<0.40	<0.40	0.81	<0.40	<0.40	<0.40	<0.40	<0.40
Ethylbenzene	ug/L	<0.40	0.5	<0.40	<0.40	0.43	0.67	0.48	0.46	<0.40	0.54
Toluene	ug/L	<0.40	<0.40	<0.40	<0.40	<0.40	<0.40	<0.40	<0.40	<0.40	<0.40
o-Xylene	ug/L	<0.40	<0.40	<0.40	<0.40	4.4	<0.40	1.6	<0.40	<0.40	12
m & p-Xylene	ug/L	<0.80	<0.90	<0.80	<0.80	2.8	<0.90	1.4	<1.6	<0.80	3
<b>Volatile Organics</b>											
1,1,1,2-tetrachloroethane	ug/L	<2.0	<2.0	<2.0	<2.0	<2.0	<2.0	<2.0	<2.0	<2.0	<2.0
1,1,1-trichloroethane	ug/L	<0.50	<0.50	<0.50	<0.50	<0.50	<0.50	<0.50	<0.50	<0.50	<0.50
1,1,2,2-tetrachloroethane	ug/L	<2.0	<2.0	<2.0	<2.0	<2.0	<2.0	<2.0	<2.0	<2.0	<2.0
1,1,2-trichloroethane	ug/L	<0.50	<0.50	<0.50	<0.50	<3.6	<0.50	<0.50	<0.50	<0.50	<0.50
1,1-dichloroethane	ug/L	<0.50	<0.50	<0.50	<0.50	<0.50	<0.50	<0.50	<0.50	<0.50	<0.50
1,1-dichloroethene	ug/L	<0.50	<0.50	<0.50	<0.50	<0.50	<0.50	<0.50	<0.50	<0.50	<0.50
1,2,3-trichlorobenzene	ug/L	<1.0	<1.0	<1.0	<1.0	<1.0	<1.0	<1.0	<1.0	<1.0	<1.0
1,2,4-trichlorobenzene	ug/L	<1.0	<1.0	<1.0	<1.0	<1.0	<1.0	<1.0	<1.0	<1.0	<1.0
1,2,4-trimethylbenzene	ug/L	0.9	<0.50	0.94	0.89	1	<0.50	<0.50	<0.50	<0.50	<0.50
1,2-dibromoethane	ug/L	<2.5	<0.65	<1.8	<2.5	<3.0	<0.65	<0.50	<0.50	<0.50	<0.50
1,2-dichlorobenzene	ug/L	<0.50	<0.50	<0.50	<0.50	<0.50	<0.50	<0.50	<0.50	<0.50	<0.50
1,2-dichloroethane	ug/L	<0.50	<0.50	<0.50	<0.50	<0.50	<0.50	<0.50	<0.50	<0.50	<0.50
1,2-dichloropropane	ug/L	<0.50	<0.50	<0.50	<0.50	<0.50	<0.50	<0.50	<0.50	<0.50	<0.50
1,3,5-trichlorobenzene	ug/L	<0.50	<0.50	<0.50	<0.50	<0.50	<0.50	<0.50	<0.50	<0.50	<0.50
1,3,5-trimethylbenzene	ug/L	<0.50	<0.50	<0.50	<0.50	0.75	<0.50	<0.50	<0.50	<0.50	1.3
1,3-dichlorobenzene	ug/L	<0.50	<0.50	<0.50	<0.50	<0.50	<0.50	<0.50	<0.50	<0.50	<0.50
1,4-dichlorobenzene	ug/L	<0.50	<0.50	<0.50	<0.50	<0.50	<0.50	<0.50	<0.50	<0.50	<0.50
Bromodichloromethane	ug/L	<0.50	<0.50	<0.50	<0.50	<0.50	<0.50	<0.50	<0.50	<0.50	<0.50
Bromoform	ug/L	<0.50	<0.50	<0.50	<0.50	<0.50	<0.50	<0.50	<0.50	<0.50	<0.50
Bromomethane	ug/L	<2.0	<2.0	<2.0	<2.0	<2.0	<2.0	<2.0	<2.0	<2.0	<2.0
Carbon tetrachloride	ug/L	<0.50	<0.50	<0.50	<0.50	<0.50	<0.50	<0.50	<0.50	<0.50	<0.50
Chlorobenzene	ug/L	<0.50	<0.50	<0.50	<0.50	<0.50	<0.50	<0.50	<0.50	<0.50	<0.50
Chlorodibromomethane	ug/L	<1.0	<1.0	<1.0	<1.0	<1.0	<1.0	<1.0	<1.0	<1.0	<1.0
Chloroethane	ug/L	<1.0	<1.0	<1.0	<1.0	<1.0	<1.0	<1.0	<1.0	<1.0	<1.0
Chloroform	ug/L	<0.50	<0.50	<0.50	<0.50	<0.50	<0.50	<0.50	<0.50	<0.50	<0.50
Chloromethane	ug/L	<2.0	<2.0	<2.0	<2.0	<2.0	<2.0	<2.0	<2.0	<2.0	<2.0
cis-1,2-dichloroethene	ug/L	<0.50	<0.50	<0.50	<0.50	<0.50	<0.50	<0.50	<0.50	<0.50	<0.50
cis-1,3-dichloropropene	ug/L	<0.50	<0.50	<0.50	<0.50	<0.50	<0.50	<0.50	<0.50	<0.50	<0.50
Dichloromethane	ug/L	<2.0	<2.0	<2.0	<2.0	<2.0	<2.0	<2.0	<2.0	<2.0	<2.0
Methyl methacrylate	ug/L	<0.50	<0.50	<0.50	<0.50	<5.5	<0.50	<0.50	<0.50	<0.50	<0.50
Methyl-tert-butylether	ug/L	<0.50	<0.50	<0.50	<0.50	<2.5	<0.50	<0.50	<0.50	<0.50	<0.50
Styrene	ug/L	<0.50	<0.50	<0.50	<0.50	<0.50	<0.50	<0.50	<0.50	<0.50	<0.50
Tetrachloroethene	ug/L	<0.50	<0.50	<0.50	<0.50	<0.50	<0.50	<0.50	<0.50	<0.50	<0.50
Total Trihalomethanes	ug/L	<2.0	<2.0	<2.0	<2.0	<2.0	<2.0	<2.0	<2.0	<2.0	<2.0
trans-1,2-dichloroethene	ug/L	<0.50	<0.50	<0.50	<0.50	<0.50	<0.50	<0.50	<0.50	<0.50	<0.50
trans-1,3-dichloropropene	ug/L	<0.50	<0.50	<0.50	<0.50	<0.50	<0.50	<0.50	<0.50	<0.50	<0.50
Trichloroethene	ug/L	<0.50	<0.50	<0.50	<0.50	<0.50	<0.50	<0.50	<0.50	<0.50	<0.50
Trichlorofluoromethane	ug/L	<0.50	<0.50	<0.50	<0.50	<0.50	<0.50	<0.50	<0.50	<0.50	<0.50
Vinyl chloride	ug/L	<0.50	<0.50	<0.50	<0.50	<0.50	<0.50	<0.50	<0.50	<0.50	<0.50

VOCs, BTEX and F1 & F2 (TPH) in Water by HS GC/MS analyses conducted by Maxxam Labs, Calgary using EPA Method EPA 8260C

Table S6 (b): VOC concentrations in OSPW after R1.

VOLATILES		Sample Location	
		2A	2A
		25-Jun-12	26-Jun-12
<b>TPH</b>			
F1 (C6-C10)	mg/L	<0.10	<0.10
F2 (C10-C16)	mg/L	<0.10	<0.10
<b>BTEX</b>			
Benzene	ug/L	<0.40	<0.40
Ethylbenzene	ug/L	<0.40	<0.40
Toluene	ug/L	<0.40	<0.40
o-Xylene	ug/L	<0.40	<0.40
m & p-Xylene	ug/L	<0.80	<0.80
<b>Volatile Organics</b>			
1,1,1,2-tetrachloroethane	ug/L	<2.0	<2.0
1,1,1-trichloroethane	ug/L	<0.50	<0.50
1,1,2,2-tetrachloroethane	ug/L	<2.0	<2.0
1,1,2-trichloroethane	ug/L	<0.50	<0.50
1,1-dichloroethane	ug/L	<0.50	<0.50
1,1-dichloroethene	ug/L	<0.50	<0.50
1,2,3-trichlorobenzene	ug/L	<1.0	<1.0
1,2,4-trichlorobenzene	ug/L	<1.0	<1.0
1,2,4-trimethylbenzene	ug/L	<0.50	<0.50
1,2-dibromoethane	ug/L	<0.50	<0.50
1,2-dichlorobenzene	ug/L	<0.50	<0.50
1,2-dichloroethane	ug/L	<0.50	<0.50
1,2-dichloropropane	ug/L	<0.50	<0.50
1,3,5-trichlorobenzene	ug/L	<0.50	<0.50
1,3,5-trimethylbenzene	ug/L	<0.50	<0.50
1,3-dichlorobenzene	ug/L	<0.50	<0.50
1,4-dichlorobenzene	ug/L	<0.50	<0.50
Bromodichloromethane	ug/L	<0.50	<0.50
Bromoform	ug/L	<0.50	<0.50
Bromomethane	ug/L	<2.0	<2.0
Carbon tetrachloride	ug/L	<0.50	<0.50
Chlorobenzene	ug/L	<0.50	<0.50
Chlorodibromomethane	ug/L	<1.0	<1.0
Chloroethane	ug/L	<1.0	<1.0
Chloroform	ug/L	<0.50	<0.50
Chloromethane	ug/L	<2.0	<2.0
cis-1,2-dichloroethene	ug/L	<0.50	<0.50
cis-1,3-dichloropropene	ug/L	<0.50	<0.50
Dichloromethane	ug/L	<2.0	<2.0
Methyl methacrylate	ug/L	<0.50	<0.50
Methyl-tert-butylether	ug/L	<0.50	<0.50
Styrene	ug/L	<0.50	<0.50
Tetrachloroethene	ug/L	<0.50	<0.50
Total Trihalomethanes	ug/L	<2.0	<2.0
trans-1,2-dichloroethene	ug/L	<0.50	<0.50
trans-1,3-dichloropropene	ug/L	<0.50	<0.50
Trichloroethene	ug/L	<0.50	<0.50
Trichlorofluoromethane	ug/L	<0.50	<0.50
Vinyl chloride	ug/L	<0.50	<0.50

VOCs, BTEX and F1 & F2 (TPH) in Water by  
 HS GC/MS analyses conducted by Maxxam Labs,  
 Calgary using EPA Method EPA EPA 8260C

Table S6 (c): VOC concentrations in OSPW after R2 (cells).

VOLATILES		Sample Location														
		4A 26-Jun-12	4A 5-Jul-12	4A 10-Jul-12	4A 18-Jul-12	4A 25-Jul-12	4A 17-Aug-12	4A 25-Sep-12	4B 14-Jun-13	4B 28-Jun-12	4B 10-Jul-12	4B 18-Jul-12	4B 25-Jul-12	4B 17-Aug-12	4B 25-Sep-12	4B 14-Jun-13
<b>TPH</b>																
F1 (C6-C10)	mg/L	<0.10	<0.10	<0.10	<0.10	<0.10	<0.10	<0.10	<0.10	<0.10	<0.10	<0.10	<0.10	<0.10	<0.10	<0.10
F2 (C10-C16)	mg/L	<0.10	<0.10	<0.10	<0.10	<0.10	<0.10	<0.10	<0.10	<0.10	<0.10	<0.10	<0.10	<0.10	<0.10	<0.10
<b>BTEX</b>																
Benzene	ug/L	<0.40	<0.40	<0.40	<0.40	<0.40	<0.40	<0.40	<0.40	<0.40	<0.40	<0.40	<0.40	<0.40	<0.40	<0.40
Ethylbenzene	ug/L	<0.40	<0.40	<0.40	<0.40	<0.40	<0.40	<0.40	<0.40	<0.40	<0.40	<0.40	<0.40	<0.40	<0.40	<0.40
Toluene	ug/L	<0.40	<0.40	<0.40	<0.40	<0.40	<0.40	<0.40	<0.40	<0.40	<0.40	<0.40	<0.40	<0.40	<0.40	<0.40
o-Xylene	ug/L	<0.40	<0.40	<0.40	<0.40	<0.40	<0.40	<0.40	<0.40	<0.40	<0.40	<0.40	<0.40	<0.40	<0.40	<0.40
m & p-Xylene	ug/L	<0.80	<0.80	<0.80	<0.80	<0.80	<0.80	<0.80	<0.80	<0.80	<0.80	<0.80	<0.80	<0.80	<0.80	<0.80
<b>Volatile Organics</b>																
1,1,1,2-tetrachloroethane	ug/L	<2.0	<2.0	<2.0	<2.0	<2.0	<2.0	<2.0		<2.0	<2.0	<2.0	<2.0	<2.0	<2.0	
1,1,1-trichloroethane	ug/L	<0.50	<0.50	<0.50	<0.50	<0.50	<0.50	<0.50		<0.50	<0.50	<0.50	<0.50	<0.50	<0.50	
1,1,2,2-tetrachloroethane	ug/L	<2.0	<2.0	<2.0	<2.0	<2.0	<2.0	<2.0		<2.0	<2.0	<2.0	<2.0	<2.0	<2.0	
1,1,2-trichloroethane	ug/L	<0.50	<0.50	<0.50	<0.50	<0.50	<0.50	<0.50		<0.50	<0.50	<0.50	<0.50	<0.50	<0.50	
1,1-dichloroethane	ug/L	<0.50	<0.50	<0.50	<0.50	<0.50	<0.50	<0.50		<0.50	<0.50	<0.50	<0.50	<0.50	<0.50	
1,1-dichloroethene	ug/L	<0.50	<0.50	<0.50	<0.50	<0.50	<0.50	<0.50		<0.50	<0.50	<0.50	<0.50	<0.50	<0.50	
1,2,3-trichlorobenzene	ug/L	<1.0	<1.0	<1.0	<1.0	<1.0	<1.0	<1.0		<1.0	<1.0	<1.0	<1.0	<1.0	<1.0	
1,2,4-trichlorobenzene	ug/L	<1.0	<1.0	<1.0	<1.0	<1.0	<1.0	<1.0		<1.0	<1.0	<1.0	<1.0	<1.0	<1.0	
1,2,4-trimethylbenzene	ug/L	<0.50	<0.50	<0.50	<0.50	<0.50	<0.50	<0.50		<0.50	<0.50	<0.50	<0.50	<0.50	<0.50	
1,2-dibromoethane	ug/L	<0.50	<0.50	<0.50	<0.50	<0.50	<0.50	<0.50		<0.50	<0.50	<0.50	<0.50	<0.50	<0.50	
1,2-dichlorobenzene	ug/L	<0.50	<0.50	<0.50	<0.50	<0.50	<0.50	<0.50		<0.50	<0.50	<0.50	<0.50	<0.50	<0.50	
1,2-dichloroethane	ug/L	<0.50	<0.50	<0.50	<0.50	<0.50	<0.50	<0.50		<0.50	<0.50	<0.50	<0.50	<0.50	<0.50	
1,2-dichloropropane	ug/L	<0.50	<0.50	<0.50	<0.50	<0.50	<0.50	<0.50		<0.50	<0.50	<0.50	<0.50	<0.50	<0.50	
1,3,5-trichlorobenzene	ug/L	<0.50	<0.50	<0.50	<0.50	<0.50	<0.50	<0.50		<0.50	<0.50	<0.50	<0.50	<0.50	<0.50	
1,3,5-trimethylbenzene	ug/L	<0.50	<0.50	<0.50	<0.50	<0.50	<0.50	<0.50		<0.50	<0.50	<0.50	<0.50	<0.50	<0.50	
1,3-dichlorobenzene	ug/L	<0.50	<0.50	<0.50	<0.50	<0.50	<0.50	<0.50		<0.50	<0.50	<0.50	<0.50	<0.50	<0.50	
1,4-dichlorobenzene	ug/L	<0.50	<0.50	<0.50	<0.50	<0.50	<0.50	<0.50		<0.50	<0.50	<0.50	<0.50	<0.50	<0.50	
Bromodichloromethane	ug/L	<0.50	<0.50	<0.50	<0.50	<0.50	<0.50	<0.50		<0.50	<0.50	<0.50	<0.50	<0.50	<0.50	
Bromoform	ug/L	<0.50	<0.50	<0.50	<0.50	<0.50	<0.50	<0.50		<0.50	<0.50	<0.50	<0.50	<0.50	<0.50	
Bromomethane	ug/L	<2.0	<2.0	<2.0	<2.0	<2.0	<2.0	<2.0		<2.0	<2.0	<2.0	<2.0	<2.0	<2.0	
Carbon tetrachloride	ug/L	<0.50	<0.50	<0.50	<0.50	<0.50	<0.50	<0.50		<0.50	<0.50	<0.50	<0.50	<0.50	<0.50	
Chlorobenzene	ug/L	<0.50	<0.50	<0.50	<0.50	<0.50	<0.50	<0.50		<0.50	<0.50	<0.50	<0.50	<0.50	<0.50	
Chlorodibromomethane	ug/L	<1.0	<1.0	<1.0	<1.0	<1.0	<1.0	<1.0		<1.0	<1.0	<1.0	<1.0	<1.0	<1.0	
Chloroethane	ug/L	<1.0	<1.0	<1.0	<1.0	<1.0	<1.0	<1.0		<1.0	<1.0	<1.0	<1.0	<1.0	<1.0	
Chloroform	ug/L	<0.50	<0.50	<0.50	<0.50	<0.50	<0.50	<0.50		<0.50	<0.50	<0.50	<0.50	<0.50	<0.50	
Chloromethane	ug/L	<2.0	<2.0	<2.0	<2.0	<2.0	<2.0	<2.0		<2.0	<2.0	<2.0	<2.0	<2.0	<2.0	
cis-1,2-dichloroethene	ug/L	<0.50	<0.50	<0.50	<0.50	<0.50	<0.50	<0.50		<0.50	<0.50	<0.50	<0.50	<0.50	<0.50	
cis-1,3-dichloropropene	ug/L	<0.50	<0.50	<0.50	<0.50	<0.50	<0.50	<0.50		<0.50	<0.50	<0.50	<0.50	<0.50	<0.50	
Dichloromethane	ug/L	<2.0	<2.0	<2.0	<2.0	<2.0	<2.0	<2.0		<2.0	<2.0	<2.0	<2.0	<2.0	<2.0	
Methyl methacrylate	ug/L	<0.50	<0.50	<0.50	<0.50	<0.50	<0.50	<0.50		<0.50	<0.50	<0.50	<0.50	<0.50	<0.50	
Methyl-tert-butylether	ug/L	<0.50	<0.50	<0.50	<0.50	<0.50	<0.50	<0.50		<0.50	<0.50	<0.50	<0.50	<0.50	<0.50	
Styrene	ug/L	<0.50	<0.50	<0.50	<0.50	<0.50	<0.50	<0.50		<0.50	<0.50	<0.50	<0.50	<0.50	<0.50	
Tetrachloroethene	ug/L	<0.50	<0.50	<0.50	<0.50	<0.50	<0.50	<0.50		<0.50	<0.50	<0.50	<0.50	<0.50	<0.50	
Total Trihalomethanes	ug/L	<2.0	<2.0	<2.0	<2.0	<2.0	<2.0	<2.0		<2.0	<2.0	<2.0	<2.0	<2.0	<2.0	
trans-1,2-dichloroethene	ug/L	<0.50	<0.50	<0.50	<0.50	<0.50	<0.50	<0.50		<0.50	<0.50	<0.50	<0.50	<0.50	<0.50	
trans-1,3-dichloropropene	ug/L	<0.50	<0.50	<0.50	<0.50	<0.50	<0.50	<0.50		<0.50	<0.50	<0.50	<0.50	<0.50	<0.50	
Trichloroethene	ug/L	<0.50	<0.50	<0.50	<0.50	<0.50	<0.50	<0.50		<0.50	<0.50	<0.50	<0.50	<0.50	<0.50	
Trichlorofluoromethane	ug/L	<0.50	<0.50	<0.50	<0.50	<0.50	<0.50	<0.50		<0.50	<0.50	<0.50	<0.50	<0.50	<0.50	
Vinyl chloride	ug/L	<0.50	<0.50	<0.50	<0.50	<0.50	<0.50	<0.50		<0.50	<0.50	<0.50	<0.50	<0.50	<0.50	

VOCs, BTEX and F1 & F2 (TPH) in Water by HS GC/MS analyses conducted by Maxxam Labs, Calgary using EPA Method EPA EPA 8260C

Table S6 (d): VOC concentrations in OSPW after R2 (tanks).

VOLATILES		Sample Location									
		4Ta 25-Jul-12	4Ta 30-Jul-12	4Ta 17-Aug-12	4Ta 25-Sep-12	4Ta 14-Jun-13	4Tb 25-Jul-12	4Tb 30-Jul-12	4Tb 17-Aug-12	4Tb 25-Sep-12	4Tb 14-Jun-13
<b>TPH</b>											
F1 (C6-C10)	mg/L	<0.10	<0.10	<0.10	<0.10	<0.10	<0.10	<0.10	<0.10	<0.10	<0.10
F2 (C10-C16)	mg/L	<0.10	<0.10	<0.10	<0.10	<0.10	<0.10	<0.10	<0.10	<0.10	<0.10
<b>BTEX</b>											
Benzene	ug/L	<0.40	<0.40	<0.40	<0.40	<0.40	<0.40	<0.40	<0.40	<0.40	<0.40
Ethylbenzene	ug/L	<0.40	<0.40	<0.40	<0.40	<0.40	<0.40	<0.40	<0.40	<0.40	<0.40
Toluene	ug/L	2.8	3.2	<0.40	<0.40	<0.40	2.4	2.5	0.94	<0.40	<0.40
o-Xylene	ug/L	<0.40	<0.40	<0.40	<0.40	<0.40	<0.40	<0.40	<0.40	<0.40	<0.40
m & p-Xylene	ug/L	<0.80	<0.80	<0.80	<0.80	<0.80	<0.80	<0.80	<0.80	<0.80	<0.80
<b>Volatile Organics</b>											
1,1,1,2-tetrachloroethane	ug/L	<2.0	<2.0	<2.0	<2.0		<2.0	<2.0	<2.0	<2.0	
1,1,1-trichloroethane	ug/L	<0.50	<0.50	<0.50	<0.50		<0.50	<0.50	<0.50	<0.50	
1,1,2,2-tetrachloroethane	ug/L	<2.0	<2.0	<2.0	<2.0		<2.0	<2.0	<2.0	<2.0	
1,1,2-trichloroethane	ug/L	<0.50	<0.50	<0.50	<0.50		<0.50	<0.50	<0.50	<0.50	
1,1-dichloroethane	ug/L	<0.50	<0.50	<0.50	<0.50		<0.50	<0.50	<0.50	<0.50	
1,1-dichloroethene	ug/L	<0.50	<0.50	<0.50	<0.50		<0.50	<0.50	<0.50	<0.50	
1,2,3-trichlorobenzene	ug/L	<1.0	<1.0	<1.0	<1.0		<1.0	<1.0	<1.0	<1.0	
1,2,4-trichlorobenzene	ug/L	<1.0	<1.0	<1.0	<1.0		<1.0	<1.0	<1.0	<1.0	
1,2,4-trimethylbenzene	ug/L	<0.50	<0.50	<0.50	<0.50		<0.50	<0.50	<0.50	<0.50	
1,2-dibromoethane	ug/L	<0.50	<0.50	<0.50	<0.50		<0.50	<0.50	<0.50	<0.50	
1,2-dichlorobenzene	ug/L	<0.50	<0.50	<0.50	<0.50		<0.50	0.51	<0.50	<0.50	
1,2-dichloroethane	ug/L	<0.50	<0.50	<0.50	<0.50		<0.50	<0.50	<0.50	<0.50	
1,2-dichloropropane	ug/L	<0.50	<0.50	<0.50	<0.50		<0.50	<0.50	<0.50	<0.50	
1,3,5-trichlorobenzene	ug/L	<0.50	<0.50	<0.50	<0.50		<0.50	<0.50	<0.50	<0.50	
1,3,5-trimethylbenzene	ug/L	<0.50	<0.50	<0.50	<0.50		<0.50	<0.50	<0.50	<0.50	
1,3-dichlorobenzene	ug/L	<0.50	<0.50	<0.50	<0.50		<0.50	<0.50	<0.50	<0.50	
1,4-dichlorobenzene	ug/L	<0.50	<0.50	<0.50	<0.50		<0.50	<0.50	<0.50	<0.50	
Bromodichloromethane	ug/L	<0.50	<0.50	<0.50	<0.50		<0.50	<0.50	<0.50	<0.50	
Bromoform	ug/L	<0.50	<0.50	<0.50	<0.50		<0.50	<0.50	<0.50	<0.50	
Bromomethane	ug/L	<2.0	<2.0	<2.0	<2.0		<2.0	<2.0	<2.0	<2.0	
Carbon tetrachloride	ug/L	<0.50	<0.50	<0.50	<0.50		<0.50	<0.50	<0.50	<0.50	
Chlorobenzene	ug/L	<0.50	<0.50	<0.50	<0.50		<0.50	<0.50	<0.50	<0.50	
Chlorodibromomethane	ug/L	<1.0	<1.0	<1.0	<1.0		<1.0	<1.0	<1.0	<1.0	
Chloroethane	ug/L	<1.0	<1.0	<1.0	<1.0		<1.0	<1.0	<1.0	<1.0	
Chloroform	ug/L	<0.50	<0.50	<0.50	<0.50		<0.50	<0.50	<0.50	<0.50	
Chloromethane	ug/L	<2.0	<2.0	<2.0	<2.0		<2.0	<2.0	<2.0	<2.0	
cis-1,2-dichloroethene	ug/L	<0.50	<0.50	<0.50	<0.50		<0.50	<0.50	<0.50	<0.50	
cis-1,3-dichloropropene	ug/L	<0.50	<0.50	<0.50	<0.50		<0.50	<0.50	<0.50	<0.50	
Dichloromethane	ug/L	<2.0	<2.0	<2.0	<2.0		<2.0	<2.0	<2.0	<2.0	
Methyl methacrylate	ug/L	<0.50	<0.50	<0.50	<0.50		<0.50	<0.50	<0.50	<0.50	
Methyl-tert-butylether	ug/L	<0.50	<0.50	<0.50	<0.50		<0.50	<0.50	<0.50	<0.50	
Styrene	ug/L	0.55	0.81	<0.50	<0.50		0.9	0.69	0.67	<0.50	
Tetrachloroethene	ug/L	<0.50	<0.50	<0.50	<0.50		<0.50	<0.50	<0.50	<0.50	
Total Trihalomethanes	ug/L	<2.0	<2.0	<2.0	<2.0		<2.0	<2.0	<2.0	<2.0	
trans-1,2-dichloroethene	ug/L	<0.50	<0.50	<0.50	<0.50		<0.50	<0.50	<0.50	<0.50	
trans-1,3-dichloropropene	ug/L	<0.50	<0.50	<0.50	<0.50		<0.50	<0.50	<0.50	<0.50	
Trichloroethene	ug/L	<0.50	<0.50	<0.50	<0.50		<0.50	<0.50	<0.50	<0.50	
Trichlorofluoromethane	ug/L	<0.50	<0.50	<0.50	<0.50		<0.50	<0.50	<0.50	<0.50	
Vinyl chloride	ug/L	<0.50	<0.50	<0.50	<0.50		<0.50	<0.50	<0.50	<0.50	

VOCs, BTEX and F1 & F2 (TPH) in Water by HS GC/MS analyses conducted by Maxxam Labs, Calgary using EPA Method EPA EPA 8260C

## APPENDIX B

Appendix B contains 2 Text, 13 Figures, and 2 Tables.

### *Text B1: Kinetics study*

The adsorption capacity,  $q_t$ , is determined by equation 1:

$$q_t = \frac{(C_0 - C_t)V}{m} \quad (1)$$

Where  $q_t$  is the adsorption capacity at time  $t$ ,  $C_0$  is the initial concentration of target NAs compound (mg/L),  $C_t$  is the concentration of the target NAs compound at time  $t$  (mg/L),  $V$  is the volume of the solution (L), and  $m$  is the mass of the adsorbent material, CST and PMM (mg).

The NAs concentration data for different retention times were fit to both empirical and phenomenological adsorption kinetics models (Kajjumba et al. 2018). The determination of the best fitted kinetics model for the adsorption process was based on the correlation coefficient ( $R^2$ ) provided by linear trendline of the data and the comparison between the adsorption capacity calculated by certain model and the adsorption capacity obtained experimentally (Foo and Hameed 2010).

To understand empirical principles, PFO (equation 2), PSO kinetics models (equation 3) were employed.

$$\ln(q_e - q_t) = \ln q_e - k_1 t \quad (2)$$

$$\frac{t}{q_t} = \left[ \frac{1}{k_2 q_e^2} \right] \frac{1}{t} + \frac{1}{q_e} \quad (3)$$

To understand phenomenological principles, the transport kinetics and equilibrium isotherm models were employed. The transport kinetics includes the IPD kinetics model (equation 4), and the Elovich kinetics model (equation 5).

$$q_t = k_i\sqrt{t} + C \quad (4)$$

$$q_t = \frac{1}{\beta} \ln[\alpha\beta] + \frac{1}{\beta} \ln t \quad (5)$$

Where  $q_e$  is the adsorption capacity at equilibrium,  $k_1$  is the PFO rate constant ( $h^{-1}$ ),  $k_2$  is the PSO rate constant ( $g/mg/h$ ),  $k_i$  is the IPD rate constant ( $mg/g/h^{0.5}$ ) and  $C$  is the boundary layer thickness,  $\alpha$  is the initial sorption rate ( $mg/g/h$ ),  $\beta$  is the desorption constant ( $g/mg$ ).

**Text B2: Isotherm models/ Adsorption equilibrium models**

The adsorption data of isotherm study was evaluated by both the Langmuir (Eq. 6) (Langmuir 1918) and Freundlich (Eq. 7) (Freundlich 1906) isotherms.

$$\frac{1}{q_e} = \frac{1}{K_L q_{max}} \frac{1}{C_e} + \frac{1}{q_{max}} \quad (6)$$

$$\log q_e = \log K_f + \frac{1}{n} \log C_e \quad (7)$$

Where  $K_L$  is the Langmuir rate constant ( $mg/L$ ),  $q_{max}$  is the maximum adsorption capacity ( $mg/g$ ),  $K_f$  is the Freundlich adsorption coefficient [ $(mg/g)(mg/L)^{1/n}$ ], and  $\frac{1}{n}$  is the Freundlich heterogeneity parameter (dimensionless).

**Note:**

Figure 3.9 was created with Biorender.com.



Figure S7: The raw materials and well-prepared samples.

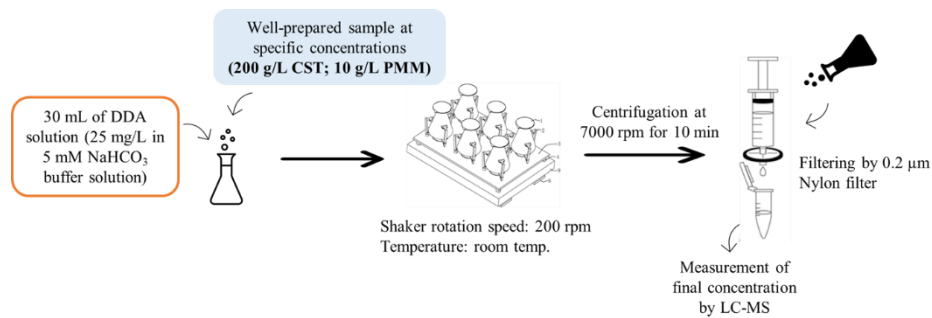


Figure S8: The scheme for the kinetics study.

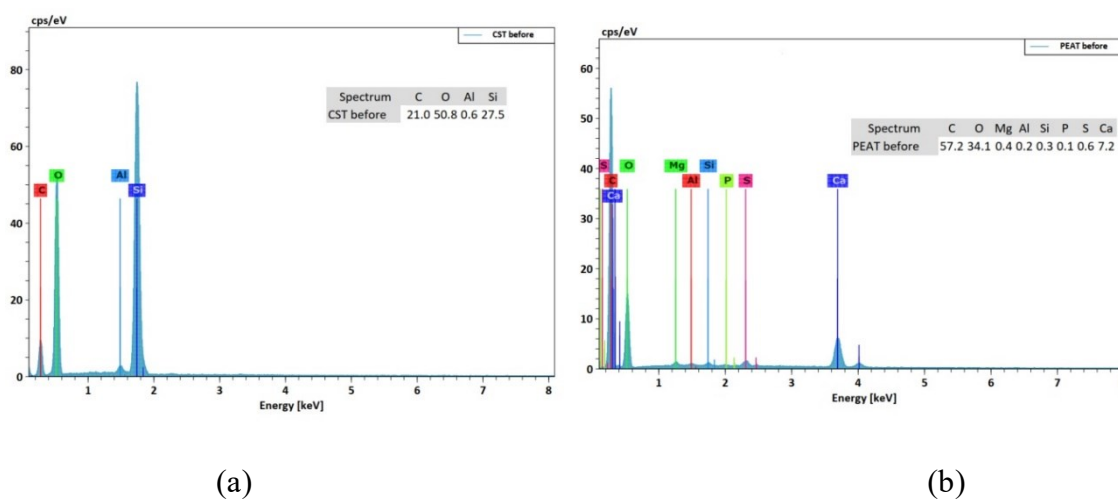


Figure S9: EDX results of CST (a) and PMM (b).

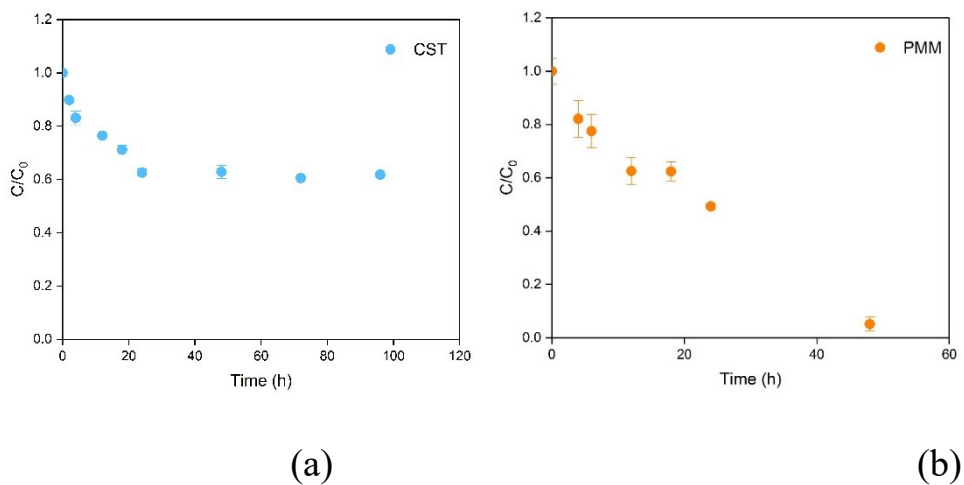
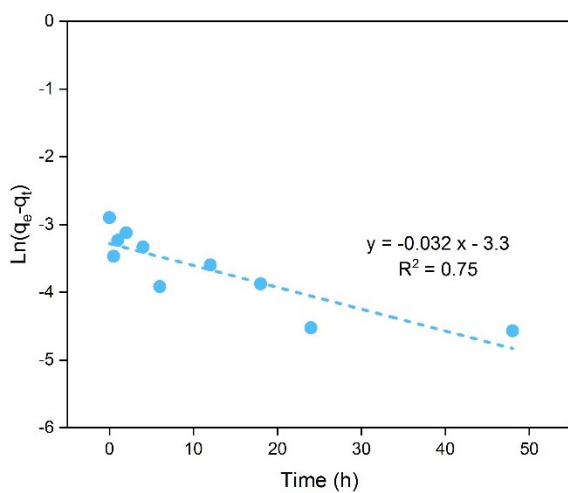
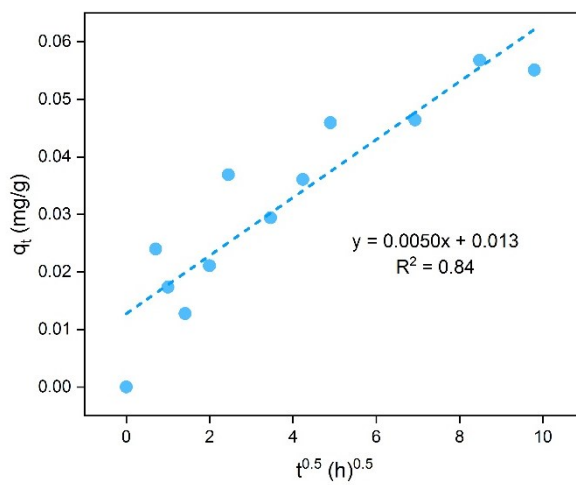


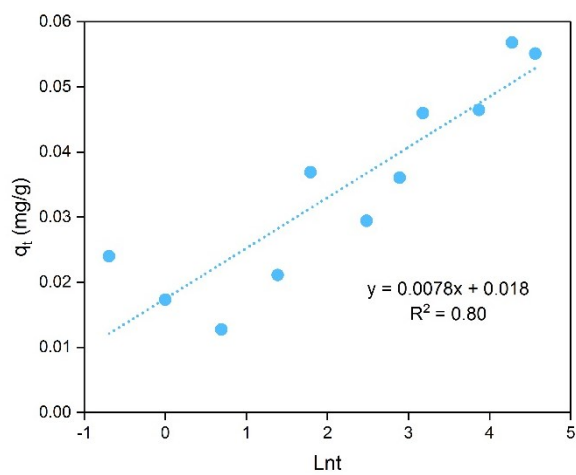
Figure S10:  $C/C_0$  vs. contact time for DDA adsorption by CST(a), and PMM (b).



(a)



(b)



(c)

Figure S11: Different kinetics models of DDA adsorption by CST: (a) PFO, (b) IPD, and (c) Elovich.

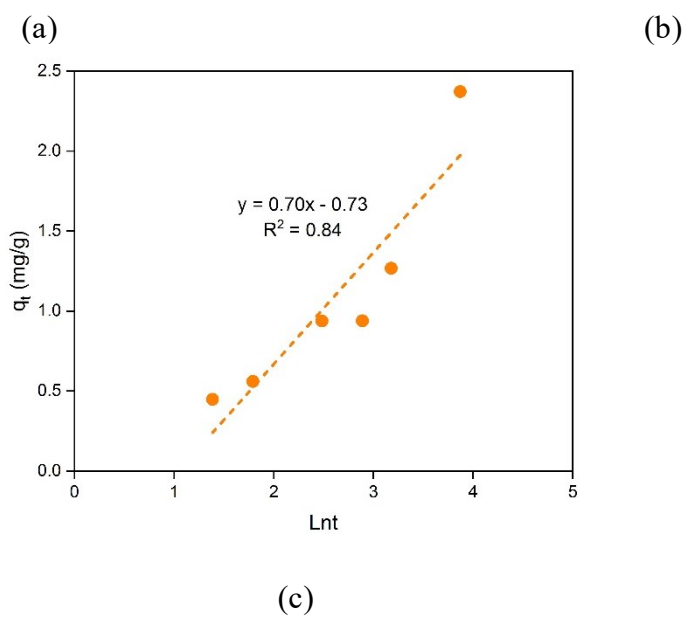
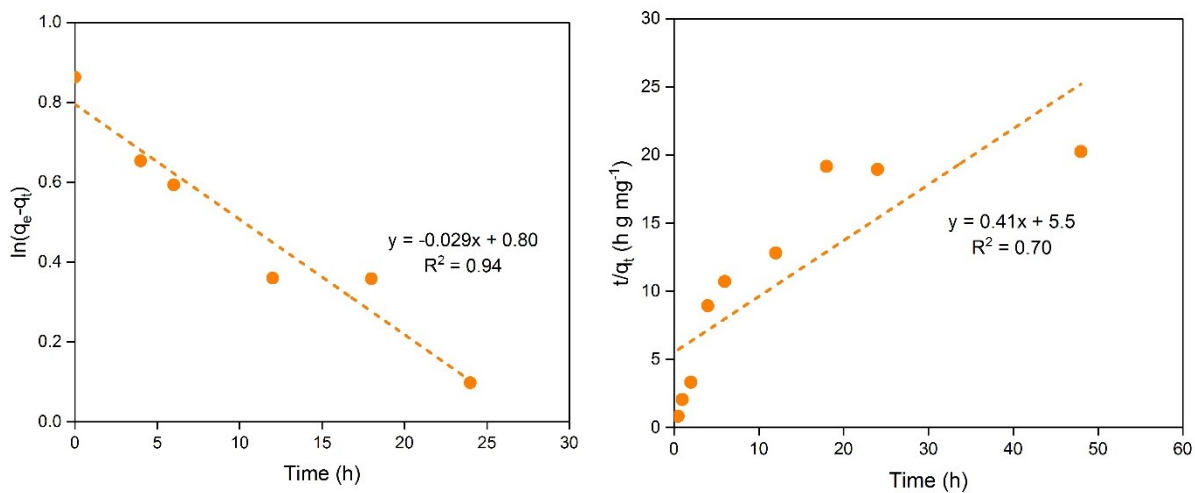


Figure S12: Different kinetics models of DDA adsorption by PMM: (a) PFO, (b) PSO, and (c) Elovich.

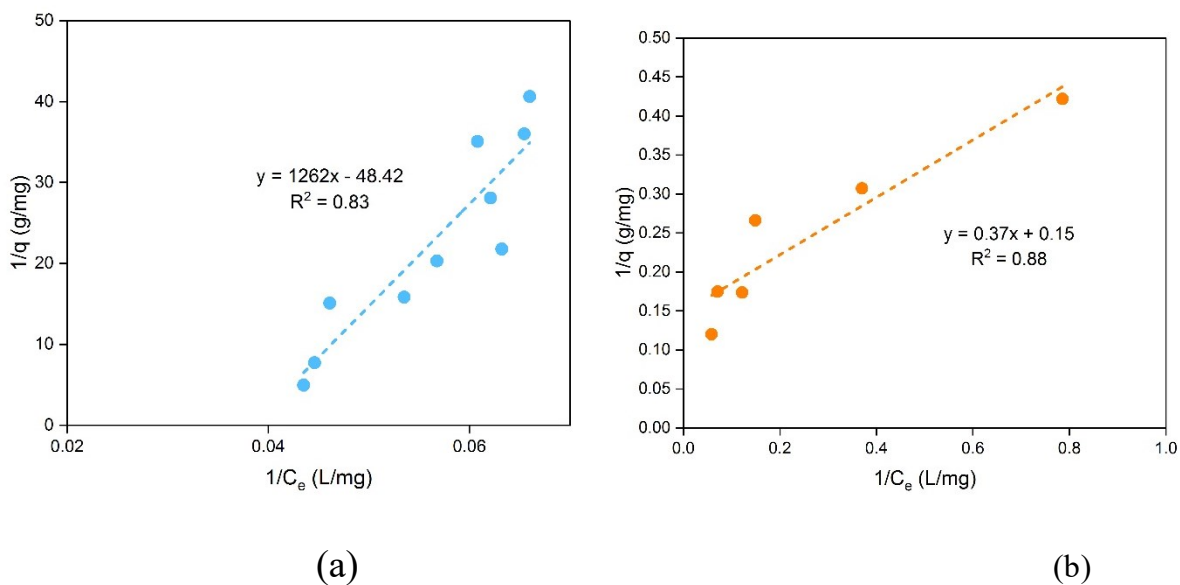


Figure S13: The linearized Langmuir models for DDA adsorption by CST (a) and PMM (b).

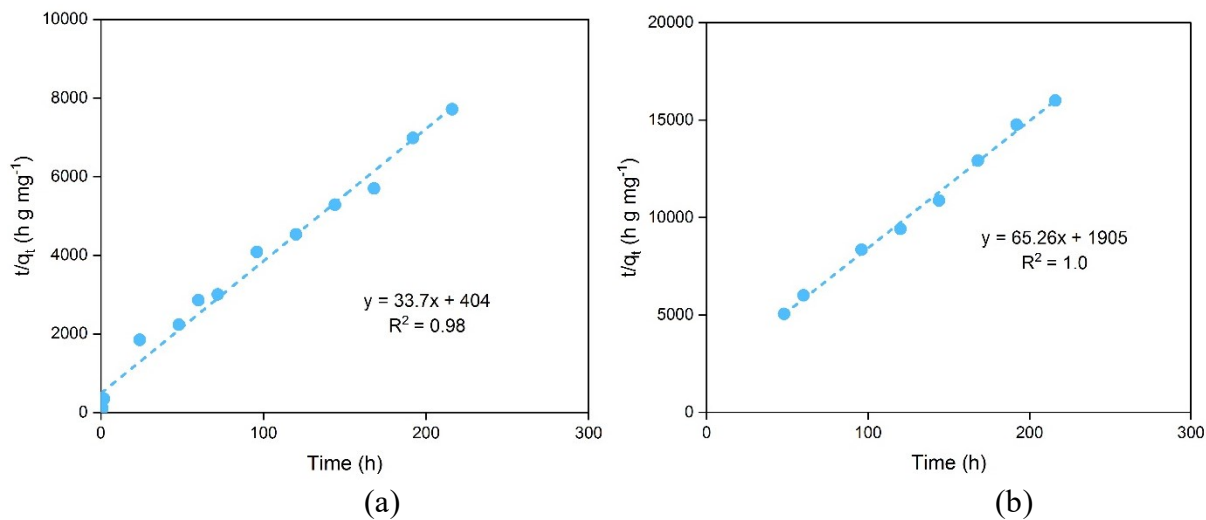
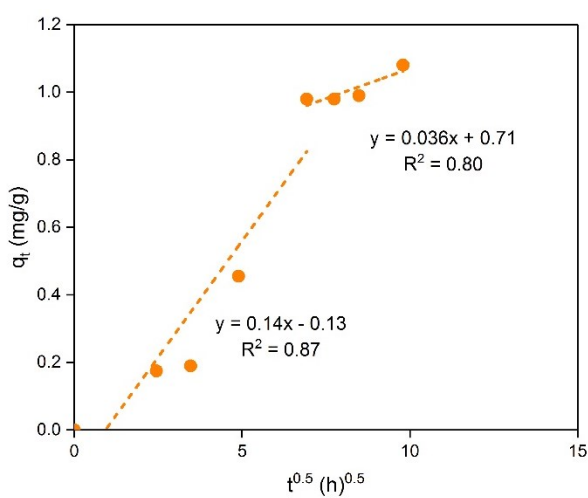
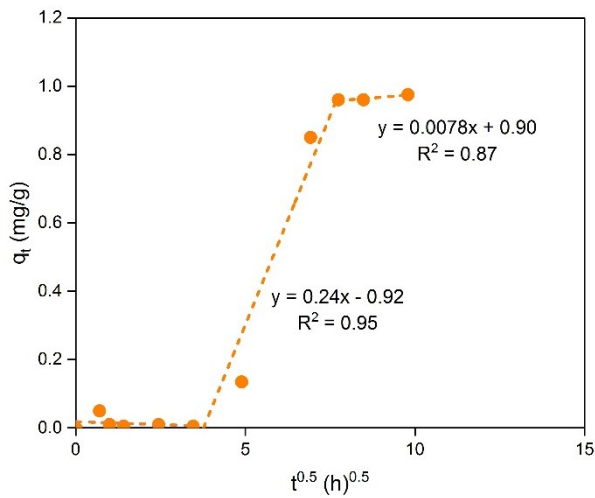


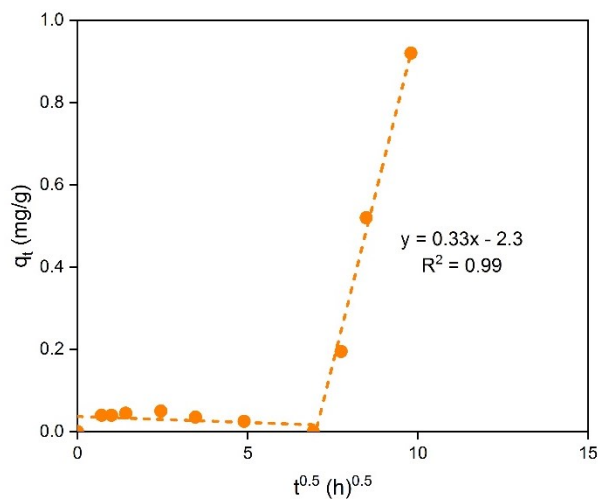
Figure S14: DDA (a) and DA (b) adsorption PSO kinetics in mixture by CST.



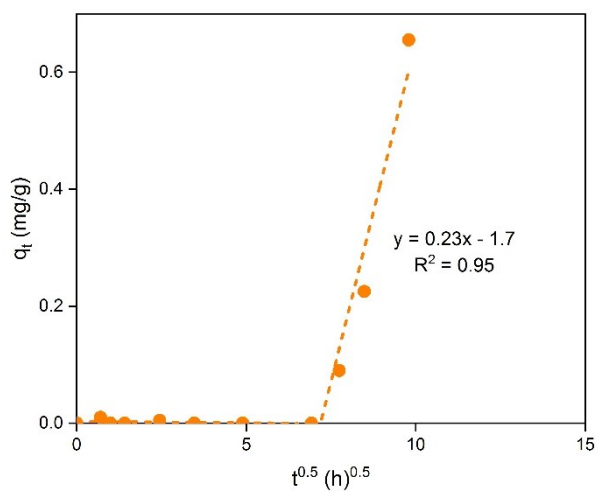
(a)



(b)

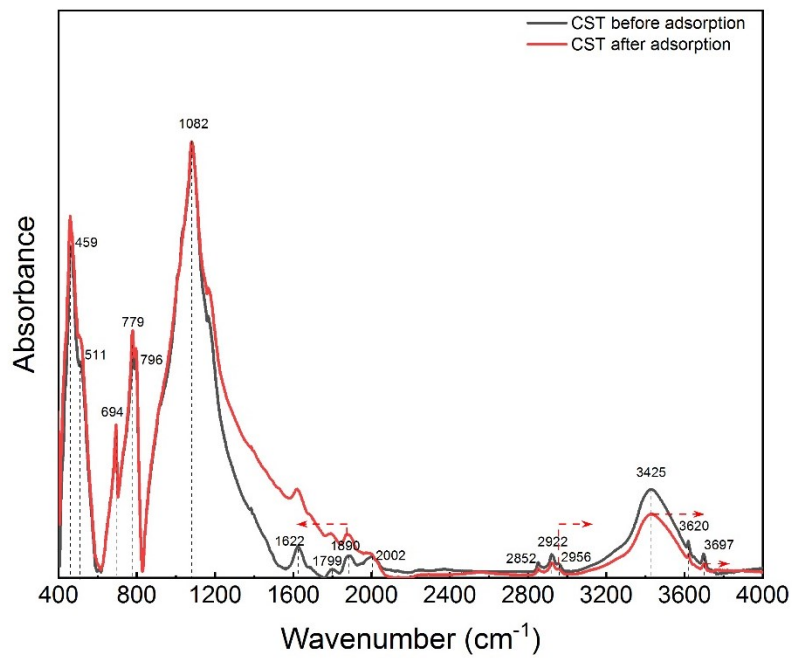


(c)

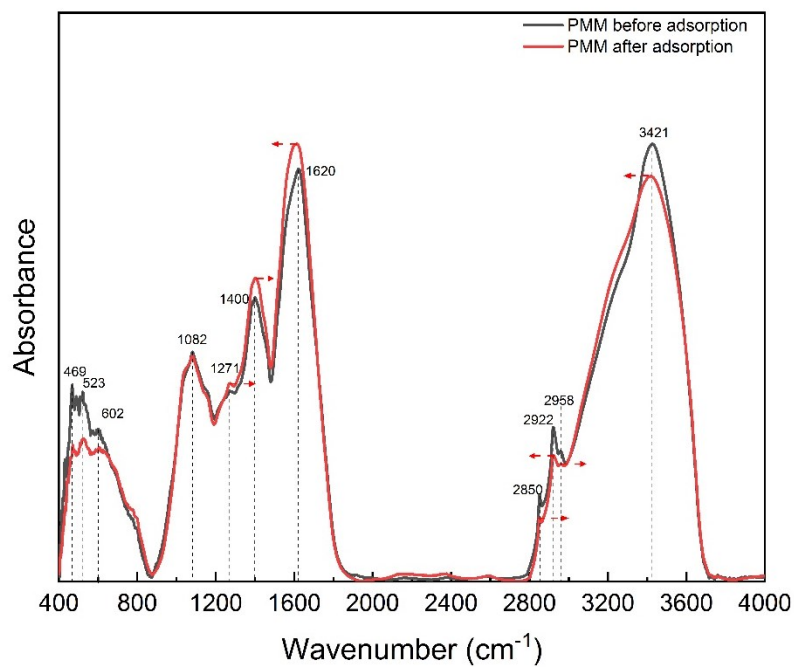


(d)

Figure S15: Adsorption kinetics (IPD model) in NAs mixture by PMM for DDA (a) DA (b), CHPA (c), and PVA (d).



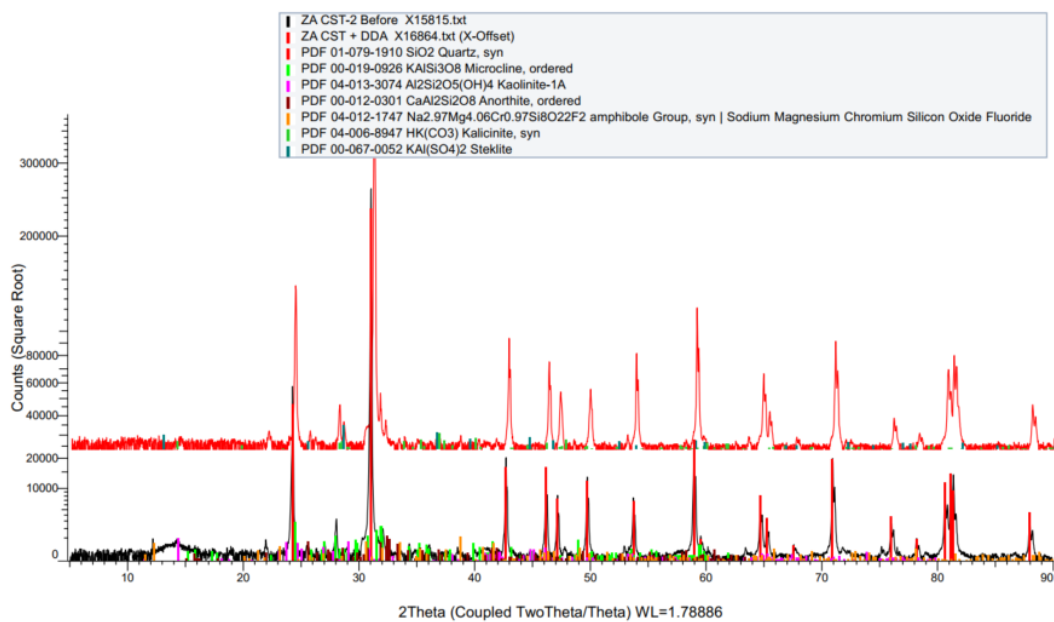
(a)



(b)

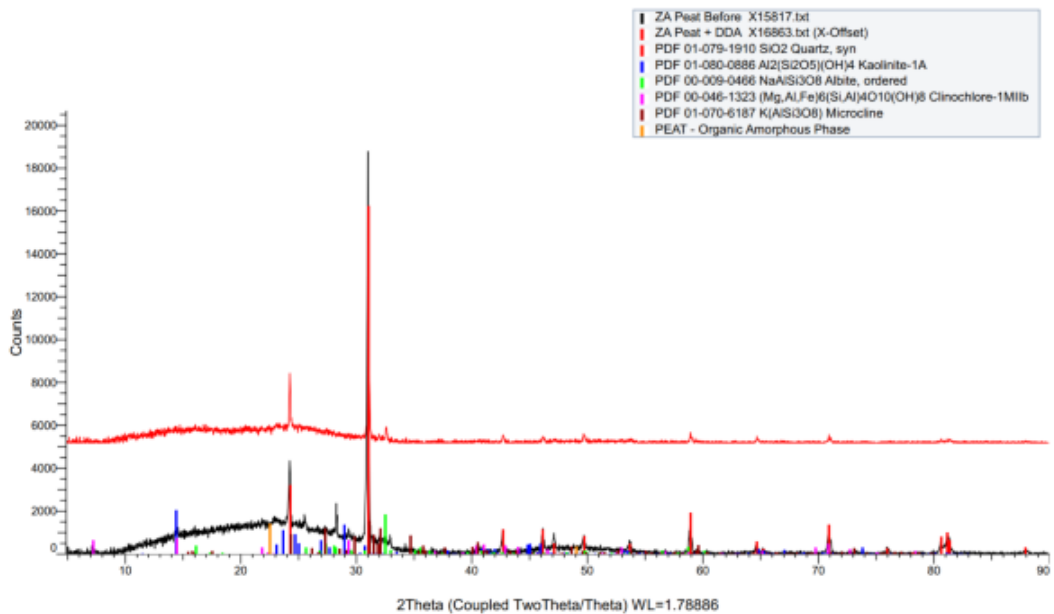
Figure S16: FTIR spectra for CST (a) and PMM (b) before and after adsorption process.

(Coupled TwoTheta/Theta)



(a)

(Coupled TwoTheta/Theta)



(b)

Figure S17: XRD results for CST (a) and PMM (b) before and after adsorption process.

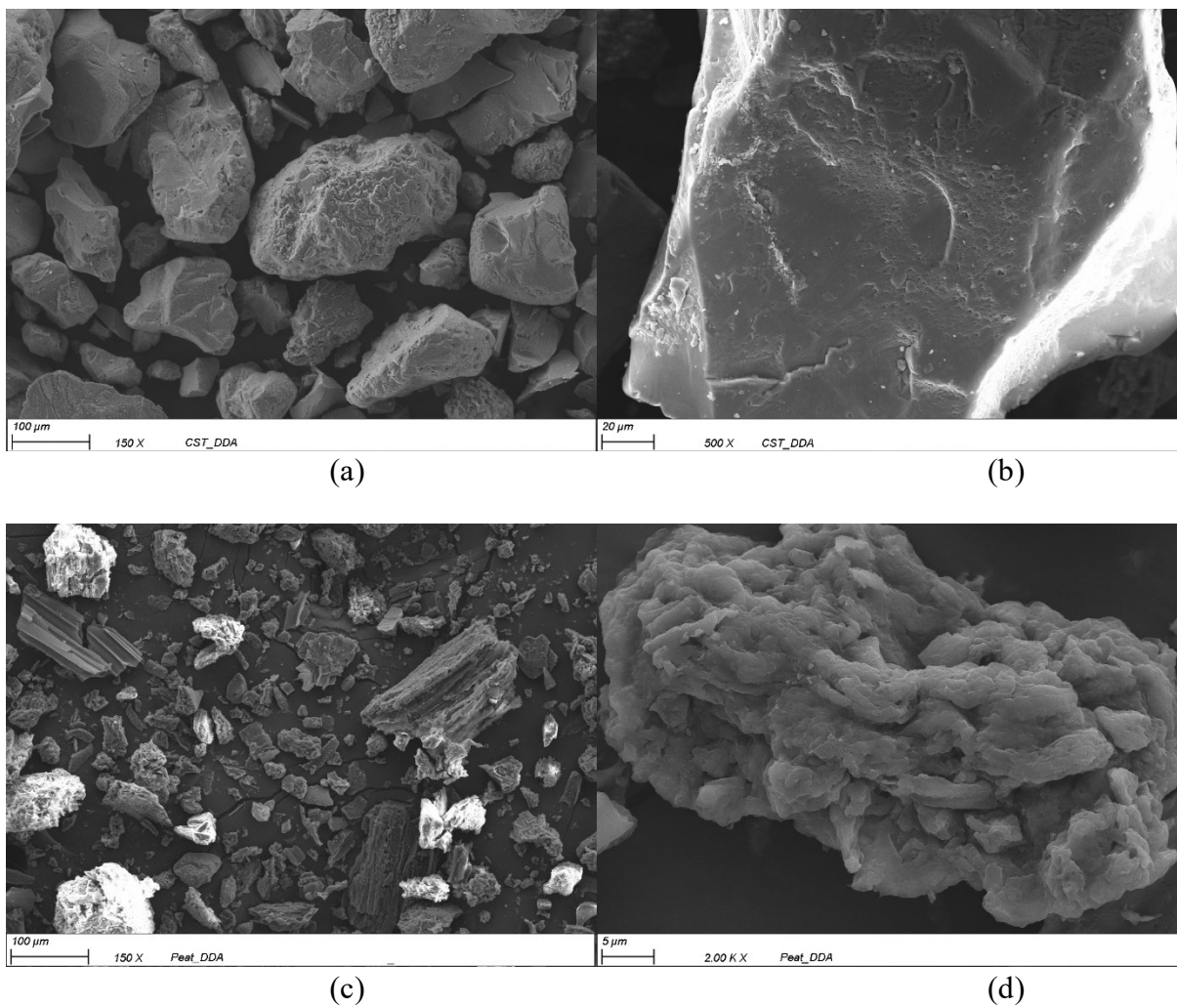


Figure S18: SEM results for CST (a, b) and PMM (c, d) after adsorption process.

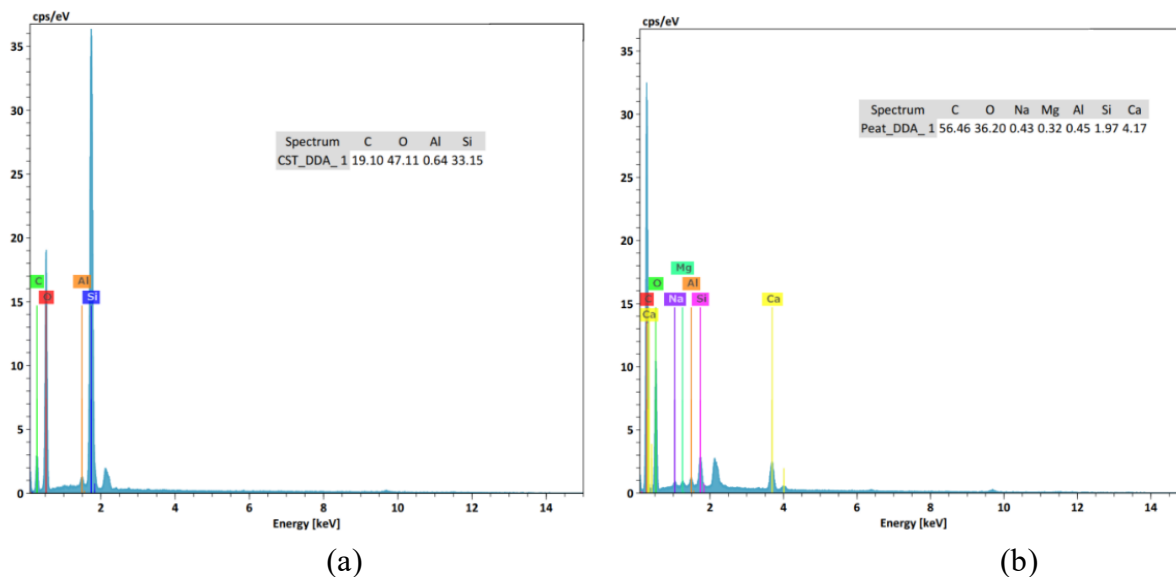


Figure S19: EDX results for CST (a) and PMM (b) after adsorption process.

Table S7: The parameters of UPLC-MS analysis of each NA compound.

Compound name	Monitored mass (m/z)	ESI mode	Cone (V)
CHA	127.0760	Negative	16
CHPA	182.8590	Negative	24
PVA	177.1900	Negative	40
DA	170.9700	Negative	36
DDA	199.0260	Negative	30

Table S8: Comparison of kinetics for different NAs sorption on CST.

Condition	Material	Best fitted model	R <sup>2</sup>	k <sub>2</sub> (g/mg/h)	q <sub>e</sub> (mg/g)	Equilibrium time (h)
Single model compound DDA	CST	PSO	0.98	2.2	0.059	24
DDA in mixture	CST	PSO	1.0	2.3	0.027	96
DA in mixture	CST	PSO	0.99	2.2	0.015	96

## APPENDIX C

**Appendix C contains 1 Text and 1 Table.**

### *Text C1: Analytical methods*

The concentrations of CHA in mono-compound solution were measured using an ultra-high-performance liquid chromatography coupled with a single quadrupole mass spectrometer (UHPLC-SQMS, Waters, USA). The electrospray ionization (ESI) mode is negative, monitored mass ( $m/z$ ) is 127.0760, and cone voltage is 16 V. Chromatographic separations were performed on an ACQUITY UPLC® BEH C18 column (1.7  $\mu\text{m}$ , 2.1  $\times$  50 mm, Waters, USA) with mobile phases of 4 mM ammonium acetate and 0.1% acetic acid in water (A), and acetonitrile (B). The elution gradient was 0-0.5 min, 5% B; 0.5-3 min, increased from 5% to 95% B; then returned to the initial condition 95% B at 3.1 min and held for 1.5 min to equilibrate the column with a flow rate of 0.4 mL/min. The column was controlled at 40 °C, and the injection volume was 5  $\mu\text{L}$ . Data were acquired using MassLynx (Waters, UAS) and processed using TargetLynx (Waters, UAS).

The quantitative analysis of all NAs in the mixture was carried out by an Agilent 1290 Infinity II UHPLC system coupled to an Agilent 6495 triple quadrupole mass spectrometer (QQMS, Agilent Technologies Inc, Canada).

Agilent Poroshell 120 EC-C18 (2.1  $\times$  50 mm, 1.9  $\mu\text{m}$ ) column was used for chromatographic separation with mobile phases of water with 0.1% acetic acid (A) and acetonitrile with 0.1% acetic acid (B). The elution gradient was 0-0.5 min, 0% B; 0.5-5 min, increased from 0% B to 100% B; 5.1 min, decreased to 0% B and held at 0% B for 2 min to equilibrate column with a flow rate of 0.4 mL/min. The column temperature was set at 40 °C throughout the run. The samples were analyzed with an injection volume of 5  $\mu\text{L}$ .

Table S9: Compound-dependent parameters in LC-QQQMS analysis.

Compound Name	Precursor ion (m/z)	Product ion (m/z)	Retention Time (min)	Collision Energy (v)	Polarity
4-MHA	143.1	143.1	4.31	0	Negative
CHA	127.1	127.1	3.80	0	Negative
CHPA	183.1	183.1	4.90	0	Negative
DA	171.1	171.1	4.90	0	Negative
HA	115.1	115.1	3.81	0	Negative
IA	130.1	112.1	0.39	12	Positive
IA	130.1	84.1	0.39	20	Positive
T-2H-T4CA	145.0	33.1	3.30	20	Negative
T-2H-T4CA	145.0	101.1	3.30	12	Negative
T4CA	129.1	129.1	2.61	0	Negative

The QQMS analysis was performed under both positive electron spray ionization (ESI<sup>+</sup>) and negative electron spray ionization (ESI<sup>-</sup>) modes with fast polarity switching. The operation conditions of the source were as follows: both dry gas and sheath gas were nitrogen with a flow rate of 12 L/min. The temperatures of dry gas and sheath gas were set at 250 °C and 400 °C, respectively. The fragmentor voltage (FV) was 166 V and the nebulizer pressure was set at 40 psi. Capillary voltages were 3500 V for both positive and negative modes. The cell accelerator voltage was set at 4 V for all compounds. Data acquisition was controlled using MassHunter software (Agilent Technologies Inc, Canada), and data were processed using Quantitative Analysis software (Agilent Technologies Inc, Canada). The dynamic multiple reaction monitoring (dMRM) transitions of all NAs are listed in Table S9.

***Note:***

Figures 4.1, 4.2, and 4.12 were created with Biorender.com.